UNIVERSITY OF CALIFORNIA SAN DIEGO

Regulation and function of branched-chain amino acid metabolism in adipocytes

A dissertation submitted in partial satisfaction of the
requirements for the degree
Doctor of Philosophy

in

Bioengineering

by

Courtney Renee Green

Committee in charge:

Professor Christian Metallo, Chair
Professor Pedro Cabrales
Professor Alan Saltiel
Professor Shankar Subramaniam
Professor Karsten Zengler

2019

The dissertation of Courtney Renee Green is approved, and it is acceptable in quality and form for publication on microfilm and electronically:

_____

_____

_____

_____

_____

Chair

University of California San Diego

2019

DEDICATION

I dedicate this dissertation to my parents for their unwavering love and support, sacrifices, and commitment to my success.

TABLE OF CONTENTS

LIST OF FIGURES

LIST OF TABLES

ACKNOWLEDGEMENTS

Thank you to everyone that supported me and guided me during my time in graduate school. I thank my advisor, Dr. Christian Metallo, for all of the time and energy he spent shaping me and my thesis work. I thank Martina Wallace for her constant support both scientifically and personally. I must thank the current and former members of the Metallo lab for the fun memories and helpful insights throughout the years: Mehmet Badur, Seth Parker, Nathaniel Vacanti, Avi Kumar, Esther Lim, Jivani Gengatharan, Anna Trimble, Hui (Sunny) Zhang, Thangaselvam Muthusamy, Michal Handzlik, and, finally, Justin Hover.

I also want to thank my friends for the support and destressing they so graciously provided. Also, I must thank my parents whose love and pride means the world to me. Finally, I want to acknowledge Alexander Keim for his daily support over all these years.

Chapter 1, titled "Studying adipose tissue branched-chain amino acid metabolism in obesity and diabetes using stable isotope tracing" is an introduction to the literature and technologies relevant to my thesis work. It covers topics in adipose biology, BCAA metabolism, and mass spectrometry.

Chapter 2, in full, is a reprint of the material as it appears in "Branched-chain amino acid catabolism fuels adipocyte differentiation and lipogenesis," *Nature Chemical Biology*, vol. 12, 2016. Courtney R. Green is the primary author of this publication. Martina Wallace, Ajit S. Divakaruni, Susan A. Phillips, Anne N. Murphy, and Theodore P. Ciaraldi are co-authors of this publication. Christian M. Metallo is the corresponding author of this publication.

Chapter 3, in full, is a reprint of the material as it appears in "Enzyme promiscuity drives branched-chain fatty acid synthesis in adipose tissues," *Nature Chemical Biology*, vol. 14, 2018. Courtney R. Green is the second author of this publication. Martina Wallace is the primary author of this publication. Lindsay S. Roberts, Yujung Michelle Lee, Justin L. McCarville, Joan Sanchez-Gurmaches, Noah Meurs, Jivani M. Gengatharan, Justin D. Hover, Susan A. Phillips, Theodore P. Ciaraldi, David A. Guertin, Pedro Cabrales, Janelle S. Ayres, Daniel K. Nomura,

and Rohit Loomba are co-authors of this publication. Christian M. Metallo is the corresponding author of this publication.

Chapter 4 is currently being prepared for submission for publication. Courtney R. Green is the primary author of this manuscript. Martina Wallace and Justin D. Hover are co-authors of this material. Christian M. Metallo is the corresponding author of this manuscript.

VITA

2019	Ph.D. in Bioengineering, University of California San Diego
2013 – 2014	Laboratory Assistant, University of California San Diego
2013	B.S. in Bioengineering: Biotechnology, University of California San Diego

PUBLICATIONS

Ramms B, Patel S, Nora C, Pessentheiner AR, Chang MW, **Green CR**, Golden GJ, Secrest P, Krauss RM, Metallo CM, Benner C, Alexander VJ, Witztum JL, Tsimikas S, Esko JD, Gordts PLSM. (2019) ApoC-III ASO Promotes Tissue LPL Activity in Absence of ApoE-Mediated TRL Clearance. *J. Lipid Res.* 60(8): 1379-1395.

Wallace M, **Green CR**, Roberts LS, Lee YM, McCarville JL, Sanchez-Gurmaches J, Meurs N, Gengatharan JM, Hover JD, Phillips SA, Ciaraldi TP, Guertin DA, Cabrales P, Ayres JS, Nomura DK, Loomba R, Metallo CM. (2018) Enzyme promiscuity drives branched-chain fatty acid synthesis in adipose tissues. *Nat. Chem. Biol.* 14(11): 1021-1031

Green CR, Wallace M, Divakaruni AS, Phillips SA, Murphy AN, Ciaraldi TP, Metallo CM. (2016) Branched-chain amino acid catabolism fuels adipocyte differentiation and lipogenesis. *Nat. Chem. Biol.* 12(1): 15-21.

Vacanti NM, Divakaruni AS, **Green CR**, Parker SJ, Henry RR, Ciaraldi TP, Murphy AN, Metallo CM. (2014) Regulation of substrate utilization by the mitochondrial pyruvate carrier. *Mol. Cell.* 56(3): 425-35.

Lewis CA*, Parker SJ*, Fiske BP, McCloskey D, Gui DY, **Green CR**, Vokes NI, Feist AM, Vander Heiden MG, Metallo CM. (2014) Tracing compartmentalized NADPH metabolism in the cytosol and mitochondria of mammalian cells. *Mol. Cell.* 55(2): 253-63.

Grassian AR*, Parker SJ*, Davidson SM, Divakaruni AS, **Green CR**, Zhang X, Slocum KL, Pu M, Lin F, Vickers C, Joud-Caldwell C, Chung F, Yin H, Handly ED, Straub C, Growney JD, Vander Heiden MG, Murphy AN, Pagliarini R, Metallo CM. (2014) IDH1 mutations alter citric acid cycle metabolism and increase dependence on oxidative mitochondrial metabolism. *Cancer Res.* 74(12): 3317-31.

CONFERENCE PRESENTATIONS

Green CR, et al. (2019) Branched chain amino acids support brown adipocyte metabolism and fatty acid biosynthesis. (Poster) Metabolism in Health and Disease Conference. Puerto Vallarta, Mexico.

Green CR, et al. (2019) Branched chain amino acids support brown adipocyte metabolism and fatty acid biosynthesis. (Poster) UCSD/UCLA Diabetes Research Center Retreat. La Jolla, CA.

Green CR, et al. (2018) Dissecting branched chain amino acid metabolism in differetiated adipocytes. (Poster) Institute for Engineering in Medicine 10th Anniversary Symposium. La Jolla, CA.

Green CR, et al. (2018) Dissecting branched chain amino acid metabolism in differetiated adipocytes. (Poster) Southern California Biomedical Sciences Graduate Student Symposium. Los Angeles, CA.

Green CR, et al. (2017) Metabolic reprogramming in adipocytes in response to inflammatory cues. (Poster) Epigenomics at VARI workshop. Grand Rapids, MI.

Green CR, et al. (2017) Metabolic reprogramming in adipocytes in response to inflammatory cues. (Poster) Cell Symposia: Cancer, Inflammation, and Immunity. San Diego, CA.

ABSTRACT OF THE DISSERTATION

Regulation and function of branched-chain amino acid metabolism in adipocytes

by

Courtney Renee Green

Doctor of Philosophy in Bioengineering

University of California San Diego, 2019

Professor Christian Metallo, Chair

Metabolism is essential for the maintenance of cellular homeostasis as cells must either import or synthesize substrates for use in biosynthetic and energy generating reactions. Different cell types have distinct metabolic functions, and adipocyte metabolism changes dramatically during adipogenesis or in response to overnutrition/obesity. The metabolism of substrates such as glucose and fatty acids (FA) are well-studied in adipocytes, but evidence suggests that the catabolism of the essential branched-chain amino acids (BCAA - leucine, isoleucine, and valine) is particularly altered in obesity. The chapters of this dissertation are independent bodies of work that explore how BCAA metabolism changes in differentiating adipocytes, contributes to *de novo* lipogenesis (DNL), and regulates the fatty acid profile within the lipidome. Chapter 1, titled "Studying adipose

tissue branched-chain amino acid metabolism in obesity and diabetes using stable-isotope tracing," is a review of the relevant adipose- and BCAA-related literature and the utility of stable-isotope tracing and metabolic flux analysis (MFA) to the study adipocyte metabolism. Chapter 2, titled "Branched-chain amino acid catabolism fuels adipocyte differentiation and lipogenesis," uses stable-isotope tracing and mass spectrometry to quantify the increase in the contribution of BCAA catabolism to the TCA cycle and DNL throughout differentiation. This chapter also details a vitamin B12 deficiency in typical adipocyte cell culture and demonstrates adipocytes' ability to reprogram metabolism to maintain BCAA levels in physiological media with lower amino acid concentrations. Chapter 3, titled "Enzyme promiscuity drives branched-chain fatty acid synthesis in adipose tissues," describes the tissue- and compartment-specific pathway of branched-chain fatty acid (BCFA) synthesis in mammals using a variety of stable-isotope tracers. We show that BCFAs are highly synthesized in adipose tissue due to expression of a critical protein in AT that facilitates their synthesis, are synthesized from intermediate metabolites in BCAA catabolism, and are decreased in a high-fat diet via a hypoxia-related mechanism. Chapter 4, titled "Altered branched-chain amino acid catabolism drives distinct changes in the TCA cycle and lipidome," is currently being prepared for submission for publication. In this manuscript, we interrogate the metabolic and functional impacts of reduced BCAA catabolism through CRISPR/Cas9-mediated deficiency of *Bckdha*. While differentiation is unaffected by *Bckdha* deficiency, oxygen consumption rates are reduced and relative glucose metabolism increases to support DNL. Furthermore, *Bckdha* deficiency decreased the levels of polyunsaturated fatty acid (PUFA)-containing sphingomyelin and increased the levels of PUFA-containing phosphatidylcholine. We hypothesize that the dramatic reduction of BCFAs and OCFAs in *Bckdha* deficient adipocytes is driving this FA reorganization phenotype. The functional impact of this change is unknown but membrane fluidity and permeability could be affected. Taken together, these collective studies demonstrate the importance of understanding the regulation and function of BCAA metabolism in adipocytes in the obese or insulin resistant state. These findings could impact biomarker development and

improve our understanding of the progression of diabetes.

Chapter 1

Studying adipose tissue branched-chain amino acid metabolism in obesity and diabetes using stable-isotope tracing

1.1 Introduction

Excess accumulation of adipose tissue (AT), or obesity, is linked to a number of metabolic syndromes and diseases including type 2 diabetes mellitus (T2DM)[1], cardiovascular disease[2], and mood disorders[3]. AT is a complex organ with endocrine roles and metabolic processes that respond to external cues and are altered in the context of obesity. The subject of this thesis is adipocyte metabolism and, in particular, the role of adipocytes in regulating branched-chain amino acid (BCAA) metabolism. Using stable-isotope tracing, mass spectrometry, and CRISPR/Cas9-based genetic perturbations, I quantitatively assess the contribution of BCAAs to adipocyte *de novo* lipogenesis (DNL) and tricarboxylic acid (TCA) cycle metabolism. I also demonstrate adipocytes' ability to synthesize monomethyl branched chain fatty acids (BCFA) and reprogram their metabolism upon knock-out of enzymes within the BCAA catabolic pathway. Impairment

of BCAA catabolism alters the lipidome and leads to substantial fatty acid (FA) reorganization between lipid classes.

1.2 Dysfunctional adipose tissue biology and metabolism drives progression to T2DM

In recent decades, there has been a greater appreciation of white adipose tissue (WAT) as more than a simple storage organ. In fact, adipocytes in WAT are known to secrete multiple cytokines that regulate the endocrine system, termed adipokines[4–6]. The first such adipokine identified was leptin, which regulates food intake, energy expenditure, and body mass[7]. Shortly thereafter, adipocytes were shown to secrete tumor necrosis factor α (TNFα)[8], which is associated with inflammation and negatively impacts insulin signal transduction. They also secrete adiponectin[9, 10], which acts through AMP kinase (AMPK) to support insulin signaling. Lipokines such as the anti-inflammatory fatty acid esters of hydroxy fatty acids (FAHFAs)[11] and insulin-sensitizing palmitoleate[12] are also secreted by adipocytes.

AT regulates whole-body metabolism particularly through its ability to both de novo synthesize lipids during feeding and subsequently release lipids to the circulation via lipolysis during fasting or exercise[13]. All of these functions of adipocytes: adipokine secretion, DNL, lipolysis, and glucose disposal in response to insulin require proper adipocyte differentiation. Adipocyte differentiation, or adipogenesis, requires specific signals such as peroxisome proliferator activator receptor γ (PPARγ) agonism[14] and suppression of Wnt/β-catenin signaling[15]. There is evidence that adipocytes in some obese individuals are poorly differentiated or dysfunctional due to chronic low-grade inflammation[16], poor vasculature/hypoxia[17], and/or mitochondrial or ER stress[18]. Prolonged exposure to these stresses is thought to contribute to tissue-specific insulin resistance (IR) and eventual T2DM.

Inflamed adipose tissue can occur in response to a number of different stresses. There is

evidence that prolonged overnutrition and overexposure to insulin, leptin, catecholamines, etc. can induce AT inflammation[16]. In addition, AT expansion, either through hypertrophy (growth of cell size) or hyperplasia (proliferation of pre-adipocytes and differentiation to adipocytes) has also been shown to differentially affect the inflammatory microenvironment. AT expansion via the former is thought to be associated with more immune cell infiltration and inflammation[19]. The latter process, hyperplasia, is associated with lower levels of inflammation and lower insulin resistance. Hyperplasia is implicated in the effectiveness of thiazolidinediones (TZD) treatments of T2DM, which often lead to weight gain and increased adiposity, but improve metabolic parameters[20, 21]. Additionally, those patients classified as "metabolically healthy obese" in that they have improved glucose homeostasis (in addition to other parameters) relative to other equally obese subjects, have smaller adipocytes than other obese people[22, 23], indicating that adipocyte size could strongly correlate with insulin sensitivity.

Beyond adipocyte size, inflammation can occur in AT through a number of other mechanisms including response to gut-derived antigens, inflammatory lipids, mechanical stresses from increased cell size straining the ECM boundaries, and hypoxia[16]. Beyond adipose-specific inflammation, there is also evidence of increased presence of macrophages within obese AT[24] and a polarization of adipose tissue macrophages to a more characteristically M1 (pro-inflammatory) macrophage[25], which is associated with development of IR[26]. The length of time before obesity leads to IR and T2DM diagnosis varies wildly but advancements have been made in predictive biomarkers.

Biomarkers for T2DM, in particular, could lead to an earlier diagnosis as once hyperglycemia is detected, pancreatic β-cell dysfunction is already very advanced[27, 28]. In 2009, Newgard and colleagues found that the concentration of BCAAs was higher in the plasma of obese individuals compared to lean controls. They also found a positive correlation between a patient's BCAA level and their Homeostatic Model Assessment of Insulin Resistance (HOMA-IR) score (i.e., higher BCAAs is associated with higher insulin resistance score)[29]. Another study

found that elevated BCAAs could serve as a predictor of future diagnosis of T2DM[30]. The next section summarizes the major studies linking BCAA metabolism to adipose tissue and adipogenesis.

1.3 BCAA catabolism and *de novo* lipogenesis are hallmarks of adipocyte metabolism

In my thesis work, I focused on the metabolism of BCAAs in adipocytes (Chapter 2), the connections between this pathway and DNL (Chapter 3), and the role this pathway plays in regulating the lipidome (Chapter 4). BCAAs – leucine, isoleucine, and valine – are essential amino acids used for protein synthesis that can also be catabolized to acetyl-CoA (AcCoA) and/or propionyl-CoA (PropCoA) for use in the TCA cycle and/or DNL. BCAAs are also potent regulators of cell growth and metabolism through the mammalian target of rapamycin (mTOR) signaling cascade[31]. Their oxidation is controlled by expression of key enzymes including BCAT, which transfers the amino nitrogen from the BCAA to α-ketoglutarate to form glutamate and a branched-chain α-ketoacid. There are 2 isoforms of BCAT: cytosolic BCAT1 (BCATc) is mainly expressed in the brain[32], while mitochondrial BCAT2 (BCATm) is more ubiquitously expressed, with the major exception of the liver[33], where very little BCAT activity exists. However, recent proteomic studies suggest that non-hepatocytes present in the liver do express BCAT[34]. The rate-limiting enzyme of BCAA catabolism is the branched-chain α-ketoacid dehydrogenase complex (BCKDH complex). The BCKDH complex is composed of 3 subunits, E1, E2, and E3. The E3 subunit is also present in other α-ketoacid dehydrogenases and is encoded by DLD[35]. The E2 subunit is encoded by DBT[36] and the E1 subunit is encoded by 2 genes, *Bckdha* and *Bckdhb*[37]. Mutations in any of these 3 genes leads to maple syrup urine disease (MSUD)[38–40], a potentially severe inborn error of metabolism that can cause neurological defects and death if untreated. These 2 enzymes, BCAT and BCKDH, act on all 3 BCAAs. After

these steps, the pathway diverges, and unique enzymes catabolize the intermediates to AcCoA and PropCoA (Fig. 1). Pathway intermediates can be used for other purposes as well though. For example, the products of BCKDH are short branched-chain fatty acyl-CoAs (SBCFA-CoA), which I show in Chapter 3 can be exported the cytosol and elongated to full-length BCFAs[41].

3T3-L1 adipocytes are a common *in vitro* model to study adipogenesis and adipocyte metabolism. These cells morphologically resemble fibroblasts when proliferating but after treatment with a differentiation cocktail for 1 week post-confluence, they differentiate to lipid-droplet-containing adipocytes that express many of the canonical markers of adipocytes[42–44]. Lackey and colleagues showed that expression of enzymes in the BCAA catabolic pathway increase during differentiation[45]. Others have demonstrated AT's ability to regulate BCAA levels. In particular the ability of wild-type AT transplantation to normalize BCAA levels in Bcat2$^{-/-}$ mice[46, 47]. In Chapter 2 of this dissertation, I quantitatively measure BCAA contribution to adipocyte metabolism – both TCA cycle metabolism and fatty acid metabolism. Using stable isotope tracing and mass spectrometry, we found that BCAAs are fully oxidized to AcCoA and PropCoA in adipocytes which labels TCA cycle metabolites and accounts for about 30% of the AcCoA used for DNL. After finding high levels of BCAA-derived methylmalonic acid and high odd-chain fatty acid (OCFA) concentrations, we determined that the cell culture system was deficient in vitamin B12. This was an exciting finding as others had detected high OCFA levels in 3T3-L1 adipocytes but the origin of these fatty acids was not known[44]. many researchers assumed they derived from α-oxidation but we show they are in fact*de novo* synthesized from BCAA-derived PropCoA[48]. We also identified a species of fatty acid – namely monomethyl branched-chain fatty acids (BCFA) – that were not thought to be synthesized by mammals as actively synthesized in 3T3-L1 adipocytes, human adipocytes, and in mice and humans[41].

The function of BCFAs in mammalian systems is not known. In lower organisms they regulate membrane fluidity[49] and their absence leads to neurological defects[50, 51]. BCFAs were known to be present in humans but they were thought to be purely diet derived. However,

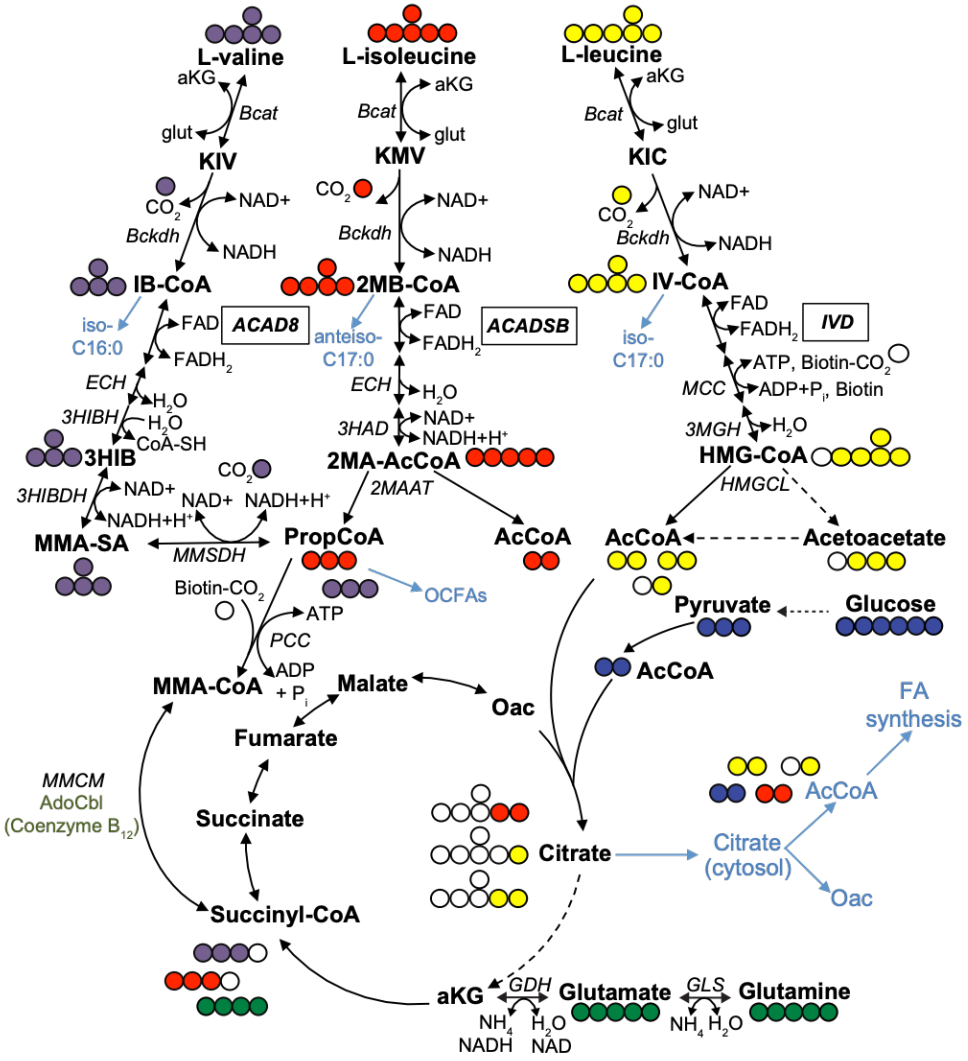

Figure 1.1: **Pathway map of BCAA catabolism.** Map of BCAA catabolism. Circles indicate a carbon atom with colored circles signifying ^{13}C labeled atoms and white circles signifying unlabeled carbon atoms. Abbreviations: aKG: α-ketoglutarate; glut: glutamate; KIV: ketoisovalerate; KMV: ketomethylvalerate; KIC: ketoisocaproate; IB-CoA: isobutyryl-CoA; 2MB-CoA: 2-methylbutyryl-CoA; IV-CoA: isovaleryl-CoA; 3HIB: 3-Hydroxyisobutyrate; MMA-SA: methylmalonyl-semialdehyde; 2MA-CoA: 2-Methylacetoacetyl-CoA; HMG-CoA: β-Hydroxy β-methylglutaryl-CoA; Oac: oxaloacetate; FA: fatty acid; AdoCbl: adenosyl-cobalamin; Bcat: branched-chain aminotransferase; Bckdh: branched-chain ketoacid dehydrogenase; ACAD: acyl-CoA dehydrogenase; IVD: isovaleryl-CoA dehydrogenase; ECH: enoyl-CoA hydratase; MCCC: methyl-crotonyl-CoA carboxylase; 3HIBH: 3-Hydroxyisobutyrate hydratase; 3HAD: 3-Hydroxyacyl-CoA dehydrogenase; 3MGH: 3-methylglutaconyl-CoA hydratase; 3HIBDH: 3-Hydroxyisobutyrate dehydrogenase; MMSDH: Methylmalonate-semialdehyde dehydrogenase; PCC: propionyl-CoA carboxylase; MMCM: methylmalonyl-CoA mutase; 2MAAT: 2MA-CoA acetyltransferase; HMGCL: 3-hydroxy-3-methylglutaryl-CoA lyase: GLS: glutaminase; GDH: glutamate dehydrogenase.

as presented in Chapter 3 of this dissertation, we demonstrate that, in fact, BCFAs are synthesized *de novo* in mammalian cells and tissues. Others reported that BCFAs are lower in obese individuals[52] and increase after gastric bypass surgery[53, 54]. Multi-branched chain fatty acids are trafficked to and oxidized by the peroxisome[55] but whether singly-branched fatty acids are trafficked in the same way and incorporated into signaling lipids such as ether lipids or plasmalogens[56, 57] is unknown at this time, though we do present evidence that this is occurring. Finally, BCFAs, due to the methyl branch near the end of the acyl chain, fluidize cell membranes in a similar manner as polyunsaturated fatty acids (PUFA) do so. One advantage to BCFAs, however, is their saturated acyl chain that is much less susceptible to oxidative stress, including lipid peroxidation[58]. Overall, the BCAA catabolic pathway is upregulated during adipocyte differentiation and homeostatic changes such as chronic low-grade inflammation in obesity reduce catabolism and synthesis of intermediates along this pathway.

The other hallmark of adipocyte metabolism is *de novo* lipogenesis. This is primarily performed by fatty acid synthase (FASN) in the cytosol. Synthesized fatty acids are primarily incorporated into triacylglycerides (TAGs) or other lipid classes such as phosphocholine (PC) and sphingomyelin (SM). Interestingly, DNL in WAT is reduced in the context of a high-fat diet, obesity, and T2DM[59, 60]. This is true for most tissues except liver where DNL actually increases on a high-fat diet to metabolize the excess fat and carbohydrates to TAGs and lipoproteins[61, 62].

As shown in Chapter 3 of this dissertation, FASN is promiscuous, meaning that it can use substrates other than AcCoA to start the FA chain. It is this promiscuity that allows SBCFA-CoAs to be elongated to full-length BCFAs. Therefore, any suppression of DNL (as in obesity) also affects BCFA levels since synthesis of these relies on high BCAA catabolism and high DNL[41]. It is likely that the coordinated upregulation of BCAA catabolism and DNL leads to increased BCFA levels after major weight loss.

The goal of biomarker research is to unify disparate findings and correlations into a

cohesive explanation. In my thesis work, I sought to understand the metabolic implications of metabolomics or transcriptomics patient studies. For example, the elevation of BCAAs in patients that ultimately develop T2DM[30] is intriguing and suggests that BCAA catabolism is impaired. If their elevation were simply due to high protein intake, all amino acids would be expected to increase. However, BCAAs and aromatic amino acids are specifically affected[29]. WAT is not the only site this decreased catabolism could occur as muscle and brown AT are also major sites of BCAA oxidation that phenotypically change and whiten during obesity[41, 63]. This reduction in BCAA catabolism could be due to inflammation, hypoxia (as shown in Chapter 3 of this thesis, hypoxia does lower BCKDHA expression), or mechanical stresses leading to adipocyte stress and dysfunction. There are still a number of unexplained phenomena such as greater improvement of BCAA homeostasis in patients that underwent gastric bypass surgery compared to those that lost an equivalent amount of weight through dietary intervention[64]. Some interpret these changes in BCAA metabolism correlating with glucose homeostasis as an indication that high BCAAs cause IR[65] but far more studies are needed to prove such a provocative hypothesis.

1.4 Mass spectrometry can elucidate changes in metabolism and *de novo* lipogenesis

Metabolic pathways are complex and can contain a dozen or more intermediates. These intermediates often intersect with other metabolic pathways and small changes to a few reaction rates can result in major changes to metabolite levels in a disparate, unexpected pathway. Tools such as gas chromatography-mass spectrometry (GC-MS), liquid chromatography-mass spectrometry (LC-MS), and nuclear magnetic resonance spectroscopy (NMR) allow for high-throughput quantitation of large numbers of metabolites within a biological matrix[66]. These technologies coupled with advancements in systems biology and computation helped make the field of biomarker identification possible[67, 68].

Public resources such as XCMS[69], Lipid Maps[70], Human Metabolome Database (HMDB)[71] and many others help make this complex field more approachable to the broader scientific community. These resources and others analyze both targeted and untargeted mass spectrometry data, display and explain structures, and summarize the typical (and atypical) concentrations of metabolites found in human fluids.

However, metabolomics alone only yields information on metabolite abundances. It is difficult, or impossible, to determine whether an elevated metabolite is synthesized more, degraded less, or simply taken up from the culture media or bloodstream more. Essentially, a flux is likely altered to drive a change in metabolite levels. Introduction of a stable-isotope tracer combined with metabolic flux analysis (MFA) is critically important to understanding metabolite alterations.

Stable-isotope tracing involves the use of substrates of interest containing non-radioactive isotopes such as glucose, glutamine, BCAAs, palmitate, etc. The type of isotope (^{13}C, ^{2}H, ^{15}N) is chosen based on which atom(s) one wants to "trace" through metabolism. Stable-isotope tracing is a powerful tool for a number of reasons.

First, stable isotope tracing introduces a time component to the analysis. Introduction of a stable isotope tracer substrate such as [U-$^{13}C_6$]glucose (where all 6 carbon atoms in the glucose molecule are ^{13}C), means that any ^{13}C mass shifts present on measured metabolites such as pyruvate, citrate, glutamate, or palmitate were newly synthesized over the course of the experiment. The labeling pattern is also important as the enzyme utilized can affect the distribution of isotopologues of the metabolite[72]. For example, if M+3 pyruvate from [U-$^{13}C_6$]glucose is oxidized by PDH to form M+2 AcCoA, ultimately an M+2 malate is formed. However, if the M+3 pyruvate is carboxylated by PC, an M+3 malate is formed. In most cells both of these pathways are active, but a myriad of factors could alter their relative utilization and drive a metabolic phenotype. Choice of tracer is critical to answering specific questions and multiple publications summarize the pros and cons of different tracers in studying specific

reactions[72–74].

Beyond central carbon metabolism and amino acid metabolism, stable isotope tracing is also useful in the context of fatty acid metabolism. Fatty acid labeling alone yields information about which substrates contribute to specific FAs. For example, this is how, in Chapter 2, I show that OCFAs were not the result of α-oxidation: they contained an M+3 shift from BCAA-derived PropCoA indicating that PropCoA initiated the FA chain and was lengthened to a full-length OCFA. However, mathematical models exist to extract more information from mass isotopomer distributions (MID) of FAs. Isotopomer spectral analysis (ISA) is used in this thesis[75]. ISA calculates 2 parameters: 1) the relative contribution of the tracer substrate to the acetyl-CoA pool used to synthesize the FA(s) being modeled (termed lipogenic AcCoA) and 2) the percentage of the FA pool that was newly synthesized over the course of the experiment (Fig. 2). The first parameter is constant over time assuming the cells are at steady state (i.e., not differentiating, reaching confluence, etc.). The second parameter will change as a function of time as, typically, a greater percentage of the FA pool will be synthesized over time because either the cells are proliferating or simply turning over their FAs.

ISA has been applied to the study of triacylglyceride (TAG) synthesis in 3T3-L1 adipocytes using an unbiased [^{13}C]acetate tracer[76]. However the use of [^{13}C]glucose and [^{13}C]BCAA tracers can yield additional information on AcCoA sourcing and alternative FA synthesis in adipocytes. Often one tracer can yield multiple measurements. For example, Collins and colleagues traced human adipocytes with [U-$^{13}C_6$]glucose and determined that the contribution of glucose to the glycerol headgroup of TAGs is much higher than glucose's contribution to the synthesized acyl chains[77]. Unbiased tracers such as deuterated or "heavy" water, $^{2}H_2O$, are also used to quantify fatty acid synthesis without relying on AcCoA generation from the tracer[78].

Further development is ongoing to improve the utility of stable isotope tracing and metabolic flux analysis. For example, the use of high-resolution mass spectrometers allows for accurate identification of metabolites and more precise labeling information, thus lowering the

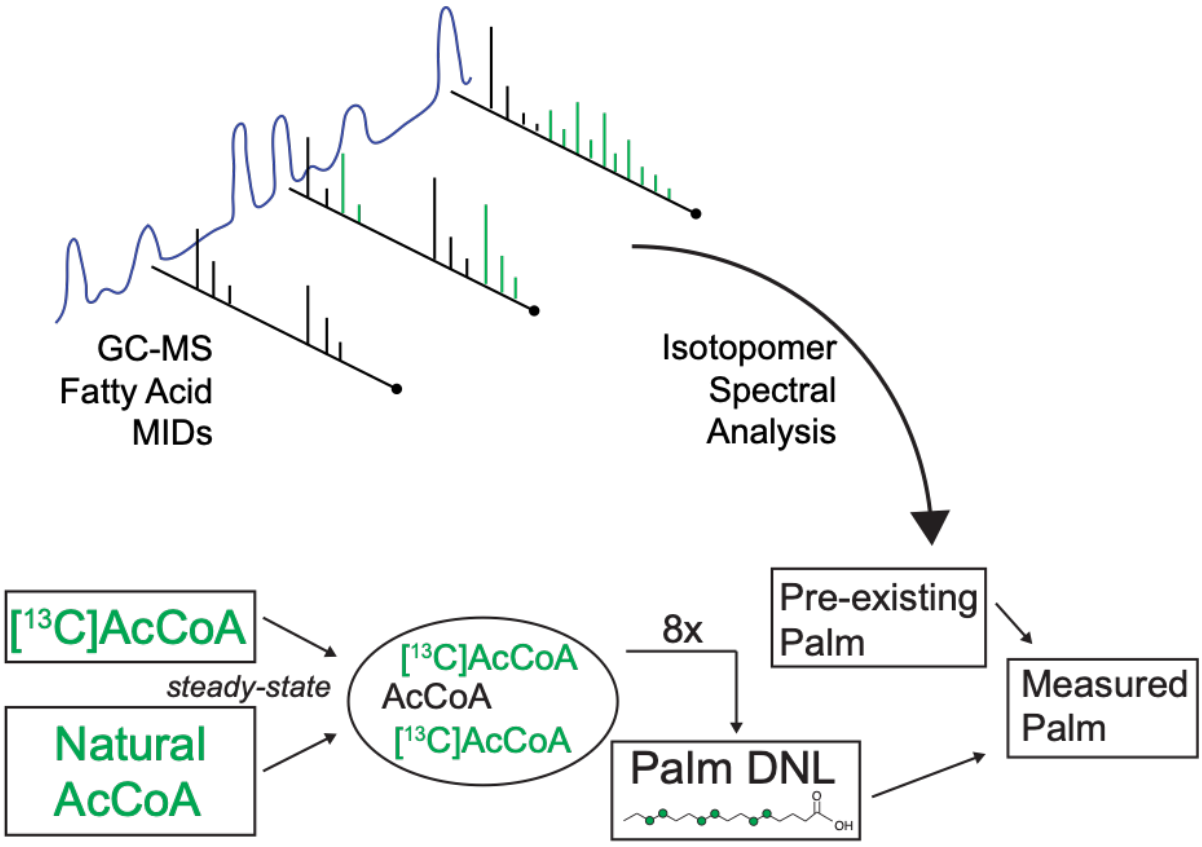

Figure 1.2: **Schematic of Isotopomer Spectral Analysis.** MIDs from GC-MS data are used to model FA biosynthesis and the contribution of specific tracers to FA biosynthesis. In this figure, Palmitate is depicted but models used in this thesis modeled multiple FAs in parallel.

confidence intervals of estimated fluxes[79]. Integration of multiple "-omics" datasets is also an active area of research as metabolomics results supported by transcriptomic and proteomic data only strengthens the conclusion reached[80].

In my thesis work, I primarily utilized gas chromatography-mass spectrometry (GC-MS) to quantify metabolites and analyze labeling patterns on polar and non-polar metabolites. However, in analyzing intact lipids for data presented in Chapter 4, I used a liquid chromatography triple-quadrupole mass spectrometer (LC-MS/MS). Using 2 different chromatography methods, I was able to measure the abundance of a variety of lipid classes including TAG, diacylglycerol, phosphatidylcholine, phosphatidylserine, phosphatidylethanolamine, sphingomyelin, ceramide, dihydroceramide, and sphingoid bases[81, 82]. I reported as many different species as possible within each lipid class as determined via a) expected retention time shift relative to a representative standard and b) significant signal increase over "blank" sample.

In the following chapters, these techniques and more are used to quantitatively understand the regulatory points within and function of BCAA metabolism and DNL in adipocytes. Chapter 2, titled "Branched-chain amino acid catabolism fuels adipocyte differentiation and lipogenesis," demonstrates a dramatic upregulation of BCAA catabolism during differentiation and identifies a cobalamin deficiency in typical cell culture media that limits BCAA catabolism to the TCA cycle. In the presence of more physiological concentrations of glucose and amino acids, 3T3-L1 adipocytes will catabolize protein to maintain the intracellular levels of BCAAs, resulting in dilution of the ^{13}C-BCAA tracer from unlabeled protein sources.

Chapter 3, titled "Enzyme promiscuity drives branched-chain fatty acid synthesis in adipose tissues," explores the regulation and tissue-specific synthesis of BCFAs in mammalian systems. It quantitatively explores the rate of BCFA synthesis *in vivo* using $^{2}H_2O$ in both mice and humans and shows that even in germ-free mice, BCFA synthesis in adipose tissue is conserved.

Chapter 4, titled "Altered branched-chain amino acid catabolism drives distinct changes in the TCA cycle and lipidome," explores the effect of BCKDHA deficiency in 3T3-L1 adipocytes

and is currently being prepared for submission for publication. The effect of blocking BCAA catabolism through CRISPR/Cas9-mediated *Bckdha* deficiency, a recapitulation of the severe inborn error of metabolism known as maple syrup urine disease[83], is contrasted with the effect of *Acad8* deficiency, a recapitulation of the milder disease isobutyryl-CoA dehydrogenase deficiency[84, 85], which blocks complete valine catabolism but does not impact BCFA synthesis[86]. We find that *Bckdha* deficiency reduces the levels of TCA cycle intermediates and lowers both the basal and maximal oxygen consumption rate. *Bckdha* deficiency also causes dramatic reorganization of PUFAs across lipid species – in particular, out of sphingomyelin pools and into phosphatidylcholine and other phospholipid pools. This phenotype is rescuable with the addition of SBCFAs, the precursor to BCFAs. We propose that this reorganization is related to the potential function of BCFAs in regulating membrane fluidity and in the absence of BCFAs, PUFAs substitute for them. Taken together, these collective studies demonstrate the importance of understanding the regulation and function of BCAA metabolism in adipocytes. These findings could impact biomarker development and improve understanding of the progression of diabetes.

1.5 Acknowledgements

Chapter 1 is an introductory chapter to this thesis. Courtney R. Green is the primary author. Christian M. Metallo is the corresponding author.

1.6 References

1. Kahn, B. & Flier, J. Obesity and insulin resistance. *Journal of Clinical Investigation* **106,** 473–481 (2000).

2. Poirier, P., Giles, T., Bray, G., Hong, Y., Stern, J., F., P. & Eckel, R. Obesity and Cardiovascular Disease: Pathophysiology, Evaluation, and Effect of Weight Loss. *Circulation* **113,** 898–918 (2006).

3. Romain, A., Marleau, J. & Baillot, A. Impact of obesity and mood disorders on physical comorbidities, psychological well-being, health behaviours and use of health services. *J Affect Disorders* **225,** 381–388 (2018).

4. Galic, S., Oakhill, J. S. & Steinberg, G. R. Adipose tissue as an endocrine organ. *Mol. Cell. Endocrinol.* **316,** 129–39 (2010).

5. Rosen, E. D. & Spiegelman, B. M. What we talk about when we talk about fat. *Cell* **156,** 20–44 (2014).

6. Stern, J., Rutkowski, J. & Scherer, P. Adiponectin, Leptin, and Fatty Acids in the Maintenance of Metabolic Homeostasis through Adipose Tissue Crosstalk. *Cell Metab* **23,** 770–784 (2016).

7. Zhang, Y., Proenca, R., Maffei, M., Barone, M., Leopold, L. & Friedman, J. Positional cloning of the mouse obese gene and its human homologue. *Nature* **372,** 425–32 (1994).

8. Hotamisligil, G. & Spiegelman, B. Tumor necrosis factor alpha: a key component of the obesity-diabetes link. *Diabetes* **43,** 1271–8 (1994).

9. Scherer, P., Williams, S., Fogliano, M., Baldini, G. & Lodish, H. A novel serum protein similar to C1q, produced exclusively in adipocytes. *J. Biol. Chem.* **270,** 26746–9 (1995).

10. Turer, A. & Scherer, P. Adiponectin: mechanistic insights and clinical implications. *Diabetologia* **55,** 2319–2326 (2012).

11. Yore, M. M., Syed, I., M, M. P., Zhang, T., Herman, M. A., Homan, E. A., Patel, R. T., Lee, J., Chen, S., Peroni, O. D., Dhaneshwar, A. S., Hammarstedt, A., Smith, U., E, M. T., Saghatelian, A. & Kahn, B. B. Discovery of a Class of Endogenous Mammalian Lipids with Anti-Diabetic and Anti-inflammatory Effects. **159** (2014).

12. Cao, H., Gerhold, K., Mayers, J. R., Wiest, M. M., Watkins, S. M. & Hotamisligil, G. S. Identification of a Lipokine, a Lipid Hormone Linking Adipose Tissue to Systemic Metabolism. **134,** 933–944 (2008).

13. Song, Z., Xiaoli, A. & Yang, F. Regulation and Metabolic Significance of De Novo Lipogenesis in Adipose Tissues. *Nutrients* **10,** 1383 (2018).

14. Rosen, E., Walkey, C., Puigserver, P. & Spiegelman, B. Transcriptional regulation of adipogenesis. *Genes Dev.* **14,** 1293–307 (2000).

15. Prestwich, T. & Ormond, M. Wnt/β-catenin signaling in adipogenesis and metabolism. *Curr Opin Cell Biol* **19,** 612–617 (2007).

16. Reilly, S. & Saltiel, A. Adapting to obesity with adipose tissue inflammation. *Nat Rev Endocrinol* **13,** 633–643 (2017).

17. Nishimura, S., Manabe, I., Nagasaki, M., Hosoya, Y., Yamashita, H., Fujita, H., Ohsugi, M., Tobe, K., Kadowaki, T., Nagai, R. & Sugiura, S. Adipogenesis in Obesity Requires Close Interplay Between Differentiating Adipocytes, Stromal Cells, and Blood Vessels. *Diabetes* **56,** 1517–1526 (2007).

18. Ferranti, S. & Mozaffarian, D. The Perfect Storm: Obesity, Adipocyte Dysfunction, and Metabolic Consequences. *Clin Chem* **54,** 945–955 (2008).

19. Chan, P. & Hsieh, P. *The Role of Adipocyte Hypertrophy and Hypoxia in the Development of Obesity-Associated Adipose Tissue Inflammation and Insulin Resistance* (2017).

20. Saltiel, A. & Olefsky, J. Thiazolidinediones in the treatment of insulin resistance and type II diabetes. *Diabetes* **45,** 1661–9 (1996).

21. Tang, W., Zeve, D., Seo, J., Jo, A. & Graff, J. Thiazolidinediones Regulate Adipose Lineage Dynamics. *Cell Metab* **14,** 116–122 (2011).

22. Klöting, N., Fasshauer, M., Dietrich, A., Kovacs, P., Schön, M., Kern, M., Stumvoll, M. & Blüher, M. Insulin-sensitive obesity. *Am J Physiol-endoc M* **299,** E506–E515 (2010).

23. Phillips, C. Metabolically healthy obesity: Definitions, determinants and clinical implications. *Rev Endocr Metabolic Disord* **14,** 219–227 (2013).

24. Weisberg, S. P., Daniel, M., Desai, M., Rosenbaum, M., Leibel, R. L. & Ferrante, A. W. Obesity is associated with macrophage accumulation in adipose tissue. *J. Clin. Invest.* **112,** 1796–808 (2003).

25. Lumeng, C., Bodzin, J. & Saltiel, A. Obesity induces a phenotypic switch in adipose tissue macrophage polarization. *J Clin Invest* **117,** 175–184 (2007).

26. Xu, H., Barnes, G. T., Yang, Q., Tan, G., Yang, D., Chou, C. J., Sole, J., Nichols, A., Ross, J. S., Tartaglia, L. A. & Chen, H. Chronic inflammation in fat plays a crucial role in the development of obesity-related insulin resistance. *J. Clin. Invest.* **112,** 1821–30 (2003).

27. Kahn, S. Clinical review 135: The importance of beta-cell failure in the development and progression of type 2 diabetes. *J. Clin. Endocrinol. Metab.* **86,** 4047–58 (2001).

28. Tabák, A. G., Jokela, M., Akbaraly, T. N., Brunner, E. J., Kivimäki, M. & Witte, D. R. Trajectories of glycaemia, insulin sensitivity, and insulin secretion before diagnosis of type 2 diabetes: an analysis from the Whitehall II study. *Lancet* **373,** 2215–21 (2009).

29. Newgard, C. B., An, J., Bain, J. R., Muehlbauer, M. J., Stevens, R. D., Lien, L. F., Haqq, A. M., Shah, S. H., Arlotto, M., Slentz, C. A., Rochon, J., Gallup, D., Ilkayeva, O., Wenner, B. R., Yancy, W. S., Eisenson, H., Musante, G., Surwit, R. S., Millington, D. S., Butler, M. D. & Svetkey, L. P. A branched-chain amino acid-related metabolic signature that differentiates obese and lean humans and contributes to insulin resistance. *Cell Metab.* **9,** 311–26 (2009).

30. Wang, T. J., Larson, M. G., Vasan, R. S., Cheng, S., Rhee, E. P., Elizabeth, M., Lewis, G. D., Fox, C. S., Jacques, P. F., Fernandez, C., J, O. C., Carr, S. A., Mootha, V. K., Florez, J. C., Souza, A., Melander, O., Clish, C. B. & Gerszten, R. E. Metabolite profiles and the risk of developing diabetes. *Nat. Med.* **17,** 448–53 (2011).

31. Laplante, M. & Sabatini, D. mTOR Signaling in Growth Control and Disease. *Cell* **149,** 274–293 (2012).

32. Hall, T., Wallin, R., Reinhart, G. & Hutson, S. Branched chain aminotransferase isoenzymes. Purification and characterization of the rat brain isoenzyme. *J. Biol. Chem.* **268,** 3092–8 (1993).

33. Hutson, S., Wallin, R. & Hall, T. Identification of mitochondrial branched chain aminotransferase and its isoforms in rat tissues. *J. Biol. Chem.* **267,** 15681–6 (1992).

34. Ding, C., Li, Y., Guo, F., Jiang, Y., Ying, W., Li, D., Yang, D., Xia, X., Liu, W., Zhao, Y., He, Y., Li, X., Sun, W., Liu, Q., Song, L., Zhen, B., Zhang, P., Qian, X., Qin, J. & He, F. A Cell-type-resolved Liver Proteome. *Mol Cell Proteomics* **15,** 3190–3202 (2016).

35. Liu, T., Kim, H., Arizmendi, C., Kitano, A. & Patel, M. Identification of two missense mutations in a dihydrolipoamide dehydrogenase-deficient patient. *Proc National Acad Sci* **90,** 5186–5190 (1993).

36. Lau, K., Herring, W., Chuang, J., M, M., Danner, D., Cox, R. & Chuang, D. Structure of the gene encoding dihydrolipoyl transacylase (E2) component of human branched chain alpha-keto acid dehydrogenase complex and characterization of an E2 pseudogene. *J. Biol. Chem.* **267,** 24090–6 (1992).

37. Mitsubuchi, H., Nobukuni, Y., Endo, F. & Matsuda, I. Structural organization and chromosomal localization of the gene for the E1 beta subunit of human branched chain alpha-keto acid dehydrogenase. *J. Biol. Chem.* **266,** 14686–91 (1991).

38. Chuang, J., Wynn, R., Moss, C., Song, J.-l., Li, J., Awad, N., Mandel, H. & Chuang, D. Structural and Biochemical Basis for Novel Mutations in Homozygous Israeli Maple Syrup Urine Disease Patients A PROPOSED MECHANISM FOR THE THIAMIN-RESPONSIVE PHENOTYPE. *J Biol Chem* **279,** 17792–17800 (2004).

39. Indo, Y., Akaboshi, I., Nobukuni, Y., Endo, F. & Matsuda, I. Maple syrup urine disease: a possible biochemical basis for the clinical heterogeneity. *Hum Genet* **80,** 6–10 (1988).

40. Robinson, B., Taylor, J. & Sherwood, W. Deficiency of dihydrolipoyl dehydrogenase (a component of the pyruvate and alpha-ketoglutarate dehydrogenase complexes): a cause of congenital chronic lactic acidosis in infancy. *Pediatr. Res.* **11,** 1198–202 (1977).

41. Wallace, M., Green, C., Roberts, L., Lee, Y., Justin, M., Joan, S., Meurs, N., Gengatharan, J., Hover, J., Phillips, S., Ciaraldi, T., Guertin, D., Cabrales, P., Ayres, J., Nomura, D., Loomba, R. & Metallo, C. Enzyme promiscuity drives branched-chain fatty acid synthesis in adipose tissues. *Nat Chem Biol* **14,** 1021 (2018).

42. Green, H. & Kehinde, O. An established preadipose cell line and its differentiation in culture II. Factors affecting the adipose conversion. *Cell* **5,** 19–27 (1975).

43. Morrison, S. & Sean, M. 3T3-L1 adipocytes display phenotypic characteristics of multiple adipocyte lineages. *Adipocyte* **4,** 295–302 (2015).

44. Roberts, L. D., Virtue, S., Antonio, V., Nicholls, A. W. & Griffin, J. L. Metabolic phenotyping of a model of adipocyte differentiation. *Physiol. Genomics* **39,** 109–19 (2009).

45. Lackey, D. E., Lynch, C. J., Olson, K. C., Mostaedi, R., Ali, M., Smith, W. H., Karpe, F., Humphreys, S., Bedinger, D. H., Dunn, T. N., Thomas, A. P., Oort, P. J., Kieffer, D. A., Amin, R., Bettaieb, A., Haj, F. G., Permana, P., Anthony, T. G. & Adams, S. H. Regulation of adipose branched-chain amino acid catabolism enzyme expression and cross-adipose amino acid flux in human obesity. *Am. J. Physiol. Endocrinol. Metab.* **304,** E1175–87 (2013).

46. Herman, M. A., She, P., Peroni, O. D., Lynch, C. J. & Kahn, B. B. Adipose tissue branched chain amino acid (BCAA) metabolism modulates circulating BCAA levels. *J. Biol. Chem.* **285,** 11348–56 (2010).

47. Zimmerman, H., Olson, K., Chen, G. & Lynch, C. Adipose transplant for inborn errors of branched chain amino acid metabolism in mice. *Mol. Genet. Metab.* **109,** 345–53 (2013).

48. Green, C. R., Wallace, M., Divakaruni, A. S., Phillips, S. A., Murphy, A. N., Ciaraldi, T. P. & Metallo, C. M. Branched-chain amino acid catabolism fuels adipocyte differentiation and lipogenesis. *Nat. Chem. Biol.* **12,** 15–21 (2016).

49. Mercier, R., Patricia, D. & Errington, J. Crucial Role for Membrane Fluidity in Proliferation of Primitive Cells. *Cell Reports* **1,** 417–423 (2012).

50. Kniazeva, M., Zhu, H., Sewell, A. & Han, M. A Lipid-TORC1 Pathway Promotes Neuronal Development and Foraging Behavior under Both Fed and Fasted Conditions in C. elegans. *Dev Cell* **33,** 260–271 (2015).

51. Kniazeva, M., Crawford, Q. T., Seiber, M., Wang, C.-Y. & Han, M. Monomethyl Branched-Chain Fatty Acids Play an Essential Role in Caenorhabditis elegans Development. *PLOS Biology* **2.** https://doi.org/10.1371/journal.pbio.0020257 (Aug. 2004).

52. Mika, A., Stepnowski, P., Kaska, L., Proczko, M., Wisniewski, P., Sledzinski, M. & Sledzinski, T. A comprehensive study of serum odd- and branched-chain fatty acids in patients with excess weight. *Obesity* **24,** 1669–1676 (2016).

53. Su, X., Magkos, F., Zhou, D., Eagon, J., Fabbrini, E., Okunade, A. & Klein, S. Adipose tissue monomethyl branched-chain fatty acids and insulin sensitivity: Effects of obesity and weight loss. *Obesity (Silver Spring)* (2014).

54. Pakiet, A., Wilczynski, M., Rostkowska, O., Korczynska, J., Jabfffdfffdonska, P., Kaska, L., Monika, P., Sobczak, E., Stepnowski, P., Magkos, F., Sledzinski, T. & Mika, A. The Effect of One Anastomosis Gastric Bypass on Branched-Chain Fatty Acid and Branched-Chain Amino Acid Metabolism in Subjects with Morbid Obesity. *Obes Surg,* 1–9 (2019).

55. Verhoeven, N., Wanders, R., B., P., Saudubray, J. & Jakobs, C. The metabolism of phytanic acid and pristanic acid in man: A review. *J Inherit Metab Dis* **21,** 697–728 (1998).

56. Lodhi, I. J. & Semenkovich, C. F. Peroxisomes: a nexus for lipid metabolism and cellular signaling. *Cell Metab.* **19,** 380–92 (2014).

57. Wanders, R., Waterham, H. & Ferdinandusse, S. Metabolic Interplay between Peroxisomes and Other Subcellular Organelles Including Mitochondria and the Endoplasmic Reticulum. *Frontiers Cell Dev Biology* **3,** 83 (2016).

58. Gaschler, M. & Stockwell, B. Lipid peroxidation in cell death. *Biochem Bioph Res Co* **482,** 419–425 (2017).

59. Duarte, J., Carvalho, F., Pearson, M., Horton, J., Browning, J., Jones, J. & Burgess, S. A high-fat diet suppresses de novo lipogenesis and desaturation but not elongation and triglyceride synthesis in mice. *J Lipid Res* **55,** 2541–2553 (2014).

60. Nadler, S., Stoehr, J., Schueler, K., Tanimoto, G., Yandell, B. & Attie, A. The expression of adipogenic genes is decreased in obesity and diabetes mellitus. *Proc National Acad Sci* **97,** 11371–11376 (2000).

61. Eissing, L., Scherer, T., Tödter, K., Knippschild, U., Greve, J., Buurman, W., Pinnschmidt, H., Rensen, S., Wolf, A., Bartelt, A., Heeren, J., Buettner, C. & Scheja, L. De novo lipogenesis in human fat and liver is linked to ChREBP-β and metabolic health. *Nat Commun* **4,** 1528 (2013).

62. Hellerstein, M., Neese, R. & Schwarz, J. Model for measuring absolute rates of hepatic de novo lipogenesis and reesterification of free fatty acids. *Am. J. Physiol.* **265,** E814–20 (1993).

63. Neinast, M., Jang, C., Hui, S., Murashige, D., Chu, Q., Morscher, R., Li, X., Zhan, L., White, E., Anthony, T., Rabinowitz, J. & Arany, Z. Quantitative Analysis of the Whole-Body Metabolic Fate of Branched-Chain Amino Acids. *Cell Metab* (2018).

64. Laferrère, B., Reilly, D., Arias, S., Swerdlow, N., Gorroochurn, P., Bawa, B., Bose, M., Teixeira, J., Stevens, R. D., Wenner, B. R., Bain, J. R., Muehlbauer, M. J., Haqq, A., Lien, L., Shah, S. H., Svetkey, L. P. & Newgard, C. B. Differential metabolic impact of gastric bypass surgery versus dietary intervention in obese diabetic subjects despite identical weight loss. *Sci Transl Med* **3,** 80re2 (2011).

65. Jang, C., Oh, S. F., Wada, S., Rowe, G. C., Liu, L., Chan, M., Rhee, J., Hoshino, A., Kim, B., Ibrahim, A., Baca, L. G., Kim, E., Ghosh, C. C., Parikh, S. M., Jiang, A., Chu, Q., Forman, D. E., Lecker, S. H., Krishnaiah, S., Rabinowitz, J. D., Weljie, A. M., Baur, J. A., Kasper, D. L. & Arany, Z. A branched-chain amino acid metabolite drives vascular fatty acid transport and causes insulin resistance. *Nat. Med.* **22,** 421–426 (2016).

66. Marshall, D. & Powers, R. Beyond the paradigm: Combining mass spectrometry and nuclear magnetic resonance for metabolomics. *Prog Nucl Mag Res Sp* **100,** 1–16 (2017).

67. Johnson, C., Ivanisevic, J. & Siuzdak, G. Metabolomics: beyond biomarkers and towards mechanisms. *Nat Rev Mol Cell Bio* **17,** 451–459 (2016).

68. Newgard, C. Metabolomics and Metabolic Diseases: Where Do We Stand? *Cell Metab* **25,** 43–56 (2017).

69. Tautenhahn, R., Patti, G., Rinehart, D. & Siuzdak, G. XCMS Online: A Web-Based Platform to Process Untargeted Metabolomic Data. *Anal Chem* **84,** 5035–5039 (2012).

70. Fahy, E., Sud, M., Cotter, D. & Subramaniam, S. LIPID MAPS online tools for lipid research. *Nucleic Acids Res* **35,** W606–W612 (2007).

71. Wishart, D., Tzur, D., Knox, C., Eisner, R., Guo, A., Young, N., Cheng, D., Jewell, K., Arndt, D., Sawhney, S., Fung, C., Nikolai, L., Lewis, M., Coutouly, M., Forsythe, I., Tang, P., Shrivastava, S., Jeroncic, K., Stothard, P., Amegbey, G., Block, D., Hau, D., Wagner, J., Miniaci, J., Clements, M., Gebremedhin, M., Guo, N., Zhang, Y., Duggan, G., Glen, M., Weljie, A., Dowlatabadi, R., Bamforth, F., Clive, D., Greiner, R., Li, L., Marrie, T., Sykes, B., Vogel, H. & Querengesser, L. HMDB: the Human Metabolome Database. *Nucleic Acids Res* **35,** D521–D526 (2007).

72. Buescher, J., Antoniewicz, M., Boros, L., Burgess, S., Brunengraber, H., Clish, C., Ralph, D., Feron, O., Frezza, C., Ghesquiere, B., Gottlieb, E., Hiller, K., Jones, R., Kamphorst, J., Kibbey, R., Kimmelman, A., Locasale, J., Lunt, S., Maddocks, O., Malloy, C., Metallo, C., Meuillet, E., Munger, J., Nöh, K., Rabinowitz, J., Ralser, M., Sauer, U., Stephanopoulos, G., Julie, S., Tennant, D., Wittmann, C., Heiden, M., Vazquez, A., Vousden, K., Young, J., Zamboni, N. & Fendt, S. A roadmap for interpreting 13C metabolite labeling patterns from cells. *Curr Opin Biotech* **34,** 189–201 (2015).

73. Crown, S., Ahn, W. & Antoniewicz, M. Rational design of 13C-labeling experiments for metabolic flux analysis in mammalian cells. *Bmc Syst Biol* **6,** 43 (2012).

74. Metallo, C., Walther, J. & Stephanopoulos, G. Evaluation of 13C isotopic tracers for metabolic flux analysis in mammalian cells. *J Biotechnol* **144,** 167–174 (2009).

75. Young, J. D. INCA: a computational platform for isotopically non-stationary metabolic flux analysis. *Bioinformatics* (2014).

76. Kharroubi, A., Masterson, T., Aldaghlas, T., Kennedy, K. & Kelleher, J. Isotopomer spectral analysis of triglyceride fatty acid synthesis in 3T3-L1 cells. *Am. J. Physiol.* **263,** E667–75 (1992).

77. Collins, J., Neville, M., Pinnick, K., Hodson, L., Ruyter, B., Dijk, T., Reijngoud, D., Fielding, M. & Frayn, K. De novo lipogenesis in the differentiating human adipocyte can provide all fatty acids necessary for maturation. *J Lipid Res* **52,** 1683–1692 (2011).

78. Strawford, A., Antelo, F., Christiansen, M. & Hellerstein, M. Adipose tissue triglyceride turnover, de novo lipogenesis, and cell proliferation in humans measured with 2H2O. *AJP: Endocrinology and Metabolism* **286,** E577–E588 (2004).

79. Long, C. & Antoniewicz, M. High-resolution 13C metabolic flux analysis. *Nat Protoc* **14,** 2856–2877 (2019).

80. Sauer, U. High-throughput phenomics: experimental methods for mapping fluxomes. *Curr Opin Biotech* **15,** 58–63 (2004).

81. Benjamin, D., Cozzo, A., Ji, X., Roberts, L., Louie, S., Mulvihill, M., Luo, K. & Nomura, D. Ether lipid generating enzyme AGPS alters the balance of structural and signaling lipids to fuel cancer pathogenicity. *Proc National Acad Sci* **110,** 14912–14917 (2013).

82. Bielawski, J., Pierce, J. S., Snider, J., Rembiesa, B., Szulc, Z. M. & Bielawska, A. in *Lipidomics: Volume 1: Methods and Protocols* (ed Armstrong, D.) 443–467 (Humana Press, Totowa, NJ, 2009).

83. Mitsubuchi, H., Owada, M. & Endo, F. Markers associated with inborn errors of metabolism of branched-chain amino acids and their relevance to upper levels of intake in healthy

people: an implication from clinical and molecular investigations on maple syrup urine disease. *J Nutrition* **135,** 1565S–70S (2005).

84. Andresen, B., Christensen, E., Corydon, T., Bross, P., Pilgaard, B., Wanders, R., Ruiter, J., Simonsen, H., Winter, V., Knudsen, I., Schroeder, L., Gregersen, N. & Skovby, F. Isolated 2-methylbutyrylglycinuria caused by short/branched-chain acyl-CoA dehydrogenase deficiency: identification of a new enzyme defect, resolution of its molecular basis, and evidence for distinct acyl-CoA dehydrogenases in isoleucine and valine metabolism. *Am. J. Hum. Genet.* **67,** 1095–103 (2000).

85. Koeberl, D. D., Young, S. P., Gregersen, N., Vockley, J., Smith, W. E., Benjamin Jr., D. K., An, Y., Weavil, S. D., Chaing, S. H., Bali, D., McDonald, M. T., Kishnani, P. S., Chen, Y.-T. & Millington, D. S. Rare Disorders of Metabolism with Elevated Butyryl- and Isobutyryl-Carnitine Detected by Tandem Mass Spectrometry Newborn Screening. *Pediatr Res* **54,** 219–223 (2003).

86. Burrage, L., Nagamani, S., Campeau, P. & Lee, B. Branched-chain amino acid metabolism: from rare Mendelian diseases to more common disorders. *Hum Mol Genet* **23,** R1–R8 (2014).

Chapter 2

Branched-chain amino acid catabolism fuels adipocyte differentiation and lipogenesis

2.1 Abstract

Adipose tissue plays important roles in regulating carbohydrate and lipid homeostasis, but less is known about the regulation of amino acid metabolism in adipocytes. Here we applied isotope tracing to pre-adipocytes and differentiated adipocytes to quantify the contributions of different substrates to tricarboxylic acid (TCA) metabolism and lipogenesis. In contrast to proliferating cells, which use glucose and glutamine for acetyl-coenzyme A (AcCoA) generation, differentiated adipocytes showed increased branched-chain amino acid (BCAA) catabolic flux such that leucine and isoleucine from medium and/or from protein catabolism accounted for as much as 30% of lipogenic AcCoA pools. Medium cobalamin deficiency caused methylmalonic acid accumulation and odd-chain fatty acid synthesis. Vitamin B12 supplementation reduced these metabolites and altered the balance of substrates entering mitochondria. Finally, inhibition

of BCAA catabolism compromised adipogenesis. These results quantitatively highlight the contribution of BCAAs to adipocyte metabolism and suggest that BCAA catabolism has a functional role in adipocyte differentiation.

2.2 Introduction

Adipose tissue has a major role in glucose and lipid homeostasis via the storage of excess nutrients in lipid droplets and the release of bioenergetic substrates through lipolysis. Adipocytes, the major cellular constituent of adipose tissue, execute important regulatory functions through endocrine and paracrine signaling[1]. For example, the synthesis and release of lipids and adipokines influence fatty acid metabolism in the liver, appetite, inflammation and insulin sensitivity[2–4]. Dysfunction in these pathways can contribute to insulin resistance[5]. Beyond these signaling functions, the increased adiposity associated with obesity and type 2 diabetes mellitus (T2DM) highlights the need to better understand metabolic regulation and activity in adipocytes.

Insulin stimulates glucose utilization and *de novo* lipogenesis (DNL) in the liver and adipose tissue, and glucose and fatty acids are considered the primary carbon sources fueling anaplerosis and AcCoA generation in these sites[6]. Beyond carbohydrates and fat, both essential and nonessential amino acids also contribute significantly to AcCoA metabolism in cells. The branched-chain amino acids (BCAAs) leucine, isoleucine, and valine are important ketogenic and/or anaplerotic substrates in a number of tissues[7, 8]. In fact, clinical metabolomics studies have recently suggested that plasma levels of BCAAs, their downstream catabolites (such as acylcarnitines) and other essential amino acids become elevated in the context of insulin resistance[9–11]. However, the mechanisms leading to these changes and their ultimate consequences in the context of metabolic syndrome are not fully understood.

Several past studies provide evidence that adipose tissue plays a role in BCAA homeostasis,

though the quantitative contribution of these amino acids to TCA metabolism relative to those of other nutrients is not well defined. Enzyme activity, substrate oxidation and systems-based profiling of 3T3-L1 metabolism suggest that BCAA consumption increases precipitously during differentiation to adipocytes[12–14]. In addition, the transcription of BCAA catabolic enzymes increases significantly during 3T3-L1 differentiation[15]. Whereas genetic modulation of Bcat2 in mice alters circulating BCAA levels, transplantation of wild-type adipose tissue to *Bcat2*$^{-/-}$ mice normalizes plasma BCAAs[16–18]. Finally, treatment of human subjects and animals with thiazolidinediones (TZDs), clinically used activators of peroxisome proliferator-activated receptor-γ (PPARγ), increases the transcription of BCAA catabolic genes in adipose tissue[19, 20], suggesting that this metabolic activity may have beneficial effects in the context of T2DM.

To date, the extent to which oxidation of BCAAs, relative to other substrates, contributes to anaplerosis and DNL has not been quantitatively determined in adipocytes. Here we employed ^{13}C-labeled isotope tracers, mass spectrometry and isotopomer spectral analysis (ISA) to quantify BCAA utilization in proliferating pre-adipocytes and differentiated adipocytes. Whereas proliferating pre-adipocytes did not appreciably catabolize these substrates, BCAAs accounted for as much as one-third of the mitochondrial AcCoA in terminally differentiated 3T3-L1 adipocytes as well as in adipocytes isolated from human subcutaneous and visceral adipose tissues. Furthermore, inadequate cobalamin availability in 3T3-L1 cultures perturbed BCAA and fatty acid metabolism and led to the non-physiological accumulation of methylmalonate (MMA) and synthesis of odd-chain fatty acids (OCFAs). Finally, inhibition of BCAA catabolism negatively influenced 3T3-L1 adipogenesis. These results highlight the complex interplay between cellular differentiation and metabolic pathway flux in adipocyte biology.

2.3 Materials and Methods

2.3.1 Cell culture and reagents

All reagents were purchased form Sigma-Aldrich unless otherwise noted. All media and sera were purchased from Life Technologies unless otherwise stated. Murine 3T3-L1 pre-adipocytes were purchased from the American Type Culture Collection and cultured in high glucose Dulbecco's modified Eagle medium (DMEM) (Life Technologies) supplemented with 10% bovine calf serum (BCS) below 70% confluence. Cells were regularly screened for mycoplasma contamination. For differentiation, 10,000 cells/well were seeded into 12-well plates (ThermoFisher) and allowed to reach confluence (termed Day -2). On Day 0 differentiation was induced with 0.5 mM 3-isobutyl-1-methylxanthine (IBMX), 0.25 μM dexamethasone, 1 μg/ml insulin, and 100 nM rosiglitazone in DMEM containing 10% FBS (FBS). Medium was changed on Day 2 to DMEM + 10% FBS with 1 μg/ml insulin. Day 4, and thereafter DMEM + 10% FBS was used. Cobalamin (500 nM) or 5'-adenosylcobalamin (AdoCbl; 100 nM) were supplemented to cultures when noted.

2.3.2 Human subjects

Weight stable obese subjects undergoing elective laparoscopic gastric bypass via Roux-en-Y for the treatment of obesity were recruited for the study to provide material for pre-adipocyte isolation. The Institutional Review Boards of Scripps Memorial Hospital and the University of California, San Diego, approved the studies. All subjects gave informed consent.

2.3.3 Adipose tissue (AT) biopsy

Subcutaneous (S) AT biopsies were obtained from the superficial abdominal SAT depot and visceral (V) AT was obtained from the greater omentum[21]. Biopsy tissue was placed in a

sterile HEPES salts solution as previously described[22] and transported to the lab for immediate processing.

2.3.4 Human pre-adipocyte isolation

All procedures for AT explant culture were carried out using sterile techniques. Fresh SAT was minced and placed into a 4% BSA/HEPES salts buffer containing 333 units collagenase (Worthington Biochemical Corp.) per mL buffer (about 1,000 units per gram of AT) and incubated for 1 hour in a 37°C shaking water bath. Following digestion, the suspension was filtered through a 450 μm nylon mesh (Component Supply Company) and centrifuged at 50g for 10 min at 25°C. The pellet and infranatant containing the SVF was aspirated and centrifuged through 250 μm nylon mesh, then centrifuged at 800g for 10 min at 20°C. Further pre-adipocyte isolation and culture was performed as previously described[23].

2.3.5 Human adipocyte differentiation

Human pre-adipocytes were maintained in DMEM/F12 + 10% FBS. At Day 0 (2 days after confluence was reached), cells were differentiated in DMEM/F12 + 3% FBS, 0.5 mM IBMX, 100 nM insulin, 100 nM dexamethasone, 2 nM T3, 10 μg/ml transferrin, 1 μM rosiglitazone, 33 μM biotin and 17 μM pantothenic acid[24] induction cocktail for 7 days with medium changes every 2 days. After induction, cells were maintained in DMEM/F12 with 10 nM insulin and 10 nM dexamethasone until metabolic tracing experiments were conducted on Day 14.

2.3.6 Extracellular flux measurements

A Yellow Springs Instruments (YSI) 2950 was used to obtain extracellular flux measurements. Briefly, spent media was centrifuged at 300g for 5 min to remove cell debris. Culture medium supernatants were centrifuged at 21,000g for 15 min to remove impurities and analyzed

for glucose, lactate, glutamine and glutamate measurements. Amino acid uptake and secretion was calculated using GC-MS derivatization of fresh and spent media with internal labeled standards for quantification.

2.3.7 Respirometry

Respirometry was conducted using a Seahorse XF96 Analyzer. For respiration in intact cells, cells were plated at 5 x 10^3 cells/well and maintained and differentiated as described above. 10 days after differentiation was initiated, growth medium was replaced with unbuffered DMEM (Sigma #5030) supplemented with 8 mM glucose, 3 mM glutamine, 1 mM pyruvate and 0.5 mM carnitine. Mitochondrial respiration is calculated as the oxygen consumption rate sensitive to 1 μM rotenone and 2 μM antimycin A. Immediately after the experiment, rates were normalized for cell number using CyQuant (Life Technologies) and scaled appropriately.

For respiration in permeabilized cells, cells were seeded onto XF96 plates at 1 x 10^4 cells/well and were maintained and differentiated as described above. Measurements of differentiated cells were conducted 10-14 days after differentiation was initiated. Respiration was initially measured in MAS medium supplemented with 0.2% (w/v) BSA, 4 mM ADP and 3 nM recombinant Perfringolysin O (purchased as XF Plasma Membrane Permeabilizer, Seahorse Bioscience)[25] and sequentially offered 2 μg/ml oligomycin, successive additions of 2 μM FCCP, and 2 μM antimycin A. Permeabilized adipocytes were offered 5 mM branched chain ketoacids with 0.5 mM malate (except KIV, for which only FADH2-linked respiration was measured) and concentrations for commonly used respiratory substrates are as described previously[26]. Uncoupler-stimulated respiration was calculated as the difference between the maximum respiratory rate in response to FCCP that was sensitive to antimycin A. All data were normalized to total cell protein as measured by the bicinchoninic acid assay (Pierce) with matched plates of whole cells.

2.3.8 Imaging

A 0.35% (w/v) Oil Red O stock was prepared in isopropanol and filtered through a 0.22 μm filter. Cells were washed with PBS, fixed with 4% paraformaldehyde for 30 min at room temperature, washed 2x in milli-Q water, washed once with 60% isopropanol, and finally stained with 3:2 (stock:water) solution for 30 min. Stain solution was removed from cells and cells were washed 4x with milli-Q water.

2.3.9 Isotopomer Spectral Analysis

Mass isotopomer distributions were determined by integrating metabolite ion fragments[4] summarized in Supplementary Table 3 and corrected for natural abundance using in-house algorithms. ISA analysis was conducted using INCA[27] and a more complete model for fatty acid synthesis that accounted for production of myristate, palmitate, oleate and stearate (Supplementary Table 1).

2.3.10 Tracing experiments

All [^{13}C] glucose and amino acid tracers were purchased from Cambridge Isotopes Inc. Stable isotope labeling of intracellular metabolites in differentiated 3T3-L1 cells was accomplished by culturing cells 7 days post-induction in tracer medium for 24 h unless otherwise stated. Proliferating 3T3-L1, A549, HuH-7 and 143B cells were seeded at 10,000 cells/cm^2 and cultured in tracer medium for 48 h. Custom DMEM or DMEM/F12 (Hyclone Laboratories, Inc.) was formulated with the specified tracer, unlabeled versions of other chemical components, and 10% dialyzed FBS such that all nutrients were available to cells in all experiments (with one or more labeled). Complete formulation of DMEM and Low gluc+AA media can be found in Supplementary Table 3. Mole percent enrichment (MPE) of isotopes was calculated as the percent of all atoms within the metabolite pool that are labeled:

$$\frac{\sum_{i=1}^{n} M_i \cdot i}{n}$$

where n is the number of carbon atoms in the metabolite and M_i is the relative abundance of the i^{th} mass isotopomer.

2.3.11 Gas chromatography/mass spectrometry (GC/MS) analysis

Polar metabolites and fatty acids were extracted using methanol/water/chloroform and analyzed as previously described[28]. Proliferating 3T3-L1 cells and primary human adipocytes were cultured in 6-well plates, while differentiated 3T3-L1 cells were cultured in 12-well plates and the volumes of extraction buffers were adjusted accordingly. Polar metabolites were derivatized in 20 μl of 2% (w/v) methoxyamine hydrochloride (Thermo Scientific) in pyridine and incubated at 37°C for 60-90 min. Samples were then silylated with 30 μl of N-tert-butyldimethylsilyl-N-methyltrifluoroacetamide (MTBSTFA) with 1% tert-butyldimethylchlorosilane (tBDMS) (Regis Technologies) at 37°C for 30-45 min. Samples were centrifuged at 21,000g for 5 min and supernatant was transferred to GC sample vials for analysis. Extracted nonpolar metabolites were evaporated, saponified and esterified to form fatty acid methyl esters (FAMEs) through addition of 500 μl 2% (v/v) H_2SO_4 in methanol and incubation at 50°C for 90-120 min. FAMEs were extracted after addition of 100 μl saturated NaCl solution with two 500 μl hexane washes and evaporated to dryness before redissolving in 50-100 μl of hexane and transfer to glass GC vials for analysis. Derivatized samples were analyzed by GC-MS using a DB-35MS column (30 m x 0.25 mm i.d. x 0.25 μm, Agilent J&W Scientific) installed in an Agilent 7890A gas chromatograph (GC) interfaced with an Agilent 5975C mass spectrometer (MS).

For quantitation of amino acids in plasma samples, an isotope-labeled internal standard mixture was prepared and added during extraction.

2.3.12 Lentiviral production and shRNA KD of *Bckdha*

Glycerol stocks of TRC2-pLKO.1-puro shRNA targeting mouse *Bckdha* (KD1: NM_007533.2-421s1c1: CCGGTCCTTCTACATGACCAACTATCTCGAGATAGTTGGTCATGTAGAAGGATTTTTG; KD2: NM_007533.2-1188s1c1: CCGGGCAGTCACGAAAGAAGGTCATCTCGAGATGACCTTCTTTCGTGACTGCTTTTTG), and a non-targeting control

fection agent Fugene 6 and required packaging plasmids VSV-G, gag/pol, and rev. HEK293T medium containing lentiviral constructs was collected two days later and filtered (0.45 μm). Polybrene was added to a final concentration of 6 μg/ml. 3T3-L1 pre-adipocytes were infected with 0.5 ml of virus-containing medium in a 6-well plate for 4 h before addition of 2 ml of virus-free medium. After 24 h of recovery, transduced cells were selected with 2 μg/ml puromycin. Cells were then plated to 12-well plates for differentiation as described above but without rosiglitazone. Puromycin was removed from the medium beginning on Day 0.

2.3.13 RNA isolation and quantitative RT-PCR

Total RNA was purified from cultured cells using Trizol Reagent (Life Technologies) per manufacturer's instructions. First-strand cDNA was synthesized from 1 μg of total RNA using iScript Reverse Transcription Supermix for RT-PCR (Bio-Rad Laboratories) according to the manufacturer's instructions. Individual 20 μl SYBR Green real-time PCR reactions consisted of 2 μl of diluted cDNA, 10 μl of SYBR Green Supermix (Bio-Rad), and 1 μl of each 5 μM forward and reverse primers. For standardization of quantification, 18S was amplified simultaneously. The PCR was carried out on 96-well plates on a CFX Connect Real time System (Bio-Rad), using a three-stage program provided by the manufacturer: 95°C for 3 min, 40 cycles of 95°C for 10 s and 60°C for 30 s. Gene-specific primers used are listed in Supplementary Table 4.

2.3.14 Western blots

3T3-L1 adipocytes with Control KD or *Bckdha* KD were lysed in ice-cold RIPA buffer with 1x protease inhibitor (Sigma-Aldrich. 30 μg of total protein was separated on 12% SDS-PAGE gel. The proteins were transferred to a nitrocellulose membrane and immunoblotted with rabbit anti-Bckdha (Novus Biologicals NBP1-79616) (1:1,000 dilution) and mouse anti-Beta-Actin (Cell Signaling 8H10D10) (1:5,000). Specific signal was detected with horseradish peroxidase-conjugated secondary antibody goat anti-rabbit (1:2,500) or rabbit anti-mouse (1:10,000) using SuperSignal West Pico Chemiluminescent Substrate (Thermo Scientific) and developed using Blue Devil Autoradiography film (Genesee Scientific).

2.3.15 Statistical analyses

Results shown as averages of technical replicates are presented as mean $\pm$ s.d. and are representative two or more independent experiments (biological replicates). Biological replicates are defined as separate experiments temporally; technical replicates are defined as separate spatial replicates (i.e., wells of a tissue culture plate) within an experiment. Respirometry results are averages of multiple independent experiments and presented as mean $\pm$ s.e.m. P values were calculated using Student's two-tailed t test or ANOVA, as required; *, P value between 0.01 and 0.05; **, P value between 0.001 and 0.01; ***, P value $<$0.001. Errors associated with ISA of lipogenesis are 95% confidence intervals determined via confidence interval analysis.

2.4 Results

2.4.1 Adipogenesis reprograms amino acid metabolism

To understand how mitochondrial substrate utilization changes during adipogenesis, we quantified the sources of lipogenic AcCoA before and after differentiation. 3T3-L1 adipocytes dis-

played substantial lipid accumulation 7 d after induction of differentiation (Supplementary Results, Supplementary Fig. 1a). Palmitate (total from saponified nonpolar extracts) in proliferating and differentiated 3T3-L1 cells cultured with [U-$^{13}C_6$]glucose (Supplementary Fig. 1b) had the expected pattern of labeling arising via pyruvate dehydrogenase (PDH)-mediated generation of M2 AcCoA (i.e., AcCoA containing two ^{13}C isotopes). Isotopic enrichment from [U-$^{13}C_5$]glutamine (Supplementary Fig. 1c) was lower than that observed with labeled glucose. ISA was employed to quantify the relative contributions of [U-$^{13}C_6$]glucose and [U-$^{13}C_5$]glutamine to *de novo* palmitate synthesis in 3T3-L1 pre-adipocytes versus adipocytes and compared to results in cancer cell lines of various tissue origins (Fig. 1a). Notably, glucose and glutamine accounted for $\geq$80% of the lipogenic AcCoA in all proliferating cells. In contrast to cells with an active cell cycle, in differentiated cells a substantially greater fraction of lipid carbon arose from substrates other than glucose and glutamine. As expected, absolute lipogenic flux from glucose and glutamine to palmitate increased dramatically after differentiation (Supplementary Fig. 1d).

When normalized to protein levels, glucose uptake, lactate secretion and glutamine uptake were all significantly reduced in differentiated 3T3-L1 cells as compared to those at the pre-adipocyte stage (Fig. 1b). Proliferating 3T3-L1 pre-adipocytes secreted more lactate per mole of glucose taken up - a hallmark of rapidly proliferating cells[29]. Importantly, the use of stable isotope tracers allowed us to measure the percentage of each amino acid pool that was newly synthesized in each cell type. Despite their lack of proliferation, several nonessential amino acids initially present at high levels in the culture medium were synthesized at strikingly high rates in differentiated 3T3-L1 adipocytes, including glutamine, glycine and serine (Fig. 1c), whereas none of the proliferating cells tested synthesized glutamine *de novo*. After 24 h of culture in medium containing 4 mM glutamine, approximately 20% of the pool was newly synthesized, such that glutamine was secreted into the culture medium at a considerable rate (while still being consumed) (Supplementary Fig. 1e), in line with results from studies in adipose tissue[30]. Given that *de novo* synthesis of glutamine and other amino acids was occurring at significant rates

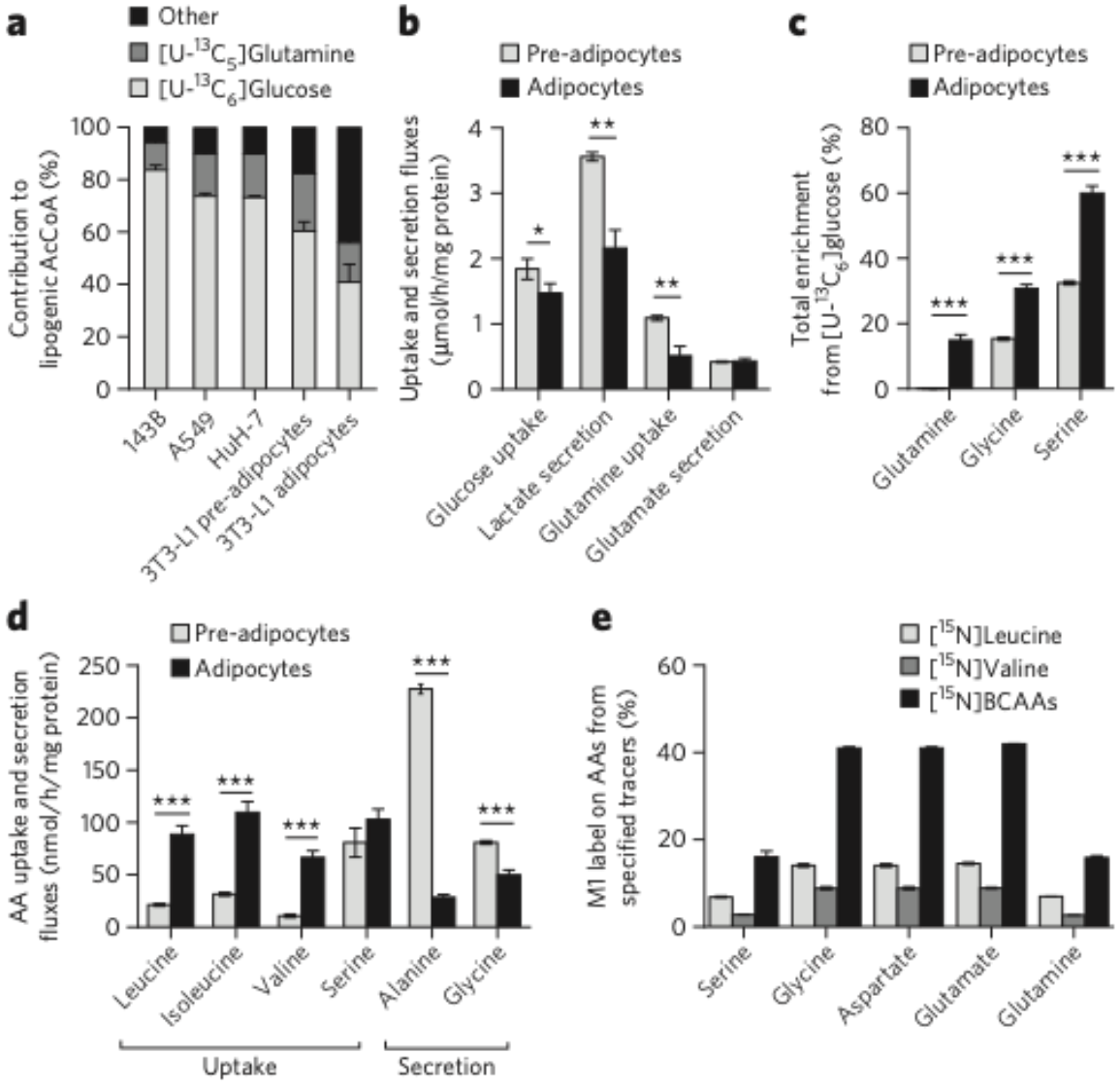

Figure 2.1: **Characterization of metabolic reprogramming during adipocyte differentiation. a**. Contribution of [U-$^{13}C_6$]glucose and [U-$^{13}C_5$]glutamine to lipogenic AcCoA for palmitate synthesis in 143B, A549, HuH-7 cancer cells and 3T3-L1 pre-adipocytes and adipocytes. **b**. Uptake and secretion fluxes in 3T3-L1 pre-adipocytes and adipocytes. **c**. Percentage of intracellular glutamine, serine and glycine pools that were newly synthesized (labeled) from [U-$^{13}C_6$]glucose in 3T3-L1 pre-adipocytes and adipocytes. **d**. Net amino acid uptake and secretion in 3T3-L1 pre-adipocytes and adipocytes. **e**. Percentage of amino acids that contain an M1 label indicating transamination from the indicated [^{15}N]amino acid tracers. Data presented in **a** are model output $\pm$ 95% confidence interval (CI), and those in **b-e** are mean $\pm$ s.d. Data shown in **a-e** are from three technical replicates (separate wells in cell culture) representative of three biological replicates (independent experiments); asterisks represent significant differences between groups by Student's two-tailed t-test: *P < 0.05, **P < 0.01, ***P < 0.001.

in differentiated cells, we hypothesized that consumption of other amino acids increased upon differentiation to provide the necessary nitrogen for these reactions. Indeed, quantitation of amino acid fluxes indicated that BCAA consumption increased dramatically in differentiated 3T3-L1 adipocytes as compared to pre-adipocytes (Fig. 1d), consistent with previous observations[13]. Furthermore, metabolic tracing using ^{15}N-labeled BCAAs indicated that nitrogen from these substrates contributed to amino acid synthesis in differentiated adipocytes (Fig. 1e).

2.4.2 BCAAs fuel TCA metabolism and lipogenesis in adipocytes

To better quantify the extent to which leucine or isoleucine contribute to mitochondrial metabolism and lipogenesis in cultured adipocytes, we applied [U-$^{13}C_6$]leucine or [U-$^{13}C_6$]isoleucine tracers to 3T3-L1 cultures. Figure 2a summarizes the carbon atom transitions associated with BCAA catabolism and resultant labeling in mitochondrial intermediates. For a more detailed map of BCAA catabolism, see Supplementary Figure 2a. Two M2 AcCoA and one M1 AcCoA molecules are produced from [U-$^{13}C_6$]leucine catabolism, and [U-$^{13}C_6$]isoleucine catabolism yields one M2 AcCoA and one M3 propionyl-CoA (PropCoA), which is subsequently converted to succinyl-CoA. AcCoA molecules arising from leucine and isoleucine were readily incorporated into citrate pools in differentiated adipocytes (Fig. 2b). To compare changes before and after differentiation, 3T3-L1 pre-adipocytes and those differentiated for 6-7 d were cultured in the presence of [U-$^{13}C_6$]glucose, [U-$^{13}C_5$]glutamine, [U-$^{13}C_6$]leucine or [U-$^{13}C_6$]isoleucine and the steady-state mole percent enrichment (MPE) in the citrate pool was measured (Fig. 2c and Supplementary Fig. 2b). Although incorporation of carbon atoms from leucine and isoleucine into citrate was barely detectable in pre-adipocytes, their contribution increased considerably upon adipocyte differentiation to 3.3% and 3.0%, respectively (Fig. 2c). Other TCA intermediates showed comparable levels of leucine and isoleucine enrichment (Supplementary Fig. 2c), beginning about 2 d into differentiation (Supplementary Fig. 2d).

We also quantified the relative extent of BCAA catabolism in human pre-adipocytes

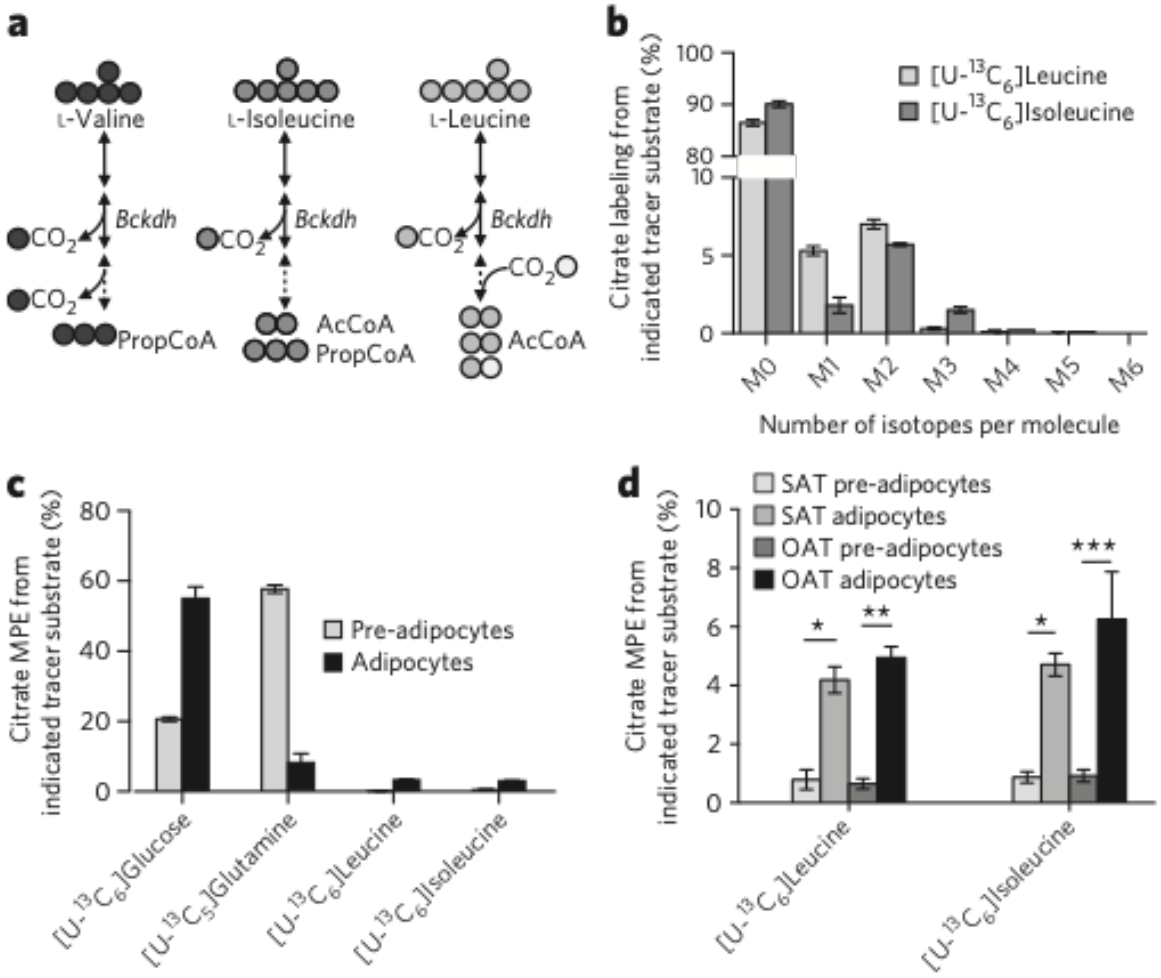

Figure 2.2: **BCAA catabolism is initiated upon adipocyte differentiation. a**. Summary of BCAA catabolism and carbon-atom transitions from each BCAA tracer. Abbreviations: Bckdh, branched-chain ketoacid dehydrogenase; AcCoA, acetyl-CoA; PropCoA, propionyl-CoA. **b**. Citrate labeling in 3T3-L1 adipocytes from [U-$^{13}C_6$]leucine and [U-$^{13}C_6$] isoleucine. **c**. Mole percent enrichment (MPE) of citrate from each tracer substrate in 3T3-L1 pre-adipocytes and adipocytes. **d**. MPE of citrate from [U-$^{13}C_6$]leucine and [U-$^{13}C_6$]isoleucine in primary human pre-adipocytes and adipocytes isolated from subcutaneous (SAT) or omental adipose tissue (OAT) depots. Data in **b-d** are from three technical replicates representative of three biological replicates and represent mean $\pm$ s.d; asterisks represent significant differences between groups by two-way ANOVA: *P < 0.05, **P < 0.01, ***P < 0.001.

isolated from subcutaneous or omental depots to observe whether induction of BCAA catabolism also occurs during human adipogenesis[21, 23, 31]. Trends observed when comparing citrate MPE from both [U-$^{13}C_6$]leucine and [U-$^{13}C_6$]isoleucine in human pre-adipocytes as compared to differentiated adipocytes were similar to those observed in 3T3-L1 cells, suggesting that human adipocytes also metabolize BCAAs at higher rates than human pre-adipocytes (Fig. 2d). In addition to carbon atom enrichment, evidence of the oxidative capacity of these cells for each of the respective branched-chain ketoacids (BCKAs) was obtained via respirometry analysis of permeabilized adipocytes[25, 26]. When comparing uncoupler-stimulated respiration of adipocytes and pre-adipocytes, we observed a marked increase in oxygen consumption from all substrates tested, but a disproportionate increase in the oxidation of the BCAT2 reaction products ketoisocaproate (KIC), ketomethylvalerate (KMV) and ketoisovalerate (KIV) was evident (Fig. 3a). The capacity to oxidize these BCKAs increased by 14- to 25-fold after differentiation, a much greater increase than was observed for other substrates, suggesting that differentiation-induced mitochondrial biogenesis does not entirely explain the increased capacity to oxidize BCKAs (Supplementary Fig. 3a).

In contrast to cultured human adipocytes, 3T3-L1 cells exhibit high levels of DNL, which facilitates quantitation of isotope enrichment in the lipogenic AcCoA pool (Fig. 3b). To determine the relative contributions of [U-$^{13}C_6$]glucose, [U-$^{13}C_5$]glutamine, [U-$^{13}C_6$]leucine and [U-$^{13}C_6$]isoleucine to this metabolic pool, we modified our ISA model to account for partially labeled AcCoA arising from [U-$^{13}C_6$]leucine catabolism (Fig. 2a and Supplementary Table 1). The contributions of both glucose and glutamine to AcCoA decreased significantly upon differentiation (Fig. 3c). On the other hand, leucine and isoleucine contributions increased from undetectable levels in pre-adipocytes to 23% and 9%, respectively, in adipocytes. These results are consistent with the pronounced induction of BCAA oxidation we observed upon adipocyte differentiation. Finally, this metabolic reprogramming toward BCAA utilization dramatically increased 3 d after induction and continued until 6 d after induction (Supplementary Fig. 3b),

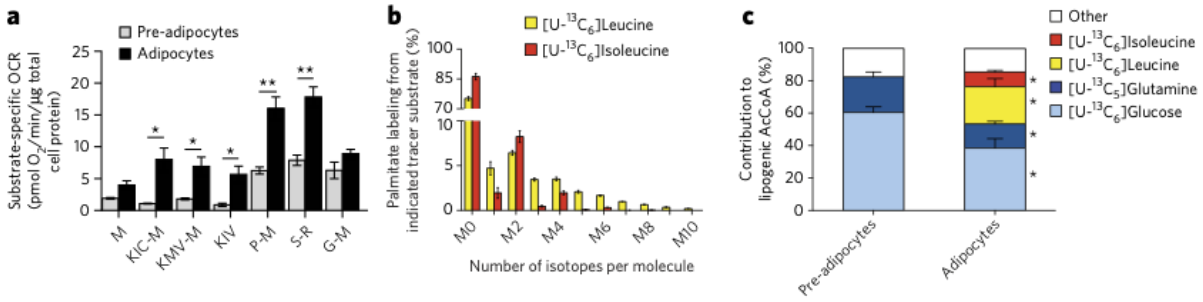

Figure 2.3: **BCAA catabolism fuels mitochondrial metabolism and lipogenesis in adipocytes a**. Substrate-specific oxygen consumption rate (OCR) in permeabilized 3T3-L1 pre-adipocytes and adipocytes. Substrate key: M, malate; KIC-M, ketoisocaproate and malate; KMv-M, ketomethylvalerate and malate; KIv, ketoisovalerate; P-M, pyruvate and malate; S-R, succinate and rotenone; G-M, glutamate and malate. 250 nM AdoCbl and biotin were added to the respirometry medium. **b**. Palmitate labeling in 3T3-L1 adipocytes from [U-$^{13}C_6$]leucine and [U-$^{13}C_6$]isoleucine. Minimal label was detected in palmitate from [U-$^{13}C_5$]valine. **c**. Contribution of each tracer substrate to lipogenic AcCoA in 3T3-L1 pre-adipocytes and adipocytes after correction due to tracer dilution. BCAA contributions were adjusted to account for dilution of intracellular amino acids from protein turnover using the average BCAA labeling over the course of the experiment. Data presented in **a** are mean ± s.e.m., data in **b** are mean ± s.d. and data in **c** are model output ± 95% CI. Data in **a** represent at least five biological replicates each with four technical replicates, while those in **b** and **c** are three technical replicates representative of three biological replicates. *P < 0.05, **P < 0.01 by Student's two-tailed t-test.

coinciding with the accumulation of palmitate and other fatty acids (Supplementary Fig. 3c).

2.4.3 Protein catabolism supports BCAA metabolism

Elevated nutrient concentrations can influence metabolic activity through mass action or the regulation of cell signaling pathways, particularly in the case of glucose and BCAAs[32]. Indeed, BCAA levels in standard adipocyte medium (that is, DMEM) are over four-fold higher than those measured in human and mouse plasma[9]. To test whether the high concentrations of amino acids and glucose in 3T3-L1 cultures influences the extent of BCAA catabolism, we cultured adipocytes in medium with glucose and the full complement of amino acids present at more physiological levels (termed "Low gluc+AA" - for example, 6 mM glucose, 1 mM glutamine and 200 μM for each BCAA; see Supplementary Table 2 for complete formulation). In comparing the metabolism of 3T3-L1 adipocytes in control versus Low gluc+AA media, we observed a significant reduction in glycolysis and amino acid uptake and secretion (Fig. 4a,b). On the other hand, total fatty acid pools and synthesis rates were unchanged (Supplementary Fig. 4a,b). ISA using specific tracers indicated that the contribution of glucose to AcCoA increased, while the relative contribution of BCAAs to fatty acids decreased (Fig. 4c). Notably, the increased glucose contribution could be almost entirely accounted for by increased labeling of glutamine from glucose (Supplementary Fig. 4c). Perhaps more importantly, the decrease in BCAA-derived label in AcCoA pools was strongly affected by dilution from unlabeled protein turnover (the only other source of essential amino acids present): within 24 h, approximately 50% of the intracellular BCAA pool became unlabeled (Fig. 4d). Notably, the final concentrations of each BCAA (25 μM leucine, 40 μM isoleucine and 75 μM valine) were well below those observed in plasma from fasting human subjects[33] (125 μM leucine, 75 μM isoleucine and 200 μM valine), which would strongly induce protein catabolism at the end of culture. However, these data provide evidence that amino acids (BCAAs in particular) from both extracellular sources and protein catabolism are highly utilized by differentiated adipocytes. Though not surprising

given the coordinate regulation of protein synthesis and catabolism[34], the marked dilution of [^{13}C]BCAAs observed here highlights the importance of amino acid recycling in metabolically active cells and tissues.

2.4.4 Medium B12 deficiency affects BCAA and lipid metabolism

Intriguingly, we failed to observe prominent M3 labeling of citrate (Fig. 2b) or other TCA intermediates (data not shown) when culturing differentiated 3T3-L1 cells with [U-$^{13}C_6$]isoleucine, suggesting that PropCoA and methylmalonyl CoA (MMA-CoA) derived from isoleucine did not enter the TCA cycle (Supplementary Fig. 2a). We also failed to detect 13C incorporation in any TCA metabolite from [U-$^{13}C_5$]valine (data not shown). Notably, we measured substantial accumulation of methylmalonic acid (MMA) in differentiated 3T3-L1 cells, which was surprisingly present at intracellular levels similar to those of BCAAs (Supplementary Fig. 5a). Furthermore, high levels of OCFAs accumulated in 3T3-L1 adipocytes but not pre-adipocytes, including C15:0 and C17:0 species (Fig. 5a). These fatty acids have previously been observed in other reports using 3T3-L1 cells, but their origin has remained unclear[35].

Distinct M3 labeling was observed in MMA after 24 h of culture with [U-$^{13}C_6$]isoleucine or [U-$^{13}C_5$]valine (Supplementary Fig. 5b), as expected on the basis of known pathway architecture. Similarly, the C15:0 and C17:0 OCFAs also contained a prominent M3 peak after culture with these BCAA tracers (Fig. 5b and Supplementary Fig. 5c), providing evidence that these fatty acids arose from BCAA-derived DNL rather than via α-oxidation. These data suggest that MMA and PropCoA accumulate in differentiated 3T3-L1 adipocytes, presumably due to defects in BCAA catabolism. MMA accumulates in patients with the genetic disorder methylmalonic aciduria. This phenotype may be caused by mutations in the gene encoding MMA-CoA mutase (MUT) or genes involved in cobalamin metabolism, as the conversion of MMA-CoA to succinyl-CoA requires the coenzyme 5'-deoxyadenosylcobalamin (AdoCbl)[36]. Notably, the human adipocytes analyzed in this study were cultured in DMEM/F12, which contains 500 nM

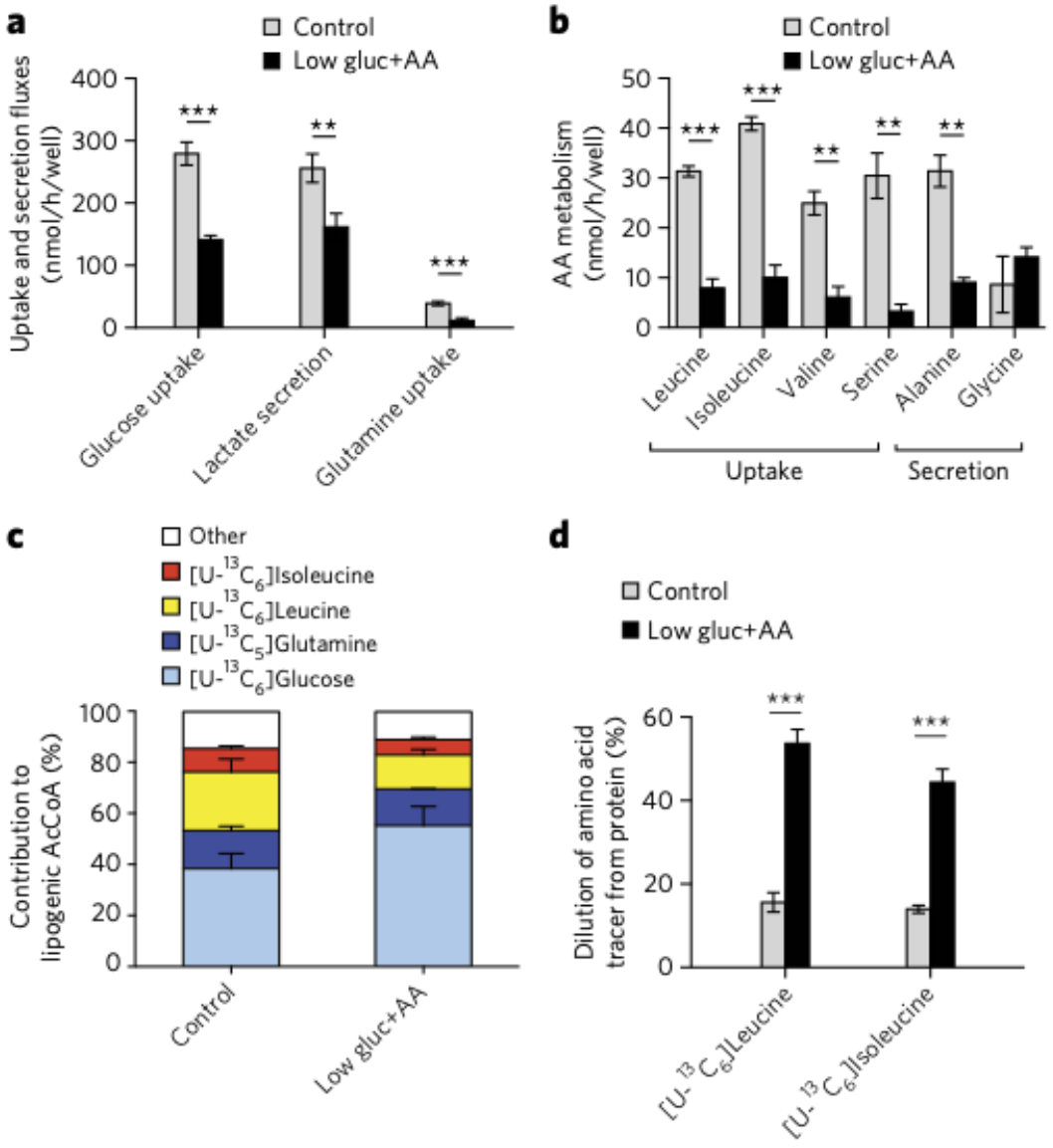

Figure 2.4: **BCAA utilization is supported by protein catabolism. a**. Uptake and secretion fluxes in 3T3-L1 adipocytes cultured in control and low gluc+AA media. **b**. Amino acid uptake and secretion in control and low gluc+AA media. **c**. Contribution of each tracer to lipogenic AcCoA in 3T3-L1 adipocytes cultured in control and low gluc+AA media. BCAA contributions were adjusted to account for dilution of intracellular amino acids from protein turnover using the average BCAA labeling over the course of the experiment. Glutamine dilution occurred primarily via glucose-derived synthesis. **d**. Percentage of pool without label when cultured in indicated tracer substrate in control and low gluc+AA for 24 h. Data presented in **a,b,d** are mean $\pm$ s.d.; data in **c** are model output $\pm$ 95% CI. Data shown in **a-d** are from three technical replicates representative of three biological replicates; $^{**}P < 0.01$, $^{***}P < 0.001$ by Student's two-tailed t-test.

cobalamin, and both OCFAs and MMA were undetectable in these cultures. Because typical 3T3-L1 culture conditions employ DMEM lacking cobalamin, and supplementation with 10% dialyzed or untreated serum might not be sufficient to support this metabolism, we hypothesized that deficiencies in cobalamin availability led to the accumulation of MMA and OCFAs. Indeed, addition of cobalamin to media at levels ranging from 2 nM (the approximate concentration in human plasma) to 500 nM (DMEM/F12) prevented the accumulation of these metabolites (Fig. 5c and Supplementary Fig. 5d). We obtained similar results when we added cobalamin or AdoCbl to 3T3-L1 culture medium (Supplementary Fig. 5e and Fig. 5d). Supplementation of cobalamin influenced the relative abundance of fatty acid species as well as the contribution of BCAAs to TCA metabolism. For example, addition of cobalamin from day 0 to day 7 of differentiation reduced OCFA levels as a percentage of the total intracellular fatty acids, with a concomitant increase occurring in the relative amount of palmitate (Fig. 5e). At the same time, cobalamin supplementation promoted anaplerosis of valine, as evidenced by increased enrichment of fumarate, malate and other TCA intermediates from [U-$^{13}C_5$]valine (Supplementary Fig. 5f-h). Furthermore, 3T3-L1 adipocytes took up more BCAAs, including leucine, when cultured in cobalamin-supplemented medium (Fig. 5f), suggesting that cobalamin deficiency and/or the accumulation of MMA and OCFAs results in broader regulation of the pathway. On the other hand, enrichment from [U-$^{13}C_6$]glucose decreased across all TCA intermediates in 3T3-L1 adipocytes cultured with 500 nM cobalamin (Supplementary Fig. 5i). These data indicate that accumulation of MMA, OCFAs and presumably their precursor, PropCoA, due to inadequate cobalamin availability perturbs BCAA, fatty acid and mitochondrial metabolism in cultured adipocytes.

2.4.5 BCAA metabolism contributes to adipogenesis

Given the high catabolic flux of BCAAs observed in differentiated adipocytes, we next examined whether this pathway plays a functional role in adipogenesis. To address this question,

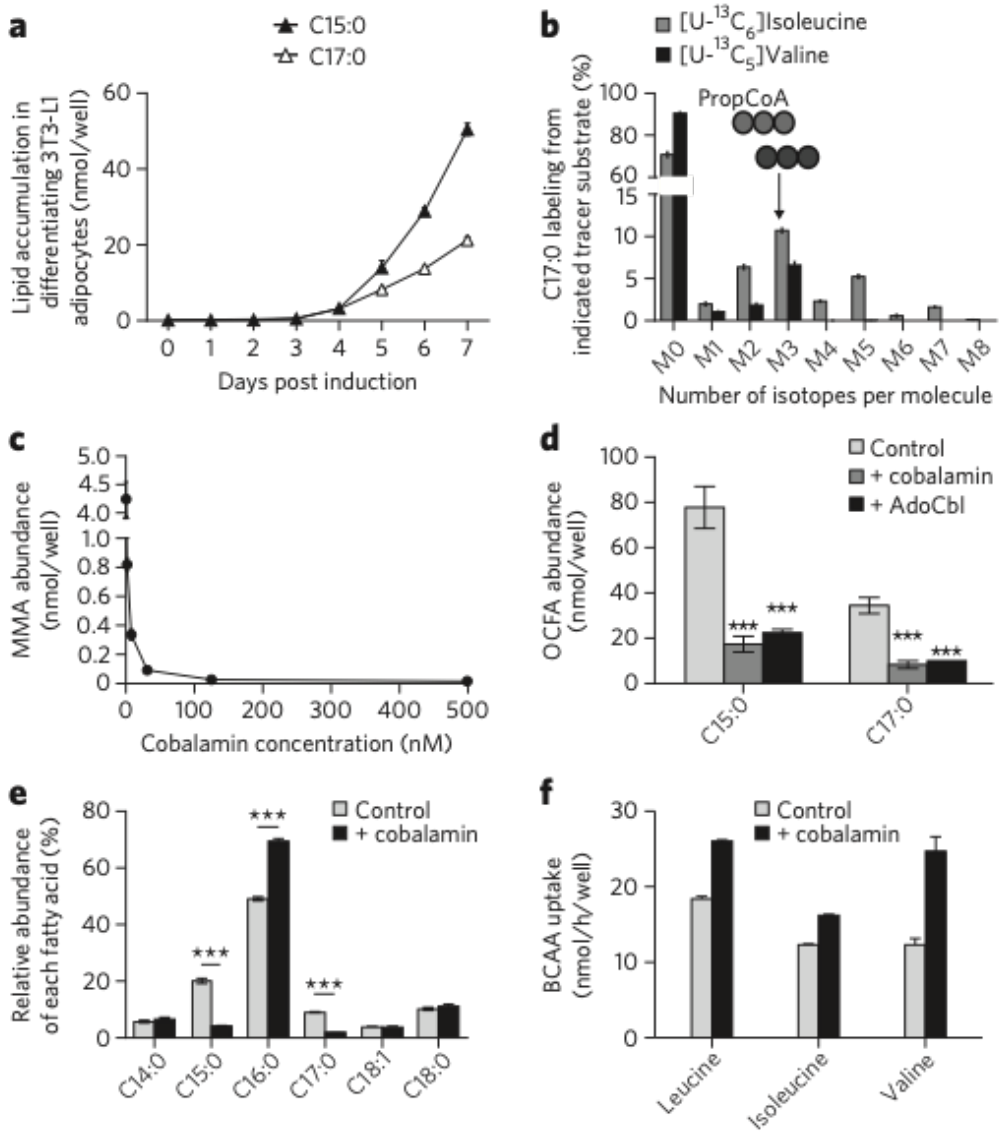

Figure 2.5: **BCAAs contribute to MMA, oCFAs and BCFAs in differentiated 3T3-L1 adipocytes.** **a**. Odd-chain fatty acid (OCFA) accumulation in 3T3-L1 adipocytes 0-7 d after induction. **b**. C17:0 labeling from [U-$^{13}C_6$]isoleucine and [U-$^{13}C_5$]valine in 3T3-L1 adipocytes. **c**. MMA abundance in cells cultured in DMEM +10% FBS and 0, 2, 8, 32, 125 or 500 nM cobalamin beginning on day 0 of differentiation. **d**. OCFA levels in 3T3-L1 adipocytes after culture with 500 nM cobalamin or 100 nM AdoCbl. ***$P < 0.001$ compared to control condition by two-way ANOVA and Holm-Sidak's multiple-comparison test. **e**. Relative abundance of the most abundant fatty acids in control and + cobalamin conditions. ***$P < 0.001$ compared to control condition by Student's two-tailed t-test. **f**. Uptake of BCAAs in control and + cobalamin condition. Data presented in **a-f** are mean $\pm$ s.d. and represent three technical replicates representative of three biological replicates.

we generated polyclonal populations of 3T3-L1 cells that stably express either short hairpin RNAs (shRNAs) targeting *Bckdha* (knockdown (KD) using one of two unique sequences) or nonspecific sequences (control). At confluence these cells were subjected to differentiation in the absence of cobalamin and rosiglitazone and each characterized with respect to their metabolism, morphology and differentiation markers. After differentiation, *Bckdha* KD cells exhibited lower Bckdha protein levels than control cells (Fig. 6a). Respiration and BCAA uptake were also significantly lower in KD cells than in controls (Fig. 6b,c). Consistent with this observation, lipogenic flux of [U-$^{13}C_6$]leucine to fatty acids was markedly lower in KD cells (Fig. 6d). Furthermore, the abundance of numerous fatty acids was decreased in differentiated KD cells, including fatty acids synthesized *de novo* as well as those taken up from the medium (Fig. 6e). Finally, the transcription of selected adipogenic genes (*Pparg*, *Glut4*, *Plin4*, *Adipoq*, and *Lep*) was significantly lower in the KD condition than in the control cells (Fig. 6f), further suggesting that BCAA catabolism contributes to adipogenesis. Representative images of differentiated cultures also suggested that *Bckdha* KD negatively affected adipogenic differentiation, as evidenced by decreased lipid droplet formation (Fig. 6g). Supplementation of cobalamin did not observably affect adipogenic differentiation (data not shown), suggesting that some metabolite or pathway flux upstream of MMA-CoA mutase contributes to adipogenesis.

2.5 Discussion

Here we have explored how specific nutrients differentially contribute to mitochondrial metabolism as a function of adipocyte differentiation. Human and mouse cell lines of diverse tissue origins, including human visceral and subcutaneous pre-adipocytes, predominantly obtained AcCoA for DNL from glucose and glutamine when proliferating. Upon differentiation, the relative conversion of glucose and glutamine carbon to fatty acids was reduced, while significant de novo glutamine synthesis was initiated. At the same time, differentiated adipocytes catabolized BCAAs

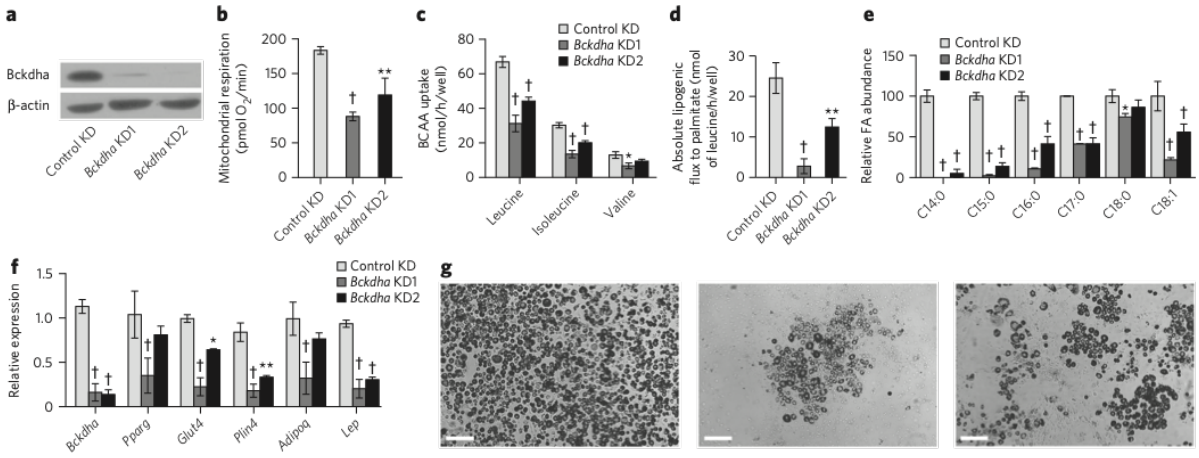

Figure 2.6: **Inhibition of BCAA catabolism impairs adipocyte differentiation. a**. Western blot of Bckdha and β-actin in differentiated 3T3-L1 adipocytes. Full gel is shown in Supplementary Figure 6. **b**. Basal respiration in control and Bckdha KD adipocytes (two cell lines separately derived using unique hairpins) normalized to nuclear quantitation. Data are from four technical replicates representative of three biological replicates. **c**. BCAA uptake in control KD and Bckdha KD adipocytes. **d**. Absolute lipogenic flux of leucine to palmitate synthesis. **e**. Relative abundance of the most abundant fatty acids. **f**. Quantitative PCR analysis of adipocyte-specific gene expression. **g**. Representative images of adipocyte differentiation (scale bars, 200 μm). From left: control KD, Bckdha KD1, Bckdha KD2. Data presented in **b-f** are mean $\pm$ s.d. Asterisks in b-e represent significance compared to control KD: *P < 0.05, **P < 0.01, †P < 0.001. Unless otherwise specified, data are from three technical replicates representative of three (**a-e**) or two (**f**) biological replicates (independent lentiviral knockdown and differentiation such that KD1 and KD2 were each derived two or three times) analyzed by two-way ANOVA with Holm-Sidak's multiple-comparison test.

such that leucine and isoleucine accounted for approximately one-third of lipogenic AcCoA. Even in the presence of more physiological concentrations of BCAAs, this catabolism was sustained via protein catabolism, as significant dilution arising from protein turnover was observed in differentiated adipocytes. These data indicate that proteinogenic amino acids serve as a significant carbon source for mitochondrial metabolism (and DNL) in differentiated adipocytes, a result similar to those obtained with pancreatic cancer cells cultured in low-glutamine medium[37].

The suppression of BCAA catabolism during cell proliferation is consistent with the dedicated utilization of these nutrients for protein biosynthesis. Mammalian target of rapamycin (mTOR) activity and associated protein translation required for proliferation is sensitive to leucine availability in particular[32, 38]. The differentiation-dependent induction of BCAA catabolism in 3T3-L1 cells and human pre-adipocytes demonstrated here may therefore serve as a model system for identifying key activators or suppressors of BCAA metabolism. Activity of PPARγ, a target of TZDs, increases significantly during early adipogenesis and has recently been associated with BCAA catabolic enzyme expression in human tissues, animals and cell models[13, 15, 19, 20]. However, additional transcription factors and coactivators driving this process may be identified through more systematic analyses.

Our results also demonstrate the critical role of vitamins as enzyme cofactors in mediating important metabolic processes and highlight potential deficiencies that could affect various model systems. In our hands and in other published studies, differentiated 3T3-L1 cells accumulated significant levels of OCFAs[35]. We confirmed that these metabolites arose from the accumulation of PropCoA and extension by fatty acid synthase (FASN) rather than α-oxidation[39]. Supplementation of cobalamin suppressed OCFA and MMA abundances in culture, suggesting that 3T3-L1 cells have the appropriate mitochondrial machinery for converting cobalamin to the activated AdoCbl cofactor necessary for MUT activity. Given the severe pathologies associated with acute, untreated methylmalonic aciduria[40], our results highlight the importance of investigating mitochondrial function as it correlates with cobalamin availability in other cell types

that catabolize BCAAs. These findings also demonstrate that standard culture conditions for differentiated 3T3-L1 cells are inadequate to support complete BCAA oxidation. Indeed, the heart, muscle and kidney are known to metabolize BCAAs and may be particularly affected by deficiencies in this cofactor[7, 8, 41]. Numerous biological models that are routinely used to represent these tissues (such as rat cardiomyocytes, primary murine myocytes and adipocytes) employ media that may lack sufficient cobalamin for BCAA catabolism, as has been observed in glial cells[42]. MMA and OCFA accumulation may affect results obtained from such systems given the demonstrated pathology associated with these metabolites[43].

Elevated plasma BCAAs, methionine and OCFAs, as well as C3- and C5-acylcarnitine species, have all been associated with obesity and insulin resistance[44, 45]. Although biotin availability is hypothesized to be a potential unifying cause of perturbations in these pathways[10], cobalamin-deficiency might also compromise BCAA catabolism in a similar manner to biotin. Indeed, a recent flux model of adipocyte metabolism that incorporated clinical proteomic and transcriptional data identifies MMA-CoA conversion to succinyl-CoA as a pathway that is downregulated in obese as compared to lean patients[46]. We observed that cobalamin deficiency induces the accumulation of downstream intermediates arising from BCAA catabolism (carnitine is also notably limited in culture systems employing dialyzed serum). Notably, several studies indicate that patients with T2DM are commonly deficient in cobalamin as a result of malabsorption due to metformin or other causes[47, 48]. Furthermore, the expression of cobalamin transporters and cobalamin availability itself can influence the composition of the gut microbiome[49], highlighting the complexity of the ways in which this cofactor can affect human health.

While BCAA catabolism is clearly induced during adipogenesis, functional knockdown of the pathway in pre-adipocytes impaired lipid accumulation and differentiation. These data provide the first direct evidence that BCAA oxidation is important for adipogenic differentiation. Presumably, some metabolite(s) along the BCAA catabolic pathway that are upstream of PropCoA and AcCoA could mediate the observed effects on adipogenesis, though additional studies are

required to identify such a regulatory effect. Our demonstration of a link between BCAA catabolism and adipogenesis is consistent with previous observations in *Bcat2*$^{-/-}$ mice, which exhibit decreased adiposity among other metabolic changes[16–18]. These results may also provide insights into potential adipose-mediated pathogenesis in patients with maple syrup urine disease (MSUD). However, cell-autonomous BCAA catabolism is likely not a prerequisite for adipogenic differentiation, as demonstrated by the moderate effects noted here and the (relative) health of individuals with MSUD. Collectively, our quantitative findings highlight critical roles for BCAA catabolism and vitamin availability in adipocyte differentiation, lipogenesis and bioenergetics.

2.6 Acknowledgements

We thank R.R. Henry (R.R.H.; Veterans Affairs San Diego Healthcare System, San Diego, California, USA) for human adipocyte material. This work was supported, in part, by US National Institutes of Health (NIH) grant R01CA188652 (C.M.M.), California Institute of Regenerative Medicine (CIRM) Award RB5-07356 (C.M.M.), US Department of Defense (DOD) grant W81XWH-13-1-0105 (C.M.M.) and a Searle Scholar Award (C.M.M.), as well as grants from the American Diabetes Association (7-05-DCS-04), the Medical Research Service (1 I010X00635-01A1), the US Department of Veterans Affairs and the VA San Diego Healthcare System (R.R.H.), NIH grant 1R01NS087611 (A.N.M.) and a grant from Seahorse Bioscience.

Chapter 2, in full, is a reprint of the material as it appears in "Branched-chain amino acid catabolism fuels adipocyte differentiation and lipogenesis," *Nature Chemical Biology*, vol. 12, 2016. Martina Wallace, Ajit S. Divakaruni, Susan A. Phillips, Anne N. Murphy, and Theodore P. Ciaraldi were co-authors of this publication. Courtney R. Green is the primary author of this publication. Christian M. Metallo is the corresponding author of this publication.

2.7 References

1. Rosen, E. D. & Spiegelman, B. M. What we talk about when we talk about fat. *Cell* **156,** 20–44 (2014).

2. Steppan, C., Bailey, S., Bhat, S., Brown, E., Banerjee, R., Wright, C., Patel, H., Ahima, R. & Lazar, M. The hormone resistin links obesity to diabetes. *Nature* **409,** 307–12 (2001).

3. Glass, C. & Olefsky, J. Inflammation and lipid signaling in the etiology of insulin resistance. *Cell Metab.* **15,** 635–45 (2012).

4. Turer, A. & Scherer, P. Adiponectin: mechanistic insights and clinical implications. *Diabetologia* **55,** 2319–2326 (2012).

5. Herman, M. A., Peroni, O. D., Villoria, J., Schön, M. R., Abumrad, N. A., Blüher, M., Klein, S. & Kahn, B. B. A novel ChREBP isoform in adipose tissue regulates systemic glucose metabolism. *Nature* **484,** 333–8 (2012).

6. Kahn, B. & Flier, J. Obesity and insulin resistance. *Journal of Clinical Investigation* **106,** 473–481 (2000).

7. Buse, M., Biggers, J., Friderici, K. & Buse, J. Oxidation of branched chain amino acids by isolated hearts and diaphragms of the rat. The effect of fatty acids, glucose, and pyruvate respiration. *J. Biol. Chem.* **247,** 8085–96 (1972).

8. Rosenthal, J., Angel, A. & Farkas, J. Metabolic fate of leucine: a significant sterol precursor in adipose tissue and muscle. *Am. J. Physiol.* **226,** 411–8 (1974).

9. Newgard, C. B., An, J., Bain, J. R., Muehlbauer, M. J., Stevens, R. D., Lien, L. F., Haqq, A. M., Shah, S. H., Arlotto, M., Slentz, C. A., Rochon, J., Gallup, D., Ilkayeva, O., Wenner, B. R., Yancy, W. S., Eisenson, H., Musante, G., Surwit, R. S., Millington, D. S., Butler, M. D. & Svetkey, L. P. A branched-chain amino acid-related metabolic signature that differentiates obese and lean humans and contributes to insulin resistance. *Cell Metab.* **9,** 311–26 (2009).

10. Fiehn, O., Garvey, W., Newman, J. W., Lok, K. H., Hoppel, C. L. & Adams, S. H. Plasma metabolomic profiles reflective of glucose homeostasis in non-diabetic and type 2 diabetic obese African-American women. *PLoS ONE* **5,** e15234 (2010).

11. Wang, T. J., Larson, M. G., Vasan, R. S., Cheng, S., Rhee, E. P., Elizabeth, M., Lewis, G. D., Fox, C. S., Jacques, P. F., Fernandez, C., J, O. C., Carr, S. A., Mootha, V. K., Florez, J. C., Souza, A., Melander, O., Clish, C. B. & Gerszten, R. E. Metabolite profiles and the risk of developing diabetes. *Nat. Med.* **17,** 448–53 (2011).

12. Kedishvili, N., Popov, K., Jaskiewicz, J. & Harris, R. Coordinated expression of valine catabolic enzymes during adipogenesis: analysis of activity, mRNA, protein levels, and metabolic consequences. *Arch. Biochem. Biophys.* **315,** 317–22 (1994).

13. Si, Y., Yoon, J. & Lee, K. Flux profile and modularity analysis of time-dependent metabolic changes of de novo adipocyte formation. *Am. J. Physiol. Endocrinol. Metab.* **292,** E1637–46 (2007).

14. Chuang, D., Hu, C. & Patel, M. Induction of the branched-chain 2-oxo acid dehydrogenase complex in 3T3-L1 adipocytes during differentiation. *Biochem. J.* **214,** 177–81 (1983).

15. Lackey, D. E., Lynch, C. J., Olson, K. C., Mostaedi, R., Ali, M., Smith, W. H., Karpe, F., Humphreys, S., Bedinger, D. H., Dunn, T. N., Thomas, A. P., Oort, P. J., Kieffer, D. A., Amin, R., Bettaieb, A., Haj, F. G., Permana, P., Anthony, T. G. & Adams, S. H. Regulation of adipose branched-chain amino acid catabolism enzyme expression and cross-adipose amino acid flux in human obesity. *Am. J. Physiol. Endocrinol. Metab.* **304,** E1175–87 (2013).

16. She, P., Reid, T. M., Bronson, S. K., Vary, T. C., Hajnal, A., Lynch, C. J. & Hutson, S. M. Disruption of BCATm in mice leads to increased energy expenditure associated with the activation of a futile protein turnover cycle. *Cell Metab.* **6,** 181–94 (2007).

17. Herman, M. A., She, P., Peroni, O. D., Lynch, C. J. & Kahn, B. B. Adipose tissue branched chain amino acid (BCAA) metabolism modulates circulating BCAA levels. *J. Biol. Chem.* **285,** 11348–56 (2010).

18. Zimmerman, H., Olson, K., Chen, G. & Lynch, C. Adipose transplant for inborn errors of branched chain amino acid metabolism in mice. *Mol. Genet. Metab.* **109,** 345–53 (2013).

19. Sears, D., Hsiao, G., Hsiao, A., Yu, J., Courtney, C., Ofrecio, J., Chapman, J. & Subramaniam, S. Mechanisms of human insulin resistance and thiazolidinedione-mediated insulin sensitization. *Proc. Natl. Acad. Sci. U.S.A.* **106,** 18745–50 (2009).

20. Hsiao, G., Chapman, J., Ofrecio, J. M., Wilkes, J., Resnik, J. L., Thapar, D., Subramaniam, S. & Sears, D. D. Multi-tissue, selective PPARγ modulation of insulin sensitivity and metabolic pathways in obese rats. *Am. J. Physiol. Endocrinol. Metab.* **300,** E164–74 (2011).

21. Phillips, S., Ciaraldi, T., Oh, D., Savu, M. & Henry, R. Adiponectin secretion and response to pioglitazone is depot dependent in cultured human adipose tissue. **295,** E842–50 (2008).

22. Phillips, S. A., Kung, J., Ciaraldi, T. P., Choe, C., Christiansen, L., Mudaliar, S. & Henry, R. R. Selective regulation of cellular and secreted multimeric adiponectin by antidiabetic therapies in humans. *Am. J. Physiol. Endocrinol. Metab.* **297,** E767–73 (2009).

23. Tchkonia, T., Tchoukalova, Y. D., Giorgadze, N., Pirtskhalava, T., Karagiannides, I., Forse, R., Koo, A., Stevenson, M., Chinnappan, D., Cartwright, A., Jensen, M. D. & Kirkland, J. L.

Abundance of two human preadipocyte subtypes with distinct capacities for replication, adipogenesis, and apoptosis varies among fat depots. *Am. J. Physiol. Endocrinol. Metab.* **288,** E267–77 (2005).

24. Lee, M. J., Wu, Y. & Fried, S. K. A modified protocol to maximize differentiation of human preadipocytes and improve metabolic phenotypes. *Obesity (Silver Spring)* **20,** 2334–40 (2012).

25. Divakaruni, A. S., Rogers, G. W. & Murphy, A. N. Measuring Mitochondrial Function in Permeabilized Cells Using the Seahorse XF Analyzer or a Clark-Type Oxygen Electrode. *Curr Protoc Toxicol* **60,** 25.2.1–25.2.16 (2014).

26. Divakaruni, A. S., Wiley, S. E., Rogers, G. W., Andreyev, A. Y., Petrosyan, S., Loviscach, M., Wall, E. A., Yadava, N., Heuck, A. P., Ferrick, D. A., Henry, R. R., G, M. W., Colca, J. R., Simon, M. I., Ciaraldi, T. P. & Murphy, A. N. Thiazolidinediones are acute, specific inhibitors of the mitochondrial pyruvate carrier. *Proc. Natl. Acad. Sci. U.S.A.* **110,** 5422–7 (2013).

27. Young, J. D. INCA: a computational platform for isotopically non-stationary metabolic flux analysis. *Bioinformatics* (2014).

28. Metallo, C. M., Gameiro, P. A., Bell, E. L., Mattaini, K. R., Yang, J., Hiller, K., Jewell, C. M., Johnson, Z. R., Irvine, D. J., Guarente, L., Kelleher, J. K., Vander Heiden, M. G., Iliopoulos, O. & Stephanopoulos, G. Reductive glutamine metabolism by IDH1 mediates lipogenesis under hypoxia. *Nature* **481,** 380–4 (2012).

29. Vander Heiden, M. G., Cantley, L. & Thompson, C. Understanding the Warburg Effect: The Metabolic Requirements of Cell Proliferation. *Science* **324,** 1029 (2009).

30. Kowalski, T. & Watford, M. Production of glutamine and utilization of glutamate by rat subcutaneous adipose tissue in vivo. *Am. J. Physiol.* **266,** E151–4 (1994).

31. Lee, M. J., Wu, Y. & Fried, S. K. Adipose tissue heterogeneity: implication of depot differences in adipose tissue for obesity complications. *Mol. Aspects Med.* **34,** 1–11 (2013).

32. Nicklin, P., Bergman, P., Zhang, B., Triantafellow, E., Wang, H., Nyfeler, B., Yang, H., Hild, M., Kung, C., Wilson, C., Myer, V. E., P, M. J., Porter, J. A., Wang, Y., Cantley, L. C., Finan, P. M. & Murphy, L. O. Bidirectional transport of amino acids regulates mTOR and autophagy. *Cell* **136,** 521–34 (2009).

33. Cynober, L. Plasma amino acid levels with a note on membrane transport: characteristics, regulation, and metabolic significance. *Nutrition* **18,** 761766 (2002).

34. Zhang, Y., Nicholatos, J., Dreier, J., Ricoult, S., Widenmaier, S., Hotamisligil, G., Kwiatkowski, D. & Manning, B. Coordinated regulation of protein synthesis and degradation by mTORC1. *Nature* **513,** 440 (2014).

35. Roberts, L. D., Virtue, S., Antonio, V., Nicholls, A. W. & Griffin, J. L. Metabolic phenotyping of a model of adipocyte differentiation. *Physiol. Genomics* **39,** 109–19 (2009).

36. Kapadia, C. R. Vitamin B12 in health and disease: part I–inherited disorders of function, absorption, and transport. *Gastroenterologist* **3,** 329–44 (1995).

37. Commisso, C., Davidson, S. M., G, S. R., Parker, S. J., Kamphorst, J. J., Hackett, S., Grabocka, E., Nofal, M., Drebin, J. A., Thompson, C. B., Rabinowitz, J. D., Metallo, C. M., Vander Heiden, M. G. & Dafna, B. Macropinocytosis of protein is an amino acid supply route in Ras-transformed cells. *Nature* **497,** 633–7 (2013).

38. Lynch, C. J., Halle, B., Fujii, H., Vary, T. C., Wallin, R., Damuni, Z. & Hutson, S. M. Potential role of leucine metabolism in the leucine-signaling pathway involving mTOR. *Am. J. Physiol. Endocrinol. Metab.* **285,** E854–63 (2003).

39. Su, X., Han, X., Yang, J., Mancuso, D. J., Chen, J., Bickel, P. E. & Gross, R. W. Sequential Ordered Fatty Acid α-Oxidation and $\delta 9$ Desaturation Are Major Determinants of Lipid Storage and Utilization in Differentiating Adipocytes. *Biochemistry* **43,** 50335044 (2004).

40. Haarmann, A., Mayr, M., Kölker, S., Baumgartner, E., Schnierda, J., Hopfer, H., Devuyst, O. & Baumgartner, M. Renal involvement in a patient with cobalamin A type (cblA) methylmalonic aciduria: a 42-year follow-up. *Mol. Genet. Metab.* **110,** 472–6 (2013).

41. Birn, H. The kidney in vitamin B12 and folate homeostasis: characterization of receptors for tubular uptake of vitamins and carrier proteins. *Am J Physiol Renal Physiol.* **291,** F22–F36 (2006).

42. Barley, F., Sato, G. & Abeles, R. An effect of vitamin B12 deficiency in tissue culture. *Journal of Biological Chemistry* (1972).

43. Kishimoto, Y., Williams, M., Moser, H., Hignite, C. & Biermann, K. Branched-chain and odd-numbered fatty acids and aldehydes in the nervous system of a patient with deranged vitamin B 12 metabolism. *J. Lipid Res.* **14,** 69–77 (1973).

44. Newgard, C. B. Interplay between lipids and branched-chain amino acids in development of insulin resistance. *Cell Metab.* **15,** 606–14 (2012).

45. Adams, S. H. Emerging perspectives on essential amino acid metabolism in obesity and the insulin-resistant state. *Adv Nutr* **2,** 445–56 (2011).

46. Mardinoglu, A., Agren, R., Kampf, C., Asplund, A., Nookaew, I., Jacobson, P., Walley, A., Froguel, P., Carlsson, L., Uhlen, M. & Nielsen, J. Integration of clinical data with a genome-scale metabolic model of the human adipocyte. *Mol. Syst. Biol.* **9** (2013).

47. Reinstatler, L., Qi, Y., Williamson, R. S., Garn, J. V. & Oakley, G. P. Association of Biochemical B12 Deficiency With Metformin Therapy and Vitamin B12 Supplements The National Health and Nutrition Examination Survey, 1999–2006. *Diabetes Care* **35,** 327–33 (2012).

48. Kang, D., Yun, J., Ko, S., Lim, T., Ahn, Y., Park, Y. & Ko, S. Higher Prevalence of Metformin-Induced Vitamin B12 Deficiency in Sulfonylurea Combination Compared with Insulin Combination in Patients with Type 2 Diabetes: A Cross-Sectional Study. *PLoS One.* **9** (2014).

49. Degnan, P. H., Barry, N. A., Mok, K. C., Taga, M. E. & Goodman, A. L. Human gut microbes use multiple transporters to distinguish vitamin B12 analogs and compete in the gut. *Cell Host Microbe* **15,** 47–57 (2014).

Chapter 3

Enzyme promiscuity drives branched-chain fatty acid synthesis in adipose tissues

3.1 Abstract

Fatty acid synthase (FASN) predominantly generates straight-chain fatty acids using acetyl-CoA as the initiating substrate. However, monomethyl branched-chain fatty acids (mmBCFAs) are also present in mammals but are thought to be primarily diet derived. Here we demonstrate that mmBCFAs are *de novo* synthesized via mitochondrial BCAA catabolism, exported to the cytosol by adipose-specific expression of carnitine acetyltransferase (CrAT), and elongated by FASN. Brown fat exhibits the highest BCAA catabolic and mmBCFA synthesis fluxes, whereas these lipids are largely absent from liver and brain. mmBCFA synthesis is also sustained in the absence of microbiota. We identify hypoxia as a potent suppressor of BCAA catabolism that decreases mmBCFA synthesis in obese adipose tissue, such that mmBCFAs are significantly decreased in obese animals. These results identify adipose tissue mmBCFA synthesis as a

novel link between BCAA metabolism and lipogenesis, highlighting roles for CrAT and FASN promiscuity influencing acyl-chain diversity in the lipidome.

3.2 Introduction

The branched-chain amino acids (BCAAs) leucine, isoleucine, and valine are essential amino acids important for protein synthesis, signaling, and bioenergetics. BCAA catabolism is emerging as a prominently dysregulated pathway in metabolic syndrome[1, 2] and cancer[3]; as such, a greater and more quantitative understanding of this pathway in mammalian physiology is needed. BCAA catabolism is initiated by deamination via branched-chain amino acid transferases (BCATs), and these branched-chain keto acids are subsequently metabolized in mitochondria to generate various acyl-CoA species downstream of the branched-chain ketoacid dehydrogenase (BCKDH) complex. This pathway is active in both energetically demanding tissues, such as heart and muscle, and lipogenic tissues[4]. Indeed, studies indicate that adipose BCAA catabolism can compensate for whole-body genetic deficiencies in the pathway[5]. Furthermore, carbon from leucine and isoleucine contribute significantly to *de novo* lipogenesis in differentiated adipocytes[6, 7], suggesting that adipose tissue BCAA catabolism may be important for adipocyte function.

The predominant product of *de novo* lipogenesis in mammals is the saturated 16-carbon fatty acid (FA) palmitate, which is further elongated and/or desaturated in a tissue-specific manner. Both odd-chain (OCFAs) and monomethyl branched-chain FAs (mmBCFAs) are also present in mammals, but these species are considered to be predominantly diet derived outside of the skin[8, 9]. In lower organisms mmBCFAs are important for controlling membrane fluidity[10] and contribute to neural development[11]. In mammals, mmBCFAs are found in milk[12], sebum[13], and vernix[14], and mmBCFA levels differ in obese and insulin-resistant patients[15, 16]. However, little is known about the metabolism of BCFAs in mammals. Here we demonstrate

that mmBCFAs are endogenous products of fatty acid synthase (FASN) and that their *in vivo* synthesis is influenced by mitochondrial BCAA catabolism, tissue-specific expression of carnitine acetyltransferase (*Crat*), the microbiome, hypoxia, and diet. mmBCFAs are primarily synthesized in adipose depots and are decreased in the context of diet-induced obesity, in which adipose-specific hypoxia potently suppresses BCAA catabolism and lipogenesis. These results identify a metabolic pathway in mammals connecting BCAA metabolism and lipid biosynthesis to acyl-chain diversity that is coordinated across distinct tissues and potently regulated by hypoxia.

3.3 Materials and Methods

3.3.1 Materials and reagents

Media and sera were purchased from Life Technologies. Glucose and amino acid isotope tracers were purchased from Cambridge Isotopes Inc. Fatty acid standards were purchased from Larodan. All other reagents were purchased form Sigma-Aldrich unless otherwise noted.

3.3.2 Cell culture

3T3-L1 pre-adipocytes were purchased from the American Type Culture Collection and cultured in high glucose Dulbecco's modified Eagle medium (DMEM; Life Technologies) supplemented with 10% bovine calf serum (BCS) below 70% confluence. For differentiation, cells were allowed to reach confluence (day -2), and 2 d post confluence (day 0) differentiation was induced with 0.5 mM 3-isobutyl-1-methylxanthine (IBMX), 0.25 μM dexamethasone, and 1 μg/ml insulin in DMEM containing 10% FBS. Media was changed on day 2 to DMEM + 10% FBS with 1 μg/ml insulin. On day 4 and thereafter, DMEM + 10% FBS was used. Cobalamin (500 nM) was supplemented to cultures when noted. Isotope tracing was carried out 7 d post induction of differentiation unless otherwise noted. Cells were incubated in custom DMEM in

which the metabolite specified was replaced with the ^{13}C- or ^{2}H-labeled version for 24 h unless otherwise specified. For short-chain fatty acid addition experiments, individual short-chain fatty acids were added to the media at the indicated concentration for 24 h, after which total fatty acids were extracted as described below. Fatty acids were then calculated as percent total fatty acids and normalized to control conditions. For LC-MS analysis of [U-$^{13}C_5$]valine incorporation into lipids, 3T3-L1 cells were incubated in tracer media for 4 d.

BAT depots were isolated from the interscapular area of neonate mice as previously described[17]. Once cells reached confluency, differentiation was induced by addition of DMEM containing 10% FBS, 20 nM insulin, 1 nM triiodothyronine, 0.5 mM 3-isobutyl-1-methylxanthine, 2 μg/mL dexamethasone, and 0.25 mM indomethacin for 2 d and then switched to differentiation media containing 20 nM insulin, and 1 nM triiodothyronine for 5-6 d. Isotope tracing was carried out 7 d post induction of differentiation.

Primary human white pre-adipocytes and muscle satellite cells were isolated, propagated and differentiated and then cultured for 24 h in tracer media as previously described[7, 18]. Weight stable obese subjects undergoing elective laparoscopic gastric bypass via Roux-en-Y for the treatment of obesity were recruited for the study to provide material for pre-adipocyte isolation. Both human skeletal muscle biopsies and material for pre-adipocyte isolation were obtained with approval from the University of California San Diego's Committee on Human Investigation and VA San Diego Medical Center's Institutional Review Board. All donors provided informed written consent after listening to an explanation of the protocol, and the study complied with all relevant regulations.

All hypoxia experiments were carried out in a Coy hypoxia chamber, which allows media changes under hypoxic conditions. ND-646 (1,4-dihydro-1-[(2R)-2-(2-methoxyphenyl)-2-[(tetrahydro-2H-pyran-4-yl)oxy]ethyl]-a,a,5-trimethyl-6-(2-oxazolyl)-2,4-dioxothieno[2,3-d]pyrimidine-3(2H)-acetamide) was solubilized in DMSO and added to cells at a final concentration of 100 nM for 24 h in the presence of tracer.

3.3.3 Lipolysis assay

Differentiated 3T3-L1 adipocytes were washed twice with PBS and incubated with serum-free DMEM containing P/S, 2% FA-free BSA, and 10 μM isoproterenol for 1 h. 100 μL was extracted for GC-MS analysis.

3.3.4 Oil Red O staining

A 0.35% (w/v) Oil Red O stock was prepared in isopropanol and filtered through a 0.22 μm filter. Cells were washed with PBS, fixed with 4% paraformaldehyde for 30 min at room temperature, washed 2x in milli-Q water, washed once with 60% isopropanol, and finally stained with 3:2 (stock:water) Oil Red O solution for 30 min. Stain solution was removed from cells and cells were washed 4x with milli-Q water before imaging.

3.3.5 Lentiviral production and shRNA KD of acyl-CoA dehydrogenases

Glycerol stocks of TRC2-pLKO.1-puro shRNA (Supplementary Table 3) and a nontargeting control construct were purchased from Sigma-Aldrich and packaged in HEK293FT cells using the transfection agent Fugene 6 and required packaging plasmids VSV-G, gag/pol, and rev. HEK293FT medium containing lentiviral constructs was collected 2 d later and filtered (0.45 μm). Polybrene was added to a final concentration of 6 μg/ml. 3T3-L1 pre-adipocytes were infected with 0.5 ml of virus-containing medium in a 6-well plate for 4 h before addition of 2 ml of virus-free medium. After 24 h of recovery, transduced cells were selected with 3 μg/ml puromycin. Cells were then plated to 12-well plates for differentiation as described above. Puromycin was removed from the medium beginning on day 0 of differentiation.

3.3.6 Pooled CRISPR-Cas9 KO of Crat and Fasn in 3T3-L1 adipocytes

Fasn, NT, and CrAT target sequences (Supplementary Table 4) were cloned into the lentiCRISPRv2 plasmid (Addgene plasmid #52961). For lentivirus production, 2-2.5 million HEK293FT cells were placed in 10-cm tissue culture plates in 10 ml of DMEM (containing 1% penicillin/streptomycin, 10% FBS). 24 h later, transfection was performed using Lipofectamine 3000 (Invitrogen) with 1.3 μg VSV.G/PMD2.G, 5.3 μg of lenti-gag/pol/PCMVR8.2 and 4 μg of lentiviral vector. Lentivirus-containing supernatants were harvested 48 and 72 h later and concentrated using Amicon Ultra-15 centrifugal filters, 100,000 NMWL (Millipore) following the manufacturer's protocol. 3T3-L1 pre-adipocytes were infected with 10 μL of virus in 1 ml of medium containing 7.5 μg of polybrene in a 6-well plate for 4 h before addition of an extra 1 ml of virus-free medium. After 24 h of recovery, transduced cells were selected with 3 μg/mL puromycin. Cells were then plated to 12-well plates for differentiation as described above. Puromycin was removed from the medium beginning on day 0 of differentiation.

3.3.7 RNA isolation and quantitative RT-PCR

Total RNA was purified from cultured cells using Trizol Reagent (Life Technologies) per the manufacturer's instructions. First-strand cDNA was synthesized from 1 μg of total RNA using iScript Reverse Transcription Supermix for RT-PCR (Bio-Rad Laboratories) according to the manufacturer's instructions. Individual 10 μl SYBR Green real-time PCR reactions consisted of 2 μl of diluted cDNA, 5 μl of SYBR Green Supermix (Bio-Rad), and 1 μl of each 5 μM forward and reverse primers. For standardization of quantification, 18S was amplified simultaneously. The PCR was carried out on 96-well plates on a CFX Connect Real time System (Bio-Rad) using a three-stage program provided by the manufacturer: 95°C for 3 min, 40 cycles of 95°C for 10 s and 60°C for 30 s. Gene-specific primers used are listed in Supplementary Table 5. PCR data for intergene comparison were corrected for primer efficiency.

3.3.8 Western blots

3T3-L1 adipocytes or 100-150 mg of ground eWAT were lysed in ice-cold RIPA buffer with 1x protease inhibitor (Sigma-Aldrich). 30 μg total protein was separated on a 12% SDS-PAGE gel for BCKDH blots or 20 μg of total protein was separated on a 4-20% SDS-PAGE gel (mini-protean TGX gels, Bio-Rad) for CrAT and FASN blots. The proteins were transferred to a nitrocellulose membrane and immunoblotted with anti-Bckdha (Novus Biologicals NBP1-79616) (1:1,000 dilution), anti-β-actin (Cell Signaling 4970S) (1:5,000), anti-GAPDH (Cell Signaling 5174S), anti-CrAT (Novus NBP2-15999), anti-FASN (Proteintech 10624-2-AP). Specific signal was detected with horseradish peroxidase-conjugated secondary antibody goat anti-rabbit (1:2,500-1:10,000) using SuperSignal West Pico Chemiluminescent Substrate (Thermo Scientific) and developed using Blue Devil Autoradiography film (Genesee Scientific) or Bio-Rad Chemidoc XRS+.

3.3.9 Animal studies

Animal handling and care followed the NIH Guide for Care and Use of Laboratory Animals. The experimental protocols were approved by either the UCSD, Salk, or UMMS Institutional Animal Care and Use Committee. C57BL/6J and ob/ob(B6.Cg-Lepob/J) were obtained from Jackson Laboratories.

3.3.10 Mouse fasting study

Food was removed from cages containing 12-week-old male or female C57BL/6J mice (3-4 mice per cage) at 7:00 a.m. Blood was collected via tail bleed at baseline, 2, 6, 12, and 24 h post-removal of food. Mice remained in their original cage with original bedding (nonsynthetic shavings) for the duration of the experiment.

3.3.11 ^2H_2O administration to animals

For the comparison of germ free and specific pathogen free mice, male Swiss Webster mice were bred and maintained in sterile semi-flexible isolators and screened for bacterial, viral, and fungal contamination. Age-matched male specific pathogen-free mice were used for comparison and obtained from Charles River at 5 weeks of age. Mice were maintained under a 12 h light/dark cycle and given a standard chow diet *ad libitum*. At 6 weeks of age, mice were subcutaneously injected with 0.035 ml/g body weight 0.9% NaCl ^2H_2O, and drinking water was replaced with 8% ^2H_2O-enriched water. 8 d later, mice were fasted for 6 h (9 a.m. to 3 p.m.) and tissues collected and snap frozen in liquid nitrogen.

For the high-fat study, 5-week-old C57BL/6 J mice were obtained from Jackson Laboratories and *ad libitum* fed a 45% high-fat diet (D12451) or a 10% low-fat diet (D12450K) for 15 weeks from 6 weeks of age. Diets were obtained from Research Diets, Inc. 7-21 d before termination, mice were injected intraperitoneally with 0.035 ml/g body weight 0.9% NaCl ^2H_2O, and drinking water was replaced with 8% ^2H_2O-enriched water. Mice were fasted for 6 h before plasma, and tissue collection and samples were immediately snap frozen in liquid nitrogen.

Thermovariation experiments were carried out as previously described[19]. Briefly, 10-week-old C57BL/6 J mice were simultaneously housed in two rodent incubators (RIT33SD, Powers Scientific) within the Animal Medicine facilities of the UMMS for 4 weeks. One of them had the temperature adjusted to 30°C (thermoneutrality group). Another incubator had its temperature decreased by 4°C weekly until reaching 6°C, and the mice stayed at this temperature for a week (severe cold group). Room-temperature group mice were in a clean room set at 22°C co-housed in the same facility as the mice in rodent incubators. Mouse cages were changed weekly using components pre-adjusted to temperature. Three days before termination, mice were intraperitoneally injected with 0.035 ml/g body weight 0.9% NaCl ^2H_2O (Sigma, 151882), and drinking water was replaced with 8% ^2H_2O-enriched water.

3.3.12 Isotope-labeled chow study

5-week-old C57BL/6 J mice were obtained from Jackson Laboratories and *ad libitum* fed a custom 60% kcal high fat diet (TD.160092) or a 20% kcal fat diet (TD. 160091) for 15 weeks from 6 weeks of age. Diets and incorporated isotopes were obtained from Envigo Teklad Diets and Cambridge isotopes, respectively. For the final 3 weeks, 25% of the total valine and leucine in the diet was replaced with [U-$^{13}C_5$,^{15}N]valine and [U-$^{13}C_6$,^{15}N]leucine so that there was 3 g [U-$^{13}C_5$,^{15}N]valine /100 g protein and 4 g [U-$^{13}C_6$,^{15}N]leucine/100 g protein in both diets. Mice were fasted overnight before plasma and tissue collection, and samples were immediately snap frozen in liquid nitrogen.

3.3.13 Tissue pO_2 and organ blood flow in HFD/LFD mice

To determine the impact of obesity on tissue pO_2, blood flow and BCKDHA levels in eWAT, 5-week-old C57BL/6J mice were obtained from Jackson Laboratories and *ad libitum* fed a 60% kcal high fat diet (D12492) or a 10% kcal fat diet (D12450K) from research diets for 8 weeks from 6 weeks of age.

3.3.14 Electrodes for oxygen measurements

The oxygen partial pressure was measured using carbon fiber electrodes (Carbostar-1, Kation Scientific; Minneapolis, MN) in which the tip of the electrode was coated with 5% Nafion (Sigma; St. Louis, MO) to increase oxygen specificity. The process consisted of three individual Nafion coats. The microelectrodes were polarized at -0.8 V relative to a silver-silver chloride reference electrode (Cypress Systems; Lawrence, KS). Oxygen measurements were performed using the two electrodes system (working and reference electrode), and the current generated was measured with a potentiostat and electrometer (Keithley model 610 C; Cleveland, OH). The microelectrodes were calibrated at 37°C with 0, 5, 10, and 21% oxygen gases (Airgas; Los

Angeles, CA). Tissues were superfused (0.1 ml/min) with physiological Krebs salt solution, and the tissue was maintained at 35-37°C by the heated Krebs solution. The solution was spread on the tissue as a thin film, drained into a platter, and drawn off by suction. The solution was equilibrated with 95% N_2 and 5% CO_2, which maintained the superfusate at a pH of 7.4 and minimized O_2 delivery to the tissue from the atmosphere. Oxygen measurements were made by penetrating the tissue with the microelectrode tip. The reference electrode was placed in the bath, and the microelectrode was placed in a shielded holder and advanced toward the measurement site with a micromanipulator. A long-working distance X10 Leitz objective was used to direct the electrode to the measurement site. Before measurements, the electrode tip was immersed in the supernatant suffusion solution and the current was registered. The supernatant suffusion solution was set as 0 mmHg reference point. Upon introduction into the tissue, the microelectrodes responded with a time constant that is estimated to be of the order of 10 s. A stable reading is obtained within 30 s, and upon reaching the current plateau value, the electrode is extracted from the tissue and the tip maintained within the suffusing saline solution.

3.3.15 Organ blood flow distribution

The fluorescent-labeled microsphere (FLM) method was used to determine organ blood flow. Briefly, fluorescent microspheres (Molecular Probes, Eugene, OR), 15 μm in diameter with a single color (green, yellow, red, or scarlet) were suspended in saline and injected over a short 10 s period (100 μL) at the time point of interest. At the end of the protocol, animals were euthanized with a lethal dose of sodium pentobarbital, and eight vital tissues were harvested. The tissues were digested in 1 N KOH in separate containers for 24 h and then filtered. Fluorescent dye extraction was accomplished using Cellosolve (Fisher Scientific Co., Pittsburg, PA), and the number of FLMs was quantified as a function of the florescent signal at each specific FluoSphere wavelength (LS50B, PerkinElmer Corp., Norwalk, CT)[20].

3.3.16 NAFL/NASH patient sample collection

Sixteen subjects undergoing diagnostic liver biopsy for suspected NAFLD were recruited by the NAFLD Research Center at the University of California, San Diego. Subjects were carefully screened and excluded for liver diseases other than NAFLD and secondary causes of hepatic steatosis[21]. Subjects drank 50 ml of 70% ^2H_2O three times per day for 4 d, followed by twice a day until the date of liver biopsy, for a total period of 3-5 weeks. Plasma was collected weekly from the start of heavy water labeling until the time of biopsy. All procedures used in this study were approved by the University of California, San Diego Human Research Protections Program. Subjects provided written informed consent, and Declaration of Helsinki protocols were followed.

3.3.17 GC-MS analysis of fatty acids and polar metabolites

For cell culture, polar metabolites and fatty acids were extracted using methanol / water / chloroform and analyzed as previously described[7]. For tissue and plasma, metabolites and total fatty acids were extracted from tissues and plasma using a Folch-based methanol / chloroform / saline extraction at a ratio of 1:2:1 with inclusion of [$^2H_{31}$]palmitate and unlabeled norvaline as lipid and polar internal standards, respectively. Briefly, 250 μl MeOH, 500 μl $CHCl_3$, 250 μl saline and fatty acid isotope internal standards were added to weighed pre-ground tissue. This was vortexed for 10 min followed by centrifugation at 10,000 g for 5 min. Polar metabolites were derivatized in 2% (w/v) methoxyamine hydrochloride (Thermo Scientific) in pyridine and incubated at 37°C for 60 min. Samples were then silylated with N-tertbutyldimethylsilyl-N-methyltrifluoroacetamide (MTBSTFA) with 1% tert-butyldimethylchlorosilane (tBDMCS) (Regis Technologies) at 37°C for 30-45 min. Polar derivatives were analyzed by GC-MS using a DB-35MS column (30 m x 0.25 mm i.d. x 0.25 μm, Agilent J&W Scientific) installed in an Agilent 7890A gas chromatograph (GC) interfaced with an Agilent 5975C mass spectrometer

(MS). The lower chloroform phase was dried and then derivitized to form fatty acid methyl esters (FAMES) via addition of 500 μl 2% H_2SO_4 in MeOH and incubation at 50°C for 2 h. FAMES were extracted via addition of 100 μl saturated salt solution and 500 μl hexane and these were analyzed using a Select FAME column (100 m x 0.25 mm i.d.) installed in an Agilent 7890A GC interfaced with an Agilent 5975C MS using the following temperature program: 80°C initial, increase by 20°C/min to 170°C, increase by 1°C/min to 204°C, then 20°C/min to 250°C and hold for 10 min. The percent isotopologue distribution of each fatty acid and polar metabolite was determined and corrected for natural abundance using in-house algorithms adapted from Fernandez et al.[22]. The metabolite ion fragments used are summarized in Supplementary Table 6. Mole percent enrichment (MPE) was calculated via the following equation:

$$\frac{\sum_{i=1}^{n} M_i \cdot i}{n}$$

where n is the number of carbon atoms in the metabolite and M_i is the relative abundance of the i^{th} mass isotopomer.

Molar enrichment was determined by multiplying the MPE by the abundance.

YSI (Yellow Springs Instrument) was used to quantify glucose, lactate, glutamine, and glutamate in cell culture media.

3.3.18 Isotopomer spectral analysis

The contribution of oxPPP-derived NADPH to lipogenesis using the [3-^{2}H]glucose tracer was determined via isotopomer spectral analysis (ISA) using INCA as previously described[7]. The ISA compares a measured fatty acid isotopomer distribution (determined by integrating metabolite ion fragments of fatty acids summarized in Supplementary Table 6) to one that is simulated using a reaction network for palmitate synthesis, whereby 14 NADPH molecules are consumed to form one palmitate molecule. Models were also generated for mmBCFA and

OCFA synthesis, whereby 12 NADPH molecules are consumed to form one branched- or odd-chain fatty acid (Supplementary Tables 7 and 8). Parameters for the relative enrichment of the lipogenic NADPH pool from a given [^{2}H] tracer and the percentage of fatty acids that are *de novo* synthesized are extracted from a best-fit model using INCA 4.6 metabolic flux analysis software package[23]. The 95% confidence intervals for both parameters were estimated by evaluating the sensitivity of the sum of squared residuals between measured and simulated fatty acid mass isotopomer distributions to small flux variations.

3.3.19 GC-MS analysis of short-chain fatty acids

Cecal content was weighed, and 2 μl of water was added per mg of cecum. The sample was vortexed for 5 min and then centrifuged at 18,000 g for 5 min at 10°C. The resultant cecal water was used for SCFA analysis, and the cecal pellet was dried overnight at 60°C to obtain the dry weight.

For cecal SCFA quantification, 50 μl of cecal water was added to a 2 ml eppendorf microcentrifuge tube, followed by 150 μl water, 10 μl 5 mM 2-ethylbutyrate, 30 μl 10 mM sodium acetate-d_3, 50 μl 1-propanol and 50 μl pyridine. The tube was placed on ice for 5 min, which was followed by addition of 100 μl 1 M NaOH and 30 μl methylchloroformate. The sample was then vortexed for 20 s followed by addition of 300 μl MTBE and then vortexed for another 20 s followed by centrifugation at 10,000g for 5 min at 4°C. 100 μl of the upper phase was then transferred in duplicate to GC vials for analysis. Samples were analyzed by GC-MS using a DB-35MS column (30 m x 0.25 mm i.d. x 0.25 μm, Agilent J&W Scientific) installed in an Agilent 7890B gas chromatograph (GC) interfaced with an Agilent 5977B mass spectrometer (MS) using the following temperature program: 50°C initial with a hold time of 0.8 min, followed by an increase of 25°C/min to 120°C and then an increase of 100°C/min to 280°C. Samples were injected using split mode (25 ml/min split flow), and the mass spectrometer was operated in scan mode between 50-150 AMU. Acetate was quantified from the internal acetate isotope standard

and all other SCFAs were quantified from a standard curve extracted in parallel.

The isotopologue distributions of acetate and isovalerate were obtained via diethyl ether extraction and TBDMS derivatization of cecal water. Briefly, 10 μl concentrated HCl (37%) and 1 ml diethyl ether was added to 100 μl cecal water, which was followed by 10 min of vortexing and centrifugation at 18,000g at 15°C for 5 min. The upper phase was added to a new tube and the diethyl ether extraction step was repeated. 250 μl of the extract was aliquoted in triplicate to GC vials, and 25 μl MTBSTFA + 1% tBDMS was added followed by incubation at room temperature for 1 h before GC-MS analysis with the following temperature program: 80°C initial with a hold time of 0.8 min, followed by an increase of 15°C/min to 150°C with a hold time of 2 min, then an increase by 50°C/min to 280°C. Samples were injected using split mode (25 ml/min split flow) and the mass spectrometer was operated in scan mode between 50-500 AMU.

3.3.20 Plasma ^2H_2O enrichment analysis

The ^{2}H labeling of water from samples or standards was determined via deuterium acetone exchange. 5 μl of sample or standard was reacted with 4 μl of 10 N NaOH and 4 μl of a 5% (v/v) solution of acetone in acetonitrile for 24 h. Acetone was extracted by the addition of 600 μl chloroform and 0.5 g sodium sulfate followed by vigorous mixing. 100 μl of the chloroform was then transferred to a GC-MS vial. Acetone was measured using an Agilent DB-35MS column (30 m x 0.25 mm i.d. x 0.25 μm, Agilent J&W Scientific) installed in an Agilent 7890A gas chromatograph (GC) interfaced with an Agilent 5975C mass spectrometer (MS) with the following temperature program: 60°C initial, increase by 20°C/min to 100°C, increase by 50°C/min to 220°C, and hold for 1 min. The split ratio was 40:1 with a helium flow of 1 ml/min. Acetone eluted at approximately 1.5 min. The mass spectrometer was operated in the electron impact mode (70 eV). The mass ions 58 and 59 were integrated and the percent M1 (m/z 59) calculated. Known standards were used to generate a standard curve and plasma percent enrichment was determined from this. All samples were analyzed in triplicate.

3.3.21 *In vivo de novo* lipogenesis calculations

Calculation of the fraction of newly synthesized fatty acids (FNS) was based on the method described by Lee et al.[24], where FNS is described by the following equation:

$$FNS = \frac{ME}{n \times p}$$

where ME is the average number of deuterium atoms incorporated per molecule (ME = $1\times m_1$ + $2\times m_2$ + $3\times m_3$...), p is the deuterium enrichment in water and n is the maximum number of hydrogen atoms from water incorporated per molecule. N was determined using the following equation:

$$\frac{m_2}{m_1} = \frac{(n-1)}{2} \times \frac{p}{q}$$

As described by Lee et al.[24], where q is the fraction of hydrogen atoms and $p + q = 1$. The molar amount of newly synthesized fatty acids (MNS) was determined by: MNS = FNS $\times$ total fatty acid amount (nmoles/mg tissue).

3.3.22 LC-MS lipidomic analysis

Lipid extraction was carried out using a Folch-based methanol/chloroform/saline extraction at a ratio of 1:2:1 with the inclusion of C12:0 dodecylglycerol and [$^2H_{31}$]palmitate as internal standards. The methanol phase was washed a second time with chloroform after addition of 1 μl formic acid. Metabolite separation was achieved with a Luna reverse-phase C5 column (50 x 4.6 mm, with 5-μm-diameter particles; Phenomenex). Mobile phase A was composed of a 95:5 ratio of water:methanol, and mobile phase B consisted of isopropanol, methanol, and water in a 60:35:5 ratio. Solvent modifiers 0.1% formic acid with 5 mM ammonium formate and 0.1% ammonium hydroxide were used to assist ion formation and to improve the LC resolution in both positive and

negative ionization modes, respectively. The flow rate for each run started at 0.1 ml/min for 5 min to alleviate backpressure associated with injecting chloroform. The gradient started at 0% B and increased linearly to 100% B over the course of 45 min with a flow rate of 0.4 ml/min, followed by an isocratic gradient of 100% B for 17 min at 0.5 ml/min before equilibrating for 8 min at 0% B with a flow rate of 0.5 ml/min. MS analysis was performed with an electrospray ionization (ESI) source on an Agilent 6430 QQQ LC-MS/MS. The capillary voltage was set to 3.0 kV, and the fragmentor voltage was set to 100 V. The drying gas temperature was 350°C, the drying gas flow rate was 10 L/min, and the nebulizer pressure was 35 psi. Representative lipids were quantified by SRM of the transition from precursor to product ions at associated optimized collision energies as previously described58. Briefly, for the SRM transitions in which the transition of parent masses to the loss of the headgroup (for example, loss of phosphocholine from phosphatidylcholine) is monitored, the acyl chain specificities were determined from previously described procedures[25]. For phospholipids such as PCs and PEs, the fatty acid acyl chain composition was determined from phospholipids using a mobile phase containing both ammonium hydroxide and formic acid and the fatty acid fragmentations were monitored from [M-H + HCO_2H] m/z at 40 V collision energy in negative ionization mode. For other phospholipids such as PAs and PIs, the fatty acid fragmentations from [M-H] m/z at 40 V collision energy in negative ionization mode in mobile phase containing just ammonium hydroxide were monitored. The identifying ion and the M + 4 (mass increment of 4) ion of each lipid was monitored, and relative abundance was determined by integrating the area under the curve followed by normalization to internal standard values. Significant incorporation of [U-$^{13}C_5$]valine into lipids was determined by comparing the relative abundance of the M + 4 ion of each lipid species targeted in [U-$^{13}C_5$]valine-traced cells versus cells that had no tracer added (no trace) via fold change differences and Student's t-test. Percentage enrichment of each lipid species was determined via:

$$\%E = [\frac{^{13}CM_4}{^{13}CM_0} - \frac{^{12}CM_4}{^{12}CM_0}] \cdot 100\%$$

Where M_4 is the M + 4 abundance of each lipid, M_0 is the identifying ion abundance and ^{13}C and ^{12}C denote cells cultured in [U-$^{13}C_5$]valine and ^{12}C valine, respectively.

3.3.23 Statistical analysis

All results are shown as mean ± s.e.m. P values were calculated using Student's two-tailed t-test unless otherwise specified; *P value between 0.01 and 0.05; **P value between 0.001 and 0.01; ***P < 0.001. t-tests were carried out in GraphPad Prism, version 7. Errors associated with ISA of lipogenesis are 95% confidence intervals determined via sensitivity analysis. All cell culture experiments were replicated at least 3 independent times.

3.4 Results

3.4.1 Mammalian adipocytes synthesize mmBCFAs via FASN

Adipocytes undergo substantial mitochondrial and cytosolic metabolic reprogramming upon differentiation. We and others have previously shown that a distinct feature of this metabolic reprogramming is upregulation of BCAA catabolism, which becomes a substantial source of carbon for both TCA cycle metabolism and lipogenic acetyl-CoA[6, 7, 26]. In cultured adipocytes, odd-chain FAs (C15:0 and C17:0) synthesized from valine- and isoleucine-derived propionyl-CoA can also accumulate as a result of vitamin B12 deficiency and decreased activity of the B12-dependent enzyme methylmalonyl-CoA mutase[6, 7]. In addition to the increased BCAA catabolism and OCFA synthesis observed in differentiated 3T3-L1 adipocytes, we detected accumulation of several mass isomers of the FAs C16:0 (palmitate) and C17:0 (heptadecanoate), which eluted before the predominant straight-chain isomers in our gas chromatography-mass spectrometry (GC-MS) analysis. As compromised B12 metabolism can lead to accumulation of monomethyl branched-chain FAs (mmBCFAs) in the brain[27], we hypothesized that these alternate mass

isomers were mmBCFAs and subsequently used analytical standards to confirm their identities. We detected increases in 14-methylpentadecanoate (iso-C16:0), 14-methylhexadecanoate (anteiso-C17:0) and 15-methylhexadecanoate (iso-C17:0) during differentiation of 3T3-L1 adipocytes, with iso-C16:0 occurring at the highest abundance (Fig. 1a). These FAs have a single branch at either the penultimate or antepenultimate carbon of the acyl chain (Supplementary Fig. 1a), with the position impacting elution times (Supplementary Table 1). Interestingly, the relative abundance of anteiso-C17:0 was impacted by B12 availability in this culture system (Fig. 1b), suggesting that these species were actively metabolized by adipocytes.

Figure 3.1: **Mammalian adipocytes synthesize mmBCFAs via fatty acid synthase. a**. mmBCFA abundance in differentiating 3T3-L1 adipocytes. **a**. mmBCFA abundance in 3T3-L1 adipocytes differentiated for 7 d with or without 500 nM B12. Two-tailed Student's t-test was performed on three cellular replicates (P = 0.000019) with no adjustment for multiple comparisons. **c**. Atom-transition map demonstrating isotope incorporation into *de novo* synthesized fatty acids from [U-$^{13}C_6$]glucose. Closed circles indicate ^{13}C carbon. DNL, *de novo* lipogenesis. **d**. Isotopologue distribution of iso-C16:0 from [U-$^{13}C_6$]glucose-traced 3T3-L1 cells. **e**. Percent enrichment from [U-$^{13}C_6$]isoleucine-derived acetyl-CoA (M1-M2 only) in 3T3-L1 adipocytes with or without 100 nM ND646 for 24 h. **f**. Atom-transition map depicting transfer of isotope [3-^{2}H]glucose through glycolysis, the pentose phosphate pathway and reductive biosynthesis. Open circles indicate carbon and small red circles indicate a deuterium label from [3-^{2}H]glucose. TPI, triose phosphate isomerase. **g**. Contribution of [3-^{2}H]glucose-labeled NADPH to fatty acid *de novo* synthesis determined via ISA. 3T3-L1 adipocytes cultured in tracer for 72 h. PGD, phosphogluconate dehydrogenase. **h**. Iso-C16:0 levels as percent total FA in pooled CRISPR-Cas9 FASN KO 3T3-L1 adipocytes following addition of isobutyrate for 24 h. **i**. Relative abundances of mmBCFAs and C16:0 in differentiated 3T3-L1s following addition of isobutyrate for 24 h. Two-tailed Student's t-test was performed on three cellular replicates for each comparison with no adjustment for multiple comparisons. All data are presented as means $\pm$ s.e.m. with dot plots overlaid except for **g**, where 95% confidence intervals from ISA model are shown. All data are representative of three cellular replicates, and each experiment was repeated three independent times with the exception of **h**, for which two separate infections were carried out. The same result was obtained in each independent experiment. *P < 0.05, **P < 0.01, ***P < 0.001.

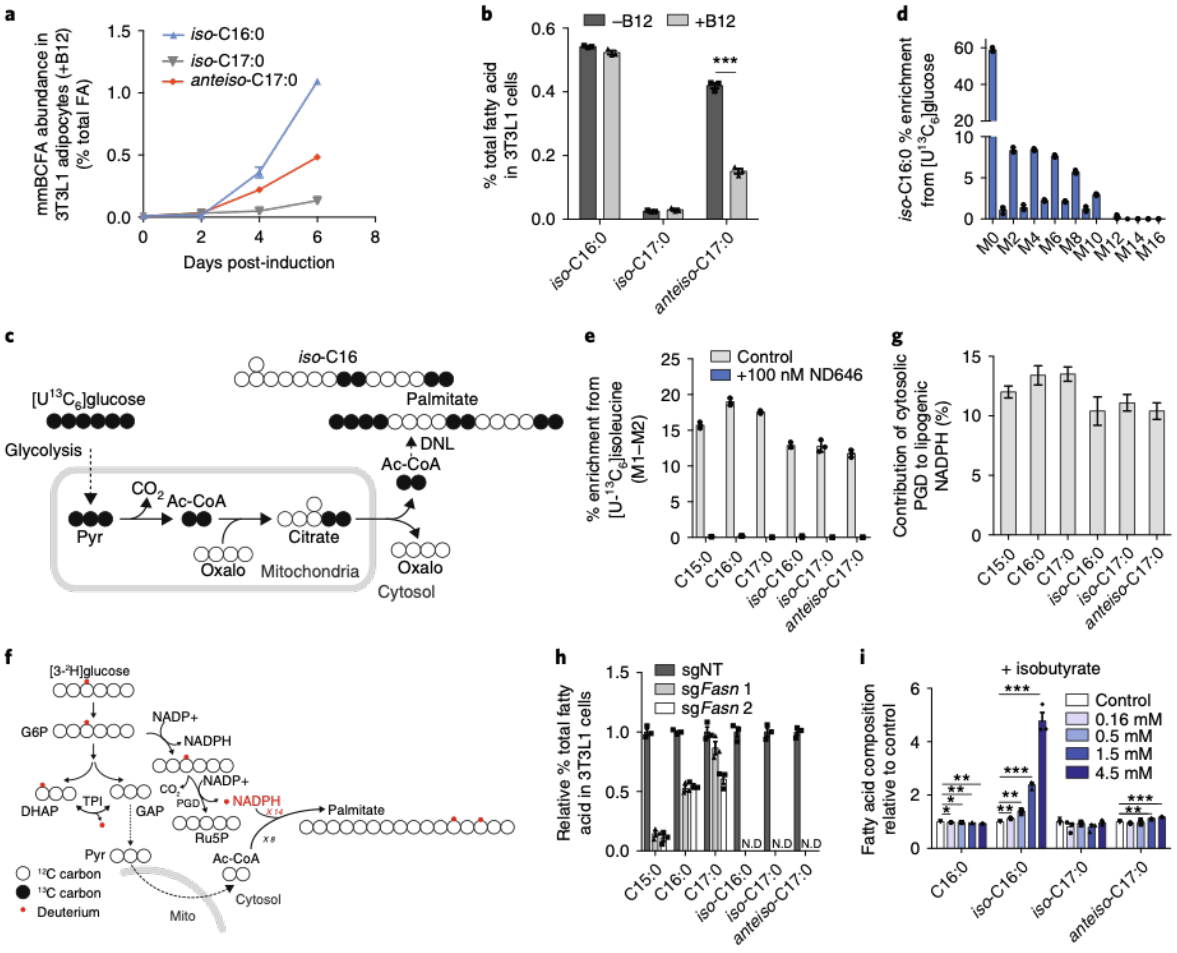
a
mmBCFA abundance in 3T3L1 adipocytes (+B12) (% total FA)
iso-C16:0
iso-C17:0
anteiso-C17:0
Days post-induction
b
% total fatty acid in 3T3L1 cells
–B12
+B12
***
iso-C16:0
iso-C17:0
anteiso-C17:0
d
iso-C16:0 % enrichment from [U13C6]glucose
M0 M2 M4 M6 M8 M10 M12 M14 M16
c
iso-C16
[U13C6]glucose
Palmitate
Glycolysis
DNL
Ac-CoA
CO2 Ac-CoA
Pyr
Citrate
Oxalo
Mitochondria
Oxalo
Cytosol
e
% enrichment from [U-13C6]isoleucine (M1–M2)
Control
+100 nM ND646
C15:0 C16:0 C17:0 iso-C16:0 iso-C17:0 anteiso-C17:0
g
Contribution of cytosolic PGD to lipogenic NADPH (%)
C15:0 C16:0 C17:0 iso-C16:0 iso-C17:0 anteiso-C17:0
f
[3-2H]glucose
G6P
NADP+
NADPH
DHAP
TPI
GAP
CO2
PGD
NADP+
NADPH
Ru5P
x 14
x 8
Palmitate
Pyr
Ac-CoA
12C carbon
13C carbon
Deuterium
Mito
Cytosol
h
Relative % total fatty acid in 3T3L1 cells
sgNT
sgFasn 1
sgFasn 2
N.D
C15:0 C16:0 C17:0 iso-C16:0 iso-C17:0 anteiso-C17:0
i
+ isobutyrate
Fatty acid composition relative to control
Control
0.16 mM
0.5 mM
1.5 mM
4.5 mM
C16:0 iso-C16:0 iso-C17:0 anteiso-C17:0

To determine whether mmBCFAs were synthesized *de novo*, we cultured 3T3-L1 adipocytes with [U-$^{13}C_6$]glucose, which generates ^{13}C fully labeled acetyl-CoA units and a distinct M + 2 isotopologue pattern in newly synthesized FAs (Fig. 1c; Supplementary Fig. 1b). We detected significant enrichment in mmBCFAs (Fig. 1d; Supplementary Fig. 1c,d), demonstrating that these FAs are synthesized in a similar manner to palmitate, via acetyl-CoA incorporation. Additionally, treatment with the ACC inhibitor ND646[28] led to a significant decrease in ^{13}C enrichment of both straight-chain FAs and mmBCFAs, indicating that their synthesis is dependent on malonyl-CoA from ACC (Fig. 1e).

Although cytosolic FASN is the predominant enzyme used for *de novo* lipogenesis in mammalian cells, mitochondrial FAS II has been proposed as a hypothetical route for mmBCFA synthesis in eukaryotes[29]. To determine whether the cellular location of mmBCFA synthesis differed from that of palmitate, we traced adipocytes with [3-^{2}H]glucose. Deuterium labeling on the third carbon of glucose specifically labels cytosolic NADPH via the oxidative pentose phosphate pathway but is lost in glycolysis and does not label citrate, acetyl-CoA, or mitochondrial NADPH (Fig. 1f)[30]. If a significant portion of mmBCFAs were synthesized within mitochondria, decreased ^{2}H enrichment relative to palmitate would be expected. We found that cytosolic NADPH effectively labeled both mmBCFAs and palmitate, suggesting that these FAs were primarily synthesized in the cytosol by FASN (Fig. 1g), albeit at slower rates than palmitate (Supplementary Fig. 1e,f). Next, we generated pooled cultures of 3T3-L1 adipocytes with CRISPR-Cas9-mediated FASN knockout (KO) before differentiation (Supplementary Fig. 2a-b). Though the abundance of all FAs decreased, mmBCFAs were undetectable in all FASN KO cells and abundant in sgNT cells (Fig. 1h). However, differentiation was significantly impaired (Supplementary Fig. 2c).

To further confirm that FASN deficiency rather than impaired differentiation and lack of substrate decreased BCFA synthesis, we supplemented cultures with the short branched-chain FAs isobutyrate, isovalerate, 2-methyl-butyrate, and propionate. Addition of these substrates increased

the abundance of mmBCFA and OCFA in a dose-dependent manner (Fig. 1i; Supplementary Fig. 1d-f). Whereas iso-C16:0 levels significantly increased in control adipocytes and in non-differentiated pre-adipocytes upon addition of isobutyrate, iso-C16:0 levels were still undetectable in FASN KO cells (Supplementary Fig. 2g), indicating that lack of FASN rather than impaired differentiation was the primary reason for the absence of BCFA synthesis. Furthermore, treatment with the FASN inhibitor TVB3166 significantly decreased the synthesis of both iso-C16:0 and palmitate (Supplementary Fig. 2h). Although the mitochondrial FAS II system may also contribute to mmBCFA synthesis, our results demonstrate that cytosolic *de novo* lipogenesis via FASN promiscuity is the primary driver of mmBCFA production in adipocytes[31].

3.4.2 BCAA catabolic intermediates drive mmBCFA synthesis

The minor impact of B12 availability on iso-C16:0 and iso-C17:0 suggests that these FAs are not synthesized via elongation of methylmalonyl-CoA. Administration of radioisotopes in rats has indicated that BCAAs are precursors for mmBCFAs in skin[32]. In addition, provision of isovaleryl-CoA, isobutyryl-CoA or 2-methylbutyryl-CoA to enzyme extracts from rat epididymal tissue results in the production of mmBCFAs[31]. To confirm that this pathway architecture exists within intact adipocytes, we cultured adipocytes with uniformly ^{13}C-labeled BCAAs and quantified labeling via GC-MS. This resulted in distinct labeling patterns for each of their respective mmBCFAs (Fig. 2a-d). Carbon from [U-$^{13}C_5$]valine was only incorporated into iso-C16:0 and resulted in a prominent M + 4 peak in the isotopologue distribution, indicating that the valine catabolic intermediate isobutyryl-CoA was used to synthesize iso-C16:0 (Fig. 2a,b). Similarly, iso-C17:0 from [U-$^{13}C_6$]leucine and anteiso-C17:0 from [U-$^{13}C_6$]isoleucine exhibited distinct M + 5 shifts, indicating that isovaleryl-CoA and 2-methylbutyryl-CoA were used for mmBCFA synthesis (Fig. 2a,c,d). Notably, we detected no FA isotopologues of M + 8 or M + 10, demonstrating that only a single incorporation of these branched intermediates into the acyl chain was occurring in these cells. This result, combined with the observation that only mmBCFAs with

a branch at the penultimate or antepenultimate end were detected, supports a mechanism whereby FASN is promiscuous and can use short acyl-CoAs to initiate synthesis of long-chain FAs.

Multiple acyl-CoA dehydrogenases (ACAD) are annotated to carry out the dehydrogenations of isovaleryl-CoA, 2-methylbutyryl-CoA, and isobutyryl-CoA. To evaluate the specific roles of these enzymes in BCAA catabolism and mmBCFA synthesis, we targeted various ACAD enzymes via shRNA-mediated knockdown and quantified FA abundances after adipocyte differentiation (Supplementary Fig. 3a-c). Knockdown of ACAD8, IVD and ACADSB specifically and significantly increased levels of iso-C16:0, iso-C17:0 and anteiso-C17:0, respectively (Fig. 2e-g; Supplementary Fig. 3d-f). Targeting of ACADM and ACADS did not impact mmBCFA levels appreciably. Each mmBCFA accumulated differently, with valine-derived iso-C16:0 having the highest abundance (Fig. 1a; Supplementary Fig. 3d), inversely consistent with the relative expression of each dehydrogenase (Fig. 2h). These findings indicate that ACAD enzyme expression influences the metabolic fate of BCAAs and mmBCFA production.

3.4.3 mmBCFAs are incorporated into distinct lipid species

The above data are representative of total hydrolyzed FA pools in the cell. To further characterize the metabolic fate of mmBCFAs, we next sought to determine whether mmBCFAs were incorporated into distinct lipid species. Distinguishing lipids containing different acyl chain isomers such as iso-C16:0 and C16:0 (palmitate) with liquid chromatography is challenging because of the decreased isomer resolution compared to gas chromatography, and there have been limited reports of mmBCFAs in specific, intact lipids[11, 33]. To circumvent this issue we used [U-$^{13}C_5$]valine tracing to differentiate lipids containing C16:0 versus iso-C16:0 acyl-chains, as lipids synthesized with the latter would contain distinct M + 4 peaks (Supplementary Fig. 4a-c). We quantified M + 0 and M + 4 isotopologue abundances using targeted LC-MS/MS in 46 lipid species containing 16-carbon acyl chains in adipocytes cultured with [U-$^{13}C_5$]valine or [^{12}C]valine. Of those measured species, 11 lipids had significant enrichment of M + 4 ions in

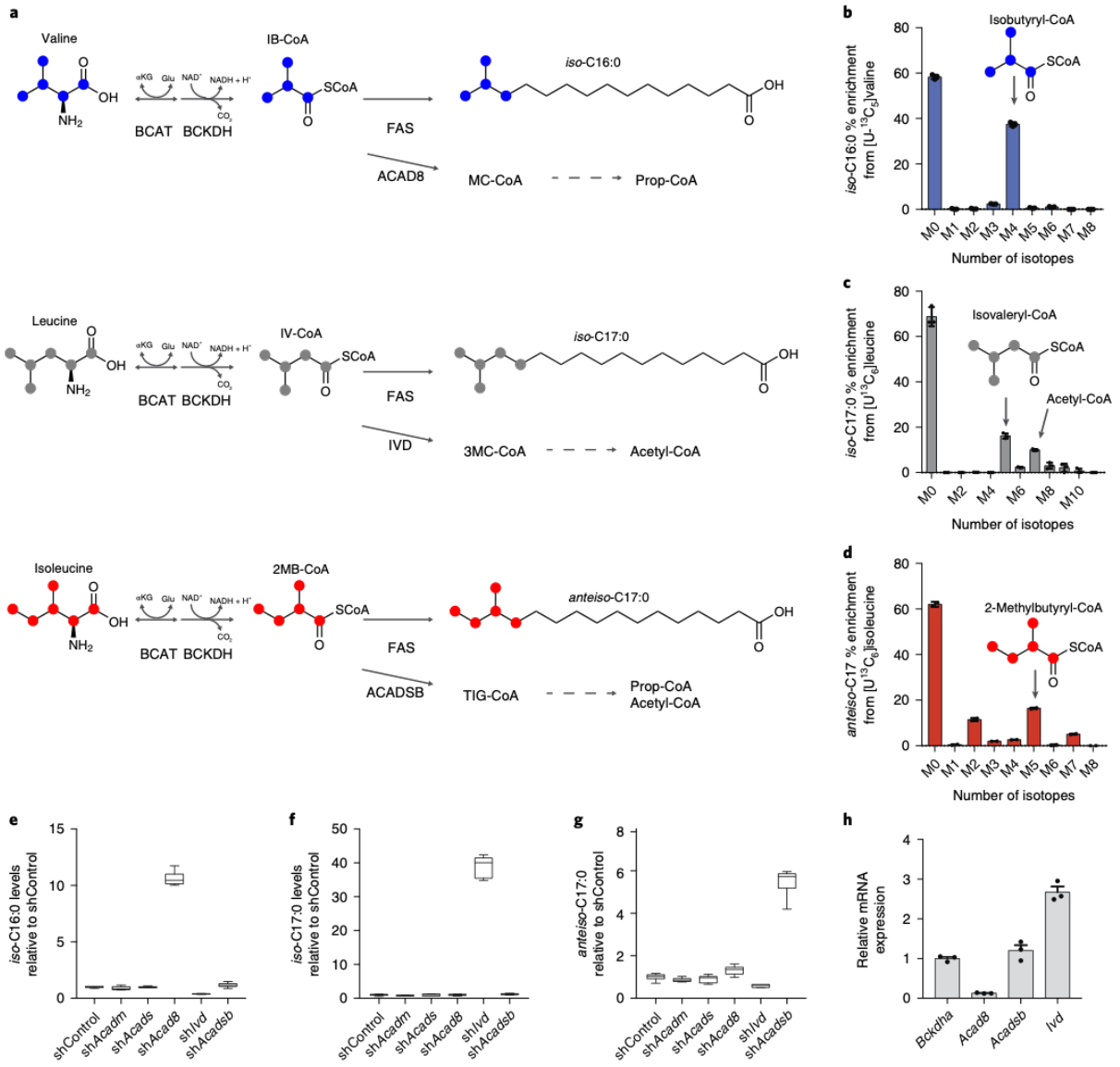

Figure 3.2: **BCAA catabolic intermediates drive mmBCFA synthesis. a**. Pathway depicting BCAA catabolism and mmBCFA synthesis. **b-d**. Isotopologue distributions of **b**, iso-C16:0 from [U-$^{13}C_5$]valine, **c**, iso-C17:0 from [U-$^{13}C_6$]leucine, and **d**, anteiso-C17:0 from [U-$^{13}C_6$]isoleucine. Representative data from three cell replicates in **b-d**. **e-g**. Relative abundance of **e**, iso-C16:0, **f**, iso-C17:0, and **g**, anteiso-C17:0 following knock down of ACAD enzymes. Representative data from six cell replicates are shown in **e-g**. **h**. Relative mRNA expression. Representative data are shown from three cell replicates. All experiments were carried out in 3T3-L1 adipocytes. All experiments were repeated three independent times with similar results. Data in **b-d, h** are presented as means ± s.e.m. with dot plots overlaid. Data in **e-g** as or box (25th to 75th percentile with median line) and whiskers (min. to max. values).

[U-$^{13}C_5$]valine-traced cells over [^{12}C]valine-traced cells (Supplementary Fig. 4d,e). The highest percent of total enrichments was observed in species containing alkyl chains, suggesting that iso-C16:0 may be selectively incorporated into ether lipids. Notably, some BCFAs (for example, phytanic acid) must be trafficked to the peroxisome for α-oxidation, and peroxisomes are the site for ether lipid synthesis because of the presence of alkyl DHAP synthase and DHAPAT. As such, mmBCFAs may be similarly directed to the peroxisome, leading to the observed high enrichment in abundant alkyl-lipids. Other significantly enriched lipids included sphingomyelin, phosphatidylserine, phosphatidylcholine, phosphatidylinositol, and triacylglycerols (TAGs). In fact, induction of lipolysis via isoproterenol treatment resulted in significant mmBCFA secretion into culture medium, indicating that these FAs are present in lipid droplets (Supplementary Fig. 4f).

3.4.4 mmBCFAs are *de novo* synthesized *in vivo*

To determine whether mmBCFA synthesis occurs *in vivo*, we quantified the abundances of each mmBCFA across various tissues in male and female C57BL/6J mice. Consistent with our observation of mmBCFA synthesis in adipocytes, white and brown adipose tissues (WAT and BAT) exhibited the highest abundances of all mmBCFAs, including iso-C18:0, an elongated derivative of iso-C16:0 that was not detectable in 3T3-L1 cultures (Fig. 3a, b; Supplementary Fig. 5a,b). Liver and brain exhibited the lowest abundances of mmBCFAs, suggesting that FA composition is regulated in a tissue-specific manner. In addition, iso-C17:0 abundance differed between males and females, potentially because of hormonal effects on BCAA catabolism[34]. With the exception of anteiso-C17:0, total mmBCFAs (free and lipid bound) were present in plasma at micromolar concentrations (Supplementary Fig. 5c), and their abundances increased 2-3 fold in plasma upon prolonged fasting (Fig. 3c; Supplementary Fig. 5d). Although these measurements are of total rather than free FAs, these data suggest that iso-BCFAs are released from adipose tissue via lipolysis along with other FAs.

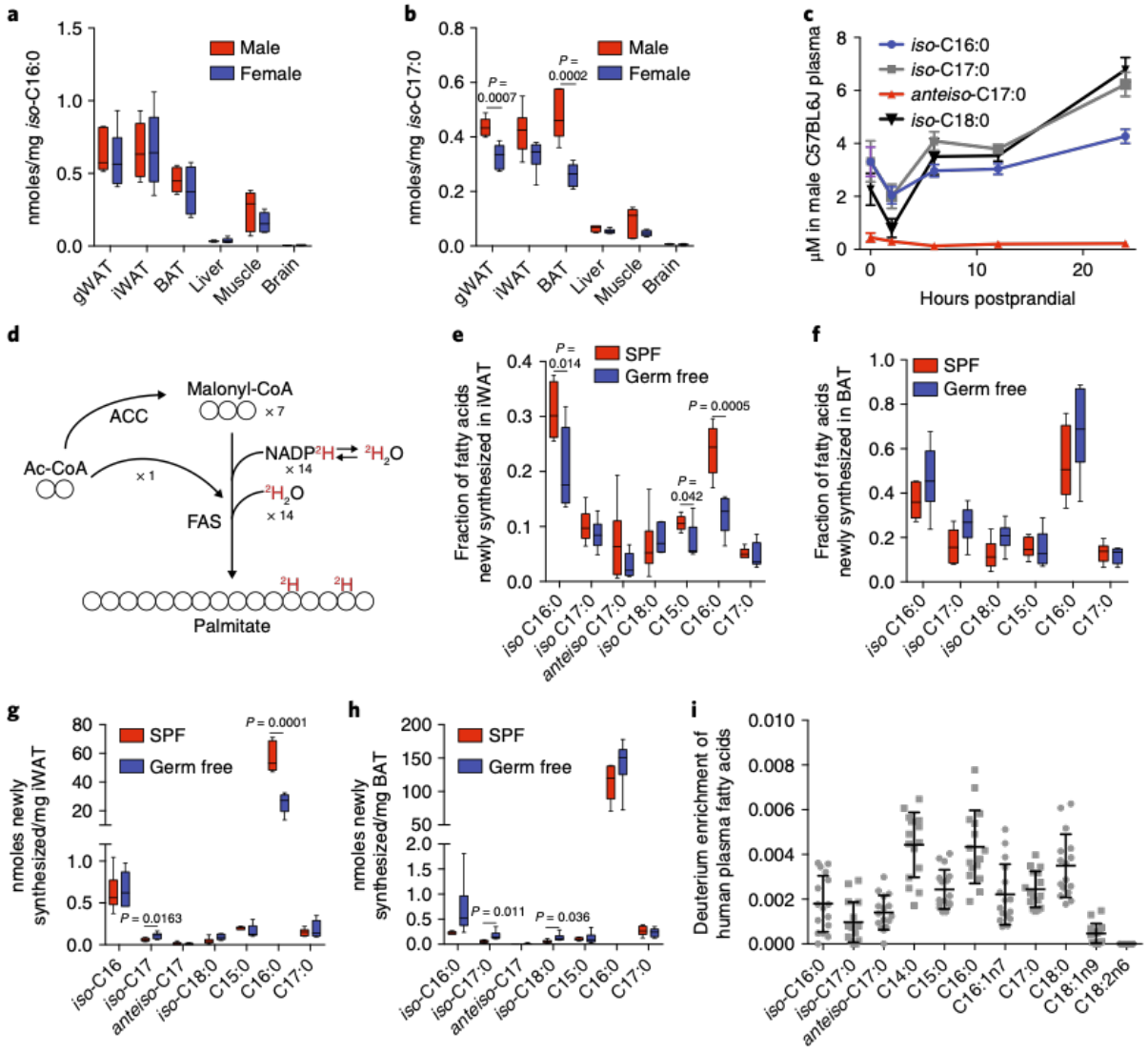

Figure 3.3: **mmBCFAs are *de novo* synthesized *in vivo*. a-b**. Abundance of **a**, iso-C16:0 and **b**, iso-C17:0 in various tissues from C57BL/6J male (n = 6) and female mice (n = 6). **c**. Plasma concentration of total hydrolyzed mmBCFAs from C57BL/6J male mice (n = 8) following removal of food at time 0 (7 a.m.), sampled at 2 h, 6 h, 12 h and 24 h. **d**. Incorporation of $^{2}H_2O$ into newly synthesized fatty acids. **e-f**. Fractional synthesis of fatty acids in **e**, iWAT and **f**, BAT of germ-free (n = 6) and SPF mice (n = 6). **g-h**. Amount of newly synthesized fatty acids present in **g**, iWAT and **h**, BAT of germ-free (n = 6) and SPF mice (n = 6). **i**. Deuterium enrichment of plasma FAs in NAFLD patients (n = 16) normalized to the area under the curve of plasma $^{2}H_2O$ levels from day 0 to day 21 for each patient. Two-tailed Student's t-test was performed for each comparison in this figure with no adjustment for multiple comparisons. Data are presented in **c** as means ± s.e.m., **i** as means ± s.d. with dot plots overlaid, or **a, b, e-h** as box (25th to 75th percentile with median line) and whiskers (min. to max. values).

As microbial metabolism is a source of both long and short BCFAs[35, 36] (Supplementary Fig. 6a), the gut microbiome could be a significant source of mmBCFAs in animals. In addition, mmBCFAs are present in chow (Supplementary Fig. 6b), and thus diet will also contribute to mmBCFA levels *in vivo*. To determine the relative contribution of *de novo* synthesis versus diet and the impact of microbiota on mmBCFA levels, we administered ^2H_2O to germ-free and specific pathogen-free (SPF) control mice for 8 d and measured enrichment of FAs in lipogenic tissues[37] (Fig. 3d). A significant fraction of the mmBCFAs present were newly synthesized in both germ free and SPF mice (Fig. 3e, f; Supplementary Fig. 6c,d). Valine-derived iso-C16:0 was the most abundantly synthesized mmBCFA (Fig. 3g, h; Supplementary Fig. 6e,f), and the fraction of newly synthesized iso-C16:0 was similar to that for palmitate (C16:0) in eWAT, iWAT and BAT (Fig. 3e, f; Supplementary Fig. 6c). Overall, these data indicate that *de novo* synthesis is a significant source of mmBCFAs in vivo, and their production can occur in the absence of microbiota. However, both levels (Supplementary Fig. 6g-j) and synthesis of mmBCFAs and other FAs differed significantly in the adipose tissues of germ-free and SPF mice, indicating that microbiota impacts lipogenesis and FA diversity.

To confirm that *de novo* synthesis of mmBCFAs occurs in humans, we analyzed plasma from NAFLD patients who were administered ^2H_2O (Supplementary Table 2 and Supplementary Fig. 6k,l). Analysis of deuterium enrichment of FAs demonstrated that both OCFAs and mmBCFAs were synthesized *de novo* in humans (Fig. 3i). Plasma mmBCFAs were present in the range of 1-20 μM in these patients (Supplementary Fig. 6m), comparable to those of other long and very long chain FAs such as C20:0 and C24:0[38].

3.4.5 BCAA flux to mmBCFAs is decreased by diet-induced obesity

Clinical studies have indicated that BCAA metabolism is dysregulated in the context of metabolic syndrome, as plasma BCAAs and some catabolites are elevated in insulin-resistant patients[1, 2]. Additionally, BCAA catabolic enzyme expression is decreased in rodents fed a high-

fat diet (HFD)[26]. Conversely, plasma mmBCFAs are decreased in morbidly obese patients[15]. To determine whether mmBCFA levels change in mouse models of obesity, we quantified total FAs in plasma and WAT of mice fed a HFD or low-fat diet (LFD) for 15 weeks. Although intake of all FAs (including mmBCFAs) was increased in the HFD cohort (Supplementary Fig. 7a), iso-BCFA abundances were significantly lower (Fig. 4a,b; Supplementary Fig. 7b-c). In terms of fold changes, valine-derived iso-C16:0 and iso-C18:0 were the most differentially abundant FAs in these tissues. Relative abundances of straight-chain FAs increased or remained unchanged, with the exceptions of C16:1 (palmitoleate) and C15:0 (Fig. 4a). Similar results were observed in ob/ob mice, in which mmBCFAs were significantly decreased in iWAT relative to control mice (Supplementary Fig. 7d). Notably, anteiso-C17:0 levels increase in the plasma of HFD mice (Fig. 4b). Given that synthesis of anteiso-C17:0 was nearly undetectable in $^{2}H_{2}O$ traced mice (Fig. 3g,h), this FA is primarily diet derived and synthesis from isoleucine is not significant *in vivo*. These results demonstrate that individual FAs change distinctly with the onset of obesity depending on their origin and metabolism.

To directly investigate altered BCAA catabolism in the context of metabolic syndrome, we fed C57BL/6J mice a HFD or LFD for 12 weeks and then identical diets formulated with 25% enriched [U-$^{13}C_5$,^{15}N]valine and [U-$^{13}C_6$,^{15}N]leucine for 3 weeks (Supplementary Fig. 8a). Although fasting plasma glucose levels were elevated (Supplementary Fig. 8b), plasma BCAA levels were unchanged (Supplementary Fig. 8c), consistent with recent studies in C57BL/6J mice[39], and we observed no differences in enrichment of plasma leucine and valine (Supplementary Fig. 8d). However, significant differences were present within tissues (Supplementary Fig. 8e,f). We detected significant ^{13}C enrichment of citrate and palmitate in all tissues measured (Fig. 4c,d), indicating that leucine catabolism is a significant source of acetyl-CoA *in vivo*. In the HFD cohort, ^{13}C enrichment and molar abundance in citrate and palmitate, respectively, were significantly decreased in all tissues, with BAT being the most impacted, demonstrating that diet-induced obesity decreases BCAA catabolism (Fig. 4c,d). The leucine- and valine-derived

mmBCFAs had characteristic mass shifts of M + 4 and M + 5, indicating that these FAs were synthesized *de novo* from BCAAs *in vivo* (Fig. 4e; Supplementary Fig. 8g,h). Importantly, molar enrichment of iso-BCFAs from valine and leucine were decreased in total FA pools from almost all tissues analyzed (Fig. 4f; Supplementary Fig. 8i,j). The highest abundances of newly synthesized, long-chain iso-BCFAs were present in BAT, although cross-tissue transport is likely significant given the high FA enrichments detected in muscle and heart. Collectively, these data indicate that diet-induced obesity significantly decreases BCAA catabolic flux, and a downstream result of this regulation is lower mmBCFA synthesis and abundance throughout the body.

In contrast to mmBCFAs, we did not detect a pronounced M + 3 shift in OCFAs (Supplementary Fig. 8k), consistent with the abundance of other propionate sources in animals (for example, gut microbes, OCFA oxidation, and cholesterol breakdown) or their production via α-oxidation[40]. Although valine is a source of propionate in cultured adipocytes, this pathway is not a major source of OCFAs *in vivo* under normal physiological conditions[6, 7]. However, we did note some incorporation of BCAA-derived carbon into OCFAs via acetyl-CoA (Supplementary Fig. 8l,m), indicating that OCFAs are also *de novo* synthesized to some extent *in vivo*.

3.4.6 Adipose tissue mmBCFA synthesis is facilitated by CrAT

The above results demonstrate that BCAA catabolic flux contributes significantly to *de novo* lipogenesis *in vivo*, and mmBCFAs are abundant products of this pathway. The large (approximately 10-fold) differences in abundance within liver and adipose tissues (Fig. 3a,b) suggest that mmBCFA synthesis is regulated distinctly in these tissues. To assess the impact of diet on tissue-specific mmBCFA synthesis and enable a comparison to synthesis of other FAs, we administered $^{2}H_2O$ to HFD and LFD mice and measured enrichment in lipogenic tissues. Newly synthesized iso-C16:0 and iso-C18:0 were decreased in livers of HFD mice more than any other FA in terms of fold-change (Fig. 5a). In contrast, straight-chain and monounsaturated

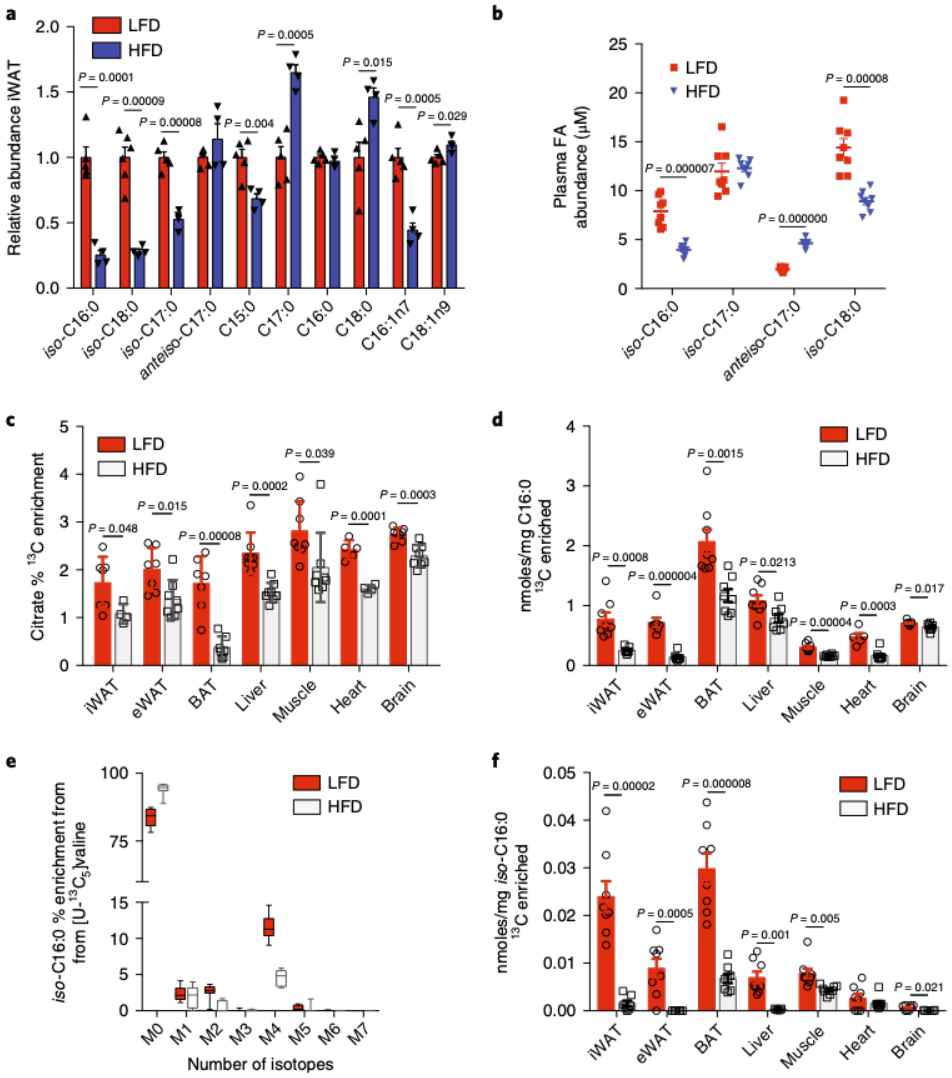

Figure 3.4: **BCAA flux to mmBCFAs is decreased by diet-induced obesity.** **a**. Relative abundances of FAs in iWAT from C57BL/6J mice fed a HFD (n = 4) or a LFD (n = 5) for 15 weeks. **b**. Total FA abundances in plasma from C57BL/6J mice fed a HFD (n = 8) or a LFD (n = 8) for 15 weeks. **c-f**. ^{13}C enrichment in specified metabolites from HFD or LFD fed mice with 25% of valine and leucine supplied as [U-^{13}C,^{15}N] isotope. **c**. Citrate percent ^{13}C enrichment. N = 8 for all comparisons except LFD iWAT (n = 7), eWAT (n = 7), BAT (n = 7), heart (n = 5) and HFD iWAT (n = 4), BAT (n = 7), heart (n = 4). **d**. ^{13}C molar enrichment of C16:0. N = 8 for all comparisons except LFD eWAT (n = 7), heart (n = 5) and HFD iWAT (n = 7). **e**. Isotopologue distribution of iso-C16:0 from [U-$^{13}C_5$]valine (HFD, n = 8; LFD, n = 8). **f**. ^{13}C molar enrichment of iso-C16:0. N = 8 for all comparisons except HFD iWAT (n = 7), liver (n = 5) and brain (n = 6). Two-tailed Student's t-test was performed for each comparison in this figure with no adjustment for multiple comparisons. Data are presented in **a-d, f** as means ± s.e.m. with dot plot overlaid or **e** as box (25th to 75th percentile with median line) and whiskers (min. to max. values).

FA synthesis in the liver was increased or remained the same (Fig. 5a; Supplementary Fig. 9a). Within adipose tissues, HFD feeding decreased lipogenesis of all FAs, indicating that pathway activity is generally suppressed (Fig. 5b; Supplementary Fig. 9b-d) as previously observed[41, 42]. We next estimated FA synthesis and turnover occurring in each tissue on the basis of the molar abundance of each FA, fraction synthesized, and length of time the tracer was administered. mmBCFA turnover was highest in white and brown adipose tissues but substantially lower in liver (Fig. 5c; Supplementary Fig. 9e-g). Though brown adipose tissue exhibited the highest synthesis and turnover for all FAs, these measurements are likely a lower estimate because they do not account for β-oxidation and futile FA cycling, which are likely quite high in brown adipocytes[19]. HFD suppressed the synthesis of all FAs in adipose tissues but increased palmitate synthesis and turnover in liver (Fig. 5d). These results suggest that subcutaneous and brown adipocytes exhibit a high capacity for mmBCFA synthesis when lipogenesis is active in these depots. Indeed, mmBCFA synthesis in brown adipose tissue is significantly increased in cold-exposed mice (Fig. 5e), similar to the increased *de novo* lipogenesis of other FAs[19].

Liver exhibited relatively low abundances of newly synthesized mmBCFAs compared to other lipogenic tissues, and these levels decreased further in response to HFD, which contrasts to the changes observed for other FAs in the liver. Importantly, this tracing method does not account for lipid efflux and intertissue FA transport, and thus likely underestimates absolute FA synthesis in liver. Nevertheless, our collective data on abundance and synthesis of all FAs strongly indicate that mmBCFAs are synthesized in adipose tissues but not liver.

BCAA catabolism and lipogenesis are highly active in liver, so we next attempted to address why mmBCFA synthesis is specific to adipose tissues. mmBCFA synthesis requires BCAA catabolic intermediates to be exported from the mitochondria into the cytosol for elongation by FASN. Prior studies have demonstrated that CrAT, but not carnitine palmitoyltransferase 2 (CPT2), exhibits enzyme activity toward BCAA-derived, short branched-chain-CoAs[43]. Therefore, we hypothesized that CrAT facilitates mmBCFA synthesis in adipose tissues. Crat mRNA

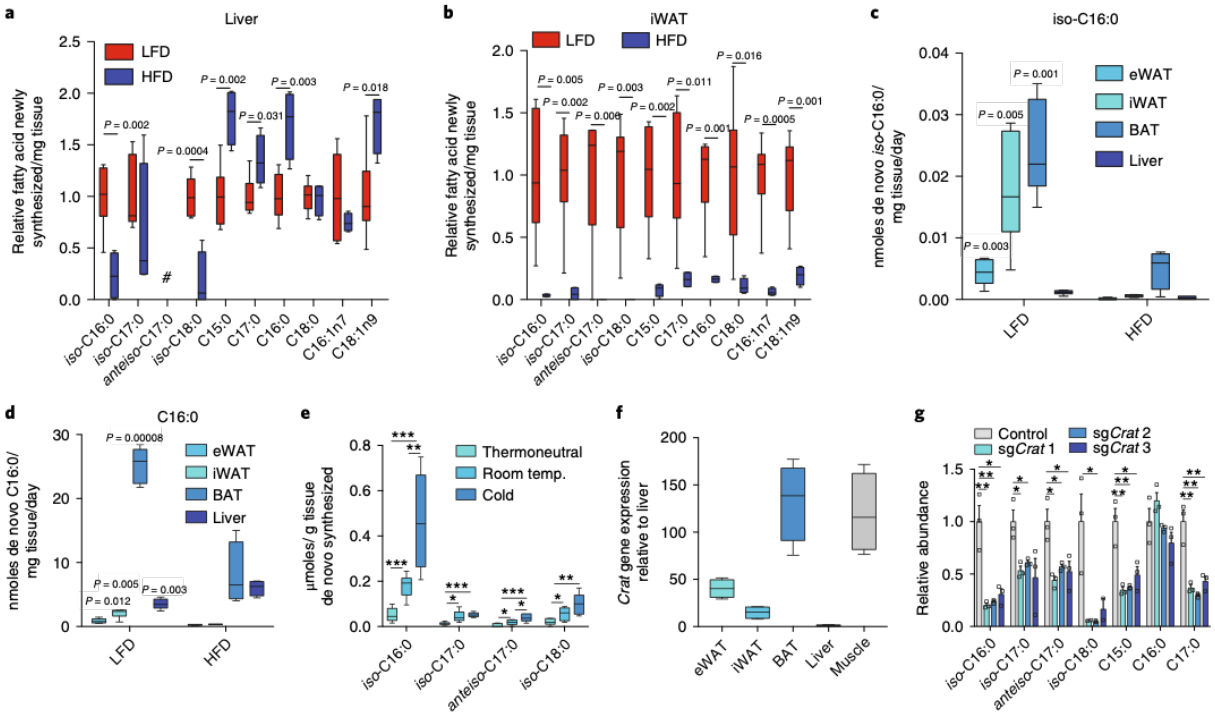

Figure 3.5: **Adipose tissue mmBCFA synthesis is facilitated by CrAT. a-b**. Fold difference in the levels of newly synthesized FAs present in **a**, liver and **b**, iWAT. LFD (n = 6) and HFD (n = 4) were compared in **a** and **b**. **c**. *De novo* lipogenic turnover of iso-C16:0 across the primary lipogenic tissues. **d**. *De novo* lipogenic turnover of C16:0 across the primary lipogenic tissues. LFD (n = 6) and HFD (n = 4) for all comparisons. P values indicate intra-tissue comparison between HFD and LFD. **e**. Amount of newly synthesized FAs in BAT of mice exposed to thermoneutral (30 °C), room temperature (22 °C), or acclimatized to severe cold (6 °C) over 1 month (n = 6 per group). **f**. Crat expression relative to liver in tissues from male C57BL/6J mice (n = 4). **g**. Relative abundance of total FAs in pooled CRISPR-Cas9 Crat KO 3T3-L1 adipocytes. Representative data from three cell replicates. Three independent infections have been carried out with the same result. Data is presented in **a-f** as box (25th to 75th percentile with median line) and whiskers (min. to max. values) or in **g** as means ± s.e.m. with dot plots overlaid. Two-tailed Student's t-test or 2-way ANOVA was performed for each comparison, as appropriate, in this figure with no adjustment for multiple comparisons. *P < 0.05, **P < 0.01, ***P < 0.001.

is expressed at low levels in liver but exhibits high expression in muscle and adipose tissues (Fig. 5f). Additionally, quantitative proteomics indicates that CrAT is expressed at higher levels in white and brown adipose tissue compared to liver and brain (Supplementary Fig. 10a)[44]. Thus, tissue-specific CrAT expression may be a driver of the observed differences in mmBCFA abundance and synthesis between liver, brain, and adipose tissues.

To more directly determine how CrAT influences mmBCFA synthesis, we generated CrAT KO 3T3-L1 cells using CRISPR-Cas9 (Supplementary Fig. 10b). In contrast to the results with FASN KO, CrAT KO did not appreciably impact adipogenesis (Supplementary Fig. 10c,d). However, CrAT KO adipocytes had significantly decreased levels of both mmBCFAs and OCFAs (Fig. 5g), with minimal differences in the levels of other FAs (Supplementary Fig. 10e). These data indicate that CrAT is an important component of the mmBCFA synthesis pathway, facilitating cytosolic export of precursor acyl-CoAs (Supplementary Fig. 10f). Differential expression of this enzyme in liver versus BAT and WAT likely contributes to the tissue specificity of mmBCFA synthesis and abundance.

3.4.7 Hypoxia suppresses BCAA catabolism and mmBCFA synthesis

Our data indicate that mmBCFAs are predominantly synthesized in adipose depots, and they decrease in the context of diet-induced obesity and increase in plasma during prolonged fasting. Given the adipose origin of mmBCFAs, we sought to determine the physiological factors that drive decreased BCAA catabolism and mmBCFA synthesis in obesity *in vivo*. Hypoxia has been proposed as a key contributory factor to adipose tissue dysfunction in obesity[45], and increasing adipose vascularization improves insulin sensitivity[46]. To test the impact of hypoxia on BCAA metabolism in adipocytes, we incubated differentiated 3T3-L1 adipocytes in 1% oxygen for 24 h before switching to hypoxia-equilibrated media containing uniformly ^{13}C-labeled amino acids or glucose for an additional 24 h. Intracellular BCAAs and α-ketoisocaproate accumulated significantly in hypoxic cultures along with lactate and

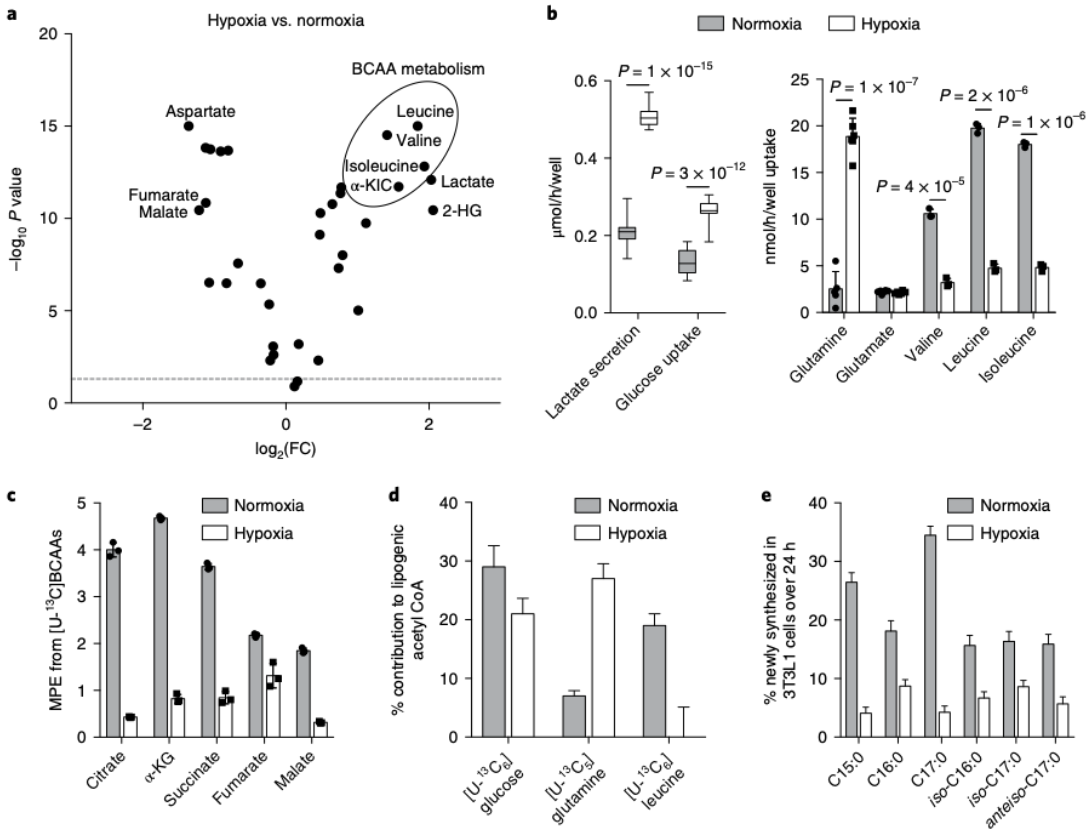

Figure 3.6: **Hypoxia suppresses BCAA catabolism and mmBCFA synthesis in adipocytes.** **a**. Volcano plot of changes in metabolite abundance in 3T3-L1 cells exposed to hypoxia (1% oxygen) or normoxia for 48 h. 12 cell replicates. **b**. Glucose and amino acid uptake by 3T3-L1 cells in hypoxia (1%) or normoxia. 14 cell replicates for lactate and glucose; 6 cell replicates for glutamine and glutamate; 3 cell replicates for leucine, isoleucine and valine. Two-tailed Student's t-test was performed for each comparison in **a** and **b** with no adjustment for multiple comparisons. **c**. Mole percent enrichment (MPE) of TCA intermediates from [U-^{13}C]BCAAs in 3T3-L1s following 24 h of tracing in hypoxia (1%) or normoxia. **d**. Relative contribution of different substrates to lipogenic acetyl-CoA in 3T3-L1s as determined by ISA following 24 h of tracing in hypoxia (1%) or normoxia. **e**. Percent of each FA newly synthesized over 24 h in hypoxia (1%) or normoxia. Three cell replicates are shown in **c-e**. All experiments were repeated three independent times with the same results. Data are presented in all panels as means ± s.e.m. with dot plots overlaid, with exception of **b**, in which data is presented as box (25th to 75th percentile with median line) and whiskers (min. to max. values), and **d-e** as mean ± 95% confidence interval.

2-hydroxyglutarate (Fig. 6a). Media analysis demonstrated that glycolytic flux increased along with net glutamine consumption, whereas BCAA uptake decreased approximately 3-4 fold (Fig. 6b). Consistent with these flux changes, TCA intermediate enrichment from [U-^{13}C]BCAAs was decreased under hypoxia (Fig. 6c). Isotopomer spectral analysis (ISA) demonstrated that the relative contribution of leucine to lipogenic acetyl-CoA decreased significantly, whereas the contribution of glutamine to FAs increased (Fig. 6d). Notably, hypoxia generally decreased the synthesis of FAs, including OCFAs and mmBCFAs (Fig. 6e). Collectively, these data indicate that hypoxia strongly decreases BCAA catabolism. These results were recapitulated in primary cells derived from various tissues, including murine brown adipocytes, human skeletal myotubes, and white adipocytes (Supplementary Fig. 11a). *Bckdha* and *Bcat2* mRNA and protein product were decreased under hypoxia in 3T3-L1 adipocytes (Supplementary Fig. 11b-d). Additionally, we observed that adipose tissue oxygen tension and arterial blood flow were specifically decreased in HFD mice along with BCKDHA protein levels (Supplementary Fig. 11e-g), corroborating previous findings in obese adipose tissue[26, 47]. Overall, these data indicate that adipose tissue in obese animals exhibits lower oxygen tension, which may contribute to the observed decreases in BCAA catabolism and the BCKDHA levels we observed in adipose tissue from HFD mice. In turn, decreased flux through this pathway decreases local and circulating iso-mmBCFA levels in obesity.

3.5 Discussion

Here, using in vitro and in vivo metabolic tracing, we define a cross-tissue metabolic pathway in which BCAA catabolic flux and the promiscuity of FASN and CrAT within brown and white adipose tissues support mmBCFA synthesis. Additionally, we demonstrate that mmBCFA turnover is suppressed by HFD and obesity-induced adipose hypoxia. Collectively, these results demonstrate that mmBCFAs are endogenous FAs produced by adipocytes that link mitochondrial

BCAA catabolism, lipogenesis, and diet to metabolic disease.

To date, the primary metabolic role of BCAA catabolism has been attributed to its importance as a nitrogen donor[48], to the production of HIBA to modulate FA uptake[49], and to the generation of branched acyl intermediates that can modulate enzyme function via post-translational modifications[50]. Our data add to this knowledge, linking BCAA catabolism to modulation of FA diversity via enzyme promiscuity. Interestingly, mmBCFAs are synthesized and present at low levels in liver despite the high abundance of BCKDH and rate of lipogenesis[51, 52]. We provide evidence that this difference is driven by differential expression of *Crat*, encoding an enzyme that has predominantly been studied in muscle, where it is thought to mitigate fatigue by facilitating acetyl-CoA consumption during exercise and preventing acetyl-CoA accumulation during rest[53], thus decreasing macronutrient-induced lysine acetylation of mitochondrial proteins[54]. However, its relevance in brown and white adipose tissues has not been explored, despite the high level of expression observed in brown adipose tissue[44]. Given recent evidence that branched acyllysine modifications also alter mitochondrial enzyme function[50], it is possible that diversion of branched CoA intermediates to long-chain FAs via CrAT is beneficial for maintaining healthy mitochondrial function.

We also highlight an underappreciated aspect of *de novo* lipogenesis, whereby the *de novo* FA composition reflects the balance of acyl-CoAs within the body. Thus, FASN promiscuity integrates changes in amino acid metabolism and short-chain FAs into the lipidome. Therefore, alterations in SCFA and acyl-CoA abundance driven by the gut microbiome, diet, or inborn errors of metabolism can influence FA diversity and must be considered when studying the pathophysiology of associated diseases. Indeed, elevated levels of mmBCFAs have been detected in the brains of patients with defects in cobalamin metabolism[27]. Supraphysiological levels of mmBCFAs could impact neuronal function and play a role in the neurological defects that occur in patients with certain organic acidemias or B12 deficiency. This work also highlights the limited resolution of most lipidomics platforms for resolving mmBCFA-containing lipids. We found that

mmBCFAs are incorporated into diverse lipid species by cultured adipocytes, including ether lipids, TAGs, and phospholipids. However, more extensive and focused approaches are needed to fully characterize their fates within different tissues.

Using ^{13}C-labeled leucine and valine chow, we observed that HFD feeding suppressed BCAA catabolism, resulting in decreased mmBCFA synthesis. This result is consistent with transcriptional and other flux-based measurements that indicate downregulation of this pathway in mouse models of obesity and in diabetic patients[26, 55]. In fact, mmBCFAs correlate negatively with metabolic disease biomarkers such as C-reactive protein and insulin resistance in patients[15, 16]. This contrasts with levels of BCAAs and their downstream catabolic intermediates, which increase in the plasma of insulin-resistant patients[1, 49]. However, BCAA levels did not increase in our model of diet-induced obesity, and thus mmBCFA levels did not correlate with BCAA levels as might be expected. This is presumably due to the adipose-specific origin of these FAs, as BCAAs are widely catabolized in energetically demanding tissues such as muscle, liver, heart and brain, which are not significant sources of mmBCFAs. Furthermore, turnover and abundance of BCAA is much greater than that of mmBCFA. Therefore, although mmBCFA synthesis is impacted by BCAA catabolic flux, differential mmBCFA production is unlikely to be a primary driver of BCAA accumulation in T2D patients. Nevertheless, mmBCFAs may be a strong biomarker of adipose tissue lipogenesis and BCAA catabolism, and, in contrast to circulating BCAA levels, are not overtly influenced by changes in protein turnover and muscle insulin resistance.

The functional consequences of decreased mmBCFA levels are unknown. Despite their abundance in tissues and presence at micromolar levels in plasma, mmBCFAs have been studied minimally in the context of mammalian biology. mmBCFA-containing lipids play critical roles in the postembryonic growth, neuronal development and the foraging behavior of C. elegans[11, 56]. In prokaryotes BCFAs influence membrane fluidity, and their abundances change in response to certain stresses[10, 35]. In mammalian biology, previous studies have suggested they influence

colon epithelial cell inflammation[57] and protect against necrotizing enterocolitis[58]. Our insights into the metabolic origins and fates of mmBCFAs suggest other potential functions. As mmBCFAs are primarily synthesized in adipose tissue, incorporated into TAGs, and increase in plasma during fasting, these lipids may be involved in nutrient sensing and signal to other tissues in the body. However, given the relatively low abundance of mmBCFAs, these FAs are unlikely to contribute significantly to energy storage or substrate oxidation and are more likely to play a role in signaling or membrane structure. Ultimately, understanding the factors that regulate mmBCFA physiology is an essential step in elucidating their function and contribution to the biological importance of the BCAA catabolic pathway.

3.6 Acknowledgements

This work was supported, in part, by US National Institutes of Health (NIH) grants R01CA188652 (C.M.M.), NIH R01CA172667 (D.K.N.), P01-HL110900 (P.C.) and R01-HL126945 (P.C.), a Searle Scholar Award (C.M.M.), a Camille and Henry Dreyfus Teacher-Scholar Award (C.M.M.), an NSF CAREER Award (#1454425 to C.M.M.), and an Ajinomoto Innovation Alliance Program Grant (C.M.M). The project was funded (in part) by a seed grant made available through the UC San Diego Larsson-Rosenquist Foundation Mother-Milk-Infant Center of Research Excellence (M.W). J.S.G. is supported by AHA award 18CDA34080527. This material is the result of work supported with resources and the use of facilities at the VA San Diego Medical Center. The contents do not represent the views of the US Department of Veterans Affairs or the United States Government. We would like to thank M. Gantner for helping with primary brown adipose tissue isolation and culture.

Chapter 3, in full, is a reprint of the material as it appears in "Enzyme promiscuity drives branched-chain fatty acid synthesis in adipose tissues," *Nature Chemical Biology*, vol. 14, 2018. Lindsay S. Roberts, Yujung Michelle Lee, Justin L. McCarville, Joan Sanchez-Gurmaches, Noah

Meurs, Jivani M. Gengatharan, Justin D. Hover, Susan A. Phillips, Theodore P. Ciaraldi, David A. Guertin, Pedro Cabrales, Janelle S. Ayres, Daniel K. Nomura, and Rohit Loomba were co-authors of this publication. Martina Wallace is the primary author of this publication. Courtney R. Green is the second author of this publication. Christian M. Metallo is the corresponding author of this publication.

3.7 References

1. Newgard, C. B., An, J., Bain, J. R., Muehlbauer, M. J., Stevens, R. D., Lien, L. F., Haqq, A. M., Shah, S. H., Arlotto, M., Slentz, C. A., Rochon, J., Gallup, D., Ilkayeva, O., Wenner, B. R., Yancy, W. S., Eisenson, H., Musante, G., Surwit, R. S., Millington, D. S., Butler, M. D. & Svetkey, L. P. A branched-chain amino acid-related metabolic signature that differentiates obese and lean humans and contributes to insulin resistance. *Cell Metab.* **9,** 311–26 (2009).

2. Wang, T. J., Larson, M. G., Vasan, R. S., Cheng, S., Rhee, E. P., Elizabeth, M., Lewis, G. D., Fox, C. S., Jacques, P. F., Fernandez, C., J, O. C., Carr, S. A., Mootha, V. K., Florez, J. C., Souza, A., Melander, O., Clish, C. B. & Gerszten, R. E. Metabolite profiles and the risk of developing diabetes. *Nat. Med.* **17,** 448–53 (2011).

3. Tönjes, M., Barbus, S., Park, Y., Wang, W., Schlotter, M., Lindroth, A. M., Pleier, S. V., Bai, A. H., Karra, D. & Piro, R. M. BCAT1 promotes cell proliferation through amino acid catabolism in gliomas carrying wild-type IDH1. *Nat. Med.* **19,** 901–908 (2013).

4. Overmyer, K., Evans, C., Qi, N., Minogue, C., Carson, J., Christopher J., C., Koch, L., Britton, S., Pagliarini, D., Coon, J. & Burant, C. Maximal Oxidative Capacity during Exercise Is Associated with Skeletal Muscle Fuel Selection and Dynamic Changes in Mitochondrial Protein Acetylation. *Cell Metab* **21,** 468–478 (2015).

5. Herman, M. A., She, P., Peroni, O. D., Lynch, C. J. & Kahn, B. B. Adipose tissue branched chain amino acid (BCAA) metabolism modulates circulating BCAA levels. *J. Biol. Chem.* **285,** 11348–56 (2010).

6. Crown, S., Marze, N. & Antoniewicz, M. Catabolism of Branched Chain Amino Acids Contributes Significantly to Synthesis of Odd-Chain and Even-Chain Fatty Acids in 3T3-L1 Adipocytes. *Plos One* **10** (2015).

7. Green, C. R., Wallace, M., Divakaruni, A. S., Phillips, S. A., Murphy, A. N., Ciaraldi, T. P. & Metallo, C. M. Branched-chain amino acid catabolism fuels adipocyte differentiation and lipogenesis. *Nat. Chem. Biol.* **12,** 15–21 (2016).

8. Ran-Ressler, R. R., Bae, S., Lawrence, P., Wang, D. H. & Brenna, J. Branched-chain fatty acid content of foods and estimated intake in the USA. *Br. J. Nutr.* **112,** 565–72 (2014).

9. Jenkins, B., West, J. & Koulman, A. A Review of Odd-Chain Fatty Acid Metabolism and the Role of Pentadecanoic Acid (C15:0) and Heptadecanoic Acid (C17:0) in Health and Disease. *Molecules* **20,** 2425–2444 (2015).

10. Mercier, R., Patricia, D. & Errington, J. Crucial Role for Membrane Fluidity in Proliferation of Primitive Cells. *Cell Reports* **1,** 417–423 (2012).

11. Kniazeva, M., Zhu, H., Sewell, A. & Han, M. A Lipid-TORC1 Pathway Promotes Neuronal Development and Foraging Behavior under Both Fed and Fasted Conditions in C. elegans. *Dev Cell* **33,** 260–271 (2015).

12. Gibson, R. & Kneebone, G. Fatty acid composition of human colostrum and mature breast milk. *Am. J. Clin. Nutr.* **34,** 252–7 (1981).

13. Grigor, M., Dunckley, G. & Purves, H. The synthesis of the branched-chain fatty acids of rat skin surface lipid. *Biochim. Biophys. Acta* **218,** 389–99 (1970).

14. Ran-Ressler, R. R., Devapatla, S., Lawrence, P. & Brenna, J. Branched Chain Fatty Acids Are Constituents of the Normal Healthy Newborn Gastrointestinal Tract. *Pediatr. Res.* **64,** 605–609 (2008).

15. Su, X., Magkos, F., Zhou, D., Eagon, J., Fabbrini, E., Okunade, A. & Klein, S. Adipose tissue monomethyl branched-chain fatty acids and insulin sensitivity: Effects of obesity and weight loss. *Obesity (Silver Spring)* (2014).

16. Mika, A., Stepnowski, P., Kaska, L., Proczko, M., Wisniewski, P., Sledzinski, M. & Sledzinski, T. A comprehensive study of serum odd- and branched-chain fatty acids in patients with excess weight. *Obesity* **24,** 1669–1676 (2016).

17. Gantner, M., Hazen, B., Eury, E., Brown, E. & Kralli, A. Complementary Roles of Estrogen-Related Receptors in Brown Adipocyte Thermogenic Function. *Endocrinology* **157,** 4770–4781 (2016).

18. Vacanti, N. M., Divakaruni, A. S., Green, C. R., Parker, S. J., Henry, R. R., Ciaraldi, T. P., Murphy, A. N. & Metallo, C. M. Regulation of substrate utilization by the mitochondrial pyruvate carrier. *Mol. Cell* **56,** 425–35 (2014).

19. Joan, S., Tang, Y., Jespersen, N., Wallace, M., Calejman, C. M., Gujja, S., Li, H., Edwards, Y. J. K., Wolfrum, C., Metallo, C. M., Nielsen, S., Scheele, C. & Guertin, D. A. Brown Fat AKT2 Is a Cold-Induced Kinase that Stimulates ChREBP-Mediated De Novo Lipogenesis to Optimize Fuel Storage and Thermogenesis. *Cell Metab* **27,** 195–209.e6 (2018).

20. Cabrales, P. & Tsai, A. Plasma viscosity regulates systemic and microvascular perfusion during acute extreme anemic conditions. *Am J Physiol-heart C* **291,** H2445–H2452 (2006).

21. Decaris, M., Li, K., Emson, C., Gatmaitan, M., Liu, S., Wang, Y., Nyangau, E., Colangelo, M., Angel, T., Beysen, C., Cui, J., Hernandez, C., Lazaro, L., Brenner, D., Turner, S., Hellerstein, M. & Loomba, R. Identifying nonalcoholic fatty liver disease patients with active fibrosis by measuring extracellular matrix remodeling rates in tissue and blood. *Hepatology* **65,** 78–88 (2017).

22. Fernandez, C. & Rosiers, D. C. Correction of 13C mass isotopomer distributions for natural stable isotope abundance. *Journal of mass spectrometry* (1996).

23. Young, J. D. INCA: a computational platform for isotopically non-stationary metabolic flux analysis. *Bioinformatics* (2014).

24. Lee, W., Bassilian, S., Ajie, H., Schoeller, D., Edmond, J., Bergner, E. & Byerley, L. In vivo measurement of fatty acids and cholesterol synthesis using D2O and mass isotopomer analysis. *Am. J. Physiol.* **266,** E699–708 (1994).

25. Louie, S., Grossman, E., Crawford, L., Ding, L., Camarda, R., Huffman, T., Miyamoto, D., Goga, A., Weerapana, E. & Nomura, D. GSTP1 Is a Driver of Triple-Negative Breast Cancer Cell Metabolism and Pathogenicity. *Cell Chem Biol* **23,** 567–578 (2016).

26. Lackey, D. E., Lynch, C. J., Olson, K. C., Mostaedi, R., Ali, M., Smith, W. H., Karpe, F., Humphreys, S., Bedinger, D. H., Dunn, T. N., Thomas, A. P., Oort, P. J., Kieffer, D. A., Amin, R., Bettaieb, A., Haj, F. G., Permana, P., Anthony, T. G. & Adams, S. H. Regulation of adipose branched-chain amino acid catabolism enzyme expression and cross-adipose amino acid flux in human obesity. *Am. J. Physiol. Endocrinol. Metab.* **304,** E1175–87 (2013).

27. Kishimoto, Y., Williams, M., Moser, H., Hignite, C. & Biermann, K. Branched-chain and odd-numbered fatty acids and aldehydes in the nervous system of a patient with deranged vitamin B 12 metabolism. *J. Lipid Res.* **14,** 69–77 (1973).

28. Svensson, R., Parker, S., Eichner, L., Kolar, M., Wallace, M., Brun, S., Lombardo, P., Nostrand, J., Hutchins, A., Vera, L., Gerken, L., Greenwood, J., Bhat, S., Harriman, G., Westlin, W., Jr, H., Saghatelian, A., Kapeller, R., Metallo, C. & Shaw, R. Inhibition of acetyl-CoA carboxylase suppresses fatty acid synthesis and tumor growth of non-small-cell lung cancer in preclinical models. *Nat Med* (2016).

29. Hiltunen, J., Schonauer, M., Autio, K., Mittelmeier, T., Kastaniotis, A. & Dieckmann, C. Mitochondrial Fatty Acid Synthesis Type II: More than Just Fatty Acids. *J Biol Chem* **284,** 9011–9015 (2009).

30. Lewis, C. A., Parker, S. J., Fiske, B. P., Douglas, M., Gui, D. Y., Green, C. R., Vokes, N. I., Feist, A. M., Vander Heiden, M. G. & Metallo, C. M. Tracing Compartmentalized NADPH Metabolism in the Cytosol and Mitochondria of Mammalian Cells. *Mol. Cell* (2014).

31. Horning, M., Martin, D. & Karmen, A. Fatty acid synthesis in adipose tissue II. Enzymatic synthesis of branched chain and odd-numbered fatty acids. *J Biol Chem* (1961).

32. Hirosuke, O., Noriyasu, Y., Junichi, N. & Isao, C. Precursor role of branched-chain amino acids in the biosynthesis of iso and anteiso fatty acids in rat skin. *Biochimica Et Biophysica Acta Bba - Lipids Lipid Metabolism* **1214,** 279–287 (1994).

33. Liu, L., Wang, Z., Park, H., Xu, C., Lawrence, P., Su, X., Wijendran, V., Walker, A. W., Kothapalli, K. & Brenna, T. J. Human fetal intestinal epithelial cells metabolize and incorporate branched chain fatty acids in a structure specific manner. *Prostaglandins Leukot Essent Fat Acids Plefa* **116,** 32–39 (2017).

34. Obayashi, M., Shimomura, Y., Nakai, N., Jeoung, N., Nagasaki, M., Murakami, T., Sato, Y. & Harris, R. Estrogen controls branched-chain amino acid catabolism in female rats. *J Nutrition* **134,** 2628–33 (2004).

35. Kaneda, T. Iso- and anteiso-fatty acids in bacteria: biosynthesis, function, and taxonomic significance. *Microbiology and Molecular Biology Reviews* **55,** 288–302 (1991).

36. Macfarlane, G., Gibson, G., Beatty, E. & Cummings, J. Estimation of short-chain fatty acid production from protein by human intestinal bacteria based on branched-chain fatty acid measurements. *Fems Microbiol Lett* **101,** 81–88 (1992).

37. Previs, S., David, M., Wang, S., Stout, S., Zhou, H., Herath, K., Shah, V., Miller, P., Wilsie, L., Jose, C., Johns, D., Cleary, M. & Roddy, T. New methodologies for studying lipid synthesis and turnover: Looking backwards to enable moving forwards. *Biochimica Et Biophysica Acta Bba - Mol Basis Dis* **1842,** 402–413 (2014).

38. Abdelmagid, S., Clarke, S., Nielsen, D., Badawi, A., Ahmed, E., Mutch, D. & Ma, D. Comprehensive Profiling of Plasma Fatty Acid Concentrations in Young Healthy Canadian Adults. *Plos One* **10,** e0116195 (2015).

39. Sailer, M., Dahlhoff, C., Giesbertz, P., Eidens, M. K., de Wit, N., Rubio-Aliaga, I., Boekschoten, M. V., Müller, M. & Daniel, H. Increased Plasma Citrulline in Mice Marks Diet-Induced Obesity and May Predict the Development of the Metabolic Syndrome. *PLOS ONE* **8,** 1–9 (May 2013).

40. Jenkins, B., Seyssel, K., Chiu, S., Pan, P., Lin, S., Stanley, E., Ament, Z., West, J., Summerhill, K., Griffin, J., Vetter, W., Autio, K., Hiltunen, K., Hazebrouck, S., Stepankova, R., Chen, C., Alligier, M., Laville, M., Moore, M., Kraft, G., Cherrington, A., King, S., Krauss,

R., Schryver, E., Veldhoven, P., Ronis, M. & Koulman, A. Odd Chain Fatty Acids; New Insights of the Relationship Between the Gut Microbiota, Dietary Intake, Biosynthesis and Glucose Intolerance. *Sci Rep-uk* **7,** srep44845 (2017).

41. Eissing, L., Scherer, T., Tödter, K., Knippschild, U., Greve, J., Buurman, W., Pinnschmidt, H., Rensen, S., Wolf, A., Bartelt, A., Heeren, J., Buettner, C. & Scheja, L. De novo lipogenesis in human fat and liver is linked to ChREBP-β and metabolic health. *Nat Commun* **4,** 1528 (2013).

42. Duarte, J., Carvalho, F., Pearson, M., Horton, J., Browning, J., Jones, J. & Burgess, S. A high-fat diet suppresses de novo lipogenesis and desaturation but not elongation and triglyceride synthesis in mice. *J Lipid Res* **55,** 2541–2553 (2014).

43. Violante, S., Lodewijk, I., Ruiter, J., Koster, J., Lenthe, H., Duran, M., Almeida, I., Wanders, R., Houten, S. & Ventura, F. Substrate specificity of human carnitine acetyltransferase: Implications for fatty acid and branched-chain amino acid metabolism. *Biochimica Et Biophysica Acta Bba - Mol Basis Dis* **1832,** 773–779 (2013).

44. Geiger, T., Velic, A., Macek, B., Lundberg, E., Kampf, C., Nagaraj, N., Uhlen, M., Cox, J. & Mann, M. Initial Quantitative Proteomic Map of 28 Mouse Tissues Using the SILAC Mouse. *Mol Cell Proteomics* **12,** 1709–1722 (2013).

45. Trayhurn, P., Wang, B. & Wood, I. Hypoxia in adipose tissue: a basis for the dysregulation of tissue function in obesity? *Brit J Nutr* **100,** 227–235 (2008).

46. Robciuc, M., Kivelä, R., Williams, I., de Boer, J., van Dijk, T., Elamaa, H., Feven, T., Molotkov, D., Leppänen, V., Käkelä, R., Eklund, L., Wasserman, D., Groen, A. & Alitalo, K. VEGFB/VEGFR1-Induced Expansion of Adipose Vasculature Counteracts Obesity and Related Metabolic Complications. *Cell Metab* **23,** 712–724 (2016).

47. Ye, J., Gao, Z., Yin, J. & He, Q. Hypoxia is a potential risk factor for chronic inflammation and adiponectin reduction in adipose tissue of ob/ob and dietary obese mice. *Am J Physiol-endoc M* **293,** E1118–E1128 (2007).

48. Mayers, J. R., Torrence, M. E., Danai, L. V., Papagiannakopoulos, T., Davidson, S. M., Bauer, M. R., Lau, A. N., Ji, B. W., Dixit, P. D., Hosios, A. M., Muir, A., Chin, C. R., Freinkman, E., Jacks, T., Wolpin, B. M., Vitkup, D. & Vander Heiden, M. G. Tissue of origin dictates branched-chain amino acid metabolism in mutant Kras-driven cancers. *Science* **353,** 1161–5 (2016).

49. Jang, C., Oh, S. F., Wada, S., Rowe, G. C., Liu, L., Chan, M., Rhee, J., Hoshino, A., Kim, B., Ibrahim, A., Baca, L. G., Kim, E., Ghosh, C. C., Parikh, S. M., Jiang, A., Chu, Q., Forman, D. E., Lecker, S. H., Krishnaiah, S., Rabinowitz, J. D., Weljie, A. M., Baur, J. A.,

Kasper, D. L. & Arany, Z. A branched-chain amino acid metabolite drives vascular fatty acid transport and causes insulin resistance. *Nat. Med.* **22,** 421–426 (2016).

50. Anderson, K., Huynh, F., Kelsey, F., Stuart, J., Peterson, B., Douros, J., Wagner, G., Thompson, J., Madsen, A., Green, M., Sivley, R., Ilkayeva, O., Stevens, R., Backos, D., Capra, J., Olsen, C., Campbell, J., Muoio, D., Grimsrud, P. & Hirschey, M. SIRT4 Is a Lysine Deacylase that Controls Leucine Metabolism and Insulin Secretion. *Cell Metab* **25,** 838–855.e15 (2017).

51. Hellerstein, M., Neese, R. & Schwarz, J. Model for measuring absolute rates of hepatic de novo lipogenesis and reesterification of free fatty acids. *Am. J. Physiol.* **265,** E814–20 (1993).

52. Shin, A., Fasshauer, M., Filatova, N., Grundell, L., Zielinski, E., Zhou, J., Scherer, T., Lindtner, C., White, P., Lapworth, A., Ilkayeva, O., Knippschild, U., Wolf, A., Scheja, L., Grove, K., Smith, R., Qian, W., Lynch, C., Newgard, C. & Buettner, C. Brain Insulin Lowers Circulating BCAA Levels by Inducing Hepatic BCAA Catabolism. *Cell Metab* **20,** 898909 (2014).

53. Seiler, S., Koves, T., Gooding, J., Wong, K., Stevens, R., Ilkayeva, O., Wittmann, A., Karen L., D., Davies, M., Lindeboom, L., Schrauwen, P., Vera B., S. & Muoio, D. Carnitine Acetyltransferase Mitigates Metabolic Inertia and Muscle Fatigue during Exercise. *Cell Metab* **22,** 65–76 (2015).

54. Davies, M., Kjalarsdottir, L., Thompson, J., Dubois, L., Stevens, R., Ilkayeva, O., Brosnan, M., Rolph, T., Grimsrud, P. & Muoio, D. The Acetyl Group Buffering Action of Carnitine Acetyltransferase Offsets Macronutrient-Induced Lysine Acetylation of Mitochondrial Proteins. *Cell Reports* **14,** 243–254 (2016).

55. Mardinoglu, A., Agren, R., Kampf, C., Asplund, A., Nookaew, I., Jacobson, P., Walley, A., Froguel, P., Carlsson, L., Uhlen, M. & Nielsen, J. Integration of clinical data with a genome-scale metabolic model of the human adipocyte. *Mol. Syst. Biol.* **9** (2013).

56. Kniazeva, M., Euler, T. & Han, M. A branched-chain fatty acid is involved in post-embryonic growth control in parallel to the insulin receptor pathway and its biosynthesis is feedback-regulated in C. elegans. *Gene Dev* **22,** 2102–2110 (2008).

57. Yan, Y., Wang, Z., Greenwald, J., Kothapalli, K., Park, H., Liu, R., Mendralla, E., Lawrence, P., Wang, X. & Brenna, J. BCFA suppresses LPS induced IL-8 mRNA expression in human intestinal epithelial cells. *Prostaglandins Leukot Essent Fat Acids Plefa* **116,** 27–31 (2017).

58. Ran-Ressler, R. R., Khailova, L., Arganbright, K. M., Adkins-Rieck, C. K., Jouni, Z. E., Koren, O., Ley, R. E., Brenna, J. T. & Dvorak, B. Branched Chain Fatty Acids Reduce the

Incidence of Necrotizing Enterocolitis and Alter Gastrointestinal Microbial Ecology in a Neonatal Rat Model. *PLOS ONE* **6,** 1–10 (Dec. 2011).

Chapter 4

Altered branched-chain amino acid catabolism drives distinct changes in the TCA cycle and lipidome

4.1 Abstract

Adipocytes upregulate branched-chain amino acid (BCAA) catabolism during differentiation, but the biological function of this tissue-specific metabolic activity is not clear. In this study, we sought to understand how BCAA catabolism and associated branched-chain fatty acid (BCFA) and odd-chain fatty acid (OCFA) synthesis affects intermediary metabolism and lipidome composition. Using CRISPR/Cas9 gene-editing, we generated branched-chain ketoacid dehydrogenase, subunit alpha (*Bckdha*) deficient pre-adipocytes and acyl-CoA dehydrogenase 8 (*Acad8*) deficient pre-adipocytes and studied their metabolism after differentiation. *Bckdha* deficiency essentially prevented BCAA-derived acetyl-CoA from entering the tricarboxylic acid (TCA) cycle but did not impact expression of differentiation markers or responsiveness to insulin. However, basal and maximal oxygen consumption rate were reduced. In response to *Bckdha* deficiency, but not

Acad8 deficiency, 3T3-L1 adipocytes reduced lactate secretion and increased the contribution of glucose into mitochondrial metabolism and lipogenesis. *Bckdha* deficiency dramatically reduced intracellular OCFA and BCFA levels and greatly impacted the lipidome of adipocytes, including reduction of OCFA-containing triacylglyceride species and overall diacylglyceride and lysophosphatidylethanolamine levels. Polyunsaturated fatty acid (PUFA)-containing sphingomyelin also decreased, while PUFA-containing phospholipids increased, indicating a potential reorganization of acyl chains between lipid species. Overall, these results identify novel molecular impacts resulting from *Bckdha* deficiency in adipocytes.

4.2 Introduction

The branched-chain amino acids (BCAAs) leucine, isoleucine, and valine are essential amino acids used for protein biosynthesis that can also be catabolized through a series of reactions to acetyl-CoA and propionyl-CoA. BCAA catabolism is highly upregulated during the initial stages of adipocyte differentiation[1–5]. Recent studies conclude that elevated BCAA levels are indicative of metabolic syndrome[6, 7] and even cancer[8–10]. Catabolism of BCAAs begins with BCAT, which transfers the amino nitrogen to α-ketoglutarate yielding glutamate and a corresponding branched-chain α-keto acids (BCKA). These BCKAs are acted upon by the branched-chain ketoacid dehydrogenase (BCKD) complex, a highly regulated, rate-limiting step in BCAA catabolism, which decarboxylates the BCKA, covalently adds a coenzyme A moiety, and yields a short branched-chain fatty acyl-CoA (SBCFA-CoA). Depending upon the SBCFA-CoA, a member of the Acad family of enzymes catalyzes the next catabolic step. Alternatively, SBCFA-CoAs can be exported to the cytosol by carnitine acyltransferase (CrAT) and elongated by fatty acid synthase (FASN) to form full-length iso- or anteiso-monomethyl branched-chain fatty acids (BCFAs)[11].

Alterations to BCAA availability and metabolism define certain Mendelian disorders

such as maple syrup urine disease (MSUD) and is hypothesized to contribute to the pathogenesis of more complex diseases such as autism and diabetes[12, 13]. In MSUD, patients have very little BCKDH complex activity, essentially blocking catabolism of all 3 BCAAs, resulting in elevated levels of these and BCKAs[14]. MSUD, left untreated, can cause mental retardation, failure to thrive, coma, and death as quickly as within the first weeks of life and even with dietary interventions, MSUD patients often show chronic neuropsychological problems[14, 15]. Inborn errors of metabolism also exist in the Acad family of enzymes, such as isobutyryl-CoA dehydrogenase deficiency (IBDD). IBDD is caused by mutations in *Acad8* which prevents complete valine catabolism. In contrast to MSUD, IBDD is often asymptomatic in infants and not always diagnosed at all as the biomarker, C4-carnitine, is not tested globally in newborns[16]. Patients with MSUD, in contrast to IBDD, are deficient in BCFAs.

BCFAs are present in most tissues in mammals with the highest levels found in skin[17], vernix[18], and breast milk[19]. Their abundance is recognized as a biomarker for obesity and metabolic syndrome[11, 20] and interventions such as gastric bypass surgery increase their abundance[20, 21].

We sought to build upon the previous two chapters and functionally interrogate the BCAA pathway further by inducing deficiencies in *Bckdha* and *Acad8* using CRISPR/Cas9 to model MSUD and IBDD, respectively, in 3T3-L1 adipocytes. The BCAA catabolic pathway, particularly in these cells, connects strongly to the *de novo* lipogenesis pathway as BCAA-derived AcCoA, propionyl-CoA (PropCoA), and SBCFAs are used to synthesized even-, odd-, and branched-chain fatty acids. Here, using stable isotope tracing and mass spectrometry, we show that impairment of BCAA catabolism is compensated by increased glucose catabolism. We also show that defective BCAA catabolism affects the lipidome via changes in the total abundance of some lipid species and the distribution of saturated and polyunsaturated fatty acids.

4.3 Materials and Methods

4.3.1 Cell culture and differentiation

All reagents were purchased form Sigma-Aldrich unless otherwise noted. All media and sera were purchased from Life Technologies unless otherwise stated. Mouse 3T3-L1 pre-adipocytes were purchased from the American Type Culture Collection and cultured in high glucose Dulbecco's modified Eagle medium (DMEM) (Life Technologies) supplemented with 10% bovine calf serum (BCS) below 70% confluence. Cells were regularly screened for mycoplasma contamination. For differentiation, 10,000 cells/well were seeded onto 12-well plates and allowed to reach confluence (termed Day -1). On Day 0, differentiation was induced with 0.5 mM 3-isobutyl-1-methylxanthine (IBMX), 0.25 μM dexamethasone, and 1 μg/ml insulin in DMEM containing 10% FBS. Medium was changed on Day 3 to DMEM + 10% FBS with 1 μg/ml insulin. Day 6, and thereafter, DMEM + 10% FBS was used. Cobalamin (500 nM) was supplemented to cultures when noted.

Isotope tracing was carried out 7d post-induction of differentiation. Cells were incubated in custom DMEM (Hyclone) in which the metabolite specified was replaced with the ^{13}C-labeled version for 24h unless otherwise specified. For short-chain fatty acid addition experiments, individual short-chain fatty acids were added to the media at a concentration of 0.5mM per SBCFA (1.5mM total) on day 3 and day 6, after which extractions were performed as described below. Fatty acids were then either calculated as percent total fatty acids and normalized to control conditions or normalized to [$^{2}H_{31}$]Palmitate internal standard and normalized to control conditions.

4.3.2 Generation of lentiviral CRISPR/Cas9 KO 3T3-L1 adipocytes

Control, Bckdha, and Acad8 target sequences (Supplementary Table 1) were cloned into the lentiCRISPRv2 plasmid, a gift from Feng Zhang (Addgene plasmid #52961)[22]. Se-

quences are summarized in Supplementary Table 1. For lentivirus production, 2-2.5 million HEK293FT cells were placed in 10cm tissue culture plates in 2mL of DMEM (containing 1% penicillin/streptomycin, 10% FBS). 24h later, transfection was performed using Lipofectamine 3000 (Invitrogen) with 1.3μg VSV.G/PMD2.G, 5.3μg of lenti-gag/pol/PCMVR8.2 and 4μg of lentiviral vector. Lentivirus-containing supernatants were harvested 48 and 72h later, combined, and concentrated using Amicon Ultra-15 centrifugal filters, 100,000 NMWL (Millipore) following the manufacturer's protocol. 3T3-L1 pre-adipocytes were infected with 7μL of concentrated virus in 2mL of medium containing 7.5μg of polybrene in a 35mm cell culture dish. Media was changed the following day and allowed to recover for 24h. Selection was performed using 2μg/mL puromycin. Cells were then plated to 12-well plates for differentiation as described above. Puromycin was removed from the medium beginning on day 0 of differentiation.

4.3.3 Western Blots

3T3-L1 adipocytes were lysed in ice-cold RIPA buffer with 1x protease inhibitor (Sigma-Aldrich). 25μg total protein was separated on a 10% SDS-PAGE gel for BCKDHA and β-actin, while 50μg total protein was loaded for ACAD8. The proteins were transferred to a nitrocellulose membrane and immunoblotted with anti-BCKDHA (Novus Biologicals NBP1-79616) (1:2,500 dilution), anti-β-Actin (Cell Signaling 4970S) (1:10,000), anti-ACAD8 (Aviva Systems Biology OAAB06085) (1:1,000 dilution). Specific signal was detected with horseradish peroxidase-conjugated secondary antibody goat anti-rabbit (1:2,500-1:10,000) using SuperSignal West Pico Chemiluminescent Substrate (Thermo Scientific) and developed using Blue Devil Autoradiography film (Genesee Scientific) or Bio-Rad Chemidoc XRS+ Imaging device.

4.3.4 Insulin-stimulated glucose uptake

Differentiated 3T3-L1 adipocytes were insulin-starved for 6h in 5mM glucose DMEM + 0.5% FBS. Cells were then glucose-starved in Kreb's Ringer Buffer (KRB) + 1.26g/L sodium bicarbonate for 1h. Cells were then incubated in 0.5mL 5mM glucose KRB + 5μCi 2-[1,2-^{3}H(N)]Deoxy-D-glucose $\pm$ 100nM insulin for 10 minutes unless otherwise stated. Cells were washed 3x in ice-cold PBS and lysed with 200μL 0.1M NaOH. Sample was neutralized with 200μL 0.1M HCl. 200μL of sample was mixed with 500μL Ultimate Gold liquid scintillation counter fluid (PerkinElmer) and read in a 24-well plate using a Perkin Elmer-Wallac 1450-021 scintillation counter running MicroBeta Workstation Software version 3.2.

4.3.5 Insulin-stimulated glucose metabolism

Differentiated 3T3-L1 adipocytes were insulin-starved for 6h in 5mM glucose DMEM + 0.5% FBS. Cells were then glucose-starved in Kreb's Ringer Buffer (KRB) + 1.26g/L sodium bicarbonate for 1 hour. Cells were labeled using 0.5mL 5mM [U-$^{13}C_6$]glucose KRB $\pm$ 100nM insulin for 10 minutes before extraction for GC-MS analysis.

4.3.6 Extraction of metabolites for GC-MS analysis

For cell culture, polar metabolites and fatty acids were extracted using methanol/water/chloroform with [$^{2}H_{31}$]palmitate and norvaline as lipid and polar internal standards, respectively, and analyzed as previously described [3, 23]. Briefly, cells were washed twice with saline, quenched with -80°C methanol and 4°C water containing norvaline, scraped into Eppendorfs, and extracted with chloroform containing [$^{2}H_{31}$]Palmitate. After centrifugation, phases are dried separately. Samples are stored at -20°C before analysis by GC-MS.

4.3.7 Extraction of lipids for LC-MS/MS analysis

Lipid extraction was carried out using a Folch-based methanol/chloroform/saline extraction at a ratio of 1:2:1 with the inclusion of 10nmol C12:0 dodecylglycerol, 10nmol [$^2H_{31}$]palmitate, 0.1nmol [$^2H_7$]DHCer, 0.2nmol [$^2H_7$]Cer, 0.1nmol [$^2H_7$]lactosyl-Cer, 0.1nmol [$^2H_7$]glycosyl-Cer, 0.01nmol [$^2H_7$]glucosyl-SO, 0.2nmol [$^2H_7$]SO, 0.02nmol [$^2H_7$]SA, 0.002nmol [$^2H_9$]deoxy-SA, 0.4nmol [$^2H_9$]SM as internal standards. 2 wells of a 12-well plate were combined to form 1 sample. The methanol phase was washed a second time with chloroform after addition of 3μL formic acid. Chloroform phase was dried under nitrogen gas at room temperature.

4.3.8 GC-MS analysis

Dried polar metabolites were derivatized in 2% (w/v) methoxyamine hydrochloride (Thermo Scientific) in pyridine and incubated at 37°C for 60 min. Samples were then silylated with N-tertbutyldimethylsilyl-N-methyltrifluoroacetamide (MTBSTFA) with 1% tert-butyldimethylchlorosilane (tBDMCS) (Regis Technologies) at 37°C for 30 min. Polar derivatives were analyzed by GC-MS using a DB-35MS column (30m x 0.25mm i.d. x 0.25μm, Agilent J&W Scientific) installed in an Agilent 7890B gas chromatograph (GC) interfaced with an Agilent 5977A mass spectrometer (MS) with an XTR ion source. The dried lower chloroform phase was derivatized to form fatty acid methyl esters (FAMEs) via addition of 500μL 2% H_2SO_4 in MeOH and incubation at 50°C for 2h. FAMEs were extracted via addition of 100μL saturated salt solution and 2 500μL hexane washes. These were analyzed using a Select FAME column (100m x 0.25mm i.d.) installed in an Agilent 7890A GC interfaced with an Agilent 5975C MS. Temperature programs are described previously [11]. The percent isotopologue distribution of each fatty acid and polar metabolite was determined and corrected for natural abundance using in-house algorithms adapted from Fernandez et al. [24]. Mole percent enrichment (MPE) was calculated via the following

equation:

$$\frac{\sum_{i=1}^{n} M_i \cdot i}{n}$$

where n is the number of carbon atoms in the metabolite and M_i is the relative abundance of the i^{th} mass isotopomer.

4.3.9 LC-MS/MS analysis

2 LC-MS/MS methods were run. The first was for broad lipidomics. Mobile phase A was composed of a 95:5 ratio of water:methanol, and mobile phase B consisted of isopropanol, methanol, and water in a 60:35:5 ratio. Solvent modifiers 0.1% formic acid with 5mM ammonium formate were used to assist ion formation and to improve the LC resolution in positive ionization mode. The flow rate for each run started at 0.1mL/min for 5 min to alleviate backpressure associated with injecting chloroform. The gradient started at 0% B and increased linearly to 100% B over the course of 45 min with a flow rate of 0.4mL/min, followed by an isocratic gradient of 100% B for 17 min at 0.5mL/min before equilibrating for 8 min at 0% B with a flow rate of 0.5mL/min. Chromatography was performed on an Agilent 1260 Infinity II HPLC using a Luna reverse-phase C5 column (50 x 4.6mm, with 5-μm-diameter particles; Phenomenex). MS analysis was performed with an electrospray ionization (ESI) source on an Agilent 6460C QQQ. The capillary voltage was set to 3.0kV, and the fragmentor voltage was set to 100V. The drying gas temperature was 350°C, the drying gas flow rate was 10L/min, and the nebulizer pressure was 35psi. Retention times were determined via analysis of a representative lipid species within each lipid class and typical retention time shifts were relied upon for identifying species with longer or more unsaturated acyl chains. Relative quantitation was performed by integrating the area under the curve and normalizing to internal standards. Where the normalized pool composition change is reported, the percentage of each category of lipid species within the lipid class is determined and then normalized to sgControl condition. Due to the ionization pattern, more detailed acyl

chain compositions were obtainable for some lipids. See Supplementary Table 2 for more detail.

The second method was used to obtain ceramide and sphingoid base measurements using an Agilent 1290 Infinity II HPLC coupled to an Agilent 6460 QQQ. Ceramides were separated on C8 column (Spectra 3ÂţmC8SR 150 x 3mm ID, Peeke Scientific) as previously described[25]. Mobile phase A was composed of 100% HPLC grade water containing 2 mM ammonium formate and 0.2% formic acid and mobile phase B consisted of 100% methanol containing 0.2% formic acid and 1 mM ammonium formate. The gradient elution program consisted of holding at 82% B for 3 min, up to 90% B over 1 min and linearly increasing to 99% B over 14 min maintaining it for 7 min and down to 82% B over 2 min. The 82% mobile phase B was maintained for 3 min followed by re-equilibration for 10 min. The capillary voltage was set to 3.5 kV, the drying gas temperature was 350°C, the drying gas flow rate was 10L/min, and the nebulizer pressure was 60psi. Ceramide species were analyzed by SRM of the transition from precursor to product ions at associated optimized collision energies and fragmentor voltages (Supplemental Table 3). All species were normalized to their most similar internal standards with deoxyceramide normalized to internal ceramide standards.

4.3.10 Isotopomer spectral analysis (ISA) of fatty acids

Mass isotopomer distributions were determined by integrating metabolite ion fragments and correcting for natural abundance using in-house algorithms as previously described [3]. The ISA compares a measured fatty acid isotopomer distribution to one that is simulated using a reaction network for palmitate synthesis, whereby 8 AcCoA molecules are consumed to form one palmitate molecule. Models were also generated for OCFA synthesis, whereby 1 PropCoA and 6-7 AcCoA molecules are consumed to form one OCFA as previously described [11]. Parameters for the relative enrichment of the lipogenic AcCoA pool from a given [^{13}C] tracer and the percentage of fatty acids that are *de novo* synthesized are extracted from a best-fit model using INCA v1.5 or v1.6 metabolic flux analysis software package [26]. The 95% confidence intervals for both

parameters were estimated by evaluating the sensitivity of the sum of squared residuals between measured and simulated fatty acid mass isotopomer distributions to small flux variations.

4.3.11 RNA isolation and quantitative RT-PCR analysis

Total RNA was purified from cultured cells using Trizol Reagent (Life Technologies) per the manufacturer's instructions. First-strand cDNA was synthesized from 0.5μg of total RNA using High-capacity cDNA Reverse Transcription Kit with RNase inhibitor (Applied Biosystems) according to the manufacturer's instructions. Individual 10μl SYBR Green real-time PCR reactions consisted of 2μL of diluted cDNA, 5μL of SYBR Green Supermix (Bio-Rad), and 1μL of primer master mix containing each forward and reverse primer at 5μM. For standardization of quantification, ribosomal RNA RPL27 was amplified simultaneously. The PCR was carried out on 96-well plates on a CFX Connect Real time System (Bio-Rad) using a three-stage program provided by the manufacturer: 95°C hot-start for 3 min, 40 cycles of 95°C for 10s and 60°C for 30s, followed by a 0.5°C/5 sec meltcurve generation protocol. Gene-specific primers used are listed in Supplementary Table 4.

4.3.12 Respirometry

Respirometry was conducted using a Seahorse XF96E Analyzer. For respiration studies, cells were plated at 6,000 cells/well and maintained in 2μg/mL puromycin-containing media until confluence was reached and differentiation was performed as described above. 8 days after differentiation was initiated, growth medium was replaced with DMEM (Sigma #5030) supplemented with 25mM HEPES, 8mM glucose, 2mM glutamine, and 1 mM pyruvate. Mitochondrial respiration is calculated as the oxygen consumption rate sensitive to 1μM rotenone and 2μM antimycin A. Maximal respiration was calculated as the difference between the maximum respiratory rate in response to 5μM FCCP that was sensitive to antimycin A. Immediately after

the experiment, cells were gently washed with PBS, fixed with 4% paraformaldehyde, and stained with CyQuant (Life Technologies) to determine cell number for normalization purposes.

4.3.13 Statistical analyses

All experiments were repeated at least 2 times and data from 1 representative experiment is shown. For analyses involving 2 groups, a two-tailed Student's t-test was performed. For analyses with 3 groups or more, a one- or two-way ANOVA was performed as appropriate. Corrections for multiple comparisons using Dunnett's post-hoc test were performed for all analyses except Seahorse measurements where no correction for multiple comparisons was performed.

4.4 Results

4.4.1 *Bckdha* deficiency prevented BCAA entry to the TCA cycle

To explore the impact of compromised BCAA catabolism in adipocytes we generated polyclonal cultures of 3T3-L1 pre-adipocytes lacking either *Bckdha* or *Acad8* with CRISPR/Cas9 (Fig 1A-B). Lipid accumulation appeared unaffected (Fig 1C), and the total amount of fatty acids was not significantly different in *Bckdha* or *Acad8* deficient adipocytes (Fig 1D). The expression of genes associated with adipogenesis was also unchanged in these polyclonal cultures (Supp. Fig 1A). To probe classic adipocyte functionality, such as insulin sensitivity, we developed a [^{13}C]-based insulin-stimulated glucose metabolism (ISGM) assay that allows for quantitation of enrichment in various metabolic pathways (Supp. Fig 1B), similar to Krycer, et al.[27] Notably, the fold-change of ^{13}C enrichment for most metabolites was significantly greater than that observed using [^{3}H]2-deoxyglucose, suggesting this is a robust method for determining not only glucose uptake but downstream metabolism (Supp. Fig 1C). We applied this assay to 3T3-L1 *Bckdha* deficient and *Acad8* deficient adipocytes and found no significant differences in

the ISGM of the cells (Supp. Fig 1D-E). In *Bckdha* deficient adipocytes we were unable to detect appreciable catabolism of [U-$^{13}C_6$]leucine to citrate (Fig. 1E) or other TCA intermediates (not shown), whereas this flux was maintained in *Acad8* deficient cells (Fig. 1E). These data confirm that BCAA catabolism is altered in *Bckdha* deficient cells without impacting adipogenesis.

4.4.2 *Bckdha* deficient adipocytes reprogram glucose metabolism to support bioenergetic demands

BCAAs contribute significantly to the TCA cycle and DNL in adipocytes[2, 3]. However, total fatty acid pools were unchanged in *Bckdha* deficient adipocytes (Fig. 1D) so we explored whether the contribution of another carbon source was increased in these cells. While BCAAs were elevated in *Bckdha* deficient adipocytes, alanine levels were dramatically decreased (Fig. 2B), likely driven by decreased Gpt2 expression in the *Bckdha* deficient adipocytes (Supp. Fig. 2A). This indicated a reprogramming of glucose metabolism and alternative usage of pyruvate (Fig. 2B). In fact, while we did not observe a consistent, significant difference in the amount of glucose taken up, we did observe a $\sim$50% decrease in the amount of lactate secreted (Fig. 2C), thereby decreasing the lactate secretion/glucose uptake ratio (Fig 2D). The intracellular lactate/pyruvate ratio also decreased slightly (Supp Fig. 2B) (driven by lower lactate levels), indicating decreased flux to lactate. Interestingly, the levels of all TCA cycle intermediates were significantly decreased in *Bckdha* deficient adipocytes, with more modest effects in *Acad8* deficient cells (Fig. 2F). Similarly, we found a consistent $\sim$25% decrease in both the basal and maximal oxygen consumption rate (Fig. 2G), similar to results in brown adipocytes with knock-out of the mitochondrial BCAA transporter, SLC25A44[28].

Uptake of leucine and isoleucine was also decreased (Supp. Fig. 2C) but the uptake and efflux of other metabolites was not consistently altered (Supp. Fig. 2D). Additionally, we did not find major differences in the percentage of newly synthesized amino acids from [U-$^{13}C_6$]glucose or [U-$^{13}C_5$]glutamine incorporated into the insoluble protein fraction (Supp Fig. 2E-F).

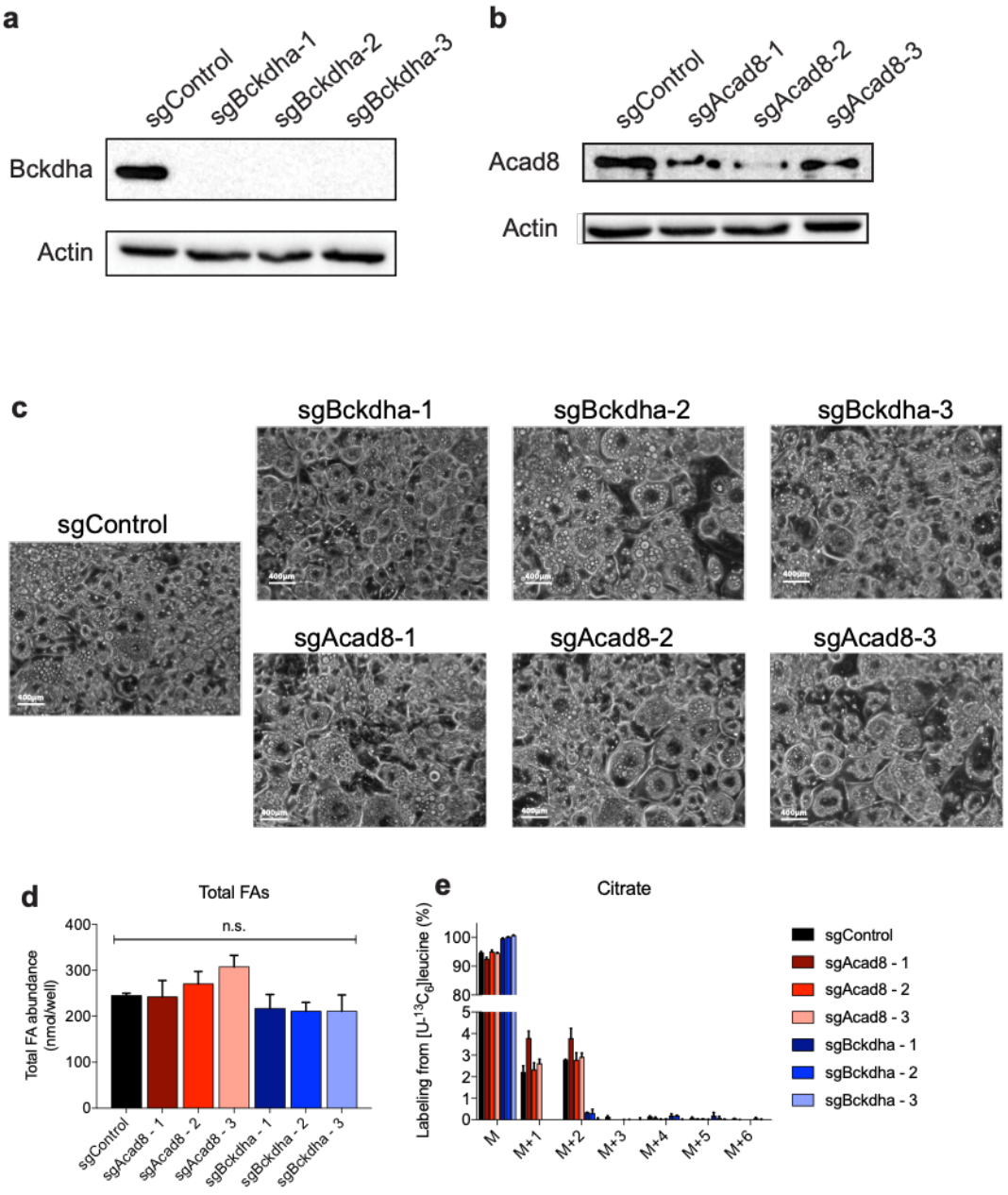

Figure 4.1: **Bckdha KO prevents BCAA entry to TCA cycle a**. Western blot of Bckdha and Actin. **b**. Western blot of Acad8 and Actin. **c**. Image of differentiated Control or *Bckdha* or *Acad8* deficient adipocytes 7 days post-induction of differentiation (scale bar = 400μm). **d**. Abundance of all fatty acids in Control, Bckdha KO, or Acad8 KO cells. **e**. Labeling on citrate from [U-$^{13}C_6$]leucine in Control, *Acad8* deficient, and *Bckdha* deficient adipocytes. All data are presented as means $\pm$ s.d.

The mass isotopomer distribution (MID) of citrate traced for 48h with [U-$^{13}C_6$]glucose shows a slight increase in glucose labeling (Supp. Fig. 2G) and [U-$^{13}C_6$]glucose enrichment of all TCA cycle intermediates is higher in *Bckdha* deficient adipocytes (Supp. Fig. 2H). Similarly, [U-$^{13}C_5$]glutamine enrichment is higher in *Bckdha* deficient adipocytes as well likely due to its role as an anaplerotic substrate (Supp. Fig. 2I). ISA revealed a significant, and larger, increase in glucose contribution to the lipogenic AcCoA pool (Fig 2H), indicating a rewiring of glucose metabolism in the absence of BCAA catabolism.

4.4.3 *Bckdha* deficiency and *Acad8* deficiency alter 3T3-L1 fatty acid metabolism

Bckdha deficiency should prevent the formation of PropCoA and SBCFA-CoAs. *Acad8* deficiency should prevent formation of PropCoA from valine, but should not affect SBCFA-CoA synthesis or PropCoA synthesis from isoleucine[11]. As expected, these deficiencies led to profound alterations on fatty acid metabolism in 3T3-L1 adipocytes. First, OCFAs were profoundly decreased in *Bckdha* deficiency, while only modestly decreased in *Acad8* deficiency (Fig. 3A). The proportion of even chain fatty acids was mostly unchanged in *Acad8* deficient cells but significantly increased in *Bckdha* deficient cells (Fig. 3A). The desaturation index (ratio of monounsaturated FA to saturated FA) was unchanged in either deficiency (Supp Fig. 3A).

The proportion of BCFAs was significantly lower in *Bckdha* deficient cells (Fig 3B). However, *Acad8* deficiency increased iso-C16:0 abundance dramatically without affecting the abundance of other BCFAs (Fig 3B), similar to results obtained using shRNA knock-down of the same enzyme[11]. ISA revealed a decrease in newly synthesized OCFAs but no significant differences in other FAs (Fig. 3C). However, the total amount of newly synthesized fatty acids (accounting for both percentage of pool newly synthesized and molar amount of FA) remained unchanged across *Acad8* or *Bckdha* deficient adipocytes (Fig 3D), indicating a clear rewiring of central carbon metabolism and FA metabolism to maintain FA levels.

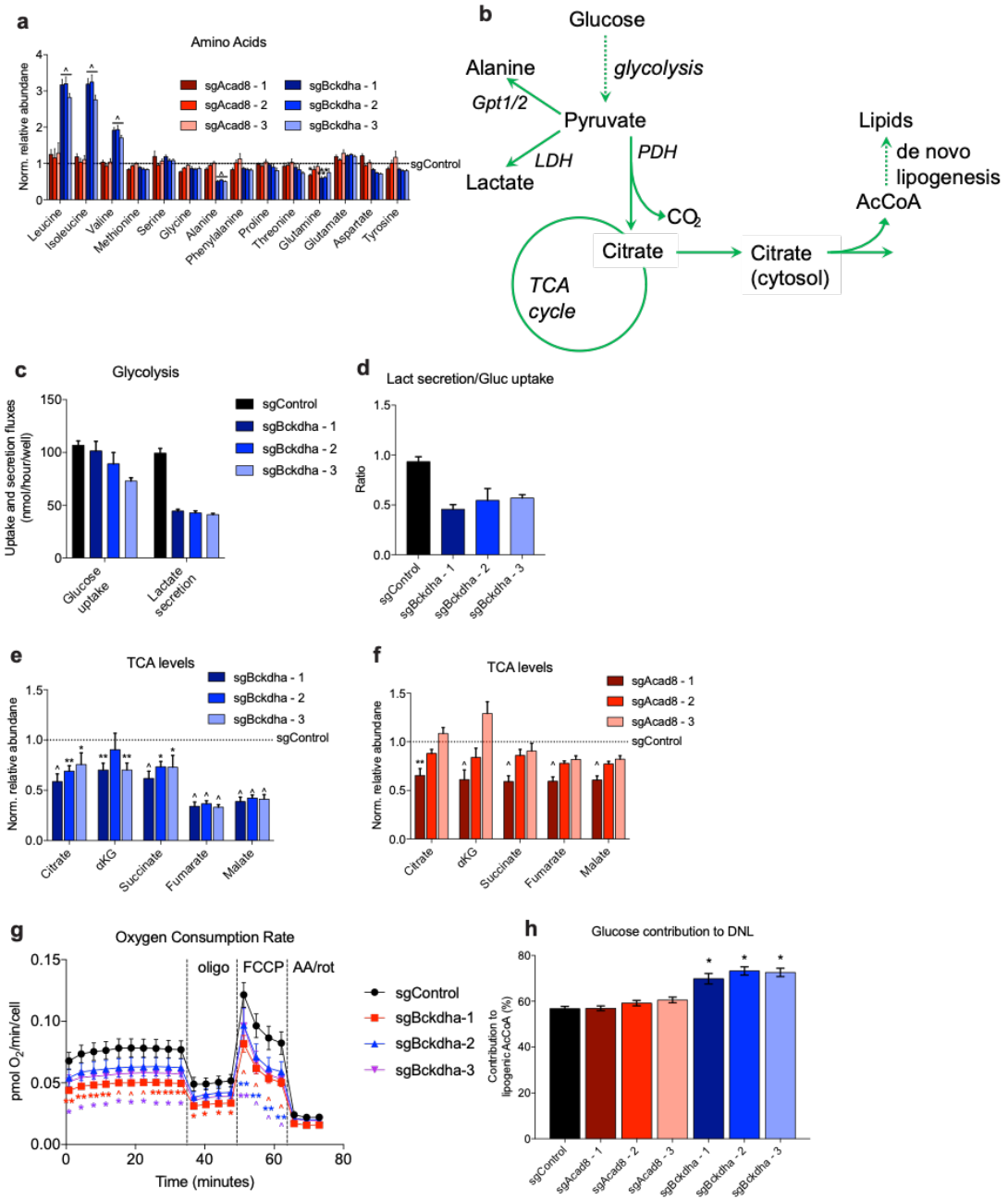

Figure 4.2: ***Bckdha* deficient adipocytes reprogram glucose metabolism to support bioenergetic demands. a**. Relative intracellular abundance of amino acids normalized to Control. **b**. Metabolic map of central carbon metabolism. **c**. Molar amount of glucose uptake or lactate secretion in Control or *Bckdha* deficient adipocytes over 48 hours. **d**. Ratio of lactate secretion to glucose uptake after 48 hours. **e-f**. Normalized relative abundance of TCA cycle intermediates in differentiated **e**, Control or *Bckdha* deficient adipocytes or **f**, Control or *Acad8* deficient adipocytes. **g**. Seahorse oxygen consumption rate (OCR) of Control and Bckdha deficient adipocytes. **h**. Contribution of [U-$^{13}C_6$]glucose to lipogenic AcCoA used for DNL. One- or Two-Way ANOVA was performed on three cellular replicates with Dunnett's multiple comparisons post-hoc test. All data are presented as means ± s.d. except **g** is means ± s.e.m. and **h** is means ± 95% C.I. Significance is calculated compared to sgControl condition. *p<0.05, **p<0.01, $^{p} < 0.001$.

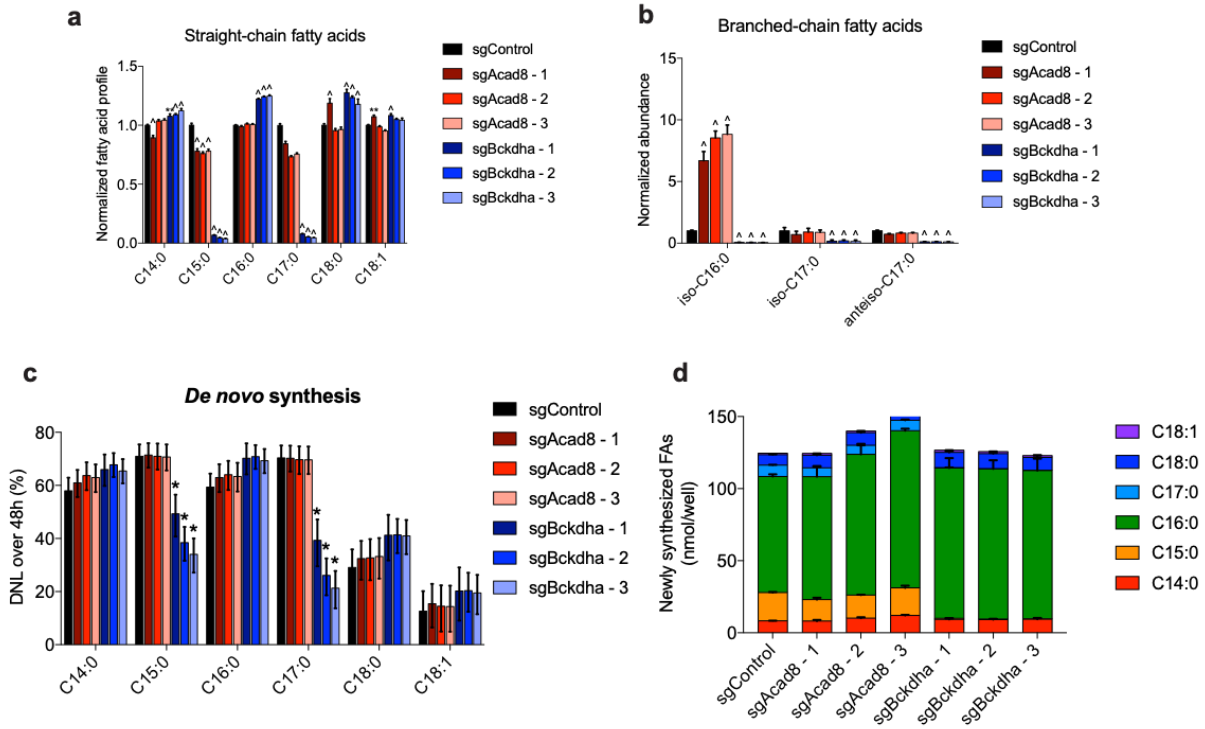

Figure 4.3: **Fatty acid metabolism is altered in *Bckdha* deficient and *Acad8* deficient adipocytes. a**. Relative change in total odd-chain and even-chain fatty acids in Control, *Acad8* deficient, or *Bckdha* deficient 3T3-L1 adipocytes. **b** Relative change in total branched chain fatty acids in Control, *Acad8* deficient, or *Bckdha* deficient 3T3-L1 adipocytes. **c**. Percent of fatty acids derived from *de novo* lipogenesis in Control, *Acad8* deficient, or *Bckdha* deficient 3T3-L1 adipocytes over 48 hours obtained via isotopomer spectral analysis (ISA). **d**. Molar amount of indicated fatty acids synthesized over 48 hours obtained by combining individual FA DNL values with pool size. Significance was determined by two-way ANOVA with Dunnett's multiple comparisons post-hoc test in **a-b** or non-overlapping 95% confidence intervals in **c**. Data are presented as means $\pm$ s.d. in all panels except **c** which is means $\pm$ 95% C.I. Significance is calculated compared to sgControl condition. *p<0.05, **p<0.01, $^{p} < 0.001$.

4.4.4 Cobalamin supplementation and *Bckdha* deficiency alters 3T3-L1 adipocyte lipidome

Due to the more pronounced effects of *Bckdha* deficiency on the 3T3-L1 adipocyte FA profile, we wanted to follow up on the lipidome changes in *Bckdha* deficient adipocytes. We chose to compare *Bckdha* deficient adipocytes to cobalamin-supplemented adipocytes as some key similarities are present - namely, the reduction of OCFAs in both interventions (Fig. 4A). With the exception of anteiso-C17:0, BCFAs were unaffected by cobalamin supplementation (Supp. Fig. 4A), consistent with prior results[11].

To further explore the changes to the lipidome of *Bckdha* deficient 3T3-L1 adipocytes or cobalamin-supplemented adipocytes, we performed a targeted lipidomic analysis using MRM-based methods to obtain positive-mode lipids, ceramides, and sphingoid bases. In performing some of the statistical analyses, all 3 replicates of the 3 *Bckdha* deficient guides were combined (9 replicates in total). Four lipid classes were significantly altered in *Bckdha* deficient adipocytes: phosphocholine (PC) and sphingomyelin (SM) decreased, and triacylglyceride (TAG) and dihydroceramide (DHCer) levels increased (Fig. 4B). Comparing cobalamin-supplemented adipocytes to control adipocytes revealed a significant reduction in total diacylglycerol (DAG), lysophosphatidylethanolamine (LPE) and lysophosphatidylcholine (LPC) species (Fig. 4C). In comparing cobalamin-supplemented adipocytes to *Bckdha* deficient adipocytes, 2 lipid species were significantly decreased: LPE and phosphatidylserine (PS) and 2 species were significantly increased: DAG and DHCer (Fig. 4D). As expected, volcano plots depicting the changes in individual species caused by *Bckdha* deficiency or cobalamin supplementation revealed that TAGs containing 2 OCFAs were the most significantly decreased lipids (Supp. Fig 4B-D). Interestingly, in addition to OCFA-containing lipids, many of the most significantly changed lipids contained polyunsaturated fatty acids (PUFA) - specifically eicosapentaenoic acid (EPA) and docosahexaenoic acid (DHA) (Supp. Fig. 4C-E).

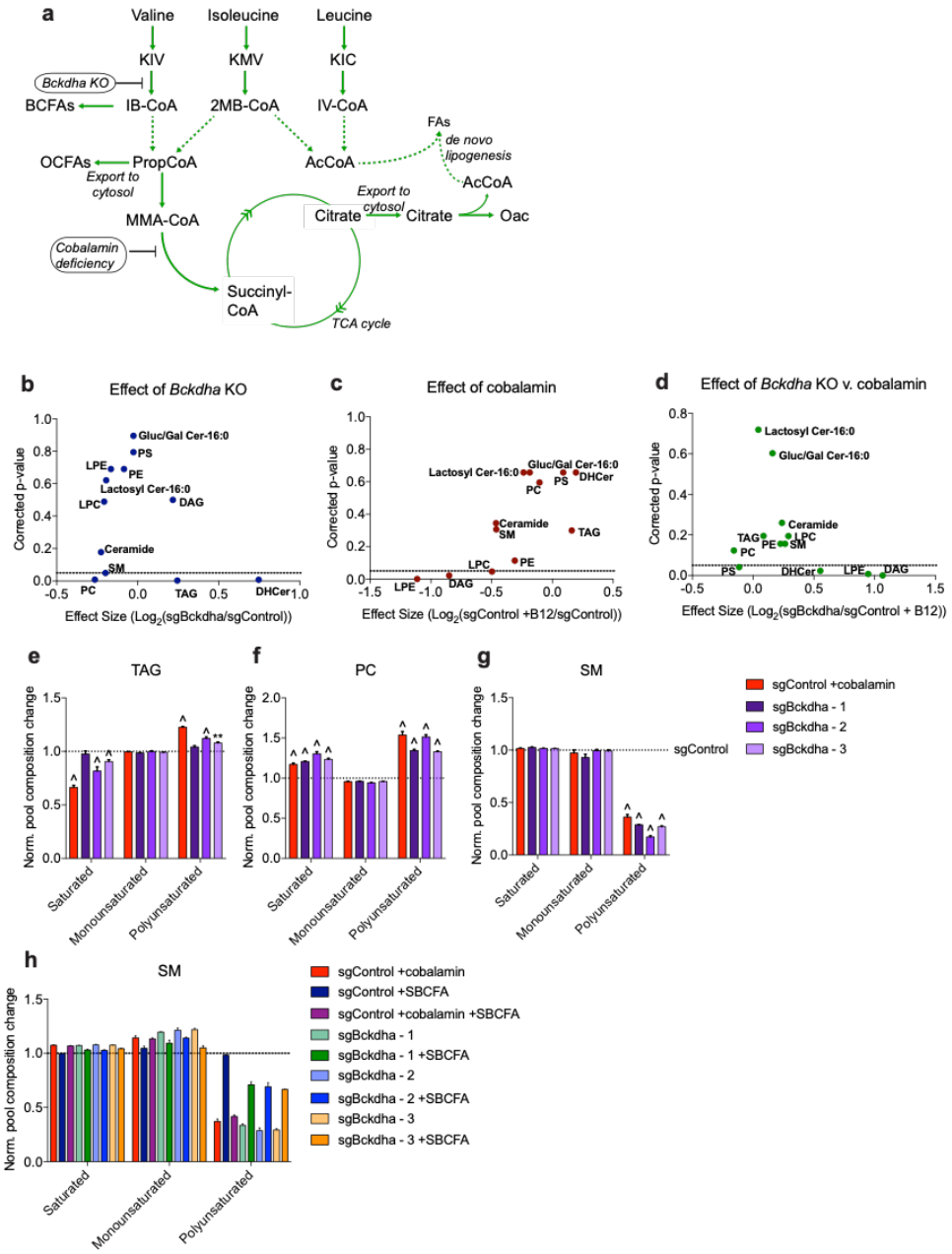

Figure 4.4: **Cobalamin supplementation and *Bckdha* deficiency alters 3T3-L1 adipocyte lipidome. a**. Metabolic map of BCAA metabolism and the impact of cobalamin supplementation and *Bckdha* deficiency on BCFAs, OCFAs, and DNL. **b-d**. Simplified Volcano plot targeting the effect of **b**, *Bckdha* deficiency v. Control, **c**, cobalamin supplementation v. Control or **d**, *Bckdha* deficiency v. cobalamin supplementation on abundance of different lipid classes. **e-g**. Percentage of pool of indicated lipid species, **e**, TAG, **f**, PC, and **g**, SM, with indicated acyl chain class normalized to sgControl. TAGs known to contain 2 monounsaturated acyl chains are included in monounsaturated category. **h**. Percentage of SM pool with indicated acyl chain class normalized to sgControl. Two-Way ANOVA was performed on three cellular replicates with Dunnett's multiple comparisons post-hoc test. All data are presented as means ± s.d. Significance is calculated compared to sgControl condition. *p<0.05, **p<0.01, $^{p} < 0.001$.

Like PUFAs, BCFAs can modulate membrane fluidity[29, 30], and in some settings BCFAs can substitute for PUFAs in living cells [31]. We therefore examined the distribution of saturated, monounsaturated, and polyunsaturated FAs in different lipid species. Importantly, total PUFA levels were not altered in *Bckdha* deficient adipocytes (Supp. Fig. 5A). In TAGs, saturated FA levels were reduced by about 40% while PUFA levels increased by about 20% in +cobalamin conditions (Fig. 4E). A similar, though less pronounced, trend was observed in *Bckdha* deficient adipocytes (Fig. 4E). PUFA-containing PC increased around 40% in *Bckdha* deficient adipocytes (Fig. 4F). Similar, but somewhat muted, trends were observed in PE and PS species as well (Supp Fig. 5B-C). Strikingly, SM displayed a distinct phenotype. Saturated and monounsaturated SM were mostly unchanged in *Bckdha* deficient and cobalamin-treated adipocytes. However, PUFA-containing SM decreased by about 80% in *Bckdha* deficient cells (Fig. 4G). If the lipid profile effects of *Bckdha* deficiency were driving this phenotype, we would expect SBCFA addition to rescue these changes. Indeed, treatment with SBCFAs (beginning on day 3 of differentiation) profoundly rescued the PUFA-SM decrease seen in *Bckdha* deficient adipocytes (Fig. 4H). These results suggest a major rewiring of acyl chain distribution in the absence of OCFAs and BCFAs.

Despite these large changes in acyl chain organization on lipid species (Supp. Fig. 6A), we did not find that Ceramide synthases, sphingomyelin dehydrogenases or synthases, or other phospholipid metabolism genes were consistently differentially expressed in *Bckdha* deficient adipocytes (Supp. Fig. 6B; Genes assayed are bold in Supp. Fig. 6A). Gene expression in *Acad8* deficient adipocytes served as a negative control (Supp. Fig. 6C). Expression of other enzymes not yet probed could still be affecting this organization. Overall, this alteration of phospholipids and glycerolipids at the expense of sphingolipids could alter cell function and lipid droplet biogenesis[32], particularly in the context of a large, dynamic tissue. The complexity of lipid metabolism and its high activity in 3T3-L1 adipocytes suggests that with the myriad of methods for removing or adding an acyl chain, reorganization of PUFAs (a small percentage of

the total FA pool) could happen without alteration of gene expression.

4.5 Discussion

Here, by lowering *Bckdha* and *Acad8* in 3T3-L1 adipocytes using CRISPR/Cas9, we showed that adipocytes are able to reprogram their metabolism to support DNL but decreased respiration signifies a metabolic impairment in Bckdha deficient adipocytes. We also demonstrated that alteration of the BCAA catabolic pathway, similar to that seen in MSUD and IBDD patients, impacted the lipidome of the cell and led to reorganization of PUFAs from SM to phospholipid and glycerol lipid pools. Collectively, these results link BCAA catabolism and cobalamin supplementation to fatty acid metabolism and lipidome composition.

The functional role of BCAA metabolism is poorly understood. BCAAs are oxidized in many tissues throughout the body, with the heart and brown adipose tissue the highest on a nmol/mg basis[33]. White adipose tissue is a very large tissue in many mammals and thus still accounts for a significant portion of overall BCAA utilization. Studies have shown that BCAA catabolism decreases in adipocytes exposed to hypoxia[11], increases in the skeletal muscle of mice during endurance exercise training[34, 35], increases in the livers of rats in response to estrogen[36], increases in mouse striated muscle exposed to insulin[33], and decreases in hepatocellular carcinoma (with extent of decrease correlating with tumor aggressiveness)[37]. Defective BCAA catabolism also sensitized mice to cardiac injury following ischemia-reperfusion[38]. Additionally, a recent study demonstrated that loss of BCAA catabolism in the brown adipose tissue of mice sensitizes them to acute cold challenge[28]. BCAAs certainly supply acetyl-CoA used in the TCA cycle and DNL but BCAA catabolism could also serve more critical roles in supplying anaplerotic substrates or yielding intermediate metabolites with signaling roles.

The lipidome in mammals is remarkably complex[39]. In CrAT-expressing, BCAA-catabolizing tissues, BCFAs almost certainly are incorporated into lipids in a highly regulated

manner[11]. BCFAs, similar to PUFAs, are known to influence fluidity[40], with the greatest biophysical alteration derived from anteiso-BCFAs[41]. For example, bacteria that contain very high levels of BCFAs such as *Bacillus*, often lack appreciable amounts of unsaturated fatty acids[42]. It was hypothesized nearly half a century ago that because BCFAs are preferentially incorporated into the -sn2 position of many phospholipids (and growth is compromised if this is prevented[43]), they may serve a similar role as PUFAs which occupy the same position in the phospholipids of higher order plants and animals[42, 44]. Additionally, in unsaturated fatty acid-depleted *E. coli*, expression of *bkd* from *B. subtilis* restored *E. coli* growth and respiration[31]. In fact, one advantage of BCFAs over PUFAs is their resistance to oxidative stress as saturated fatty acids. In fact, lipid peroxidation is proposed as a key aspect of adipose dysregulation, including impaired adipocyte differentiation[45, 46] and prolonged PUFA incorporation in lipids typically containing BCFAs could lead to greater risk of oxidative stress and ferroptosis[47].

However, loss of BCFAs may be problematic beyond fluidity effects and could affect signaling or other critical processes. In the absence of endogenously produced BCFAs (as in MSUD patients and in *Bckdha* deficiency), the fatty acid profile in lipids is disrupted. A study attempting to recapitulate MSUD in C. elegans connected the developmental defects in the worms to the low levels of BCFAs[48]. The speed of onset and severity of MSUD compared to IBDD is notable and may involve a mechanism beyond BCAA and BCKA accumulation. Given the substantial rewiring of lipid metabolism in *Bckdha* deficient adipocytes and the unique biophysical properties of BCFAs, we propose that these downstream BCAA metabolites could contribute to the pathology of MSUD, in particular the dysmyelination in the brain. Future *in vivo* studies are needed to elucidate the role of BCFAs and PUFAs in the progression and treatment of MSUD.

4.6 Acknowledgements

Chapter 4, in part, is currently being prepared for submission for publication. Courtney R. Green is the primary author of this manuscript. Martina Wallace and Justin D. Hover are co-authors of this manuscript. Christian M. Metallo is the corresponding author of this manuscript.

4.7 References

1. Chuang, D., Hu, C. & Patel, M. Induction of the branched-chain 2-oxo acid dehydrogenase complex in 3T3-L1 adipocytes during differentiation. *Biochem. J.* **214,** 177–81 (1983).

2. Crown, S., Marze, N. & Antoniewicz, M. Catabolism of Branched Chain Amino Acids Contributes Significantly to Synthesis of Odd-Chain and Even-Chain Fatty Acids in 3T3-L1 Adipocytes. *Plos One* **10** (2015).

3. Green, C. R., Wallace, M., Divakaruni, A. S., Phillips, S. A., Murphy, A. N., Ciaraldi, T. P. & Metallo, C. M. Branched-chain amino acid catabolism fuels adipocyte differentiation and lipogenesis. *Nat. Chem. Biol.* **12,** 15–21 (2016).

4. Kedishvili, N., Popov, K., Jaskiewicz, J. & Harris, R. Coordinated expression of valine catabolic enzymes during adipogenesis: analysis of activity, mRNA, protein levels, and metabolic consequences. *Arch. Biochem. Biophys.* **315,** 317–22 (1994).

5. Lackey, D. E., Lynch, C. J., Olson, K. C., Mostaedi, R., Ali, M., Smith, W. H., Karpe, F., Humphreys, S., Bedinger, D. H., Dunn, T. N., Thomas, A. P., Oort, P. J., Kieffer, D. A., Amin, R., Bettaieb, A., Haj, F. G., Permana, P., Anthony, T. G. & Adams, S. H. Regulation of adipose branched-chain amino acid catabolism enzyme expression and cross-adipose amino acid flux in human obesity. *Am. J. Physiol. Endocrinol. Metab.* **304,** E1175–87 (2013).

6. Newgard, C. B., An, J., Bain, J. R., Muehlbauer, M. J., Stevens, R. D., Lien, L. F., Haqq, A. M., Shah, S. H., Arlotto, M., Slentz, C. A., Rochon, J., Gallup, D., Ilkayeva, O., Wenner, B. R., Yancy, W. S., Eisenson, H., Musante, G., Surwit, R. S., Millington, D. S., Butler, M. D. & Svetkey, L. P. A branched-chain amino acid-related metabolic signature that differentiates obese and lean humans and contributes to insulin resistance. *Cell Metab.* **9,** 311–26 (2009).

7. Wang, T. J., Larson, M. G., Vasan, R. S., Cheng, S., Rhee, E. P., Elizabeth, M., Lewis, G. D., Fox, C. S., Jacques, P. F., Fernandez, C., J, O. C., Carr, S. A., Mootha, V. K., Florez, J. C., Souza, A., Melander, O., Clish, C. B. & Gerszten, R. E. Metabolite profiles and the risk of developing diabetes. *Nat. Med.* **17,** 448–53 (2011).

8. Hattori, A., Tsunoda, M., Konuma, T., Kobayashi, M., Nagy, T., Glushka, J., Tayyari, F., Daniel, M., Kannan, N., Tojo, A., Edison, A. & Ito, T. Cancer progression by reprogrammed BCAA metabolism in myeloid leukaemia. *Nature* (2017).

9. Mayers, J. R., Wu, C., Clish, C. B., Kraft, P., Torrence, M. E., Fiske, B. P., Yuan, C., Bao, Y., Townsend, M. K., Tworoger, S. S., Davidson, S. M., Papagiannakopoulos, T., Yang, A., Dayton, T. L., Ogino, S., Stampfer, M. J., Giovannucci, E. L., Qian, Z. R., Rubinson, D. A., Ma, J., Sesso, H. D., Gaziano, J. M., Cochrane, B. B., Liu, S., Jean, W., Manson, J. E., Pollak, M. N., Kimmelman, A. C., Souza, A., Pierce, K., Wang, T. J., Gerszten, R. E., Fuchs, C. S., Vander Heiden, M. G. & Wolpin, B. M. Elevation of circulating branched-chain amino acids is an early event in human pancreatic adenocarcinoma development. *Nat. Med.* **20,** 1193–8 (2014).

10. Tönjes, M., Barbus, S., Park, Y., Wang, W., Schlotter, M., Lindroth, A. M., Pleier, S. V., Bai, A. H., Karra, D. & Piro, R. M. BCAT1 promotes cell proliferation through amino acid catabolism in gliomas carrying wild-type IDH1. *Nat. Med.* **19,** 901–908 (2013).

11. Wallace, M., Green, C., Roberts, L., Lee, Y., Justin, M., Joan, S., Meurs, N., Gengatharan, J., Hover, J., Phillips, S., Ciaraldi, T., Guertin, D., Cabrales, P., Ayres, J., Nomura, D., Loomba, R. & Metallo, C. Enzyme promiscuity drives branched-chain fatty acid synthesis in adipose tissues. *Nat Chem Biol* **14,** 1021 (2018).

12. Burrage, L., Nagamani, S., Campeau, P. & Lee, B. Branched-chain amino acid metabolism: from rare Mendelian diseases to more common disorders. *Hum Mol Genet* **23,** R1–R8 (2014).

13. Novarino, G., Paul, E., Kayserili, H., Meguid, N. A., Scott, E. M., Schroth, J., Silhavy, J. L., Kara, M., Khalil, R. O., Tawfeg, B., AG, E., Hashish, A. F., Sanders, S. J., Gupta, A. R., Hashem, H. S., Matern, D., Gabriel, S., Sweetman, L., Rahimi, Y., Harris, R. A., State, M. W. & Gleeson, J. G. Mutations in BCKD-kinase lead to a potentially treatable form of autism with epilepsy. *Science* **338,** 394–7 (2012).

14. Strauss, K. A. & Morton, D. H. Branched-chain Ketoacyl Dehydrogenase Deficiency: Maple Syrup Disease. *Curr Treat Options Neurol* **5,** 329–341 (2003).

15. Schönberger, S., Schweiger, B., Schwahn, B., Schwarz, M. & Wendel, U. Dysmyelination in the brain of adolescents and young adults with maple syrup urine disease. *Mol Genet Metab* **82,** 69–75 (2004).

16. Santra, S., Macdonald, A., Preece, M., Olsen, R. & Andresen, B. Long-term outcome of isobutyryl-CoA dehydrogenase deficiency diagnosed following an episode of ketotic hypoglycaemia. *Mol Genetics Metabolism Reports* **10,** 28–30 (2017).

17. Grigor, M., Dunckley, G. & Purves, H. The synthesis of the branched-chain fatty acids of rat skin surface lipid. *Biochim. Biophys. Acta* **218,** 389–99 (1970).

18. Ran-Ressler, R. R., Devapatla, S., Lawrence, P. & Brenna, J. Branched Chain Fatty Acids Are Constituents of the Normal Healthy Newborn Gastrointestinal Tract. *Pediatr. Res.* **64,** 605–609 (2008).

19. Gibson, R. & Kneebone, G. Fatty acid composition of human colostrum and mature breast milk. *Am. J. Clin. Nutr.* **34,** 252–7 (1981).

20. Su, X., Magkos, F., Zhou, D., Eagon, J., Fabbrini, E., Okunade, A. & Klein, S. Adipose tissue monomethyl branched-chain fatty acids and insulin sensitivity: Effects of obesity and weight loss. *Obesity (Silver Spring)* (2014).

21. Pakiet, A., Wilczynski, M., Rostkowska, O., Korczynska, J., Jabfffdfffdonska, P., Kaska, L., Monika, P., Sobczak, E., Stepnowski, P., Magkos, F., Sledzinski, T. & Mika, A. The Effect of One Anastomosis Gastric Bypass on Branched-Chain Fatty Acid and Branched-Chain Amino Acid Metabolism in Subjects with Morbid Obesity. *Obes Surg,* 1–9 (2019).

22. Sanjana, N., Shalem, O. & Zhang, F. Improved vectors and genome-wide libraries for CRISPR screening. *Nat Methods* **11,** nmeth.3047 (2014).

23. Cordes, T. & Metallo, C. M. in *High-Throughput Metabolomics: Methods and Protocols* (ed D'Alessandro, A.) 219–241 (Springer New York, New York, NY, 2019).

24. Fernandez, C. & Rosiers, D. C. Correction of 13C mass isotopomer distributions for natural stable isotope abundance. *Journal of mass spectrometry* (1996).

25. Bielawski, J., Pierce, J. S., Snider, J., Rembiesa, B., Szulc, Z. M. & Bielawska, A. in *Lipidomics: Volume 1: Methods and Protocols* (ed Armstrong, D.) 443–467 (Humana Press, Totowa, NJ, 2009).

26. Young, J. D. INCA: a computational platform for isotopically non-stationary metabolic flux analysis. *Bioinformatics* (2014).

27. Krycer, J., Yugi, K., Hirayama, A., Fazakerley, D., Quek, L., Scalzo, R., Ohno, S., Hodson, M., Ikeda, S., Shoji, F., Suzuki, K., Domanova, W., Parker, B., Nelson, M., Humphrey, S., Turner, N., Hoehn, K., Cooney, G., Soga, T., Kuroda, S. & James, D. Dynamic Metabolomics Reveals that Insulin Primes the Adipocyte for Glucose Metabolism. *Cell Reports* **21,** 3536–3547 (2017).

28. Yoneshiro, T., Wang, Q., Tajima, K., Matsushita, M., Maki, H., Igarashi, K., Dai, Z., White, P., Robert, M., Ilkayeva, O., Deleye, Y., Oguri, Y., Kuroda, M., Ikeda, K., Li, H., Ueno, A., Ohishi, M., Ishikawa, T., Kim, K., Chen, Y., Sponton, C., Pradhan, R., Majd, H., Greiner, V., Yoneshiro, M., Brown, Z., Chondronikola, M., Takahashi, H., Goto, T., Kawada, T.,

Sidossis, L., Szoka, F., Michael, M., Saito, M., Soga, T. & Kajimura, S. BCAA catabolism in brown fat controls energy homeostasis through SLC25A44. *Nature,* 1–6 (2019).

29. Harayama, T. & Riezman, H. Understanding the diversity of membrane lipid composition. *Nat Rev Mol Cell Bio* **19,** 281 (2018).

30. Legendre, S., Letellier, L. & Shechter, E. Influence of lipids with branched-chain fatty acids on the physical, morphological and functional properties of Escherichia coli cytoplasmic membrane. *Biochimica Et Biophysica Acta Bba - Biomembr* **602,** 491–505 (1980).

31. Budin, I., de Rond, T., Chen, Y., Chan, L. G., Petzold, C. J. & Keasling, J. D. Viscous control of cellular respiration by membrane lipid composition, eaat7925 (2018).

32. Deevska, G. & Mariana, N. The expanding role of sphingolipids in lipid droplet biogenesis. *Biochimica Et Biophysica Acta Bba - Mol Cell Biology Lipids* **1862,** 1155–1165 (2017).

33. Neinast, M., Jang, C., Hui, S., Murashige, D., Chu, Q., Morscher, R., Li, X., Zhan, L., White, E., Anthony, T., Rabinowitz, J. & Arany, Z. Quantitative Analysis of the Whole-Body Metabolic Fate of Branched-Chain Amino Acids. *Cell Metab* (2018).

34. Overmyer, K., Evans, C., Qi, N., Minogue, C., Carson, J., Christopher J., C., Koch, L., Britton, S., Pagliarini, D., Coon, J. & Burant, C. Maximal Oxidative Capacity during Exercise Is Associated with Skeletal Muscle Fuel Selection and Dynamic Changes in Mitochondrial Protein Acetylation. *Cell Metab* **21,** 468–478 (2015).

35. Shimomura, Y., Murakami, T., Nakai, N., Nagasaki, M. & Harris, R. A. Exercise promotes BCAA catabolism: effects of BCAA supplementation on skeletal muscle during exercise. *J. Nutr.* **134,** 1583S–1587S (2004).

36. Obayashi, M., Shimomura, Y., Nakai, N., Jeoung, N., Nagasaki, M., Murakami, T., Sato, Y. & Harris, R. Estrogen controls branched-chain amino acid catabolism in female rats. *J Nutrition* **134,** 2628–33 (2004).

37. Ericksen, R., Lim, S., Eoin, M., Shuen, W., Vadiveloo, M., White, P., Ding, Z., Kwok, R., Lee, P., Radda, G., Toh, H., Hirschey, M. & Han, W. Loss of BCAA Catabolism during Carcinogenesis Enhances mTORC1 Activity and Promotes Tumor Development and Progression. *Cell Metab* **29,** 1151–1165.e6 (2019).

38. Li, T., Zhang, Z., Kolwicz, S., Abell, L., Roe, N., Kim, M., Zhou, B., Cao, Y., Ritterhoff, J., Gu, H., Raftery, D., Sun, H. & Tian, R. Defective Branched-Chain Amino Acid Catabolism Disrupts Glucose Metabolism and Sensitizes the Heart to Ischemia-Reperfusion Injury. *Cell Metab* **25,** 374–385 (2017).

39. Quehenberger, O., Armando, A. M., Brown, A. H., Milne, S. B., Myers, D. S., Merrill, A. H., Bandyopadhyay, S., Jones, K. N., Kelly, S., Shaner, R. L., Sullards, C. M., Wang, E.,

Murphy, R. C., Barkley, R. M., Leiker, T. J., Raetz, C. R., Guan, Z., Laird, G. M., Six, D. A., Russell, D. W., G, M. J., Subramaniam, S., Fahy, E. & Dennis, E. A. Lipidomics reveals a remarkable diversity of lipids in human plasma, *J Lipid Res* **51,** 3299–3305 (2010).

40. Mercier, R., Patricia, D. & Errington, J. Crucial Role for Membrane Fluidity in Proliferation of Primitive Cells. *Cell Reports* **1,** 417–423 (2012).

41. Kaneda, T. Iso- and anteiso-fatty acids in bacteria: biosynthesis, function, and taxonomic significance. *Microbiol. Rev.* **55,** 288–302 (1991).

42. Kaneda, T. Fatty acids of the genus Bacillus: an example of branched-chain preference. *Bacteriol Rev* **41,** 391–418 (1977).

43. Willecke, K. & Pardee, A. Fatty acid-requiring mutant of bacillus subtilis defective in branched chain alpha-keto acid dehydrogenase. *J. Biol. Chem.* **246,** 5264–72 (1971).

44. Kaneda, T. Positional distribution of fatty acids in phospholipids from Bacillus subtilis. *Biochimica Et Biophysica Acta Bba - Lipids Lipid Metabolism* **270,** 32–39 (1972).

45. Gaschler, M. & Stockwell, B. Lipid peroxidation in cell death. *Biochem Bioph Res Co* **482,** 419–425 (2017).

46. Murdolo, G., Piroddi, M., Luchetti, F., Tortoioli, C., Canonico, B., Zerbinati, C., Galli, F. & Iuliano, L. Oxidative stress and lipid peroxidation by-products at the crossroad between adipose organ dysregulation and obesity-linked insulin resistance. *Biochimie* **95,** 585–594 (2013).

47. Stockwell, B., Angeli, J., Bayir, H., Bush, A., Conrad, M., Dixon, S., Fulda, S., Gascón, S., Hatzios, S., Kagan, V., Noel, K., Jiang, X., Linkermann, A., Murphy, M., Overholtzer, M., Oyagi, A., Pagnussat, G., Park, J., Ran, Q., Rosenfeld, C., Salnikow, K., Tang, D., Torti, F., Torti, S., Toyokuni, S., Woerpel, K. & Zhang, D. Ferroptosis: A Regulated Cell Death Nexus Linking Metabolism, Redox Biology, and Disease. *Cell* **171,** 273–285 (2017).

48. Jia, F., Cui, M., Than, M. & Han, M. Developmental Defects of Caenorhabditis elegans Lacking Branched-chain /*alpha*-Ketoacid Dehydrogenase Are Mainly Caused by Monomethyl Branched-chain Fatty Acid Deficiency. *J Biol Chem* **291,** 2967–2973 (2016).

Chapter S1

Supplement to Chapter 2

S1.1 Supplemental Tables and Figures

Table S1.1: **Simplified network for Isotopomer Spectral Analysis (ISA)** Summary of Isotopomer Spectral Analysis (ISA) network for determination of substrate contribution to lipogenic AcCoA and rate of *de novo* lipogenesis in differentiated adipocytes.

Contribution to lipogenic AcCoA (%)	**Description**
AcM1.l (ab) → Ac(ab)	AcCoA containing 1 ^{13}C tracer label
AcM2.l (ab) → Ac(ab)	AcCoA containing 2 ^{13}C tracer labels
Ac.d (ab) → Ac(ab)	unlabeled AcCoA (dilution)
7*Ac(ab) → Myr.s (abcdefghijklmn)	
8*Ac(ab) → Palm.s (abcdefghijklmnop)	
9*Ac(ab) → Oleate.s (abcdefghijklmnopqr)	
9*Ac(ab) → Stear.s (abcdefghijklmnopqr)	
***de novo* lipogenesis**	
Myr.s → Myr	Newly synthesized myristate
Myr.d → Myr	Pre-existing or unlabeled myristate
0*Myr → Myr.m	Mixing of pools for measurement
Palm.s → Palm	Newly synthesized Palmitate
Palm.d → Palm	Pre-existing or unlabeled Palmitate
0*Palm → Palm.m	Mixing of pools for measurement
Oleate.s → Oleate	Newly synthesized Oleate
Oleate.d → Oleate	Pre-existing or unlabeled Oleate
0*Oleate → Oleate.m	Mixing of pools for measurement
Stear.s → Stear	Newly synthesized Stearate
Stear.d → Stear	Pre-existing or unlabeled Stearate
0*Stear → Stear.m	Mixing of pools for measurement

Table S1.2: **Control and Low Gluc + AA media formulation.** Control and Low Gluc + AA media formulation denoting those substrates with differing concentrations. All other trace components, lipids, vitamins, salts, etc. present in DMEM media were unchanged.

Amino Acid	**Control (μM)**	**Low Gluc + AA (μM)**
D-glucose	25,000	6,000
L-glutamine	4,000	1,000
L-arginine	400	100
L-cystine	200	50
Glycine	400	100
L-histidine	200	50
L-isoleucine	800	200
L-leucine	800	200
L-lysine HCl	800	200
L-methionine	200	50
L-phenylalanine	400	100
L-serine	400	100
L-threonine	800	200
L-tryptophan	78	20
L-tyrosine	400	100
L-valine	800	200

Table S1.3: **Metabolite fragment ions used for GC-MS analysis.** Fragment ions formula and m/z range used to quantify metabolite abundances.

Metabolite	Carbons	Formula	Mass (m/z)
Leucine	23456	$C_{13}H_{32}NOSi_2$	274-280
Isoleucine	23456	$C_{11}H_{26}NSi$	200-206
Isoleucine	23456	$C_{13}H_{32}NOSi_2$	274-280
Valine	2345	$C_{12}H_{30}NOSi_2$	260-288
Valine	12345	$C_{13}H_{30}NO_2Si_2$	288-296
Methylmalonate	1234	$C_{12}H_{25}O_4Si_2$	289-295
Myristate (C14:0)	1-14	$C_{15}H_{30}O_2$	242-258
Pentadecanoate (C15:0)	1-15	$C_{16}H_{32}O_2$	256-272
Palmitate (C16:0)	1-16	$C_{17}H_{34}O_2$	270-284
Heptadecanoate (C17:0)	1-17	$C_{18}H_{36}O_2$	284-294
Oleate (C18:1)	1-18	$C_{19}H_{36}O_2$	296-310
Stearate (C18:0)	1-18	$C_{19}H_{38}O_2$	298-316

Table S1.4: **Primer sequences used in gene expression analysis.** Forward and reverse primer sequences used in gene expression analysis.

Gene name	Forward sequence	Reverse sequence
PPARγ (*Pparg*)	TTCGCTGATGCACTGCCTAT	ACAGACTCGGCACTCAATGG
Adiponectin (*Adipoq*)	GACACCAAAAGGGCTCAGGA	GCCCTTCAGCTCCTGTCATT
Leptin (*Lep*)	GGGAGGAAAATGTGCTGGAGAC	AAGCCCAGGAATGAAGTCCAA
Glucose transporter type 4 (*Glut4*)	AGCCTCTGATCATCGCAGTG	ACTAAGAGCACCGAGACCAAC
Perilipin 4 (*Plin4*)	GTGTCCACCAACTCACAGATG	GGACCATTCCTTTTGCAGCAT
Branched chain ketoacid dehydrogenase (*Bckdha*)	TGGCTAGATCTCACCCCAGCA	AGAGAATGCGGTCCATGGTG
18S rRNA	AGTCCCTGCCCTTTGTACACA	CGATCCGAGGGCCTCACTA

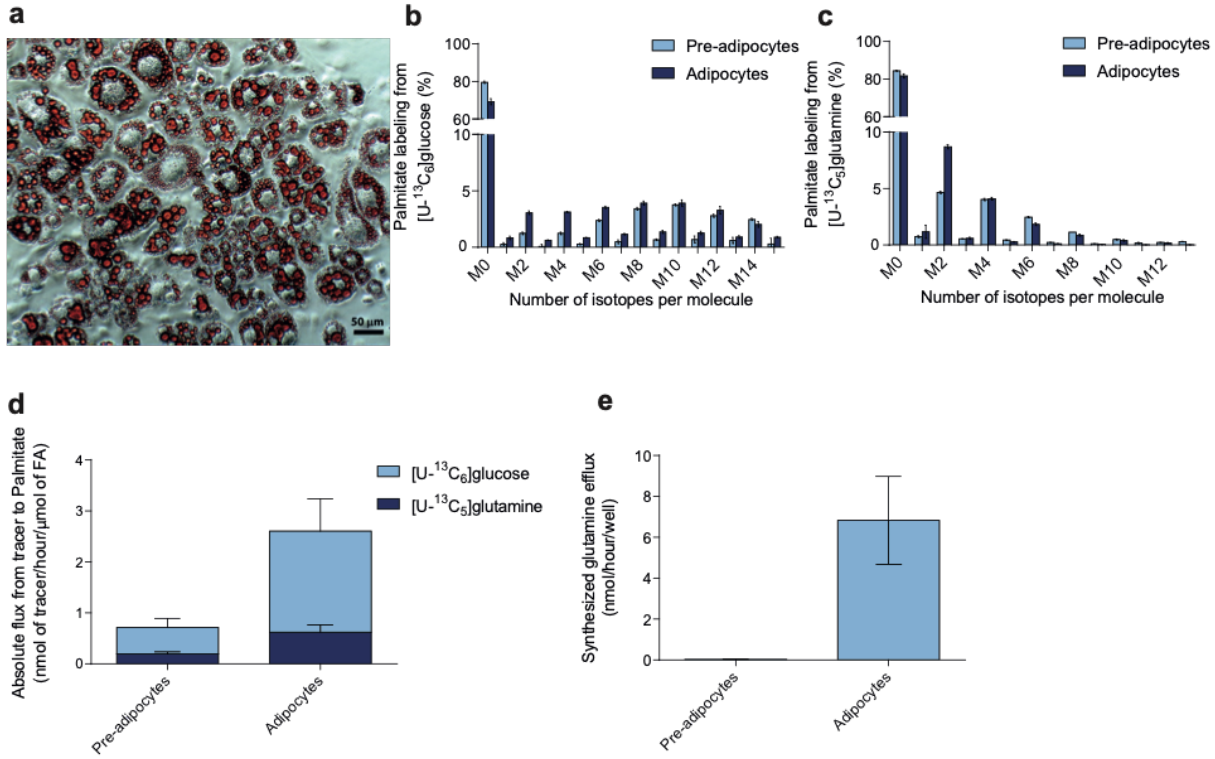

Figure S1.1: **Adipocyte differentiation reprograms intracellular metabolism.** **a**. Phase contrast image of differentiated 3T3-L1 adipocytes with Oil Red O staining of lipids. **b**. Palmitate labeling from [U-$^{13}C_6$]glucose tracer in 3T3-L1 pre-adipocytes and adipocytes. **c**. Palmitate labeling from [U-$^{13}C_5$]glutamine tracer in 3T3-L1 pre-adipocytes and adipocytes. **d**. Absolute lipogenic flux to palmitate synthesis from [U-$^{13}C_6$]glucose and [U-$^{13}C_5$]glutamine in 3T3-L1 pre-adipocytes and adipocytes. **e**. Efflux of glutamine synthesized from [U-$^{13}C_6$]glucose. Data shown in **b-e** are 3 technical replicates representative of 3 biological replicates. Data presented in **b-e** represent mean $\pm$ s.d.

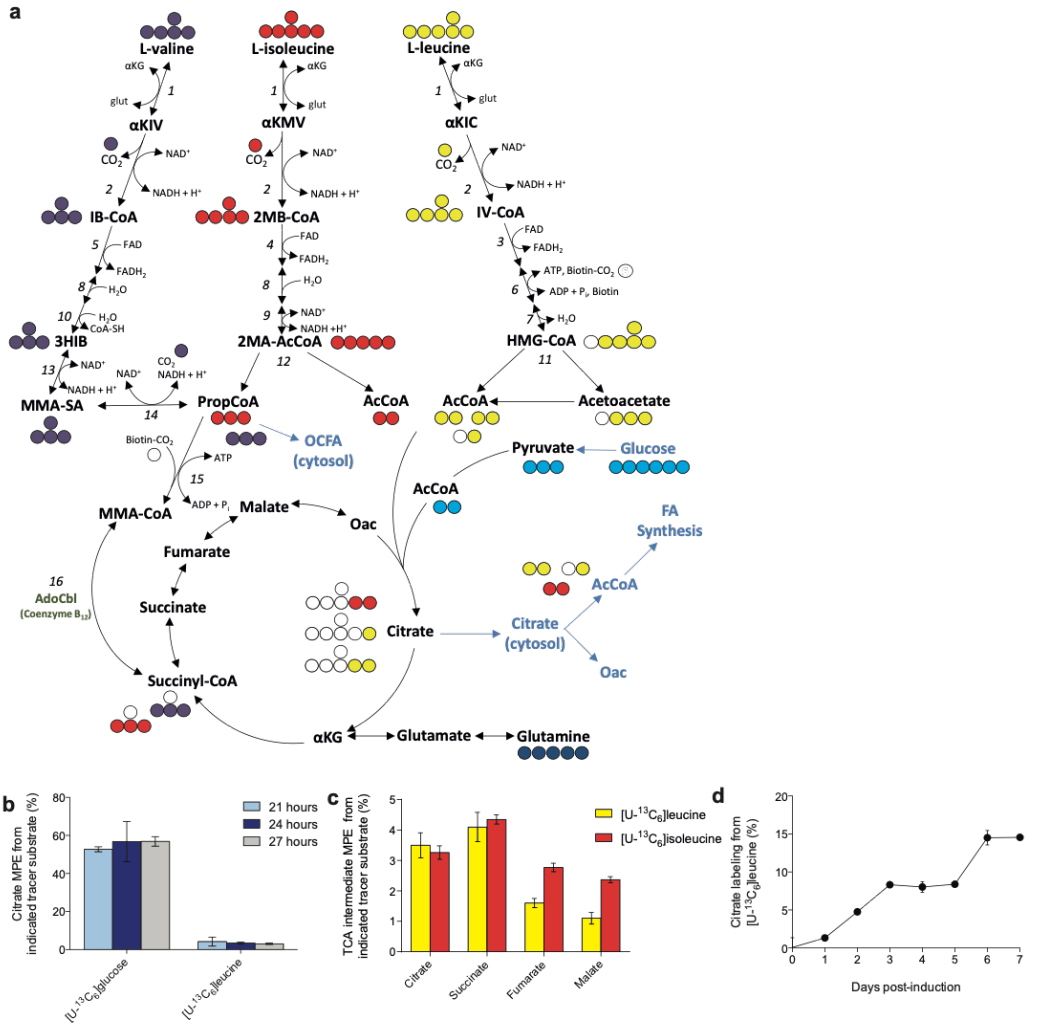

Figure S1.2: **Mitochondrial metabolism is supported by BCAA catabolism. a**. Summary of BCAA catabolism and carbon atom transitions from each BCAA tracer. Enzyme key: 1: Branched chain amino transferase, 2: Branched-chain ketoacid DH/lipoamide, 3: Isovaleryl-CoA DH, 4: Acyl-CoA DH (ACAD) short branched-chain (ACADSB) or ACAD short-chain (ACADS), 5: ACAD8 or ACADSB or ACADS, 6: Methylcrotonyl-CoA carboxylase, 7: Methylglutaconyl-CoA hydratase, 8: Enoyl-CoA hydratase, 9: 3-hydroxy-2-methylbutyryl-CoA DH, 10: 3-hydroxyisobutyryl-CoA hydrolase, 11: Hydroxymethylglutaryl-CoA lyase, 12: Acetyl-CoA acyltransferase, 13: 3-hydroxyisobutyrate DH, 14: Methylmalonate semi-aldehyde DH, 15: Propionyl-CoA carboxylase, 16: Methylmalonyl-CoA mutase; Abbreviations: αKG: α-ketoglutarate; glut: glutamate; Oac: oxaloacetate; FA: fatty acid; AdoCbl: 5'-adenosylcobalamin, DH: dehydrogenase. **b**. Mole percent enrichment (MPE) of citrate from [U-$^{13}C_6$]glucose and [U-$^{13}C_6$]leucine over 3-hour time points. **c**. MPE of TCA cycle intermediates from [U-$^{13}C_6$]leucine and [U-$^{13}C_6$]isoleucine. **d**. Citrate labeling from [U-$^{13}C_6$]leucine in 3T3-L1 adipocytes in the presence of tracer for 24 hours beginning on the indicated day of differentiation. Data shown in **b-d** are 3 technical replicates representative of 3 biological replicates. Data presented in **b-d** represent mean $\pm$ s.d.

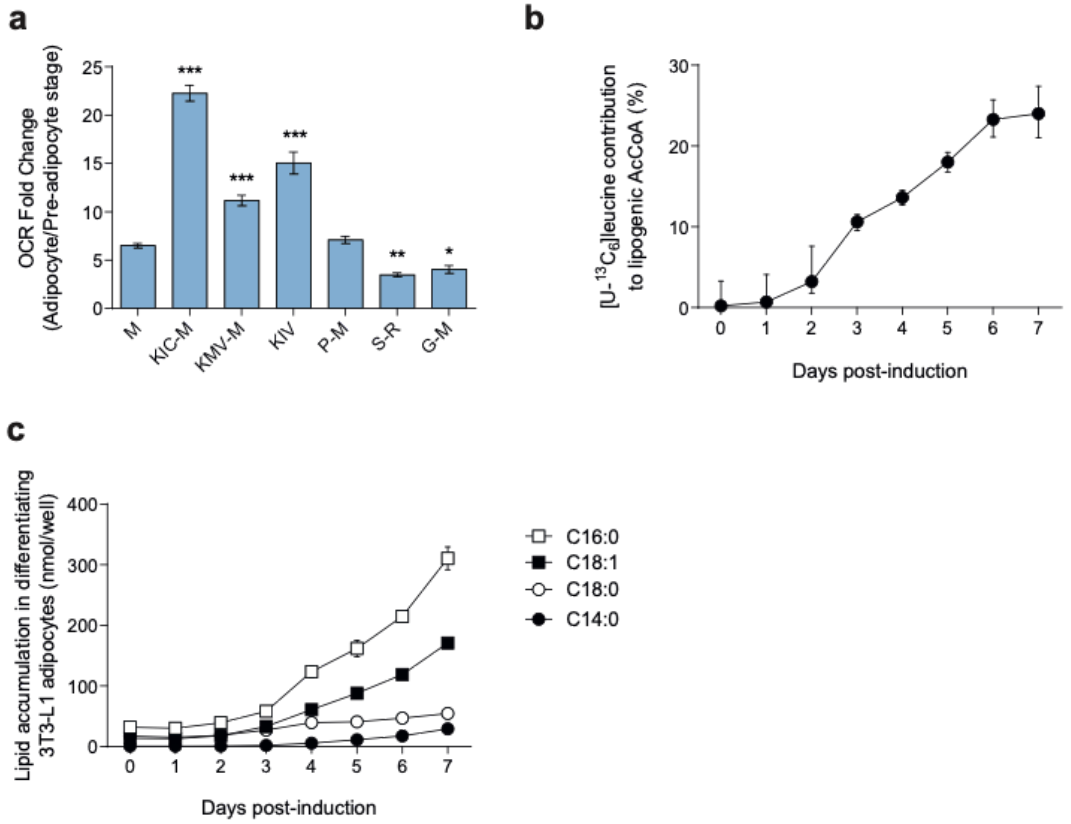

Figure S1.3: **BCAA catabolites are oxidized and used for DNL. a**. Ratio of the substrate-specific oxygen consumption rate (OCR) of adipocytes to pre-adipocytes. Substrate key: M: malate; KIC-M: keto-isocaproate-malate; KMV-M: keto-methylvalerate-malate; KIV: keto-isovalerate; P-M: pyruvate-malate; S-R: succinate-rotenone; G-M: glutamate-malate. Data shown are from at least 5 biological replicates, each with 4 technical replicates; *represents $p<0.05$, **represents $p<0.01$, and ***represents $p<0.001$ analyzed via one-way ANOVA with Holm-Sidak's multiple comparisons test. **b**. Contribution to lipogenic AcCoA from [U-$^{13}C_6$]leucine in 3T3-L1 adipocytes in the presence of tracer for 24 hours beginning on the indicated day of differentiation. **c**. Even-chain fatty acid accumulation in 3T3-L1 adipocytes in the presence of tracer for 24 hours beginning on the indicated day of differentiation. Data shown in **a** represent at least 5 biological replicates, each with 4 technical replicates. Data in **b-c** are 3 technical replicates representative of 3 biological replicates. Data plotted in **a-c** represent mean $\pm$ s.d.

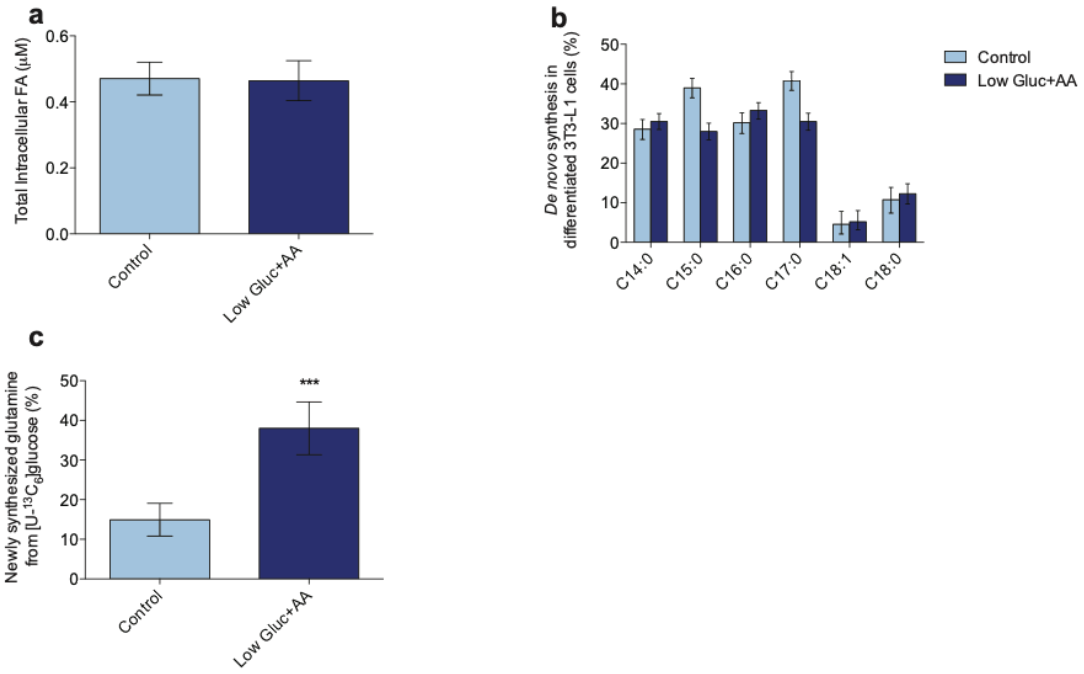

Figure S1.4: **Protein catabolism supports BCAA metabolism.** **a**. Total intracellular FA in 3T3-L1 cells between control and Low Gluc + AA conditions. **b**. FA growth rates obtained via ISA analysis in control and Low Gluc+AA conditions. **c**. Sum of M1-M5 labeled glutamine in [U-$^{13}C_6$]glucose tracer medium in control or Low Gluc + AA conditions. ***represents $p<0.001$ determined via Student's t-test. Data in **a-c** are 3 technical replicates representing 3 biological replicates and are presented as mean $\pm$ s.d.

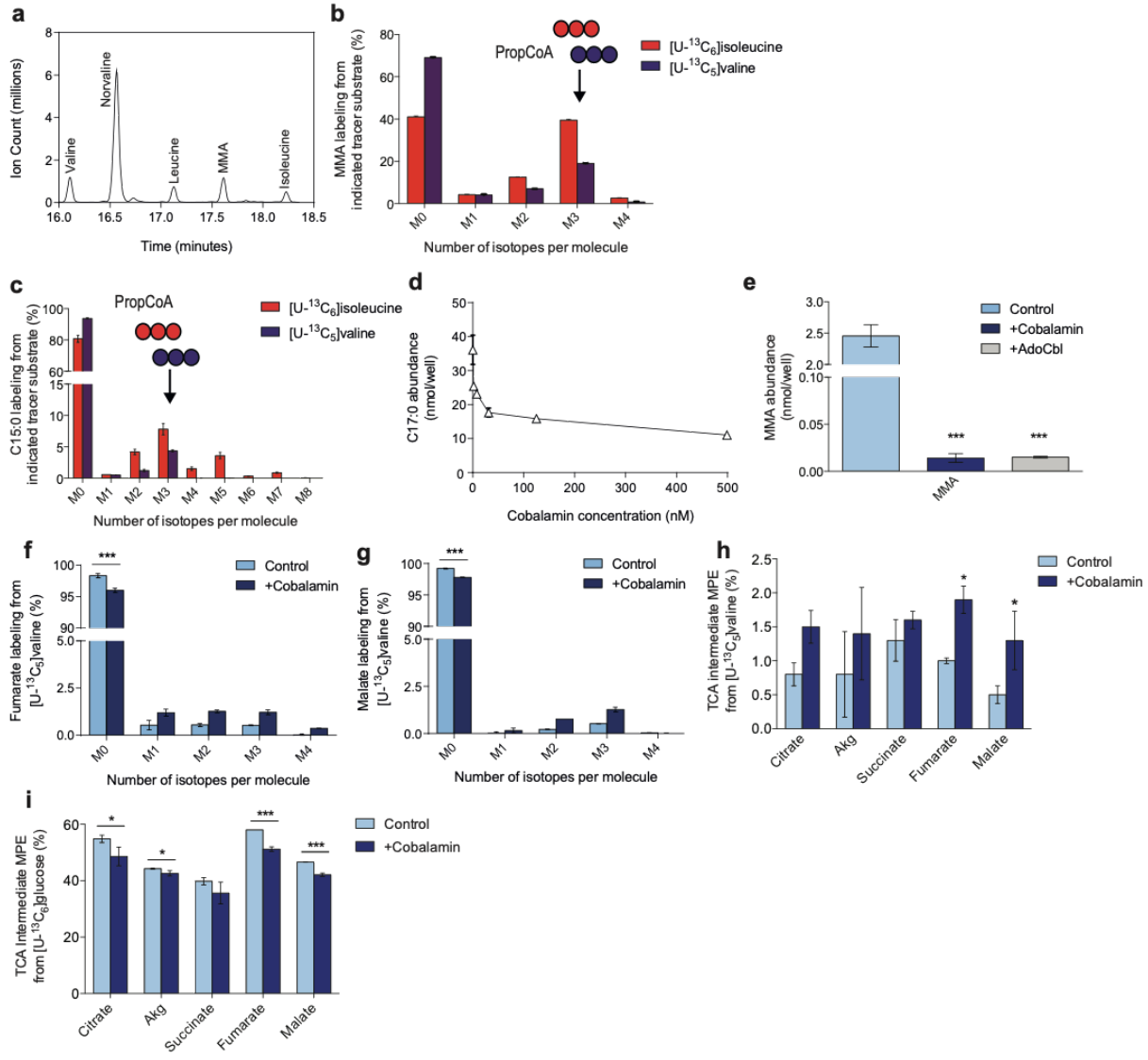

Figure S1.5: **Cobalamin supplementation alters 3T3-L1 metabolism.** **a**. Representative GC/MS chromatogram of BCAAs, norvaline internal standard, and methylmalonate (MMA) under normal culture conditions. **b**. Methylmalonate (MMA) and **c**. C15:0 labeling from [U-$^{13}C_6$]isoleucine and [U-$^{13}C_5$]valine in 3T3-L1 adipocytes. **d**. C17:0 abundance in cells cultured in DMEM +10% FBS and above cobalamin concentrations beginning on Day 0 of differentiation. **e**. MMA level in 3T3-L1 adipocytes after culture with 500 nM cobalamin or 100 nM AdoCbl. Asterisks denote significance compared to control after statistical analysis via two-way ANOVA. **f**. Fumarate labeling from [U-$^{13}C_5$]valine in control and +cobalamin conditions. **g**. Malate labeling from [U-$^{13}C_5$]valine in control and +cobalamin conditions. **h-i**. Mole percent enrichment (MPE) in TCA intermediates from **h**, [U-$^{13}C_5$]valine and **i**, [U-$^{13}C_6$]glucose in 3T3-L1 adipocytes in normal culture conditions with and without 500 nM cobalamin supplementation. Data in **b-i** are 3 technical replicates representing 3 biological replicates and are presented as mean $\pm$ s.d. *represents $p<0.05$, **represents $p<0.01$, and ***represents $p<0.001$ determined via Student's t-test unless otherwise noted.

a

Bckdha

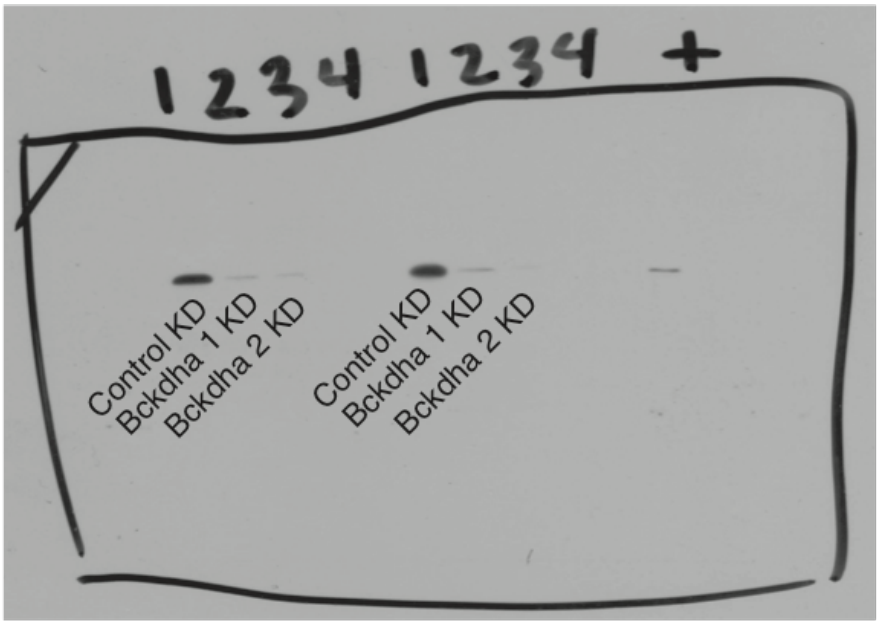

β-Actin

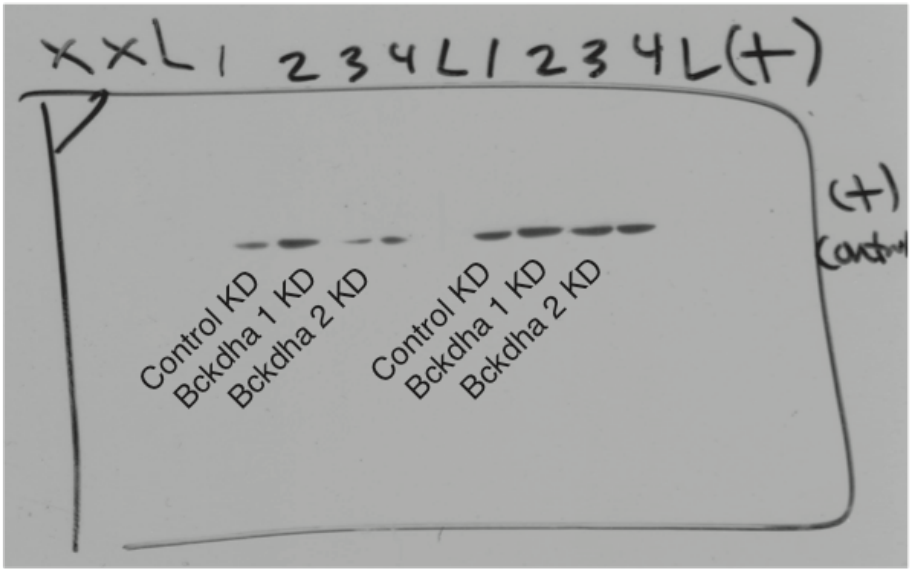

Figure S1.6: **Raw Western blot images. a**. Full, uncropped Western blot images.

Chapter S2

Supplement to Chapter 3

S2.1 Supplemental Tables and Figures

Table S2.1: **GC/MS fatty acid retention times.** Approximate retention time and molecular ion m/z.

Metabolite	**Retention time (mins)**	**m/z**
C15:0	16.9	256
iso-C16:0	17.8	270
C16:0	18.7	270
iso-C17:0	19.9	284
anteiso-C17:0	20.35	284
C17:0	21.0	284
iso-C18:0	23.7	298
C18:0	25.0	298

Table S2.2: **Baseline demographics and clinical characteristics of NAFLD patient cohort.** Data presented as mean (range).

Characteristic	**NASH (n=8)**	**NAFL (n=8)**
Sex	3M, 5F	5M, 3F
Age	47 (35-70)	55 (31-69)
BMI	34 (31-40)	31 (27-37)
AST	48 (26-102)	30 (22-46)
ALT	62 (40-122)	45 (22-96)
NAS (0-8)	5 (3-6)	3 (2-4)
Steatosis (0-3)	2 (1-3)	2 (1-3)
Fibrosis score (0-4)	2 (1-3)	0 (0-1)
Lobular inflammation (0-3)	2 (1-2)	1 (1-2)
Portal inflammation (0-2)	1 (1-2)	1 (0-1)

Table S2.3: **shRNA sequences.** Sequence of shRNAs used in KD experiments.

Gene name	shRNA sequence
Acyl-CoA dehydrogenase 8 (*Acad8*)	CCGGGCCTGGATGATTGATAGCTTTCTCGAGAAAGCTATCAATCATCCAGGCTTTTTG
Acyl-CoA dehydrogenase medium-chain (*Acadm*)	CCGGGCAAACTGCTATTGAAGCAAACTCGAGTTTGCTTCAATAGCAGTTTGCTTTTTG
Acyl-CoA dehydrogenase short-branched-chain (*Acadsb*)	CCGGGCTTCTTAGTAGACCGAGATACTCGAGTATCTCGGTCTACTAAGAAGCTTTTTG
Isovaleryl-CoA dehydrogenase (*Ivd*)	CCGGGCTGATATCCTAGTCGTGTATCTCGAGATACACGACTAGGATATCAGCTTTTTG
Acyl-CoA dehydrogenase short-chain (*Acads*)	CCGGCGTCAACAATTCTCTCTACTTCTCGAGAAGTAGAGAGAATTGTTGACGTTTTTG

Table S2.4: **CRISPR/Cas9 target sequences.** Forward and reverse single guide sequences of Fasn and Crat guides

Guide name	Forward sequence	Reverse sequence
NTC0095	CACCGGCCGTGTTGCTGGATACGCC	AAACGGCGTATCCAGCAACACGGCC
Fasn g1	CACCGTGTCTCCGAAAAGAGCCGGG	AAACCCCGGCTCTTTTCGGAGACAC
Fasn g2	CACCGTTGGTGGAGCCAATTAACAG	AAACCTGTTAATTGGCTCCACCAAC
Crat g1	CACCGTCCACAAGTGCAACTATGGG	AAACCCCATAGTTGCACTTGTGGAC
Crat g2	CACCGACCACCCACGCATATAACCG	AAACCGGTTATATGCGTGGGTGGTC
Crat g3	CACCGTTTGCTGCCAAACTCATCGA	AAACTCGATGAGTTTGGCAGCAAAC

Table S2.5: **Primer sequences used in gene expression analysis.** Forward and reverse primer sequences.

Gene name	Forward sequence	Reverse sequence
PPARγ (*Pparg2*)	TTCGCTGATGCACTGCCTAT	ACAGACTCGGCACTCAATGG
Adiponectin (*Adipoq*)	GACACCAAAAGGGCTCAGGA	GCCCTTCAGCTCCTGTCATT
Leptin (*Lep*)	GGGAGGAAAATGTGCTGGAGAC	AAGCCCAGGAATGAAGTCCAA
Acyl-CoA dehydrogenase 8 (*Acad8*)	TGGCGGAGTGGGATCAGAA	CCACATCTGTTCGCACATAGAC
Acyl-CoA dehydrogenase short-branched-chain (*Acadsb*)	CCCAACCTGCTTGTCTCCTTG	ATCCCTGGATCACCGATTTCT
Acyl-CoA dehydrogenase short-chain (*Acads*)	GACTGGCGACGGTTACACA	GGCAAAGTCACGGCATGTC
Isovaleryl-CoA dehydrogenase (*Ivd*)	GGACGGCGAGTTTCCAGTT	CCACAGGCAATATCGAGTGGG
Branched chain amino acid transaminase 2 (*Bcat2*)	CAGCCACACTAGGACAGGTCT	CAGCCTTGTTATTCCACTCCAC
Branched chain keto acid dehydrogenase A (*Bckdha*)	CTCCTGTTGGGACGATCTGG	CATTGGGCTGGATGAACTCAA
Carnitine acetyltransferase (*Crat*)	GCTGCCAGAACCGTGGTAAA	CCTTGAGGTAATAGTCCAGGGA
18S rRNA	AGTCCCTGCCCTTTGTACACA	CGATCCGAGGGCCTCACTA

Table S2.6: **GC-MS metabolite fragment ions used for analysis.** Fragment ions formula and m/z range used to quantify metabolite abundances.

Metabolite	Carbons	Formula	m/z
Acetate	12	$C_4H_9O_2Si$	117-120
Isovalerate	1-5	$C_7H_{15}O_2Si$	159-166
Leucine	2-6	$C_{13}H_{32}NOSi_2$	274-280
Isoleucine	2-6	$C_{11}H_{26}NSi$	200-206
Isoleucine	2-6	$C_{13}H_{32}NOSi_2$	274-280
Valine	2-5	$C_{12}H_{30}NOSi_2$	260-288
Valine	1-5	$C_{13}H_{30}NO_2Si_2$	288-296
Citrate	1-6	$C_{20}H_{39}O_6Si_3$	459-466
iso-C16:0	1-16	$C_{17}H_{34}O_2$	270-284
iso-C17:0	1-17	$C_{18}H_{36}O_2$	284-294
anteiso-C17:0	1-17	$C_{18}H_{36}O_2$	284-294
iso-C18:0	1-18	$C_{19}H_{38}O_2$	298-316

Table S2.7: **Simplified network for Isotopomer Spectral Analysis (ISA) used to determine contribution of oxPPP-derived NADPH to palmitate synthesis.**

Contribution to Palmitate synthesis (%)	**Description**
NADPH.l (a) → NADPH(a)	NADPH containing 1 ^{2}H tracer label
NADPH.d (a) → NADPH(a)	unlabeled NADPH (dilution)
14*NADPH (a) → Palm.s	
***de novo* lipogenesis (g(t) value)**	
Palm.s → Palm	Newly synthesized palmitate
Palm.d → Palm	Pre-existing or unlabeled palmitate
0*Palm → Palm.m	Mixing of pools for measurement

Table S2.8: **Simplified network for Isotopomer Spectral Analysis (ISA) used to determine contribution of oxPPP-derived NADPH to synthesis of BCFAs and OCFAs.**

Contribution to fatty acid synthesis (%)	**Description**
NADPH.l (a) → NADPH(a)	NADPH containing 1 ^{2}H tracer label
NADPH.d (a) → NADPH(a)	unlabeled NADPH (dilution)
12*NADPH (a) → FA.s	
***de novo* lipogenesis (g(t) value)**	
FA.s → FA	Newly synthesized FA
FA.d → FA	Pre-existing or unlabeled FA
0*FA → FA.m	Mixing of pools for measurement

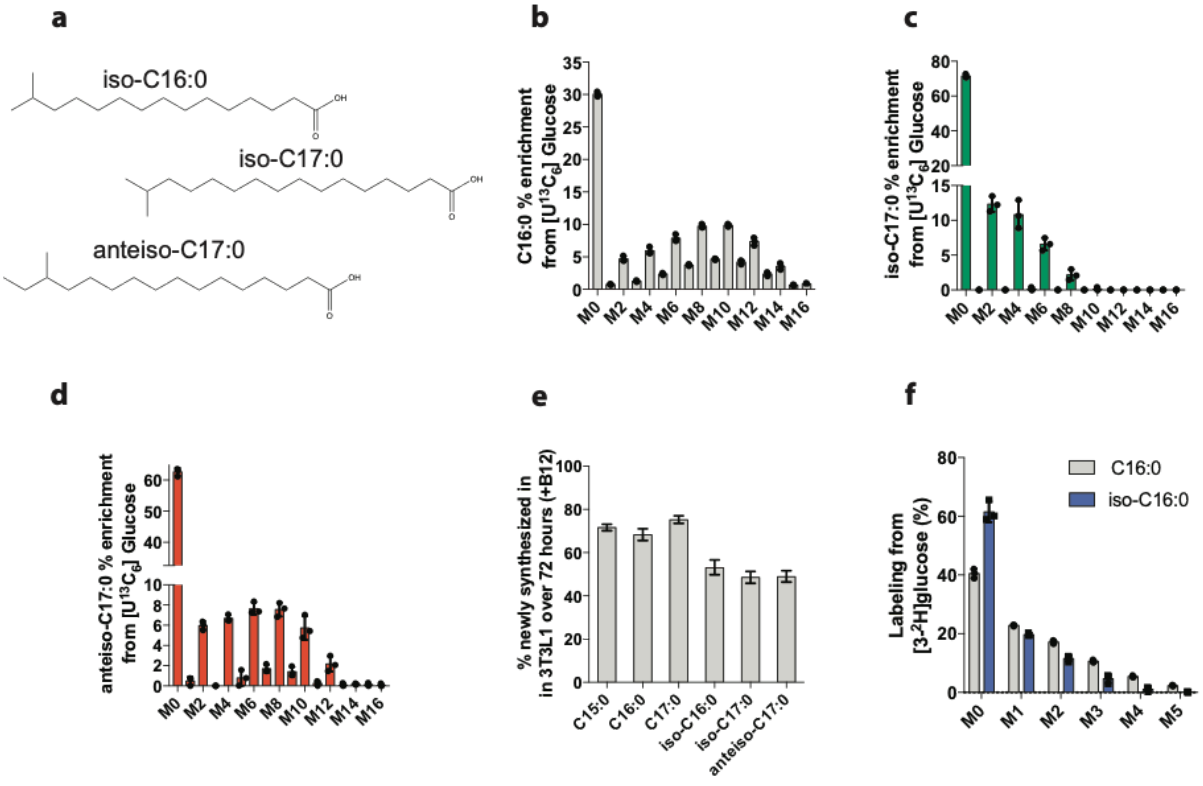

Figure S2.1: **mmBCFAs are *de novo* synthesized in 3T3-L1 cell culture. a**. Structures of mmBCFAs identified in 3T3-L1 adipocytes. **b-d**. Isotopologue distribution from [U-$^{13}C_6$]glucose in **b** palmitate, **c** iso-C17:0, and **d** anteiso-C17:0, respectively in 3T3-L1 cells. **e**. The percentage of each fatty acid newly synthesized, determined using isotopomer spectral analysis (ISA) of [3-^{2}H]glucose-traced 3T3-L1 adipocytes for 72 hours. **f**. Iso-C16:0 and palmitate labeling from [3-^{2}H]glucose in 3T3-L1 adipocytes cultured for 72 hours. All data are representative from three cell replicates and each experiment has been repeated 3 independent times with the same results obtained. Data are presented as means $\pm$ SEM with dot plots overlaid with the exception of **e**, where 95% confidence intervals from ISA model are shown.

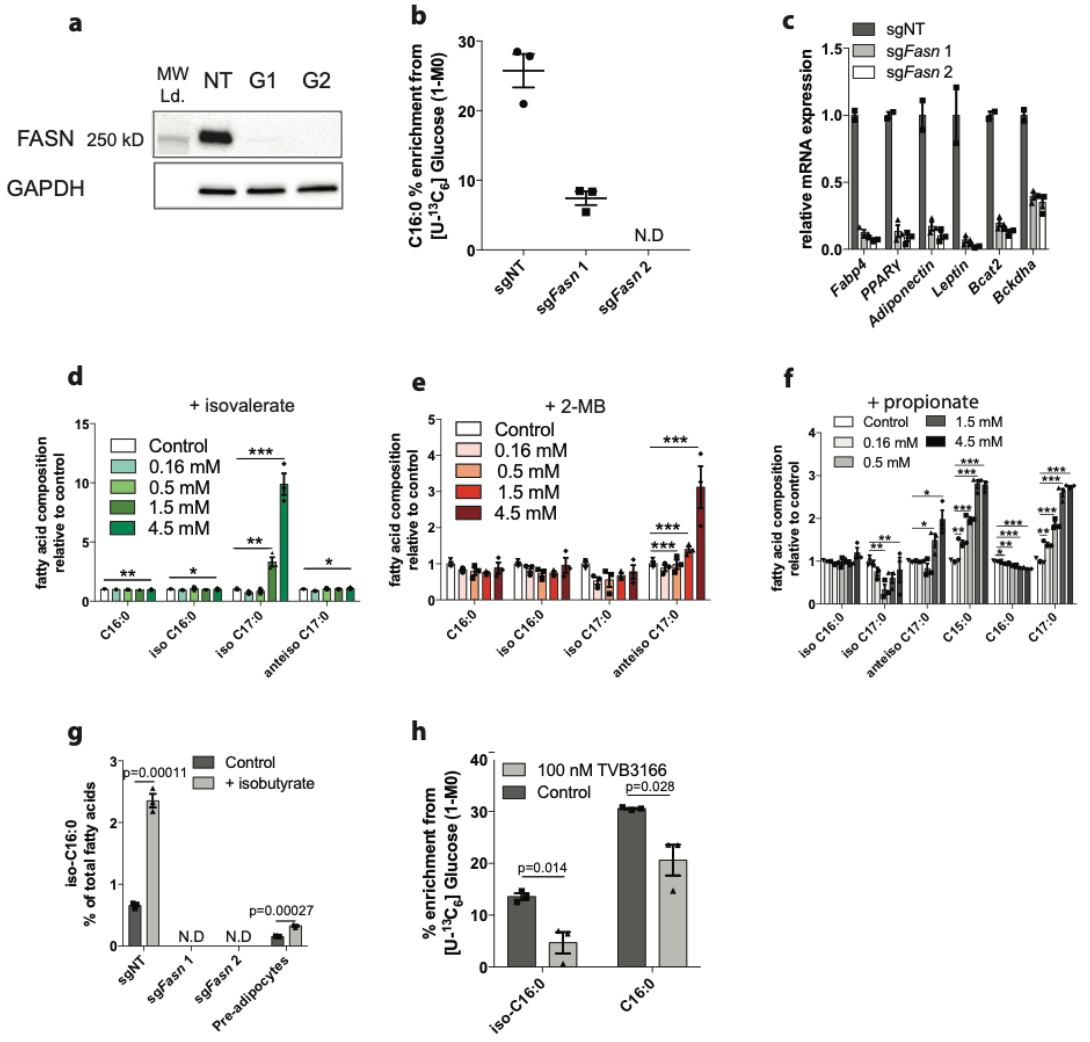

Figure S2.2: **mmBCFAs are *de novo* synthesized via FASN. a**. FASN levels in pooled CRISPR/Cas9 Fasn KO 3T3-L1 adipocytes (see 12a for full blot). **b**. Percentage enrichment of C16:0 after 48 hours in [U-$^{13}C_6$]glucose in pooled CRISPR/Cas9 Fasn KO 3T3-L1 adipocytes. **c**. Relative gene expression of adipocyte differentiation markers in Fasn KO 3T3-L1 adipocytes. **d-f**. Relative abundances of mmBCFAs and C16:0 in differentiated 3T3-L1s (day 8 post induction) following addition of **d**, isovalerate, **e**, 2-methyl-butyrate, or **f**, propionate, for 24 hours. Fatty acids calculated as percentage of total fatty acids and normalized to control conditions. Two-tailed Student's t-test was performed on three cellular replicates for each comparison with no adjustment for multiple comparisons. **g**. Iso-C16:0 levels as percentage of total fatty acid in pooled CRISPR/Cas9 Fasn KO 3T3-L1 adipocytes following addition of isobutyrate for 24 hours. **h**, Percentage enrichment of fatty acids in 3T3-L1 adipocytes after 48 hours in [U-$^{13}C_6$]glucose $\pm$ 100 nM TVB3166. Two-tailed Student's t-test was performed on three cellular replicates for each comparison with no adjustment for multiple comparisons. All data are representative from three cell replicates and each experiment has been repeated 2 independent times with the exception of **d-f** which have been repeated 3 independent times. Data are presented as means $\pm$ SEM with dot plots overlaid. *p<0.05, **p<0.01, ***p<0.001.

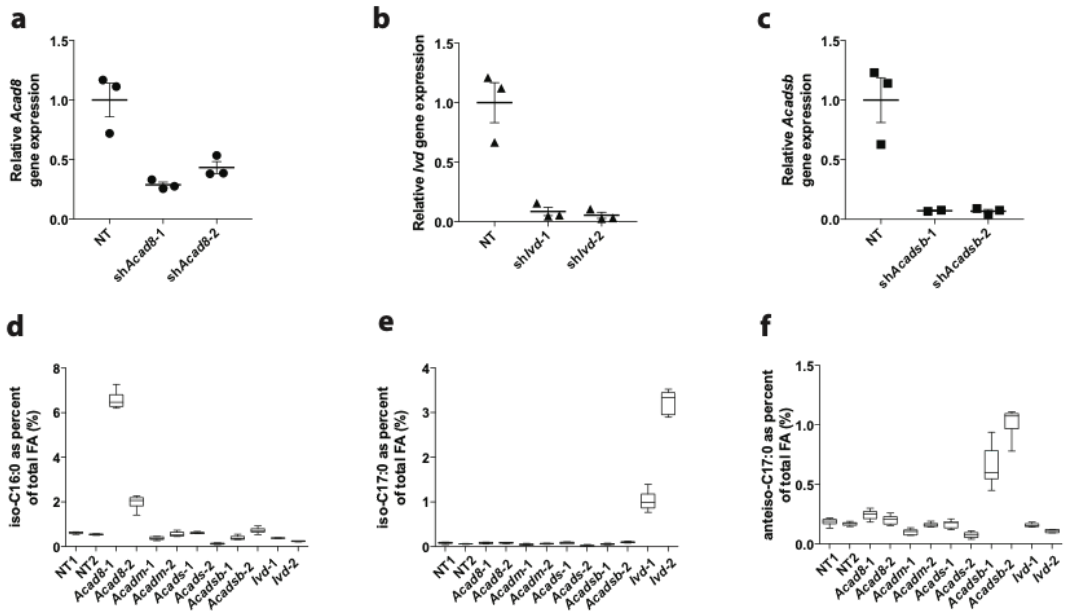

Figure S2.3: **Identification of ACADs that catabolize BCKDH products in 3T3-L1 cells.** **a-c**. mRNA levels of **a**, Acad8, **b**, Ivd, **c**, Acadsb relative to NT shRNA in 3T3-L1 adipocytes. Representative data from three cell replicates. Data are presented as means ± SEM with dot plots overlaid. **d-f**. Relative mmBCFA abundance in 3T3-L1 adipocytes following knockdown of Acad enzymes. Fatty acids are calculated as percentage of total fatty acids. Representative data from six cell replicates, data presented as box (25th to 75th percentile with median line) and whiskers (min to max values). 1 or 2 refers to different hairpins. Each experiment has been repeated 3 independent times.

Figure S2.4: **mmBCFAs are incorporated into distinct lipid species.** **a**. Differentiation between lipids (e.g. lysophosphatidylcholine; LPC) containing palmitate or iso-C16:0 in the acyl chain using stable isotope tracing and LC-MS analysis. **b-c**. Isotopologue distribution of **b**, C16:0, and **c**, iso-C16:0 from 3T3-L1 adipocytes cultured in ^{12}C or [U-$^{13}C_5$]valine and used for lipidomic analysis. Data from two cell replicates and presented as means $\pm$ SEM with dot plots overlaid. **d**. Volcano plot depicting fold change of enrichment and p-value for the M+4 ion in [U-$^{13}C_5$]valine-traced cells versus ^{12}C valine-traced cells (no isotope tracer) for 72 hours. Data from 3-4 cell replicates, p-value determined from two-tailed Student's t-test. **e**. Percentage enrichment of the most significantly enriched lipid species from [U-$^{13}C_5$]valine. Data from 3-4 cell replicates and presented as box and whiskers with error bars representing min to max values. **f**. BCFA abundance in media of 3T3-L1 cells treated with isoproterenol. Data are presented as means $\pm$ SEM with dot plots overlaid. Two-tailed Student's t-test was performed on three cellular replicates with no adjustment for multiple comparisons. Each experiment in this figure has been repeated 3 independent times.

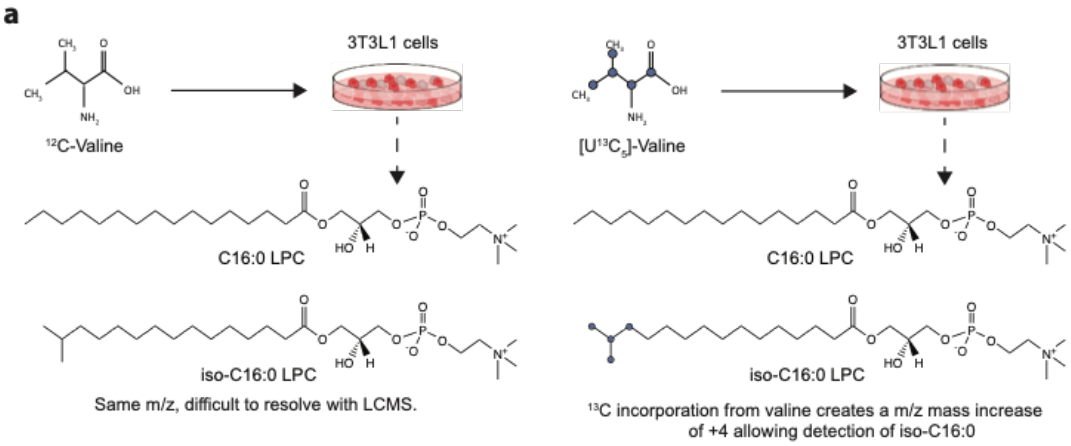
a
3T3L1 cells
^{12}C-Valine
[U^{13}C$_5$]-Valine
C16:0 LPC
iso-C16:0 LPC
Same m/z, difficult to resolve with LCMS.
^{13}C incorporation from valine creates a m/z mass increase of +4 allowing detection of iso-C16:0

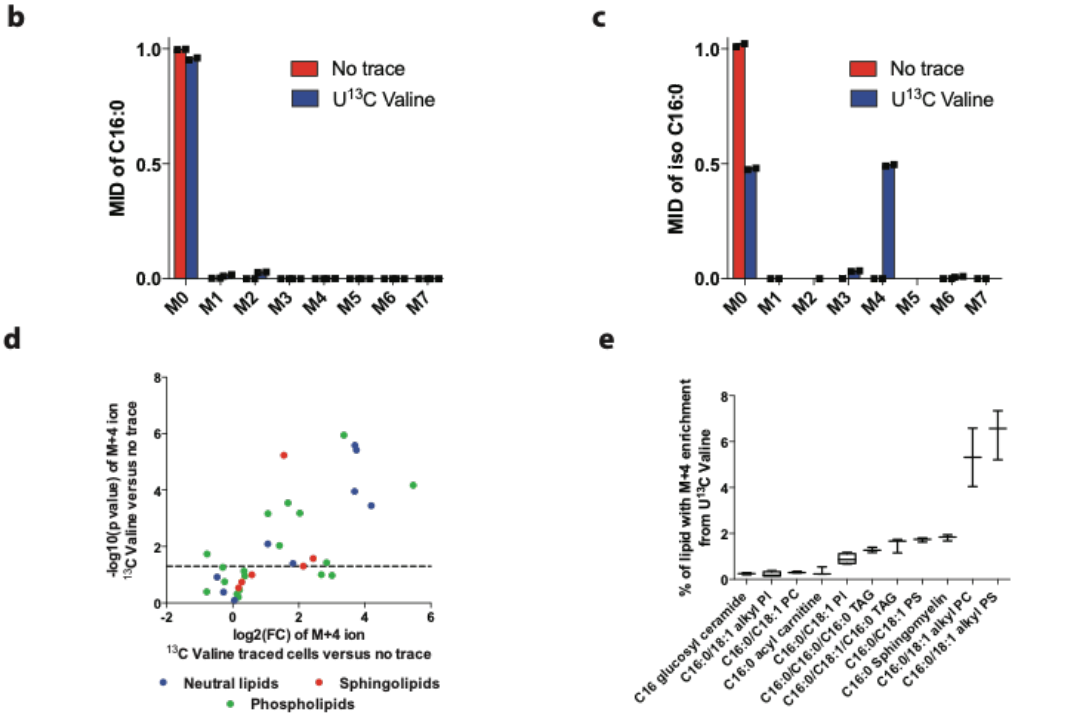
b
MID of C16:0
No trace
U^{13}C Valine
M0 M1 M2 M3 M4 M5 M6 M7
c
MID of iso C16:0
d
-log10(p value) of M+4 ion ^{13}C Valine versus no trace
log2(FC) of M+4 ion ^{13}C Valine traced cells versus no trace
Neutral lipids
Sphingolipids
Phospholipids
e
% of lipid with M+4 enrichment from U^{13}C Valine
C16 glucosyl ceramide
C16:0/18:1 alkyl PI
C16:0/C18:1 PC
C16:0 acyl carnitine
C16:0/C18:1 PI
C16:0/C16:0/C16:0 TAG
C16:0/C16:0/C18:1/C16:0 TAG
C16:0/C18:1 PS
C16:0 Sphingomyelin
C16:0/18:1 alkyl PC
C16:0/16:1 alkyl PS

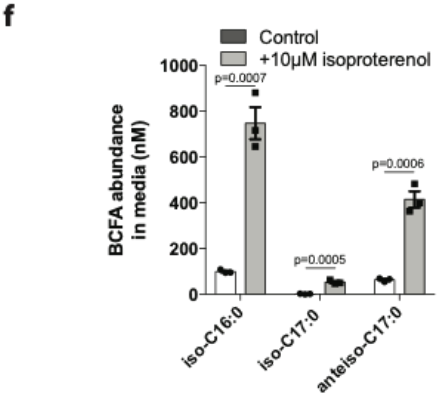
f
Control
+10μM isoproterenol
BCFA abundance in media (nM)
p=0.0007
p=0.0005
p=0.0006
iso-C16:0
iso-C17:0
anteiso-C17:0

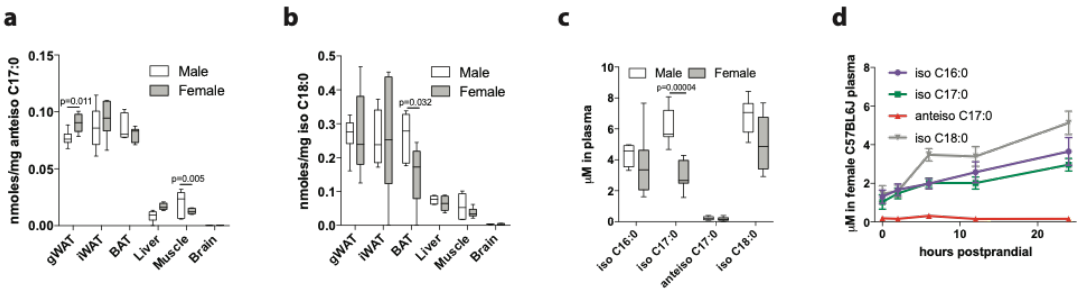

Figure S2.5: **Levels of mmBCFAs *in vivo*. a-c**. The abundance of **a**, anteiso-C17:0, and **b**, iso-C18:0, in various tissues (gWAT indicates gonadal WAT), and **c**, plasma mmBCFA levels from 16-week-old C57BL/6J male (n=6) and female mice (n=6). Two-tailed Student's t-test was performed for statistical comparison with no adjustment for multiple comparisons. Data presented as box (25th to 75th percentile with median line) and whiskers (min to max values). **d**. Plasma concentration of total hydrolyzed mmBCFAs from C57BL/6J female mice (n=8) following removal of food at time 0 (7 am) and sampled at 2hrs, 6hrs, 12hrs, and 24hrs. Data presented as means ± SEM.

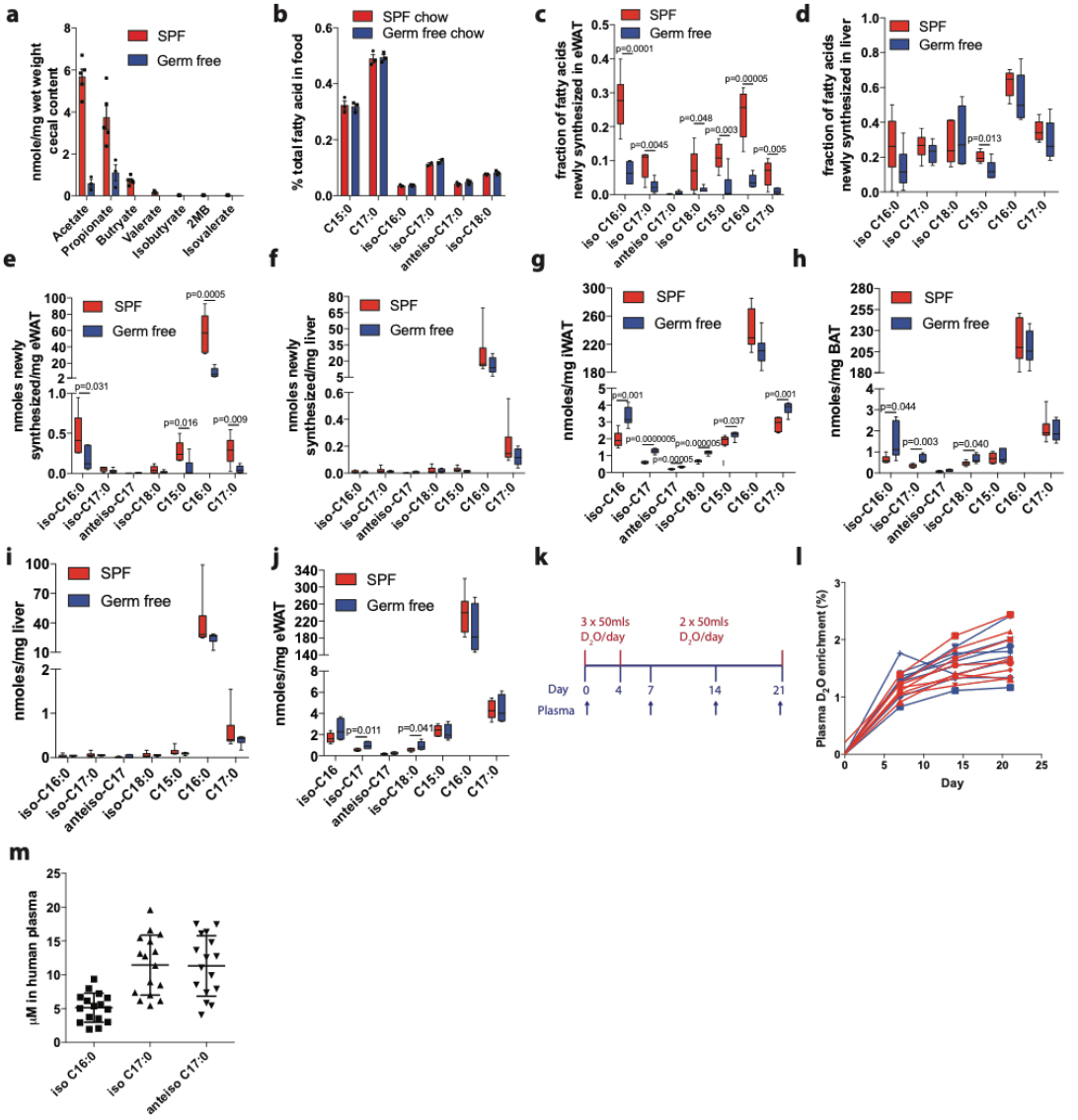

Figure S2.6: ***De novo*** **synthesis of mmBCFAs in germ-free mice and humans.** **a**. Short chain fatty acid (SCFA) levels in the cecum of germ-free (n=3) and specific pathogen free (SPF) (n=5) mice. Data presented as means ± SD with dot plot overlaid. **b**. mmBCFA and OCFA composition of chow fed to germ free and control mice (n=3 food pellets). Data presented as means ± SD with dot plot overlaid. **c-d**. Fractional synthesis of fatty acids in **c**, eWAT, and **d**, liver, **e-f**. Amount of newly synthesized fatty acids present in **e**, eWAT, and **f**, liver, **g-j**. Abundance of fatty acids in **g**, iWAT, **h**, BAT, **i**, liver, and **j**, eWAT of germ-free (n=6) and SPF mice (n=6). For **c-j**, two-tailed Student's t-test was performed for statistical comparison with no adjustment for multiple comparisons. Data presented as box (25th to 75th percentile with median line) and whiskers (min to max values). **k**. Overview of the study design for 2H2O administration and plasma collection from NAFLD patients. **l**. Plasma $^{2}H_2O$ enrichment during the 21 days of $^{2}H_2O$ administration (n=16). **m**. Levels of total plasma fatty acids in NAFLD patients (n=16). Data presented as means ± SD with dot plot overlaid.

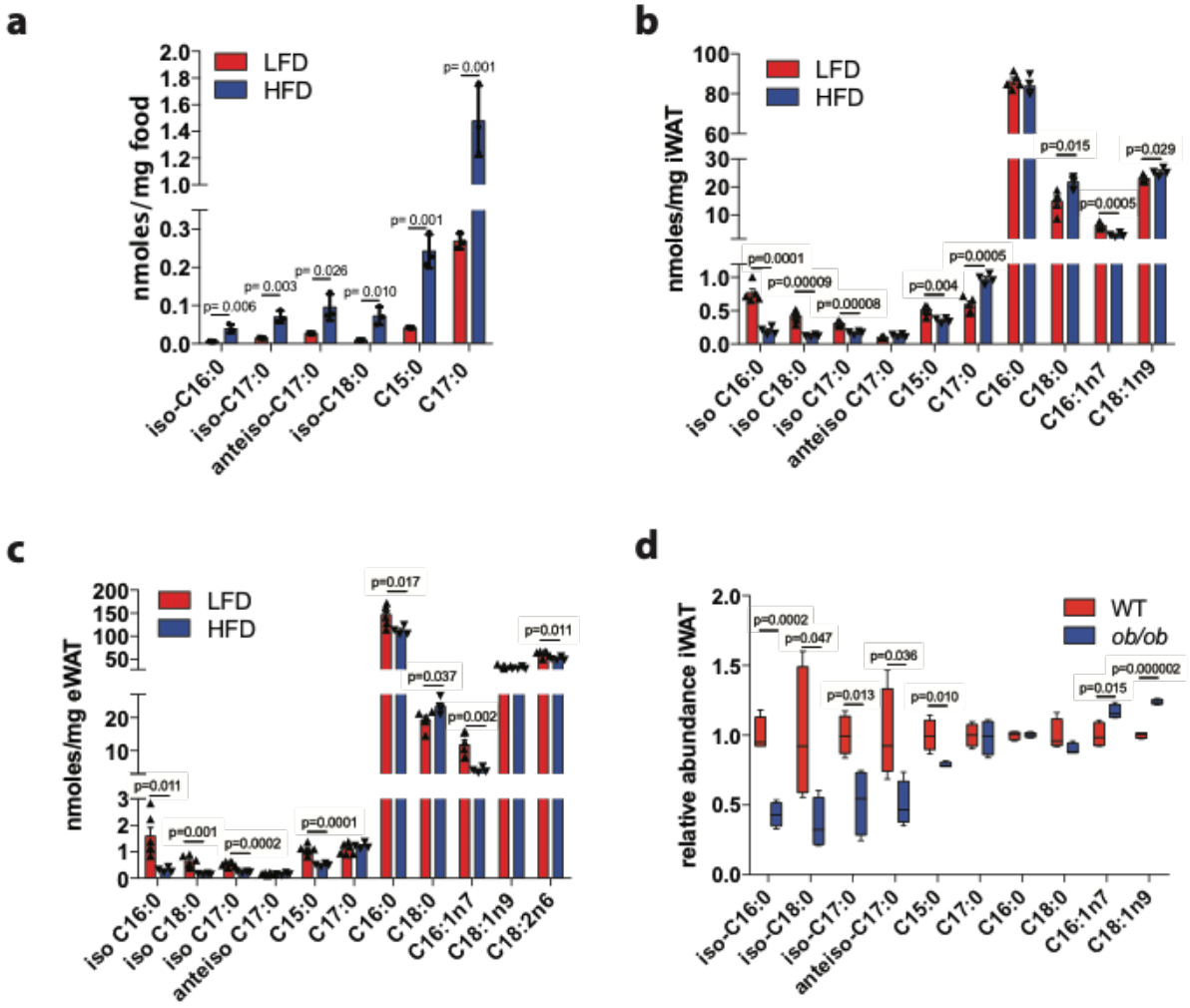

Figure S2.7: **mmBCFA levels change with high-fat diet. a**. mmBCFA and OCFA abundance in diets used (n=3 food pellets). **b**. Total fatty acid abundance in iWAT following LFD (n=5) or HFD (n=4) feeding for 15 weeks. **c**. Total fatty acid abundance in eWAT following LFD (n=6) or HFD (n=5) feeding for 15 weeks. **d**. Relative abundances of fatty acids in inguinal WAT from C57BL/6J(n=4) or ob/ob (n=4) mice. For **a-d**, two-tailed Student's t-test was performed for statistical comparison with no adjustment for multiple comparisons. Data in **a-c** presented as means $\pm$ SEM with dot plot overlaid and data presented in **d** as box (25th to 75th percentile with median line) and whiskers (min to max values).

Figure S2.8: ***De novo*** **synthesis of mmBCFAs from BCAAs *in vivo*. a**. Overview of study design for administration of isotope-enriched chow to C57BL/6J mice in the context of LFD or HFD. **b**. Fasting plasma glucose levels (n=6 HFD, n=6 LFD) and **c**, BCAA levels at termination of study (n=8 HFD, n=8 LFD). **d**. Leucine and valine plasma isotope enrichment after 3 weeks on indicated diet (n=8 HFD, n=8 LFD). **e-m**. Metabolite levels and enrichment from C57BL/6J mice fed a HFD or LFD with 25% of valine and leucine supplied as [U-^{13}C,^{15}N] isotope. **e**. leucine and **f**, valine relative abundance in tissue. N=8 for all comparisons except LFD iWAT (n=7), LFD eWAT (n=7), LFD BAT (n=7), LFD muscle (n=7), LFD heart (n=5), LFD brain (n=7), HFD iWAT(n=5), HFD BAT (n=7), HFD muscle (n=7) and HFD heart (n=5). **g-h**. Isotopologue distribution of iso-C17:0 and iso-C18:0 in BAT (n=8 HFD, n=8 LFD). **i**. ^{13}C molar enrichment of iso-C17:0. N=8 for all comparisons except LFD eWAT (n=7), LFD heart (n=5), LFD brain (n=7) and HFD iWAT (n=7). **j**. ^{13}C molar enrichment of iso-C18:0. N=8 for all comparisons except LFD heart (n=6), LFD brain (n=4) and HFD brain (n=4). **k**. Isotopologue distribution of C17:0 in the brain (n=8 HFD, n=7 LFD). **l**. Mole percent enrichment of C15:0 across tissues. N=8 for all comparisons except LFD eWAT (n=7), LFD heart (n=6), LFD brain (n=7) and HFD iWAT (n=7). **m**. Mole percent enrichment of C17:0 across tissues. N=8 for all comparisons except LFD eWAT (n=7), LFD heart (n=6), LFD brain (n=7) and HFD iWAT (n=7). Data are presented as means $\pm$ SEM with dot plots overlaid in **c-d, k**. All others are box (25th to 75th percentile with median line) and whiskers (min to max values). Two-tailed Student's t-test was performed for statistical comparisons with no adjustment for multiple comparisons.

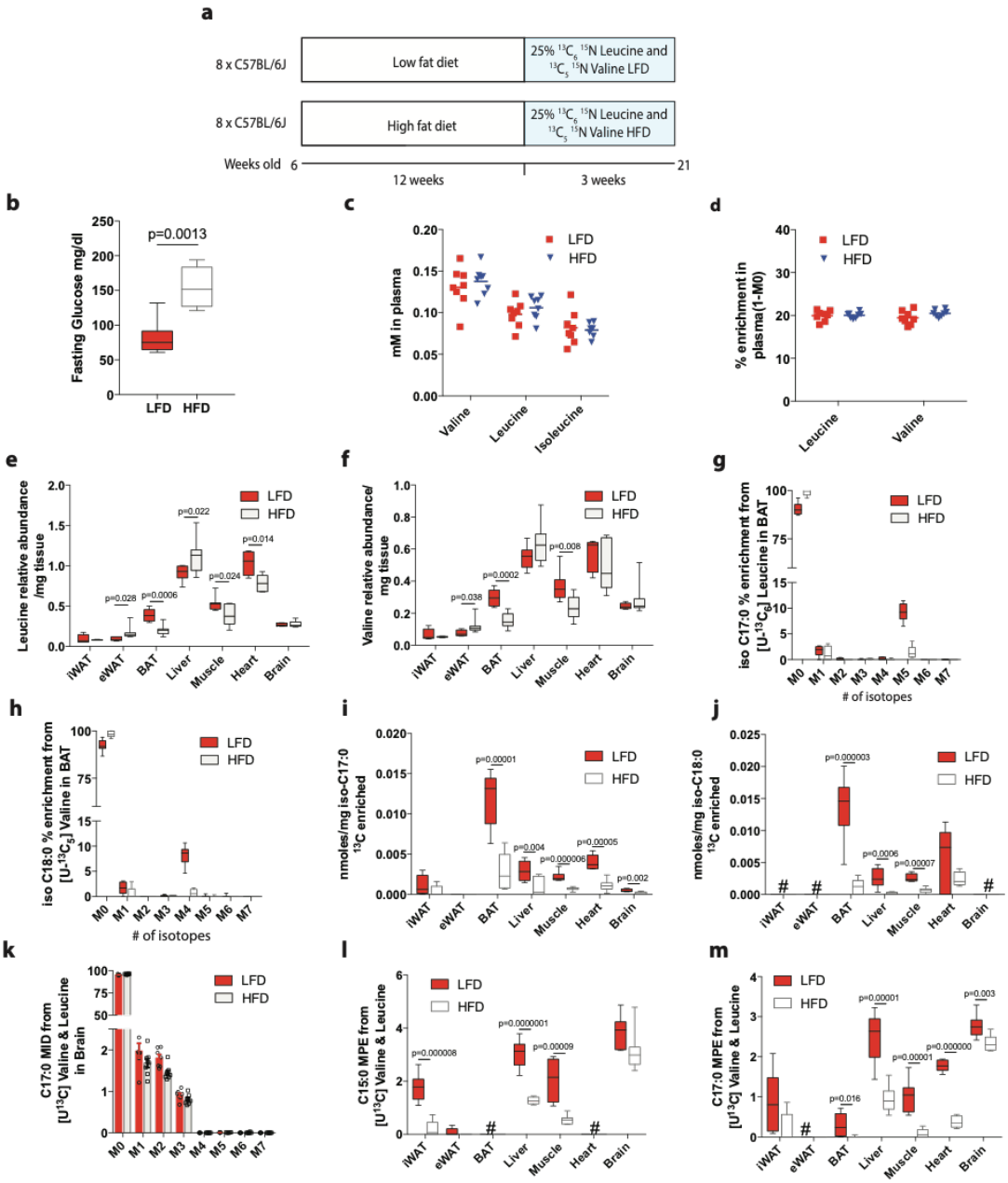
a
8 x C57BL/6J
Low fat diet
25% $^{13}C_6$ ^{15}N Leucine and $^{13}C_5$ ^{15}N Valine LFD
8 x C57BL/6J
High fat diet
25% $^{13}C_6$ ^{15}N Leucine and $^{13}C_5$ ^{15}N Valine HFD
Weeks old 6
12 weeks
3 weeks
21
b
Fasting Glucose mg/dl
p=0.0013
LFD HFD
c
mM in plasma
LFD
HFD
Valine
Leucine
Isoleucine
d
% enrichment in plasma(1-M0)
LFD
HFD
Leucine
Valine
e
Leucine relative abundance /mg tissue
LFD
HFD
p=0.028
p=0.0006
p=0.022
p=0.024
p=0.014
iWAT eWAT BAT Liver Muscle Heart Brain
f
Valine relative abundance/ mg tissue
LFD
HFD
p=0.038
p=0.0002
p=0.008
iWAT eWAT BAT Liver Muscle Heart Brain
g
iso C17:0 % enrichment from [U-$^{13}C_5$] Leucine in BAT
LFD
HFD
M0 M1 M2 M3 M4 M5 M6 M7
# of isotopes
h
iso C18:0 % enrichment from [U-$^{13}C_5$] Valine in BAT
LFD
HFD
M0 M1 M2 M3 M4 M5 M6 M7
# of isotopes
i
nmoles/mg iso-C17:0 ^{13}C enriched
LFD
HFD
p=0.00001
p=0.004
p=0.000006
p=0.00005
p=0.002
iWAT eWAT BAT Liver Muscle Heart Brain
j
nmoles/mg iso-C18:0 ^{13}C enriched
LFD
HFD
p=0.000003
p=0.0006
p=0.00007
# # # #
iWAT eWAT BAT Liver Muscle Heart Brain
k
C17:0 MID from [U-^{13}C] Valine & Leucine in Brain
LFD
HFD
M0 M1 M2 M3 M4 M5 M6 M7
l
C15:0 MPE from [U-^{13}C] Valine & Leucine
LFD
HFD
p=0.000008
p=0.0000001
p=0.00009
# #
iWAT eWAT BAT Liver Muscle Heart Brain
m
C17:0 MPE from [U-^{13}C] Valine & Leucine
LFD
HFD
p=0.00001
p=0.003
p=0.016
p=0.00001
p=0.000000
# #
iWAT eWAT BAT Liver Muscle Heart Brain

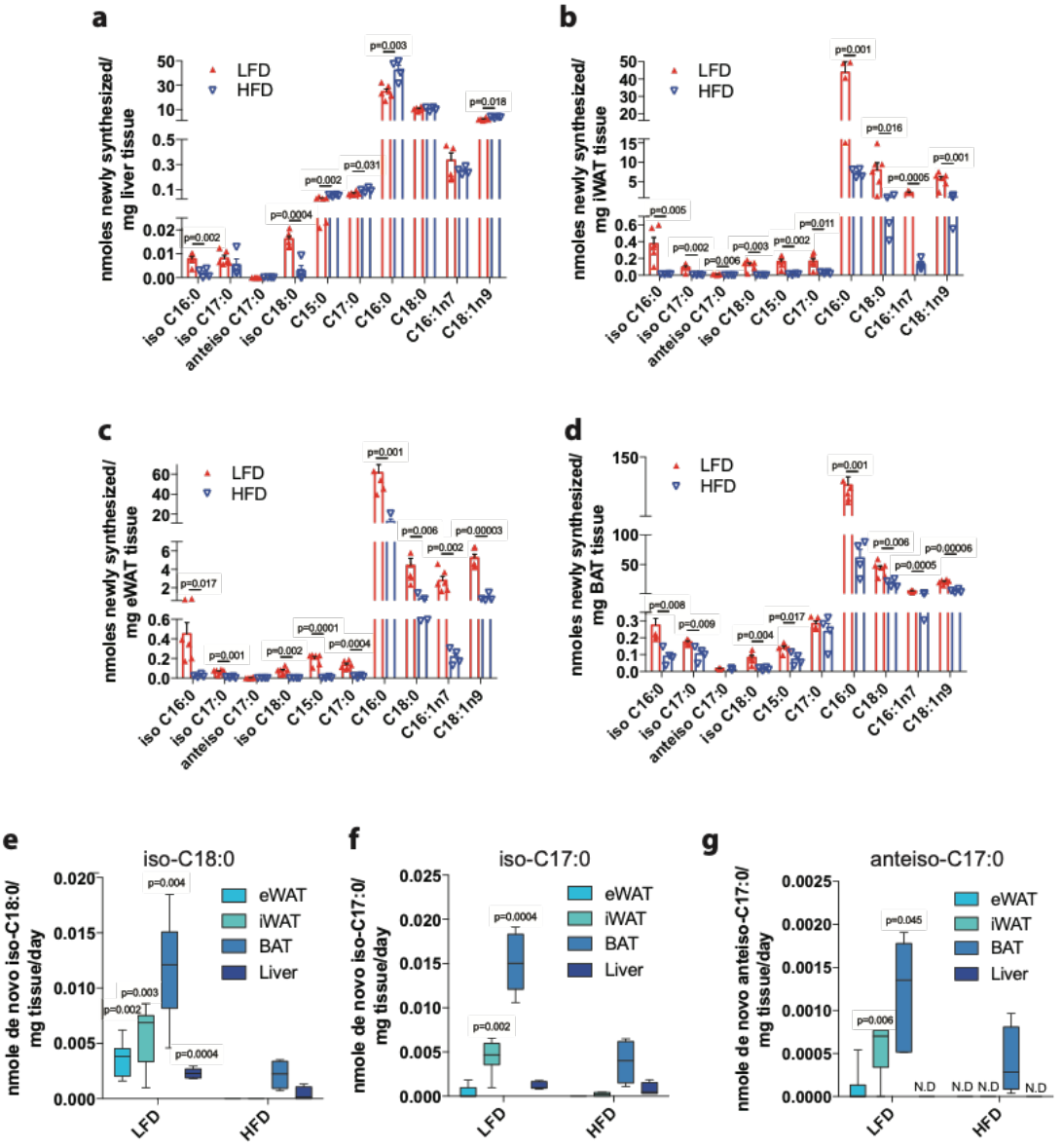

Figure S2.9: **Tissue-specific mmBCFA synthesis. a-d**. Amount of fatty acids newly synthesized over either a 3-week period (**b**, iWAT, **c**, eWAT, **d**, BAT) or 7-day period (**a**, liver) in HFD and LFD C57BL/6J mice as determined via incorporation of deuterium into newly synthesized lipids. LFD (n=6) and HFD (n=4) for all comparisons except LFD BAT iso-C16:0, iso-C17:0, anteiso-C17:0, C15:0, C17:0, C16:1n7 which had n=5. Data are presented as means ± SEM with dot plots overlaid. **e-g**. *De novo* lipogenic turnover of, **e**, iso-C18:0, **f**, iso-C17:0 and **g**, anteiso-C17:0 across the primary lipogenic tissues. Data presented as box (25th to 75th percentile with median line) and whiskers (min to max values). N.D. = not detected. Two-tailed Student's t-test was performed for all statistical comparisons with no adjustment for multiple comparisons.

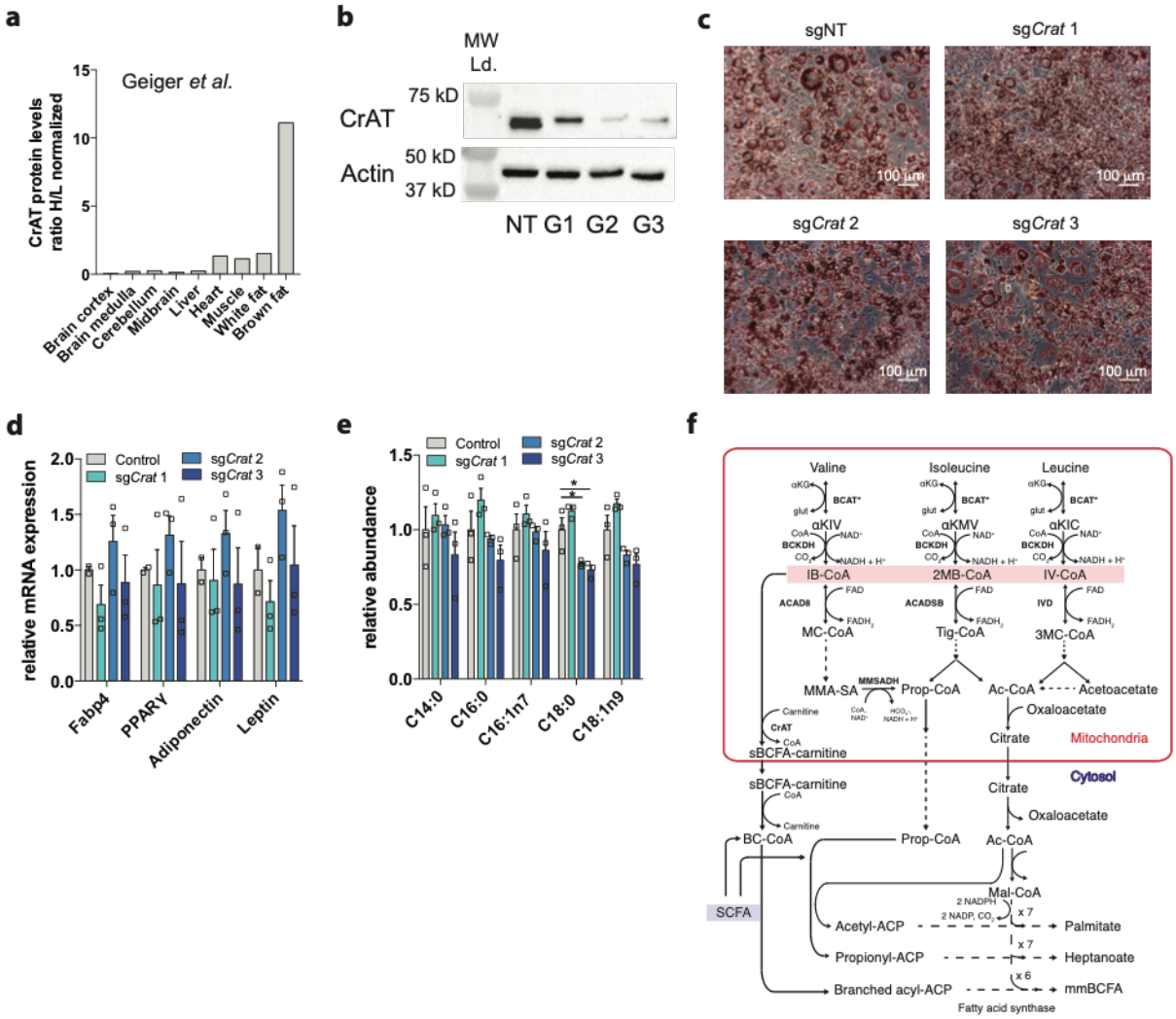

Figure S2.10: **CrAT drives mmBCFA synthesis. a**. Relative levels of CrAT across multiple tissue types determined via quantitative proteomics. Data generated from Geiger et al. **b-c**. CrAT levels (see 12b for full blot) and Oil Red O images (Scale bar represents 100 μm), of pooled CRISPR/Cas9 Crat KO 3T3-L1 adipocytes (7 days post induction of differentiation). Representative images and data from one independent experiment, three independent experiments have been carried out with the same result. **d**. Relative mRNA expression of adipocyte differentiation markers and relative fatty acid abundance in pooled CRISPR/Cas9 CrAT KO 3T3-L1 adipocytes (7 days post induction of differentiation). Representative data from three cell replicates, three independent experiments have been carried out with the same result. **f**. Pathway map depicting synthesis of OCFAs and mmBCFAs by FASN. Data are presented as means $\pm$ SEM with dot plots overlaid in **d-e**. Two-tailed Student's t-test was performed for all statistical comparisons with no adjustment for multiple comparisons. *p<0.05, **p<0.01, ***p<0.001

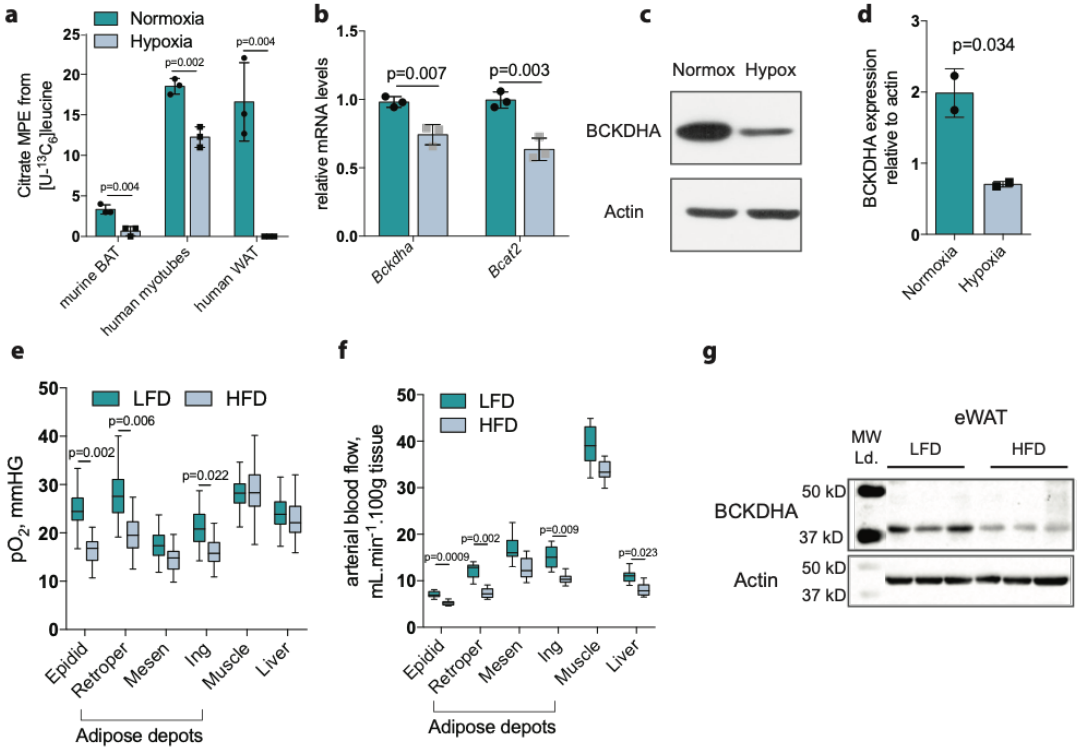

Figure S2.11: **Hypoxia suppresses BCAA catabolism.** **a**. Citrate mole percent enrichment from [U-$^{13}C_6$]leucine in primary brown adipocytes (BAT), primary human myotubes and white adipocytes (WAT) following 24 hours of tracing in hypoxia (1%) or normoxia. Representative data from 3 cell replicates, at least two independent experiments have been carried out with the same result. **b**. Relative mRNA levels of BCAA related genes in 3T3-L1 cells exposed to hypoxia (1%) or normoxia for 48 hours. Three independent replicates. **c-d**. BCKDHA protein levels in 3T3-L1 cells following exposure to hypoxia (1%) or normoxia for 48 hours (see 12c for full blot). **e**. Oxygen tension in various tissues in HFD and LFD C57BL/6J mice (n=4). **f**. Blood flow to various organs in LFD or HFD C57BL/6J mice (n=4). **g**. BCKDHA protein levels (see 12d for full blot) in epididymal white adipose tissue from LFD or HFD C57BL/6J mice (n=3 mice). Data are presented as means ± SEM overlaid with dot plots or box (25th to 75th percentile with median line) and whiskers (min to max values). Two-tailed Student's t-test was performed for all statistical comparisons with no adjustment for multiple comparisons.

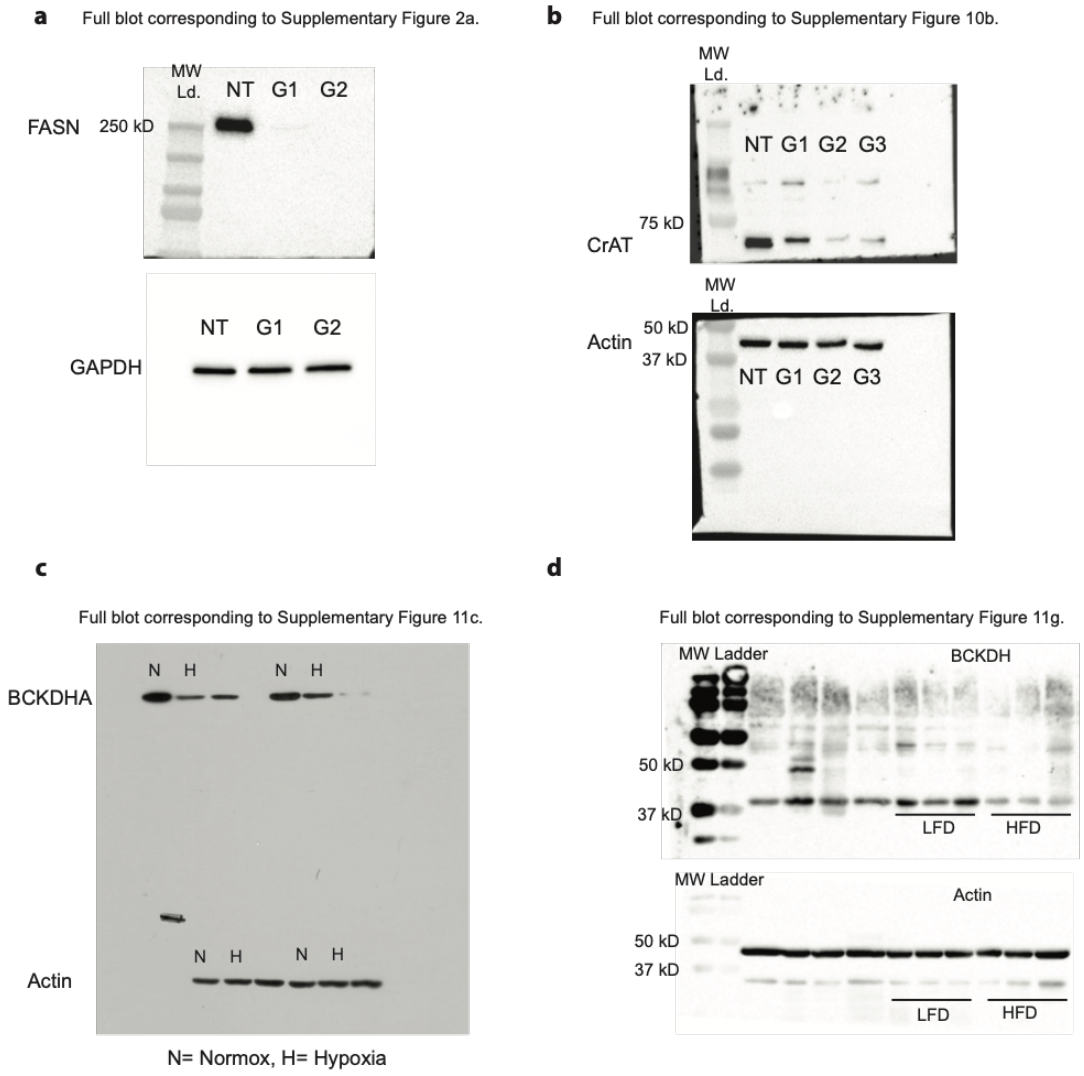

Figure S2.12: **Full Western Blots. a-d**. Full blots of **a**, corresponding to supplementary figure 2a, **b**, corresponding to supplementary figure 10b, **c**, corresponding to supplementary figure 11c, **d**, corresponding to supplementary figure 11g.

Chapter S3

Supplement to Chapter 4

S3.1 Supplemental Tables and Figures

Table S3.1: **CRISPR/Cas9 target sequences.** Sense and anti-sense single-guide sequences of Control, branched-chain ketoacid dehydrogenase alpha (Bckdha), and acyl-CoA dehydrogenase 8 (Acad8) guides used in pooled culture experiments.

Guide Target	Sense	Anti-sense
Control guide	CACCGGCCGTGTTGCTGGATACGCC	AAACGGCGTATCCAGCAACACGGCC
Bckdha guide 1	CACCGCAGCGAAATTGAAACCGGCG	AAACCGCCGGTTTCAATTTCGCTGC
Bckdha guide 2	CACCGTGAGGGATCTGCGTGGCCAG	AAACCTGGCCACGCAGATCCCTCAC
Bckdha guide 3	CACCGCATGACCAACTATGGCGAGG	AAACCCTCGCCATAGTTGGTCATGC
Acad8 guide 1	CACCGCCTTCCGCATCACATCCACA	AAACTGTGGATGTGATGCGGAAGGC
Acad8 guide 2	CACCGGCCAACAGGATTGGGACCG	AAACCGGTCCCAATCCTGTTGGCC
Acad8 guide 3	CACCGAGGTGAGTCAGACATCTATG	AAACCATAGATGTCTGACTCACCTC

Table S3.2: **Ion transitions, collision energies and fragmentor voltages for LC-MS DAG and MAG species.** Precursor ion, product ion, description of fragmentation to produce product ion, fragmentor voltage, and collision energy for each lipid species in lipidomics method.

Lipid Species	Precursor Ion	Product Ion	Description of product fragment	Frag (V)	CE
C15:0/C16:0 DAG	572.5	313.0	C16:0 loss	100	40
C15:0/C16:0 DAG	572.5	313.0	C16:0 loss	100	40
C15:0/C16:1 DAG	570.5	311.0	C16:1 loss	100	40
C15:0/C18:0 DAG	600.5	341.0	C18:0 loss	100	40
C16:0/C16:1 DAG	584.5	311.0	C16:1 loss	100	40
C15:0/C18:1 DAG	598.5	339.0	C18:1 loss	100	40
C16:0/C16:0 DAG	586.5	313.0	C16:0 loss	100	40
C16:0/C17:0 DAG	600.5	313.0	C16:0 loss	100	40
C16:0/C18:0 DAG	614.5	313.0	C16:0 loss	100	40
C16:0/C18:1 DAG	612.5	313.0	C16:0 loss	100	40
C16:0/C18:2 DAG	610.5	313.0	C16:0 loss	100	40
C16:0/C20:0 DAG	642.5	313.0	C16:0 loss	100	40
C16:0/C20:5 DAG	632.5	313.0	C16:0 loss	100	40
C16:0/C22:0 DAG	670.5	313.0	C16:0 loss	100	40
C16:0/C22:6 DAG	658.5	313.0	C16:0 loss	100	40
C16:1/C18:0 DAG	612.5	311.0	C16:1 loss	100	40
C16:1/C18:1 DAG	610.5	311.0	C16:1 loss	100	40
C17:0/C17:0 DAG	614.5	327.0	C17:0 loss	100	40
C17:0/C18:0 DAG	628.5	327.0	C17:0 loss	100	40
C17:0/C18:1 DAG	626.5	327.0	C17:0 loss	100	40
C17:0/C18:2 DAG	624.5	327.0	C17:0 loss	100	40
C17:0/C20:0 DAG	656.5	327.0	C17:0 loss	100	40
C17:0/C20:5 DAG	646.5	327.0	C17:0 loss	100	40
C17:0/C22:0 DAG	684.5	327.0	C17:0 loss	100	40
MAG 14:0	303	211.0	glycerol loss	100	8
MAG 15:0	317	225.0	glycerol loss	100	8
MAG 16:0	331	239.0	glycerol loss	100	8
MAG 17:0	345	253.0	glycerol loss	100	8
MAG 18:0	359	267.0	glycerol loss	100	8
MAG 18:1	357	265.0	glycerol loss	100	8
MAG 20:0	387	295.0	glycerol loss	100	8

Table S3.3: **Ion transitions, collision energies and fragmentor voltages for LC-MS PC and PE species.** Precursor ion, product ion, description of fragmentation to produce product ion, fragmentor voltage, and collision energy for each lipid species in lipidomics method.

Lipid Species	Precursor Ion	Product Ion	Description of product fragment	Frag (V)	CE
C32:1 PC	732.6	184.1	phosphocholine	100	40
C33:0 PC	748.5	184.1	phosphocholine	100	40
C33:1 PC	746.5	184.1	phosphocholine	100	40
C32:0 PC	734.6	184.1	phosphocholine	100	40
C34:0 PC	762.6	184.1	phosphocholine	100	40
C34:1 PC	760.6	184.1	phosphocholine	100	40
C35:0 PC	776.5	184.1	phosphocholine	100	40
C35:1 PC	774.5	184.1	phosphocholine	100	40
C36:0 PC	790.5	184.1	phosphocholine	100	40
C36:1 PC	788.5	184.1	phosphocholine	100	40
C36:2 PC	786.5	184.1	phosphocholine	100	40
C36:3 PC	784.5	184.1	phosphocholine	100	40
C38:1 PC	816.5	184.1	phosphocholine	100	40
C38:6 PC	806.5	184.1	phosphocholine	100	40
C39:1 PC	830.5	184.1	phosphocholine	100	40
C40:1 PC	844.5	184.1	phosphocholine	100	40
C40:7 PC	832.5	184.1	phosphocholine	100	40
C41:1 PC	858.5	184.1	phosphocholine	100	40
C30:0 PE	664.4	523.5	PE loss	100	40
C31:0 PE	678.4	537.5	PE loss	100	40
C32:0 PE	692.4	551.5	PE loss	100	40
C33:0 PE	706.5	565.5	PE loss	100	40
C34:0 PE	720.5	579.5	PE loss	100	40
C34:1 PE	718.5	577.5	PE loss	100	40
C34:2 PE	716.5	575.5	PE loss	100	40
C35:0 PE	734.5	593.5	PE loss	100	40
C35:1 PE	732.5	591.5	PE loss	100	40
C35:2 PE	730.5	589.5	PE loss	100	40
C36:0 PE	748.5	607.5	PE loss	100	40
C36:1 PE	746.5	605.5	PE loss	100	40
C36:2 PE	744.5	603.5	PE loss	100	40
C36:3 PE	742.5	601.5	PE loss	100	40
C36:4 PE	740.5	599.5	PE loss	100	40
C36:5 PE	738.5	597.5	PE loss	100	40
C37:0 PE	762.5	621.5	PE loss	100	40
C38:0 PE	776.5	635.5	PE loss	100	40
C38:6 PE	764.5	623.5	PE loss	100	40
C39:0 PE	790.5	649.5	PE loss	100	40
C40:0 PE	804.5	663.5	PE loss	100	40

Table S3.4: **Ion transitions, collision energies and fragmentor voltages for LC-MS LPC, LPS, and LPE species.** Precursor ion, product ion, description of fragmentation to produce product ion, fragmentor voltage, and collision energy for each lipid species in lipidomics method.

Lipid Species	Precursor Ion	Product Ion	Description of product fragment	Frag (V)	CE
C14:0 LPC	468.3	184.1	phosphocholine	100	40
C15:0 LPC	482.3	184.1	phosphocholine	100	40
C16:0 LPC	496.3	184.1	phosphocholine	100	40
C16:1 LPC	494.3	184.1	phosphocholine	100	40
C17:0 LPC	510.3	184.1	phosphocholine	100	40
C18:0 LPC	524.3	184.1	phosphocholine	100	40
C18:1 LPC	522.3	184.1	phosphocholine	100	40
C18:2 LPC	520.3	184.1	phosphocholine	100	40
C20:0 LPC	552.3	184.1	phosphocholine	100	40
C20:5 LPC	542.3	184.1	phosphocholine	100	40
C22:0 LPC	580.3	184.1	phosphocholine	100	40
C22:6 LPC	568.3	184.1	phosphocholine	100	40
C14:0 LPE	426.3	44.1	1-aminoethyl	100	40
C15:0 LPE	440.3	44.1	1-aminoethyl	100	40
C16:0 LPE	454.3	44.1	1-aminoethyl	100	40
C17:1 LPE	466.3	44.1	1-aminoethyl	100	40
C17:0 LPE	468.3	44.1	1-aminoethyl	100	40
C18:0 LPE	482.3	44.1	1-aminoethyl	100	40
C18:1 LPE	480.3	44.1	1-aminoethyl	100	40
C20:0 LPE	510.3	44.1	1-aminoethyl	100	40
C20:5 LPE	500.3	44.1	1-aminoethyl	100	40
C22:0 LPE	538.3	44.1	1-aminoethyl	100	40
C22:6 LPE	526.3	44.1	1-aminoethyl	100	40
C14:0 LPS	470.3	285.3	PS loss	100	20
C15:0 LPS	484.3	299.3	PS loss	100	20
C16:0 LPS	498.3	313.3	PS loss	100	20
C16:1 LPS	496.3	311.3	PS loss	100	20
C17:0 LPS	512.3	327.3	PS loss	100	20
C18:0 LPS	526.3	341.3	PS loss	100	20
C18:1 LPS	524.3	339.3	PS loss	100	20
C20:0 LPS	554.3	369.3	PS loss	100	20
C20:4 LPS	546.3	361.3	PS loss	100	20
C20:5 LPS	544.3	359.3	PS loss	100	20
C22:0 LPS	582.3	397.3	PS loss	100	20
C22:6 LPS	570.3	385.3	PS loss	100	20

Table S3.5: **Ion transitions, collision energies and fragmentor voltages for LC-MS TAG species C42-C50.** Precursor ion, product ion, description of fragmentation to produce product ion, fragmentor voltage, and collision energy for each lipid species in lipidomics method. Asterisk (*) indicate species that contain 2 OCFAs.

Lipid Species	Precursor Ion	Product Ion	Description of product fragment	Frag (V)	CE
TAG 42:0 (d28:0)	740.7	495.5	Loss of C14:0	100	40
TAG 43:0 (d28:0)	754.7	495.5	Loss of C15:0	100	40
TAG 44:0 (d28:0)	768.7	495.5	Loss of C16:0	100	40
TAG 44:0 (d29:0)*	768.7	509.5	Loss of C15:0	100	40
TAG 45:0 (d29:0)	782.7	509.5	Loss of C16:0	100	40
TAG 45:0 (d30:0)	782.7	523.5	Loss of C15:0	100	40
TAG 45:0 (d31:0)	782.7	537.5	Loss of C16:0	100	40
TAG 46:0 (d29:0)*	796.7	509.5	Loss of C17:0	100	40
TAG 46:0 (d31:0)*	796.7	537.5	Loss of C15:0	100	40
TAG 46:0 (d32:0)	796.7	551.5	Loss of C14:0	100	40
TAG 47:0 (d29:0)	810.7	565.5	Loss of C18:0	100	40
TAG 47:0 (d30:0)	810.7	523.5	Loss of C17:0	100	40
TAG 47:0 (d32:0)	810.7	551.5	Loss of C15:0	100	40
TAG 47:0 (d33:0)	810.7	565.5	Loss of C14:0	100	40
TAG 48:0 (d30:0)	824.7	523.5	Loss of C18:0	100	40
TAG 48:0 (d31:0)*	824.7	537.5	Loss of C17:0	100	40
TAG 48:0 (d32:0)	824.7	551.5	Loss of C16:0	100	40
TAG 48:1 (d32:0)	822.7	551.5	Loss of C16:1	100	40
TAG 48:2 (d32:1)	820.7	549.5	Loss of C16:1	100	40
TAG 48:2 (d32:2)	820.7	547.5	Loss of C16:0	100	40
TAG 48:3 (d32:2)	818.7	547.5	Loss of C16:1	100	40
TAG 49:0 (d31:0)	838.7	537.5	Loss of C18:0	100	40
TAG 49:0 (d32:0)	838.7	551.5	Loss of C17:0	100	40
TAG 49:1 (d31:0)	836.7	537.5	Loss of C18:1	100	40
TAG 50:0 (d32:0)	852.8	551.5	Loss of C18:0	100	40
TAG 50:0 (d33:0)*	852.8	565.5	Loss of C17:0	100	40
TAG 50:0 (d35:0)*	852.8	593.5	Loss of C15:0	100	40
TAG 50:1 (d32:0)	850.8	551.5	Loss of C18:1	100	40
TAG 50:2 (d32:0)	848.8	551.5	Loss of C18:2	100	40
TAG 50:2 (d32:1)	848.8	549.5	Loss of C18:1	100	40
TAG 50:3 (d32:0)	846.7	551.5	Loss of C18:3	100	40
TAG 50:3 (d32:1)	846.7	549.5	Loss of C18:2	100	40
TAG 50:3 (d32:2)	846.7	547.5	Loss of C18:1	100	40

Table S3.6: **Ion transitions, collision energies and fragmentor voltages for LC-MS TAG species C51-C56.** Precursor ion, product ion, description of fragmentation to produce product ion, fragmentor voltage, and collision energy for each lipid species in lipidomics method. Asterisk (*) indicate species that contain 2 OCFAs.

Lipid Species	Precursor Ion	Product Ion	Description of product fragment	Frag (V)	CE
TAG 51:0 (d34:0)	866.8	579.5	Loss of C17:0	100	40
TAG 51:0 (d35:0)	866.8	593.5	Loss of C16:0	100	40
TAG 51:1 (d33:0)	864.8	565.5	Loss of C18:1	100	40
TAG 52:0 (d32:0)	880.7	551.5	Loss of C20:0	100	40
TAG 52:0 (d34:0)	880.7	579.5	Loss of C18:0	100	40
TAG 52:0 (d35:0)*	880.7	593.5	Loss of C17:0	100	40
TAG 52:1 (d36:1)	878.8	605.5	Loss of C16:0	100	40
TAG 52:2 (d34:1)	876.8	577.5	Loss of C18:1	100	40
TAG 52:2 (d34:2)	876.8	575.5	Loss of C18:0	100	40
TAG 52:4 (d32:0)	872.7	551.5	Loss of C20:4	100	40
TAG 52:6 (d30:0)	868.7	523.5	Loss of C22:6	100	40
TAG 53:0 (d35:0)	894.8	593.5	Loss of C18:0	100	40
TAG 53:1 (d35:0)	892.8	593.5	Loss of C18:1	100	40
TAG 54:0 (d36:0)	908.8	607.5	Loss of C18:0	100	40
TAG 54:0 (d37:0)*	908.8	621.5	Loss of C17:0	100	40
TAG 54:0 (d38:0)	908.8	635.5	Loss of C16:0	100	40
TAG 54:6 (d32:0)	896.7	551.5	Loss of C22:6	100	40
TAG 54:6 (d36:5)	896.7	597.5	Loss of C18:1	100	40
TAG 55:6 (d33:0)	910.7	565.5	Loss of C22:6	100	40
TAG 56:6 (d34:0)	924.7	579.5	Loss of C22:6	100	40

Table S3.7: **Ion transitions, collision energies and fragmentor voltages for LC-MS PS species.** Precursor ion, product ion, description of fragmentation to produce product ion, fragmentor voltage, and collision energy for each lipid species in lipidomics method.

Lipid Species	Precursor Ion	Product Ion	Description of product fragment	Frag (V)	CE
C30:0 PS	708.4	523.5	PS loss	100	20
C31:0 PS	722.4	537.5	PS loss	100	20
C32:0 PS	736.4	551.5	PS loss	100	20
C33:0 PS	750.4	565.5	PS loss	100	20
C34:0 PS	764.5	579.5	PS loss	100	20
C34:1 PS	762.5	577.5	PS loss	100	20
C34:2 PS	760.5	575.5	PS loss	100	20
C35:0 PS	778.5	593.5	PS loss	100	20
C35:1 PS	776.5	591.5	PS loss	100	20
C36:0 PS	792.5	607.5	PS loss	100	20
C36:1 PS	790.5	605.5	PS loss	100	20
C36:2 PS	788.5	603.5	PS loss	100	20
C36:3 PS	786.5	601.5	PS loss	100	20
C36:4 PS	784.5	599.5	PS loss	100	20
C36:5 PS	782.5	597.5	PS loss	100	20
C37:0 PS	806.5	621.5	PS loss	100	20
C38:0 PS	820.5	635.5	PS loss	100	20
C38:6 PS	808.5	623.5	PS loss	100	20
C39:0 PS	834.5	649.5	PS loss	100	20
C39:6 PS	822.5	637.5	PS loss	100	20
C40:0 PS	848.5	663.5	PS loss	100	20

Table S3.8: **Ion transitions, collision energies and fragmentor voltages for LC-MS Ceramide/Sphingoid base method.** Precursor ion, product ion, description of fragmentation to produce product ion, fragmentor voltage, and collision energy for each lipid species in method.

Lipid Species	Precursor Ion	Product Ion	Frag (V)	CE
DHCer (d18:0/15:0)	526.4	508.4	100	17
DHCer (d18:0/16:0)	540.4	522.4	100	17
DHCer (d18:0/18:0)	568.4	550.4	100	17
DHCer (d18:0/20:0)	596.4	578.4	100	17
DHCer (d18:0/22:0)	624.4	606.4	100	17
DHCer (d18:0/24:0)	652.4	634.4	100	17
Cer (d18:1/16:0)	538.4	264.4	110	25
Cer (d18:1/16:1)	536.4	264.4	110	25
Cer (d18:1/18:1)	566.7	264.4	110	25
Cer (d18:1/20:0)	594.4	264.4	110	25
Cer (d18:1/20:5)	584.4	264.4	110	25
Cer (d18:1/22:0)	622.4	264.4	110	25
Cer (d18:1/22:1)	620.4	264.4	110	25
Cer (d18:1/22:6)	610.4	264.4	110	25
Cer (d18:1/24:0)	650.4	264.4	110	25
Cer (d18:1/24:1)	648.4	264.4	110	25
doxSA (m18:0)	286.4	268.4	118	13
SA (d18:0)	302.4	284.4	120	9
SO (d18:1)	300.3	282.4	112	9
Sphingomyelin (d18:1/12:0)	647.4	184.0	82	25
Sphingomyelin (d18:1/14:0)	675.4	184.0	82	25
Sphingomyelin (d18:1/15:0)	689.4	184.0	82	25
Sphingomyelin (d18:1/16:0)	703.4	184.0	82	25
Sphingomyelin (d18:1/16:1)	701.4	184.0	82	25
Sphingomyelin (d18:1/17:0)	717.4	184.0	82	25
Sphingomyelin (d18:1/18:0)	731.4	184.0	82	25
Sphingomyelin (d18:1/18:1)	729.4	184.0	82	25
Sphingomyelin (d18:1/20:0)	759.4	184.0	82	25
Sphingomyelin (d18:1/20:5)	749.4	184.0	82	25
Sphingomyelin (d18:1/22:0)	787.4	184.0	82	25
Sphingomyelin (d18:1/22:1)	785.4	184.0	82	25
Sphingomyelin (d18:1/22:6)	773.4	184.0	82	25
Sphingomyelin (d18:1/24:0)	815.4	184.0	82	25
Sphingomyelin (d18:1/24:1)	813.4	184.0	82	25
Gluc/Gal-Ceramide (d18:1/16:0)	700.4	264.2	123	37
Lactosyl-Ceramide (d18:1/16:0)	862.4	264.2	88	41

Table S3.9: **Ion transitions, collision energies and fragmentor voltages for standards used in LC-MS Ceramide/Sphingoid base method.** Precursor ion, product ion, description of fragmentation to produce product ion, fragmentor voltage, and collision energy for each lipid species in method.

Lipid Species	Precursor Ion	Product Ion	Frag (V)	CE
DHCer (d18:0-d7/13:0)	505.5	487.5	100	17
Cer (d18:1-d7/15:0)	531.4	271.4	110	25
doxSA (m18:0-d3)	289.3	271.5	118	13
SA (d18:0-d7)	309.4	291.5	120	9
SO (d18:1-d7)	307.3	289.4	112	9
Sphingomyelin (d18:1-d9/18:1)	738.4	184.0	82	25
Gluc/Gal-Ceramide (d18:1-d7/15:0)	693.5	271.2	123	37
Lactosyl-Ceramide (d18:1-d7/15:0)	855.6	271.2	88	41

Table S3.10: **Primer sequences.** Forward and reverse sequences of primers used to quantify expression of genes using quantitative RT-PCR.

Gene name	Forward sequence	Reverse sequence
RPL27 rRNA	ACATTGACGATGGCACCTC	GCTTGGCGATCTTCTTCTTG
Ceramide Synthase 1 (CerS1)	CCACCACACACATCTTTCGG	GGAGCAGGTAAGCGCAGTAG
Ceramide Synthase 2 (CerS2)	ATGCTCCAGACCTTGTATGACT	CTGAGGCTTTGGCATAGACAC
Ceramide Synthase 5 (CerS5)	CGGGGAAAGGTGTCTAAGGAT	GTTCATGCAGTTGGCACCATT
Ceramide Synthase 6 (CerS6)	GATTCATAGCCAAACCATGTGCC	AATGCTCCGAACATCCCAGTC
Sphingomyelin synthase 1 (Sgms1)	TTGGCACGCTGTACCTGTATC	CAGTCTCCAAAGAGCTTCGGA
Sphingomyelin synthase 2 (Sgms2)	GAGACAGCAAAACTTGAAGGTCA	CCCGTTGGATAAGGTCTTGGG
Acid sphingomyelinase (Smpd1)	TGGGACTCCTTTGGATGGG	CGGCGCTATGGCACTGAAT
Neutral sphingomyelinase (Smpd2)	TGGGACATCCCCTACCTGAG	TAGGTGAGCGATAGCCTTTGC
Neutral sphingomyelinase 2 (Smpd3)	ACACGACCCCCTTTCCTAATA	GGCGCTTCTCATAGGTGGTG
Lysophosphatidylcholine acyltransferase 3 (Lpcat3)	GACGGGGACATGGGAGAGA	GTAAAACAGAGCCAACGGGTAG
Phospholipase A2 group VI (Pla2g6)	GCAAGCTGATTACCAGGAAGG	GAGAGAAGAGGGGGTGAGTTG
Phosphate cytidylyltransfer 1, choline, alpha (Pcyt1a)	TCCTTCCAAAGTGCAGCGTT	CACCCTGACATAGGGCTTACTAA
Glutamate-pyruvate aminotransferase 1 (Gpt1)	TCCAGGCTTCAAGGAATGGAC	CAAGGCACGTTGCACGATG
Glutamate-pyruvate aminotransferase 2 (Gpt2)	AACCATTCACTGAGGTAATCCGA	GGGCTGTTTAGTAGGTTTGGGTA
Fatty acid binding protein 4 (Fabp4)	AGAAGTGGGAGTGGGCTTTG	CCAGCTTGTCACCATCTCGT
Carbohydrate-response element-binding protein (ChREBP)	CACTCAGGGAATACACGCCTAC	ATCTTGGTCTTAGGGTCTTCA

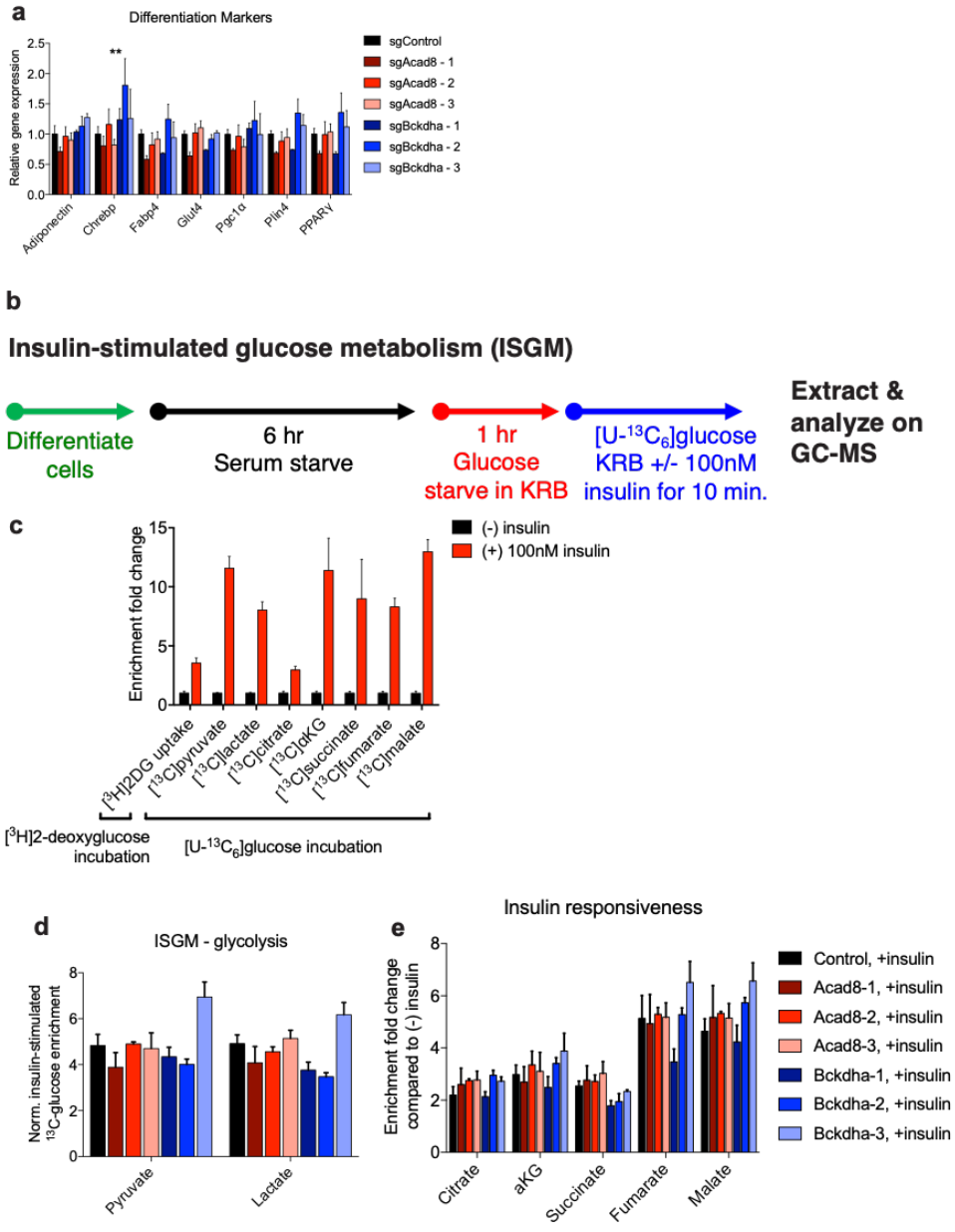

Figure S3.1: **Adipocyte differentiation markers and insulin response were not affected by *Bckdha* deficiency or *Acad8* deficiency.** **a**. Expression of adipocyte differentiation markers normalized to sgControl. **b**. Schematic of insulin-stimulated glucose metabolism (ISGM) assay. **c**. Fold change of the insulin-stimulated ^{3}H-2DG uptake or [U-$^{13}C_6$]glucose enrichment of metabolites obtained from the incorporation of pool size and mole percent enrichment of each metabolite. **d**. Fold change of the insulin-stimulated [U-$^{13}C_6$]glucose enrichment of pyruvate and lactate obtained from the incorporation of pool size and mole percent enrichment of each metabolite in Control, *Bckdha* deficient, or *Acad8* deficient cells. **e**. Fold change of the insulin-stimulated [U-$^{13}C_6$]glucose enrichment of TCA cycle intermediates citrate, α-KG, succinate, fumarate, and malate in Control, *Bckdha* deficient, or *Acad8* deficient cells.

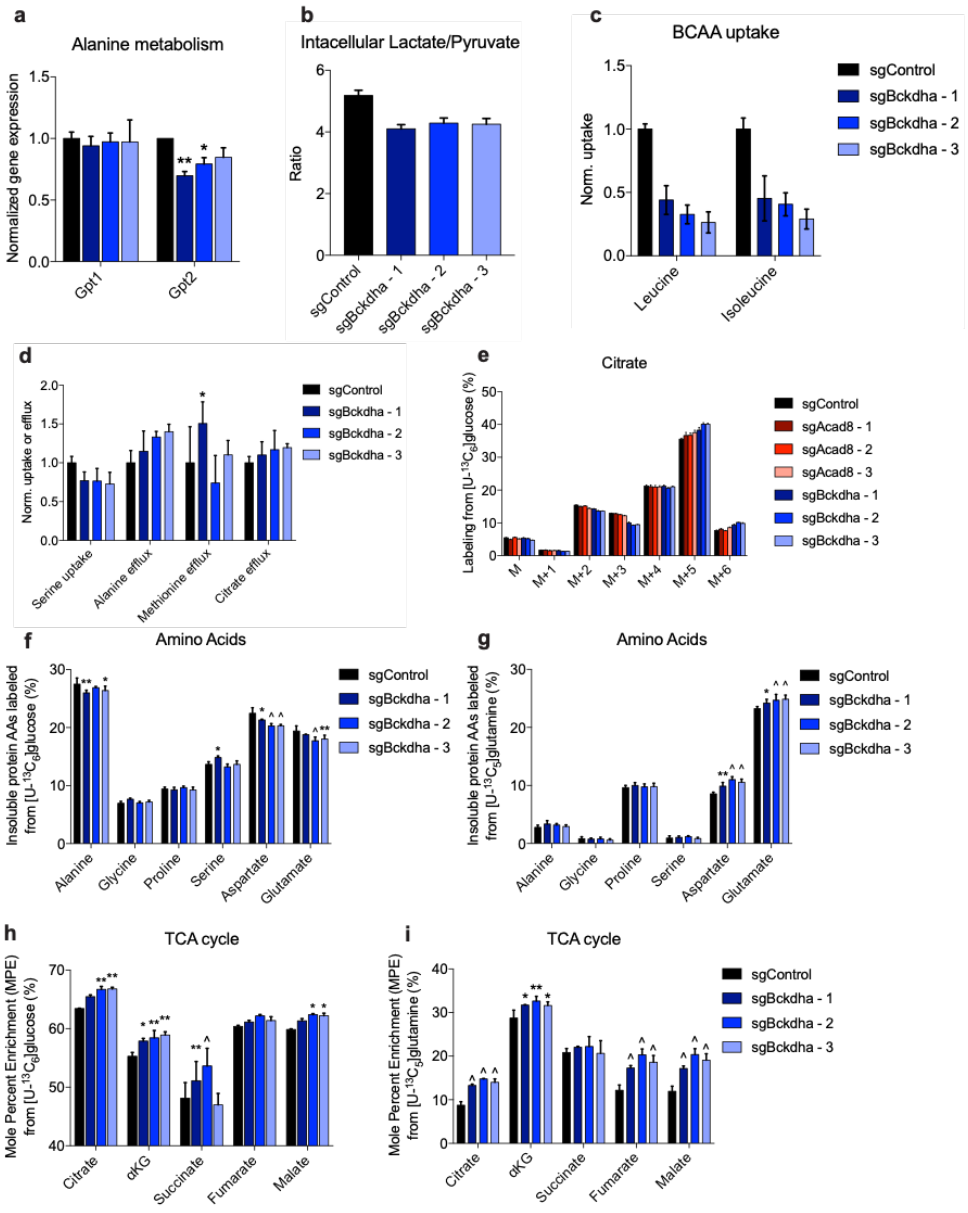

Figure S3.2: ***Bckdha* deficient adipocytes reprogram glucose metabolism to support bioenergetic demands. a**. Gene expression of glutamic-alanine transaminase 1 (Gpt1) and Gpt2 in Control and Bckdha deficient adipocytes. **b**. Intracellular lactate to pyruvate ratio. **c**. Normalized uptake of leucine and isoleucine over 48h in Control and *Bckdha* deficient adipocytes. **d**. Normalized amount of metabolite secretion or uptake in Control or *Bckdha* deficient adipocytes. **e**. Citrate labeling in *Acad8* deficient or *Bckdha* deficient adipocytes traced with [U-$^{13}C_6$]glucose. **f-g**. Percentage of insoluble protein in Control and *Bckdha* deficient adipocytes labeled from **e**, [U-$^{13}C_6$]glucose or **f**, [U-$^{13}C_5$]glutamine. **h-i**. Mole percent enrichment (MPE) of TCA cycle intermediates from **h**, [U-$^{13}C_6$]glucose or **i**, [U-$^{13}C_5$]glutamine. All data are presented as means $\pm$ s.d. Significance is calculated compared to sgControl condition using two-way ANOVA and Dunnett's multiple comparisons post-hoc test. *p<0.05, **p<0.01, $\wedge$p<0.001.

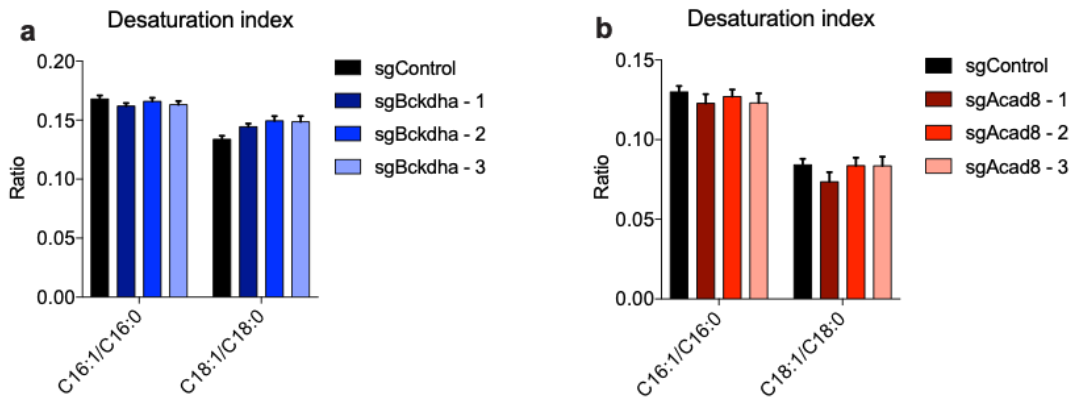

Figure S3.3: **Fatty acid desaturation index is unaffected in 3T3-L1 *Bckdha* deficient or *Acad8* deficient adipocytes.** **a**. Desaturation index in Control or *Bckdha* deficient 3T3-L1 adipocytes. **b**. Desaturation index in Control or *Acad8* deficient 3T3-L1 adipocytes. All data in are presented as means $\pm$ s.d.

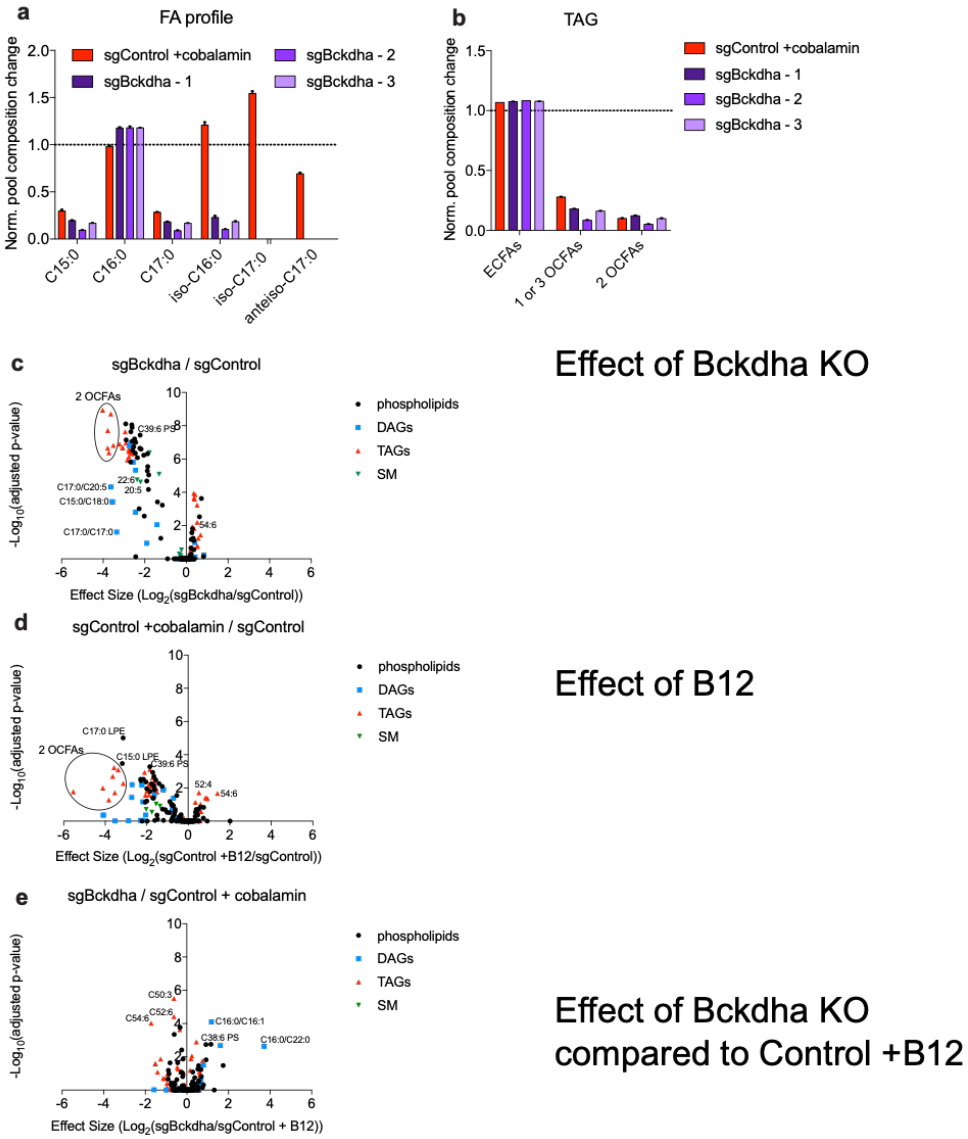

Figure S3.4: **Cobalamin supplementation and *Bckdha* deficiency alters 3T3-L1 adipocyte lipidome. a**. Change in indicated fatty acid's contribution to the total FA pool. **b**. Relative abundance of TAG acyl chain distribution of even- and odd-chain fatty acids in 3T3-L1 sgControl +cobalamin and *Bckdha* deficient normalized to 3T3-L1 sgControl -cobalamin. 1 or 3 OCFA species could not be distinguished from each other. **c**. Volcano plot of lipid species changed in *Bckdha* deficient adipocytes compared to Control adipocytes. **d**. Volcano plot of lipid species changed in Control adipocytes +cobalamin compared to Control adipocytes. **e**. Volcano plot of lipid species changed in *Bckdha* deficient adipocytes compared to Control adipocytes +cobalamin. Data in **a-b** are presented as means ± s.d.

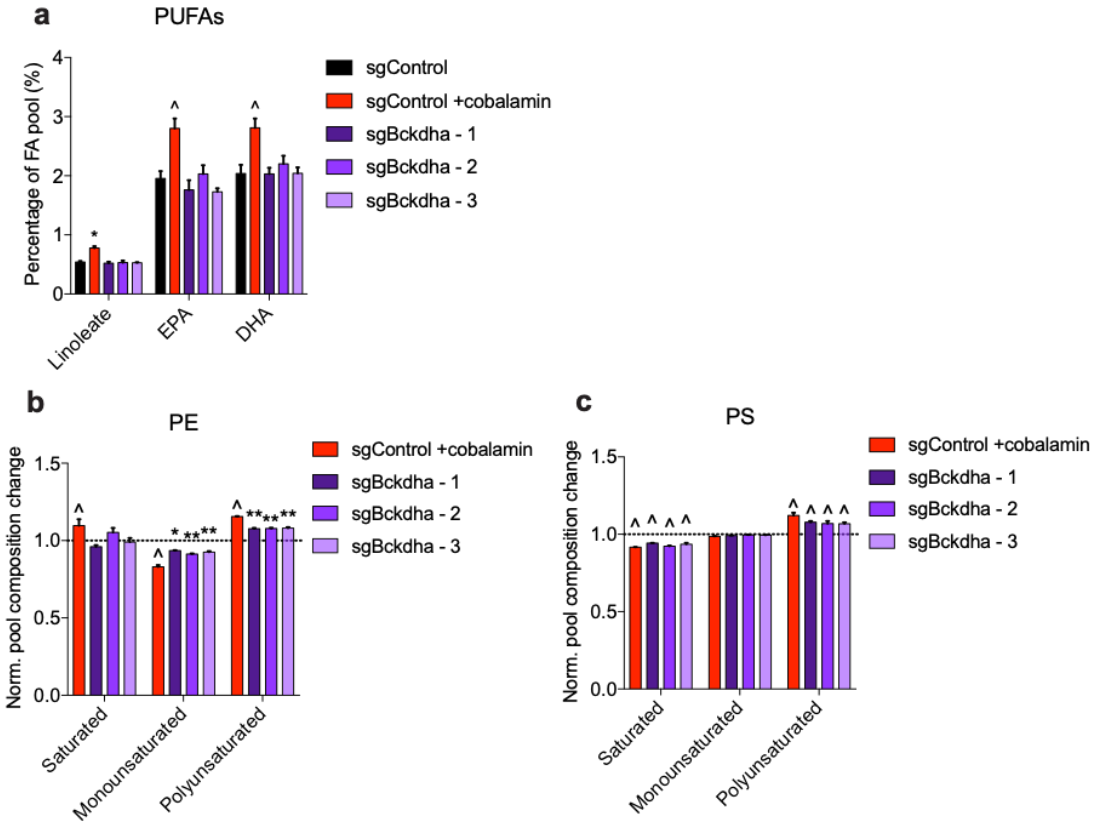

Figure S3.5: **FA composition in phospholipids is affected by cobalamin supplementation and *Bckdha* deficiency.** **a**. Indicated fatty acid's percentage of total fatty acid pool. **b-c**. Relative abundance of **d**, PE and **d**, PS acyl chain distribution of saturated, monounsaturated, and polyunsaturated fatty acids in 3T3-L1 sgControl +cobalamin and Bckdha deficient normalized to 3T3-L1 sgControl -cobalamin. Species known to contain 2 monounsaturated acyl chains are included in monounsaturated category. **d**. Normalized relative expression of genes involved in ceramide metabolism. All data are presented as means ± s.d. Significance is calculated compared to sgControl condition using two-way ANOVA and Dunnett's multiple comparisons post-hoc test. *p<0.05, **p<0.01, ∧p<0.001.

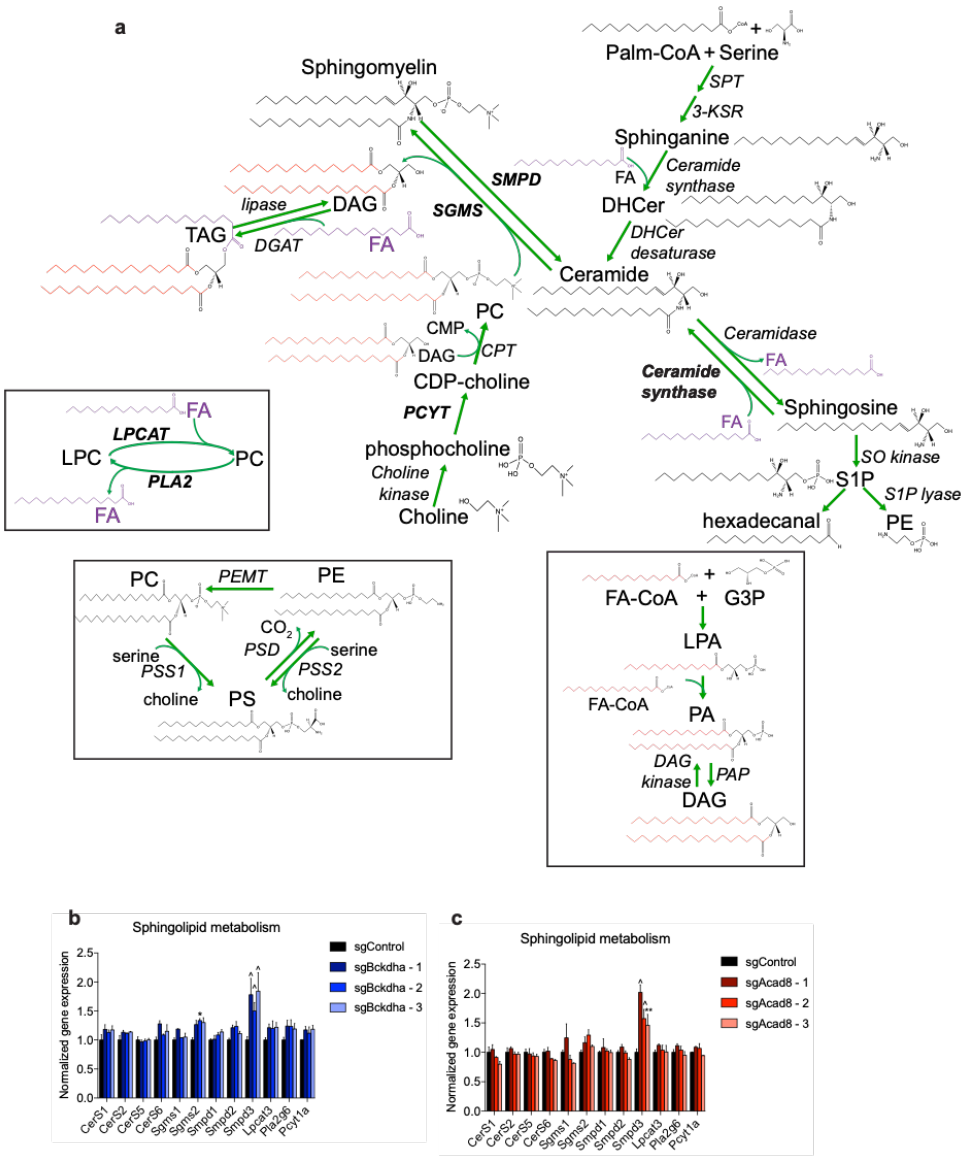

Figure S3.6: **Pathway map detailing acyl chain reorganization in lipids and gene expression of associated enzymes. a**. Map of lipid metabolism highlighting enzymes involved (italics) and points where acyl chain removal or addition occurs (purple). **b**. Normalized relative expression of genes involved in ceramide metabolism in *Bckdha* deficient cells. **c**. Normalized relative expression of genes involved in ceramide metabolism in *Acad8* deficient cells. All data are presented as means ± s.d. Significance is calculated compared to sgControl condition using two-way ANOVA and Dunnett's multiple comparisons post-hoc test. *p<0.05, **p<0.01, ∧p<0.001. Abbreviations: FA: fatty acid; SPT: serine palmitoyl transferase; 3-KSR: 3-ketosphinganine reductase; DHCer: dihydroceramide; SO: sphingosine; S1P: sphingosine 1-phosphate; PCYT1A: Phosphate Cytidylyltransferase 1, Choline, Alpha; DAG: diacylglycerol; PC: phosphatidylcholine; PE: phosphatidylethanolamine; PS: phosphatidylserine; PA: phosphatidic acid; LPA: lysophosphatidic acid; LPC: lysophosphocholine; LPCAT: Lysophosphatidylcholine (LPC) acyltransferase; PLA2: phospholipase A2; SGMS: sphingomyelin synthase; SMPD: sphingomyelinase.